UNIVERSIDAD COMPLUTENSE DE MADRID
FACULTAD DE FARMACIA

TESIS DOCTORAL

Nanovehículos basados en albúmina para terapia contra el cáncer

Albumin-based nanocarriers for cancer therapy

MEMORIA PARA OPTAR AL GRADO DE DOCTOR

PRESENTADA POR

Rama Prajapati

Director

Álvaro Somoza Calatrava

Madrid

UNIVERSIDAD COMPLUTENSE DE MADRID

FACULTAD DE FARMACIA

TESIS DOCTORAL

NANOVEHICULOS BASADOS EN ALBUMINA PARA TERAPIA CONTRA EL CÁNCER

ALBUMIN-BASED NANOCARRIERS FOR CANCER THERAPY

MEMORIA PARA OPTAR AL GRADO DE DOCTORA

PRESENTADA POR

Rama Prajapati

DIRECTOR

Álvaro Somoza Calatrava

IT IS STRANGE THAT ONLY EXTRAORDINARY MEN MAKE THE DISCOVERIES, WHICH LATER APPEAR SO EASY AND SIMPLE

Georg C. Lichtenberg

Acknowledgement

Everyone told me PhD was not everyone's cup of tea. I took it as a challenge, and I am glad I did it. I still remember vividly the day I received an e-mail mentioning I got the La Caixa fellowship in Spain. I could barely believe it, and today after more than three years, here I am, in a verge of getting a degree!!

First, I would like to thank my supervisor Álvaro Somoza for giving me this opportunity and for guiding me patiently through all the stages of my phD journey. I am sure the knowledge, experience and skills that I gained in the lab will definitely help me in the future.

Nextly, I would like to thank La Caixa for giving me the opportunity to do the PhD. I had the amazing three years in Spain. I met the amazing *Lacaixitos* who shared the same aim, same problems and mostly, who were all crazy like me. The annual programs with never ending workshops, unlimited food and fun will always be in my heart!

To all my friends from the Lab, I am glad I got to know you guys. You guys made me feel at home, away from home. Whenever I had failed experiment or needed a translator or even just had a bad day, you guys did not even think twice to lift my mood.

To Cata, my flat mate, my colleague, and my friend, you made my stay in Spain so easy. I could always count on you for anything. You were only a knock on the door away to call my internet providers, my bank, my doctor and basically everyone, provided I was (still am) terrible in Spanish. I cannot imagine how would have I managed in Madrid without you. And to Ángel, you made me less homesick by making amazing food. I tell you; you should try MasterChef España!

To Edu, you are a gem of a person! You are my lunch partner, my coffee mate, and my spicy food competitor. The lab times with you never felt like work since we were always laughing or gossiping or talking or planning for trips that were always unsuccessful! To Demi, I will always cherish the talks we had, whether it was about the lab or football or your weird stories. You guys seriously made me able to adjust in the foreign land.

What can I say about you Ciro? You have the wildest laugh, and most importantly, biggest heart, always ready to help. To Nuria, the only pharmacist in the group, you are one of the hardest

working people I came across. You helped me so much in completing my thesis, that I cannot thank you enough.

I would also like to thank Hernan, who introduced me to the vast world of molecular biology, helped me unconditionally and turned the tedious works into fun. To Maria, Carmen, Mila, Ana, and Paula, I will always remember the laughs we had, the videos that we made, the dinners we had and the times we spent together. I would not have lasted a month in Spain if it were not for you guys.

Also, I would like to thank the Rocha Lab in Leuven, Belgium, especially to my supervisors Dr. Susana Rocha and Dr. Beatrice Fortuni for your continuous support and advises. Moreover, thanks to Indra Van Zundert for helping me out in the lab. I had an amazing experience during my three months stay in Leuven.

To all my friends scattered around the globe, thank you for listening to me blabbing about how difficult PhD was and for motivating me. To Anusha and Manisha, we were all in the same boat and I am glad I had you guys who understood what I was going through.

I would like to thank my family back in Nepal, who were too supportive of whatever I did. I could not have come this far without your motivation. To my siblings, to my parents and my grandmother, you stood like a pillar beside me even from a thousand miles away. Especially to my eldest sister, Usha, who made me what I am today, sacrificing all her dreams so that I could live my dream. I hope I have made you guys proud, there is soon going to be the first Dr. in the family!

Finally, to Sushil, my husband, I cannot tell you how much you have helped me. You got up at 4 in the morning just to listen to me complaining about my failed experiments, how I wanted to give up and how you motivated me back to wanting more in life. You are my biggest support, my cheerleader and yes, “you are my ***L·O·B·S·T·E·R***”!

Table of Content

List of Figures

List of Tables

Abbreviations

ANOVA	Analysis of variance
BSA	Bovine serum albumin
CAR	Chimeric antigen receptor
Cas	CRISPR associated protein
Cav-1	Caveolin-1
CRISPR	Clustered Regularly Interspaced Short Palindromic Repeats
DLS	Dynamic Light Scattering
DMSO	Dimethyl sulfoxide
DNA	Deoxyribonucleic acid
DOX	Doxorubicin
DOX-HCl	Doxorubicin hydrochloride
DSBs	Double-stranded breaks
EGF	Epidermal growth factor
EGFR	Epidermal growth factor receptor
EMSA	Electrophoretic mobility shift assay
EPR	Enhanced permeability and retention effect
ER	Estrogen receptor
FBS	Fetal bovine serum
FcRn	Neonatal Fc receptor
FDA	Food and Drug Administration
GFP	Green fluorescent protein
GLU	Glutaraldehyde
gp	Albumin-binding glycoprotein
gRNA	Guide RNA
GSH	Glutathione
H_2DCF-DA	2',7'- dichlorodihydrofluorescein diacetate
HDR	Homology-directed repair
HER2	Human epidermal growth factor receptor 2
HSA	Human serum albumin
MDR	Multi-drug resistance

miRNAs	Micro-RNAs
MRI	Magnetic resonance imaging
mRNA	Messenger RNA
NHEJ	Non-homologous end-joining
NHS	N-Hydroxysuccinimide
NIR	Near infrared
nm	Nanometer
NP	Nanoparticle
NT	Non-targeting
p53	Tumor protein p53
PAM	Motif adjacent to the protospacer
PBS	Phosphate buffered saline
PD-1	Programmed cell death protein 1
PDI	Polydispersity index
PEG	Polyethyleneglycol
PEI	Polyethylenimine
PlK	Polo-like kinase
PR	Progesterone receptor
Rcf	Relative Centrifugal Force
Redox	Oxidation-reduction
RES	Reticuloendothelial system
RGD	Arginylglycylaspartic acid
RNA	Ribonucleic acid
RNAi	RNAs interference
RNP	Ribonucleoprotein
ROS	reactive oxygen species
Rpm	Revolutions per minute
SD	Standard deviation
SEM	Scanning electron microscopy
siRNAs	Small interfering RNAs
SN38	7-ethyl-10-hydroxy-camptothecin
SPARC	Acidic and cysteine rich secreted protein

SPDP	3-(2-Pyridyldithio)propionic acid N-hydroxysuccinimide ester
STEM	Scanning transmission electron microscope
TAE	Tris-Acetate-EDTA
TEM	Transmission electron microscopy
UV	Ultraviolet
VGFR	Vascular endothelial growth factor receptor
Vis	Visible
Vola	Volasertib
WHO	World Health Organization
ZFN	Zinc finger nucleases

Abstract/ Resumen

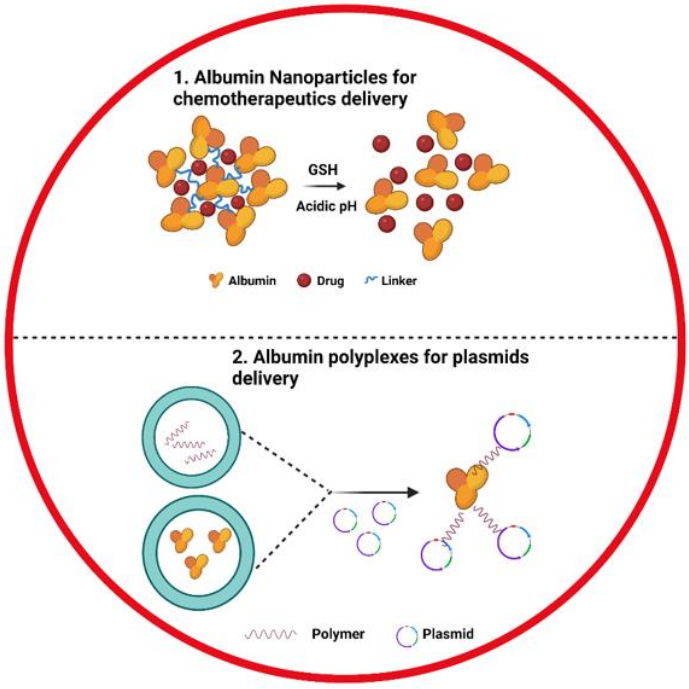

Abstract

Cancer is one of the major health problems worldwide and suitable therapies with enhanced efficacy and reduced side effects are hence being searched. In recent years, nanocarriers are gaining tremendous attention for the delivery of various therapeutic agents (both chemotherapeutics and nucleic acids) in cancer therapy. They offer multiple advantages, including improved drug delivery, targeted accumulation due to enhanced permeability and retention (EPR) effect, controlled release, improvement of circulation half-lives, biodistribution, and efficacy of encapsulated cargos, and flexibility in administration routes.

This thesis is focused on the use of albumin-based nanocarriers for cancer therapy. Albumin is a versatile protein and provides biocompatibility, tumor specificity, the possibility for surface modification, and reduces toxicity. Some of the widely investigated albumin nanocarriers include polyplexes, nanoconjugates, and nanoparticles. Despite their broad potential in oncology, many studies still need to be done regarding their safety and tumor targeting enhancement. Anyhow, the potential of albumin nanocarriers is clearly supported by the FDA and EMA approved formulation, Abraxane, which is currently used for metastatic breast cancer. Therefore, further developments based on related strategies can have a dramatic impact on cancer therapy.

In the first part of the thesis, the formulation of albumin nanoparticles with various cross-linkers will be discussed. The optimum cross-linker (SPDP) will be used for the preparation of albumin nanoparticles (ABNs) encapsulating different chemotherapeutics like Doxorubicin, SN38 and Volasertib. Then, the physicochemical properties of the nanoparticles will be assessed as well as their efficacy in various cell lines, including MCF-7, MDA-MB-231, HeLa and MCF-10A. Moreover, the role of those nanoparticles in overcoming biological barriers, along with the internalization and efficacy in 3D cancer spheroids, will also be discussed. Finally, the immunomodulatory effects of various albumin-based nanoparticles will be assessed as well.

The second part of the thesis deals with the preparation of albumin-based polyplexes with polymers based on PEI and PEG. The potential use of these systems as nanocarriers of nucleic acids will be first assessed using a Green Fluorescent Protein (GFP) plasmid as a model. Then, the optimized system will be used to conjugate a CRISPR-based plasmid targeting the mutant p53

gene in the pancreatic cancer cell line PANC-1. Overall, the results obtained in this thesis highlight the enormous potential of albumin-based nanocarriers for cancer therapy.

Resumen

El cáncer es uno de los principales problemas de salud en todo el mundo y la busqueda de terapias con mejor eficacia y menores efectos secundarios es un reto prioritario para la sociedad. En este sentido, en los últimos años, los nanovehiculos han mostrado excelentes propiedades para la administración de varios agentes terapéuticos (tanto quimioterapéuticos como ácidos nucleicos) en la terapia del cáncer. Estos sistemas ofrecen varias ventajas, como son una administración mejorada del fármaco, acumulación dirigida debido al efecto de permeabilidad y retención (EPR), liberación controlada, mejora de la vida media de la circulación, biodistribución y eficacia de las cargas encapsuladas y flexibilidad en las vías de administración.

Esta tesis se centra en el uso de nanovehiculos a base de albúmina para la terapia del cáncer. La albúmina es una proteína versátil y proporciona biocompatibilidad, especificidad tumoral, la posibilidad de modificación de la superficie y reduce la toxicidad. Algunos de los nanopovehiculos de albúmina ampliamente investigados incluyen polyplexes, nanoconjugados y nanopartículas. A pesar de su amplio potencial en oncología, aún deben realizarse muchos estudios en términos de estudios de seguridad y mejora de la orientación tumoral. En este sentido merece la pena recordar que el potencial de los nanovehiculos de albúmina ya se refleja en una formulación aprobada por la FDA y la EMA, el Abraxane, utilizado para el cáncer de mama metastásico. Por tanto, es de esperar que futuros desarrollos basados en estos sistemas tengan un gran impacto en las terapias contra el cáncer.

En la primera parte de la tesis se ha abordado la formulación de nanopartículas de albúmina con diversos conectores. El sistema óptimo, basado en el conector SPDP, se utilizó para la preparación de nanopartículas de albúmina (ABN) con diversos quimioterapéuticos como Doxorrubicina, SN38 y Volasertib. Posteriormente, se estudiaron las propiedades fisicoquímicas de las nanopartículas y se analizó su eficacia en varias líneas celulares, como son MCF-7, MDA-MB-231, HeLa y MCF-10A. Además, se evaluó el papel de las nanopartículas en la superación de barreras biológicas, así como su internalización y eficacia en modelos de cáncer en cultivos 3D (esferoides). Finalmente, se estudiaron los efectos inmunomoduladores de varias nanopartículas basadas en albúmina.

La segunda parte de la tesis aborda la preparación de polyplexes a base de albúmina con los polímeros a base de PEI y PEG. El uso de estos sistemas para el transporte de ácidos nucleicos se evaluó primero utilizando como modelo el plásmido de proteína fluorescente verde (GFP). A continuación, se utilizó el sistema optimizado para vehiculizar un plásmido para la realización de edición génica basado en CRISPR dirigido al gen p53 mutante en la línea celular de cáncer de páncreas PANC-1. En general, los resultados obtenidos en esta tesis destacan el enorme potencial de los nanovehiculos a base de albúmina para la terapia del cáncer.

Chapter 1. Introduction

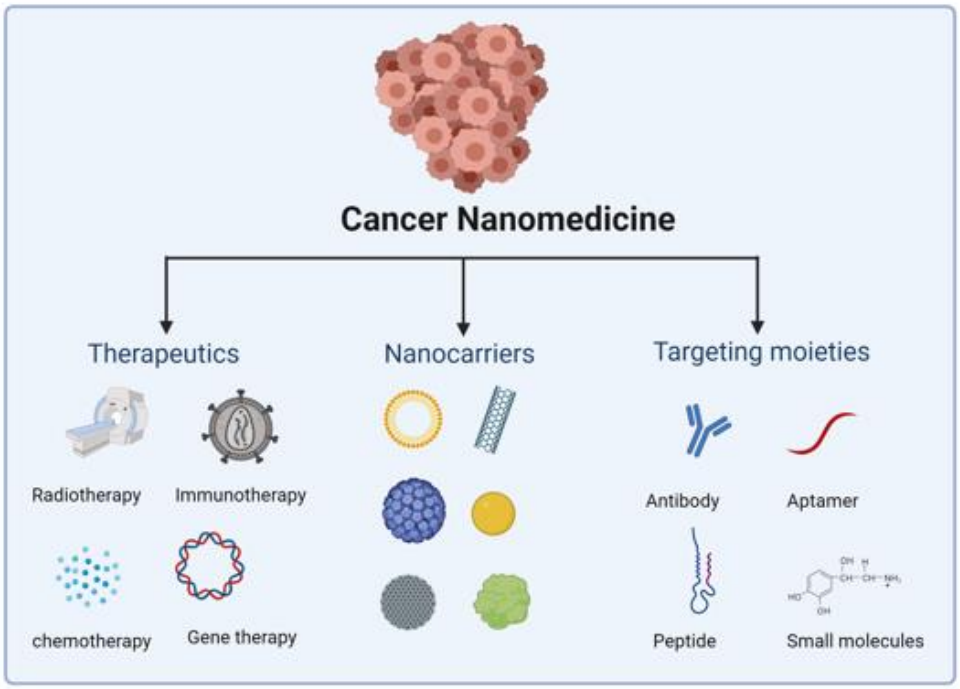

1.1. Cancer

Cancer is a complex disease condition arising due to the uncontrollable, undesired, and uncoordinated growth of a group of cells breaking the rules of cell proliferation and is one of the most dreaded diseases of the 21st century.[1] Cancers are termed according to the organs being affected, namely, breast cancer, colon cancer, blood cancer, liver cancer, etc. Cancer can affect people of all age groups; however, the risk increases with age as cellular repair mechanism is highly compromised in the older population.[2]

The causes of cancer are still intriguing to the researchers. However, thanks to the intense studies going on worldwide in the field of cancer, it has been clear that the accumulation of genetic defects is one of the major causes that triggers the development of this disease.[3,4] After the accumulation of various mutations, the cells stop responding to the growth-inhibiting signals and begin replicating uncontrollably. These rapidly dividing cells are termed malignant cells or cancer cells, or tumor cells and they vary widely from the healthy cells, in terms of appearance and behavior. Unlike normal cells, the nucleus of the cancer cells occupies most of the cell volume, are larger in size, have more permeability, possess acidic cytosol and their surface is highly crowded with various receptors, including glucose and folate receptors.[5] The cancer cells can reproduce, ignoring the restriction of space, nutrients and signals to stop cell proliferation. Moreover, in later stages, these proliferating tumorous cells may invade new locations. Based on this behavior, cancer can be classified as benign (non-invasive) or malignant (invasive) tumors.

In 2000, Hanahan and Weinberg, in their excellent review entitled “The hallmarks of cancer”, described various critical changes in healthy cells during the development of tumors.[6] These hallmarks include the acquired capability of self-sufficiency in growth signals, insensitivity to the antigrowth signals, evasion of apoptosis, the gain of limitless replicative potential, sustained angiogenesis and tissue invasion and metastasis. (Figure 1) These physiological changes in the cells were described as being responsible for the development of cancer. The understanding of cancer broadened gradually and in 2011, the authors further added other properties, like reprogramming of the energy metabolism and evasion of the immune destruction.[7]

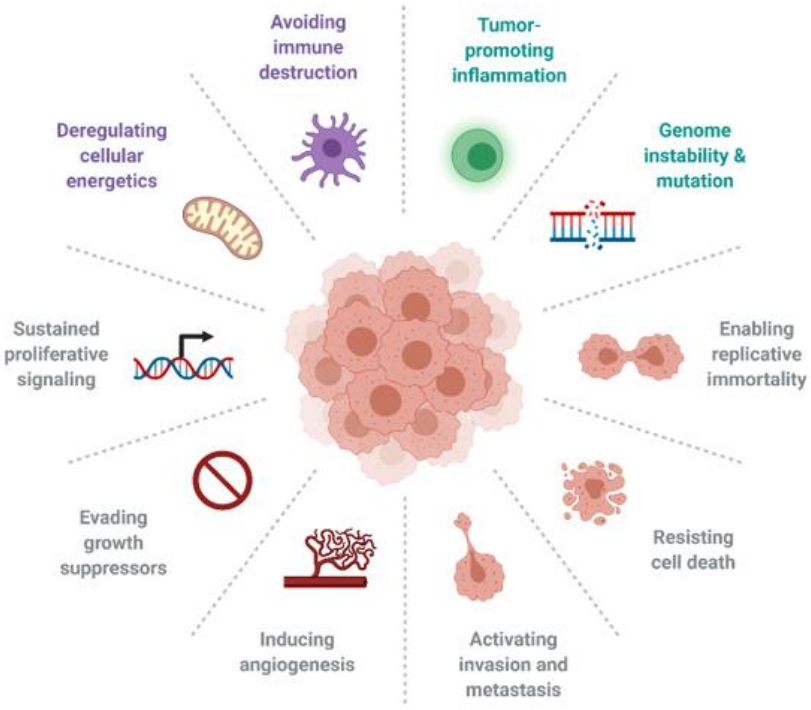

Figure 1. Hallmarks of cancer as described by Hannah and Weinberg.[6] The physiological changes that are responsible for the development of cancer are depicted.

The first description of cancer dates to 3000 BC where eight breast cancer women were reported in the Edwin Smith Papyrus, followed by mentions of cancers in different body parts by Hippocrates in 400 BC.[8] Figure 2 summarizes some of the critical discoveries of the disease and its treatments over time. The evolution of the therapies employed took place gradually, from the removal of the tumorous organs to radiotherapy and chemotherapy. However, the greater advances took place from 1971, when Richarch Nixon dramatically supported the research in this field by signing the National Cancer Act. Currently, there are over 200 anticancer drugs in the global pharmacopoeia, with most drugs derived from plants and fungi. In recent years, cancer care is focused on early diagnosis, pharmacotherapies, and other treatment modalities. The improvement in understanding the underlying pathophysiology of various cancers and molecular biology has helped in escalating the clinical management of cancers.[9] Currently, personalized cancer medicine for targeted therapy is gaining increasing popularity. Moreover, treatment

options with nucleic acids (siRNAs, long non-coding RNAs) and gene editing tools (CRISPR) are also being explored which can definitely change the future cancer therapy.[10,11]

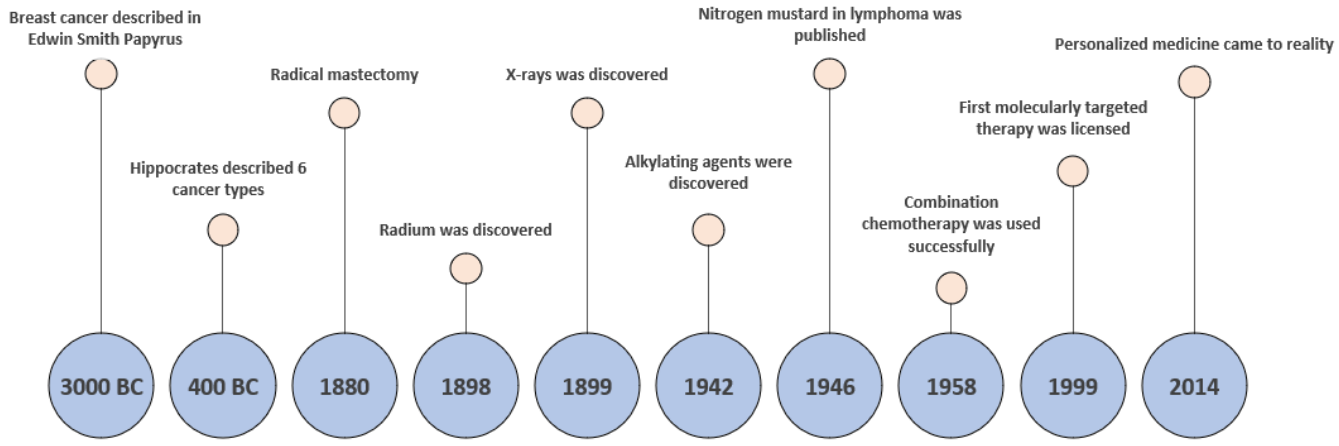

Figure 2. Timeline of cancer.[8] The progress in the knowledge of cancer, critical discoveries and advancement in treatment have been shown at different time periods.

1.2. Epidemiology of cancer

Despite the enormous amount of time and money spent on cancer research during the last decades, it is still a leading cause of morbidity and mortality (2nd place) and affects people worldwide.[12,13] Minimal improvement has been made in terms of overall cure rates in the past few decades. According to the data presented in Cancer Statistics, 2020, the 5-year relative survival rate for all cancers diagnosed from 2009 to 2015 was 67%.[13] In 2018, the cancer burden in European Union (EU) was estimated to be 3.1 million new cancer cases and 1.4 million cancer-related deaths. The health cost of cancer in the EU was 103 billion € in 2018 [2] whereas, in the United States, it was over 80 billion USD in 2015 as reported by Agency for Healthcare Research and Quality.[14] According to World Health Organization (WHO), 30.2 million people are estimated to suffer from cancer and 16.3 million deaths by 2040. The alarming situation is highlighted by the fact that every fourth person has a lifetime risk of cancer.[15]

The increase in cancer incidence is expected mainly in developing countries because of the lifestyle, including heavy smoking, pollution, and poor diet habits. The most common cancers

include breast, lung, prostate, and colon cancers based on the estimated new cases. In men, prostate, lung and colorectal cancers contributed to around 43% of all the cancers, while in women, 50% of total cancer cases were accounted by breast, lung and colorectal cancers in 2020.[16]

1.3. Cancer therapy

Based on the type, location, condition of the patient and progression of cancer, different therapeutic approaches can be employed, such as surgery, radiation therapy and chemotherapy, either alone or in combination.[17,18] In this regard, most of the treatments aim to remove the cancer cells or to cause the death of the cancer cells by interfering with essential mechanisms for survival.[19] Despite the significant progress in some particular areas, in recent years, therapies based on nucleic acids and immunotherapy have emerged as prominent methods for the management of cancers. Various treatment approaches in cancer are summarized in Figure 3.

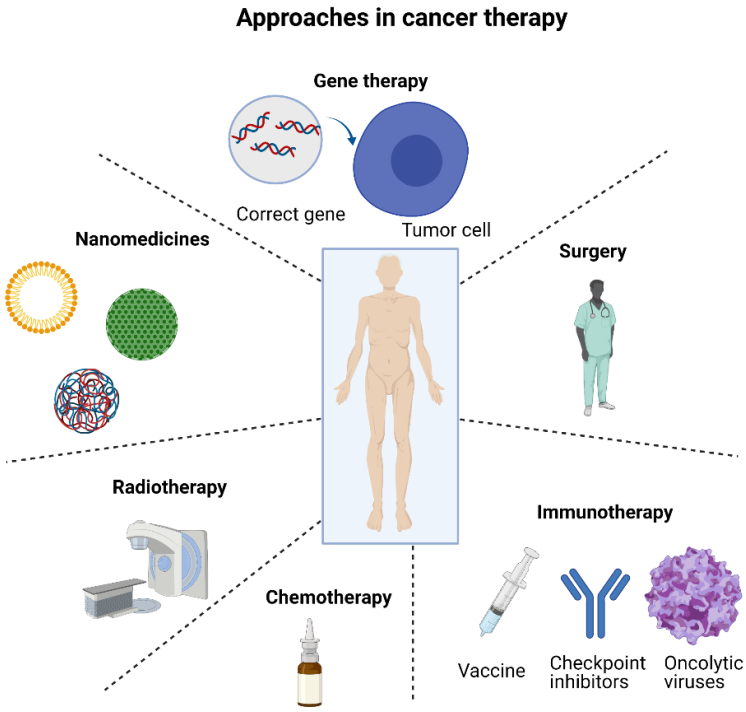

Figure 3. Various approaches for cancer treatment. The treatment options ranging from the conventional methods like surgery and chemotherapy to the more advanced gene therapy are shown in the schematic illustration.

1.3.1 Surgical intervention

Cancer surgery remains the foundation of cancer treatment, with the highest success rate to control the spread of cancer.[8] There are different types of cancer surgeries, including cryosurgery, electro surgery, laser surgery, mohs surgery, laparoscopic surgery, natural orifice surgery and robotic surgery.[20] In cancer treatment, it is often used in combination with other forms of therapies, like radiotherapy and chemotherapy. The advantages of surgical intervention in cancer include the possibility of removing a large volume of tumour, the potential of eliminating all cancer tissue in the small area, lack of systemic toxicity unlike in chemotherapy, and the reduction of the symptoms instantly. However, it is associated with various limitations, like deterioration in patient's quality of life, damage to nearby healthy tissues, and severe deformities in patients.[20] Regardless, with the advancement in techniques and procedures, it is gradually becoming more conservative, with the ability to retain organs and maintaining functions in the body.[8]

1.3.2. Radiotherapy

Radiotherapy is the most common method employed for cancer treatment. It uses ionizing radiation to induce DNA damage in the cells and is based on the fact that healthy cells demonstrate more capability in recovering from the radiation damage than tumor cells. According to studies, almost 80% of cancer patients require radiotherapy at some point of disease progression for curative or palliative reasons.[21] Radiotherapy is used for benign and malignant cancers and is used alone or combined with surgery, chemotherapy, or both.[22] The clinical radiotherapy needs to be accurate, and have a proper balance between the dose administered and the threshold of the surrounding normal tissue. The most common problems associated with radiotherapy include targeting inefficiency that damages healthy tissue surrounding the tumor cells, and long-term effects like the development of second cancer. These problems commonly arise from geometrical uncertainties resulting from the low resolution of imaging modalities, organ motion and error in dosing calculations.[23] However, multiple approaches are being carried out to enhance the efficacy while reducing the toxicity of radiotherapy. For instance, the metal-based nanoparticles are mainly being used to enhance the radiotherapeutic effects by better targeting the tumor sites since the densely packed metal particles can either selectively scatter or absorb the high energy radiations.[24]

1.3.3. Chemotherapy

The term chemotherapy was first used by Ehrlich to describe the synthetic chemicals that destroy infective agents. The chemotherapeutic agents should be toxic to the cancer cells, while not affecting the healthy cells. Cancer chemotherapy is aimed at causing cytotoxicity or apoptosis in tumor cells, primarily focused on DNA or metabolic sites responsible for causing cell replication. Chemotherapy can be adjuvant (given as a supplemental treatment after surgery or radiation to attack micrometastases) or neoadjuvant (given before the surgical procedure to shrink tumour) or maintenance (given in small doses to prolong remission).

Some prominent chemotherapeutics include alkylating agents, antimetabolites, antibiotics, monoclonal antibodies, topoisomerase inhibitors, microtubule inhibitors and plant alkaloids. Alkylating agents (e.g., mechlorethamine) covalently bind to the nucleophilic groups of the cell constituents of both resting and dividing cells leading to DNA damage. Antibiotics (e.g., doxorubicin, daunorubicin) act by intercalation in DNA, resulting in the blockage of DNA and RNA synthesis. Antimetabolites (e.g., gemcitabine, cytarabine) inhibit ribonucleotide reductase, which is responsible for DNA synthesis.

Despite the wide range of drugs, chemotherapy has several drawbacks that need to be solved. Most of the anticancer drugs are not specific towards the cancer cells, affecting normal and abnormal cells, and leads to a low therapeutic index. Hence, a system that can deliver the drugs specifically to the cancer cells is of utter importance. Moreover, the neoplastic cells may develop resistance to the cytotoxic drugs, either primary (present when the drug is administered for the first time) or acquired (develops during treatment). In addition, some of the drugs may cause treatment-induced tumors since most of the chemotherapeutics are mutagens. Those problems underline the immediate urgency to search for suitable treatment alternatives.

In this sense, the use of nanocarriers can be of help since they can encapsulate the drugs till they reach the desired tumor sites. In addition, it protects the drugs from premature degradation, enhances their cellular uptake, and promotes the delivery of hydrophobic drugs. What is more, nanocarriers can be modified to provide specificity and selectivity to the cancer areas and also be used for the co-delivery of various anticancer agents, increasing the overall efficacy, reducing side effects and preventing the generation of resistance.[25–28]

1.3.4. Immunotherapy

In addition to the conventional therapeutic approaches for cancer, namely, chemotherapy, radiotherapy and surgery, a new approach based on the exploitation of the immune system (immunotherapy) is now in the limelight.[29] Some approaches to cancer immunotherapy include immune checkpoint blockade, cancer vaccines, adoptive cell transfer therapy, and oncolytic virotherapy.[29,30] The main advantage of immunotherapy is that the immune system can remember and invade various tumor variants, unlike conventional approaches. Moreover, it can be used as combination therapy after chemotherapy or surgery to remove any surviving cancer cells. In this regard, a phase II clinical trial of a vaccine using allogeneic pancreatic cancer cells, when combined with surgery, drastically enhanced the survival rate of patients with pancreatic cancer.[31]

However, despite the tremendous potential of immunotherapy in cancer treatment, there are still some challenges that need to be addressed. For instance, cancer vaccines are dependent on autologous cells, which may be problematic in terms of expense and production time. Similarly, immune checkpoint inhibitors have gained vast success in cancer treatment, however, only a limited number of patients benefit from these therapies, where the induction of resistance and toxicity are still huge problems.[32] In addition, immunotherapy is more complicated in solid tumours since they are immunologically cold and generally do not respond to the therapies that use the body´s immune system against cancer. Recently, nucleic acid therapeutics are emerging as the potential candidate for cancer immunotherapy, which may improve the therapeutic outcome in a wide range of tumors, and even in the late stages [33]. These nucleic acids include immunostimulatory DNA/RNA, genome editing nucleic acids, and mRNA/plasmid, which can be further translated to immunotherapeutic proteins.[34] In addition, different genetic tools such as gene editing, gene silencing, or gene activating systems are also being studied extensively in cancer immunotherapy.[33]

1.3.5. Gene Therapy

The traditional chemotherapeutic regimens impart various challenges, namely, systemic toxicity, increased risk of developing other types of cancers, and side effects involving mild cognitive impairments[35,36]. In response to those challenges and to improve the survival rates of

patients, while minimizing the side effects, new treatment methods are searched for. In this regard, gene therapy is a potential treatment option for cancer. Gene therapy can be defined as the delivery of genetic material to correct defective genes or to change the properties of specific tissues to manage various disorders. In gene therapy, a defective gene can be either swapped with a normal gene by homologous recombination or repaired by selective reverse mutation, or by gene knockdown or deactivation of the problematic genes.[37] Recently, the most interesting gene therapy techniques in cancer include RNAs interference (RNAi) and gene-editing tools like CRISPR/Cas system. RNAi, often known as post-transcriptional gene silencing, causes sequence-specific gene silencing triggered by double-stranded RNA (dsRNA).[38] On the other hand, Clustered Regularly Interspaced Short Palindromic Repeats (CRISPR)/Cas9 possess Cas9 endonuclease and a short non-coding guide RNA (gRNA), where gRNA guides Cas9 to the target sequence and hence allows the modification of the genomic sequence.[39]

However, gene therapy requires a targeted and efficient delivery system to prevent undesired off-target effects, which can be fatal. The delivery methods employed include physical methods (electroporation, ultrasound), viral vectors (adenovirus, retrovirus) and non-viral vectors (liposomes, nanoparticles).[39] Among them, the viral vectors are most widely used because of their enhanced efficacy in the delivery of genes and long-term gene encoding.[40] However, various challenges, including lack of specificity to the target cells, carcinogenicity, immunogenicity, high cost and inability to deliver larger genetic material, limit their use. The physical methods (e.g., needle and jet injections, sonoporation, gene gun bombardment) are used to overcome the biological barriers that limit the gene entry to the host cells. However, they are not suitable for therapeutic applications with the exception of some ex vivo treatments. Regarding the non-viral vectors, such as lipid nanoparticles, polymeric nanoparticles and metallic nanoparticles are gaining immense popularity for gene therapy due to their improved safety profile, ability to deliver larger gene structures, and easier production than the viral vectors.[41]

1.4. Current challenges with cancer therapy

One of the major problems associated with cancer treatment is the delayed screening and diagnosis. In most cases, cancer diagnosis is inaccessible till it has reached the final stage, which makes the survival rate of patients minimal, and the treatment regimen more complicated and

expensive. Historically, cancer research is focused mainly on studying the factors contributing to cancer progression but using this knowledge for therapeutic targeting is not always successful.[42] This can be due to the lack of efficient delivery vehicles and targeted therapies, which results in undesirable toxicity and the inability to kill the cancer cells evenly.[43] The lack of targeting efficiency directly affects the survival rate of cancer patients and their quality of life. A better understanding of molecular and tumor biology has contributed to the paradigm shift of cancer treatment. It is, however, of utter importance to address the complex problems related to curing cancer and make an impact on the survival rate of patients. In this regard, an emerging platform that may handle the limitations of diagnosis and cancer therapy is nanotechnology.

1.5. Nanotechnology

Nanotechnology is defined as "the design, characterization, production and application of structures, devices and systems by controlling the size and shape in nanometric scale".[44] It deals with the structures having dimensions in the order of a billionth of a meter (1×10^{-9}). The term nanotechnology is derived from the Greek word, "nano" meaning dwarf and manufactures and engineers at a molecular level. The concept of "nanometer" was reported in 1925 by Richard Zsigmondy, the Nobel prize Laureate in chemistry.[45] The size measurement of the gold colloids particles was first done by him using a microscope.

The initial idea of nanotechnology traces back to 1959, when the Nobel Laureate Richard Feynman gave a lecture entitled "There's plenty of room at the bottom" in the annual meeting of the American Physical Society.[46] He outlined the principle of manufacturing the smaller machines by manipulating the atoms with larger machines. Afterwards, a Japanese scientist, Norio Taniguchi, first used nanotechnology to report the semiconductor processes, which were in the order of a nanometer.

Since then, nanotechnology has made tremendous progress, and the application of nanotechnology has broadened in a variety of fields, including medicine, communications, robotics, the development of electronic devices, and the study of biological processes.[47] Among many of the prevalent applications, the medical use of nanotechnology to monitor, diagnose, treat and control biological systems, known as nanomedicine, is gaining

popularity.[44,48] It is a promising field with the potential to revolutionize disease therapy and diagnosis.[49] Nanomedicine is a vast subject area that includes nanostructures as delivery systems (e.g., carbon nanotubes, magnetic nanovectors), nanodevices (silicon microchips), sensors, nanofibers and diagnostic tools.[48] Nanomedicines are being applied to enhance the physical and chemical properties of drug molecules, including biodistribution, solubility and targeted delivery.

1.6. History of nanotechnology

Nanotechnology has increased rapidly in the field of physics, chemistry, biology, and engineering. However, although the terminology is relatively new, the existence of materials and devices in the nanometric range is not novel. For instance, abalone, a type of mollusk, possesses a shell with calcium carbonate organized into the nanostructured bricks.[50] The shell protects the mollusk from any exterior cracks, which indicate the strength of nanostructures in the natural environment. It is, however, not evident when humans started to use nanosized materials. In the 4th century A.D., roman glassmakers fabricated glasses composed of nanometric metals, as in the case of the Lycurgus cup, present in the British Museum, London.[50] The dichroic glass was made from soda lime with gold and silver nanoparticles and could change the color from opaque greenish-yellow to translucent red.

The existence of nanomaterials evolved over time. In the middle ages, glass with glazed ceramics possessing optical effects was manufactured from metallic nanoparticles.[51] The red glass manufacturing occurred worldwide, and in the 19th century, the ruby-colored satsuma glasses were also produced in Japan based on the absorption properties of copper nanocrystals. Moreover, the famous Damascus blades encountered by the crusaders while fighting against the Muslims in the 17th century revealed the presence of carbon nanotubes and cementite nanowires.[52] The presence of these nanometric materials provided the blades with exceptional mechanical strength and a sharp cutting edge. The history of nanosized materials further evolved in the 18th and 19th centuries when advanced photography based on the decomposition of photographic films to produce silver nanoparticles was developed.[50]

Hence, the nanomaterials and their applications were in existence way before humans realized their importance. The most prominent period in nanotechnology began in 1980s, when Kroto, Smalley, and Curl invented fullerenes. During a similar time period, Eric Drexler proposed molecular nanotechnology, which would be able to make a copy of itself and of others with arbitrary complexity.[45] The field of nanotechnology since then has advanced a lot and is still in the progressive stage that will show its full potential in the future.

1.7. Nanotechnology and nanomedicines in cancer

In cancer therapy, nanocarriers are gaining increasing attention for the delivery of both chemotherapeutics and nucleic acids. The nanocarriers that have reached the clinical setting are usually based on biocompatible and biodegradable components (e.g., lipids, proteins, polymers), and their favorable interaction with the tumoral areas and avoidance of immune system activation are evaluated.[53] Recently, increasing research activities are also being carried out that involve the inorganic nanocarriers (gold nanoparticles, magnetic nanoparticles, silica nanoparticles). Compared to the conventional methods, the nanocarriers improve the circulation half-life, bioavailability, efficacy of the encapsulated drugs, and provide flexibility in administration routes.[54] Moreover, nanomedicines can be employed to target the tumor sites either by passive or active targeting mechanisms (Figure 4).[49,55,56]

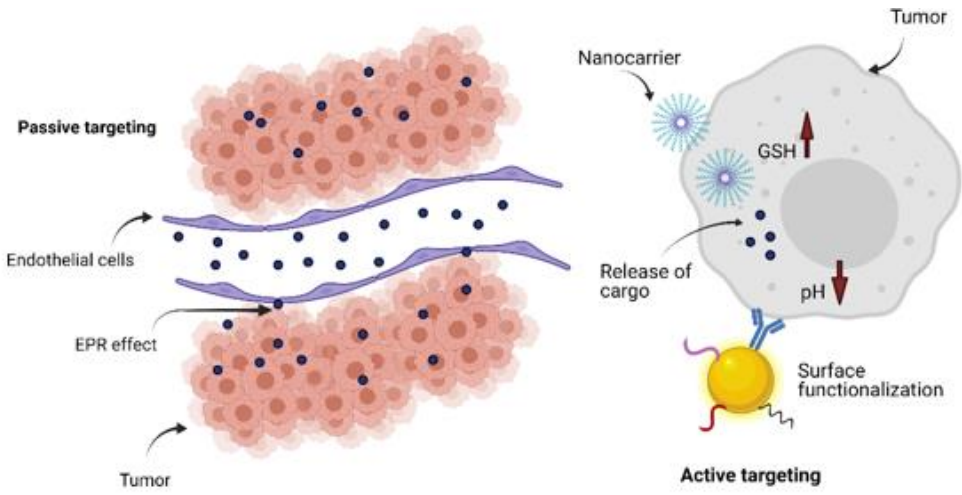

Figure 4. Targeting of tumor with nanocarriers. The passive and active targeting of cancer by the nanoparticles are depicted.

The enhanced permeability and retention (EPR) effect is the primary mode of passive targeting for nanocarriers, which is due to the characteristics of the tumoral area. [54,57,58] Particularly, the blood vessels in the tumor sites are leaky compared to the normal vasculature and permit the nanocarriers to cross the endothelial barrier.[57] Moreover, the lymphatic system in solid tumors is flawed, which further contributes to the accumulation of nanocarriers in the tumor sites.[58] In addition, active targeting can be achieved by modifying the nanocarriers with ligands, including aptamers, antibodies and proteins to increase the specificity to the tumor sites, and therefore, reduce the undesired toxicities. In addition, the nanoparticle-based delivery system can also aid in overcoming multi drug resistance (MDR) by bypassing the drug flow pumps.[59,60] Most of the free drugs enter the cells via diffusion which are susceptible to efflux mechanism whereas the nanoparticles are internalized through endocytotic routes and hence escape the efflux pumps.

The efficacy can be further enhanced by the controlled release of therapeutic agents from the nanocarriers at the tumor sites. For instance, the tumor microenvironment differs widely from the adjacent normal cells, having an acidic pH (around 5.5-6.5), compared to the healthy cells (pH of 7.4). This phenomenon, attributed to the combined effect of an increased rate of glycolysis, enhanced production of lactic acid, and inability to remove the acidic byproducts, is known as the Warburg effect.[61,62] Moreover, high glutathione (GSH) levels are usually found in the tumor sites in response to the reactive oxygen species (ROS) generated due to the additional stress of the cells.[63,64] These properties can be exploited to design nanocarriers that interact with the acidic environment or the reducing environment to control the release of encapsulated cargoes better, providing an additional way to modulate the selectivity of the therapy.[65–67]

1.8. Types of Nanocarriers

In cancer treatment, nanocarriers are gaining much attention for the delivery of therapeutics due to the enhanced efficacy and/or reduced side effects provided. Figure 5 shows the schematic representation of various nanocarriers being studied in cancer therapy, including the lipid-based nanocarriers, inorganic nanocarriers (e.g., gold, magnetic nanoparticles), carbon-based nanocarriers, and protein-mediated nanocarriers. These delivery vehicles have various advantages, such as protection from premature degradation of the cargo by biological

environment and reduction of the renal glomerular filtration rate by increasing the size of the anticancer drugs.

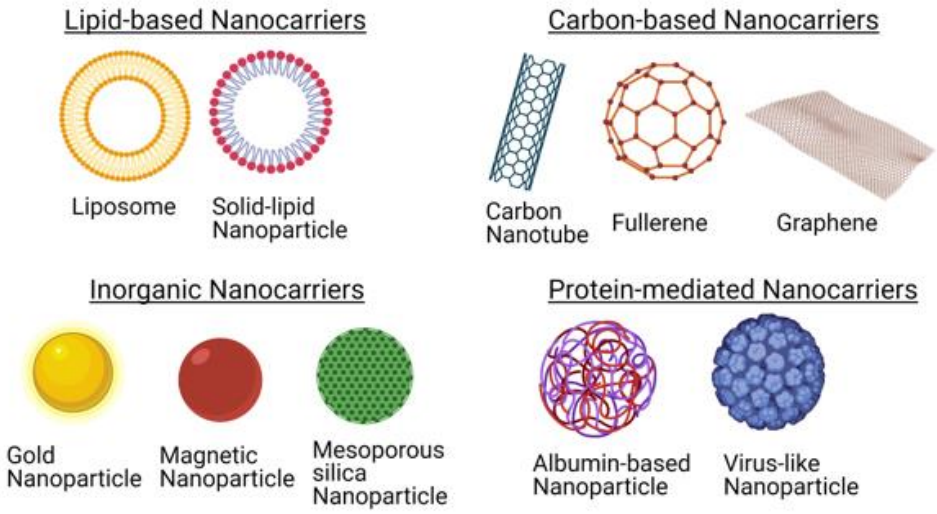

Figure 5. Schematic representation of various types of nanocarriers

1.8.1. Lipid-based nanocarriers

Lipid-based nanocarriers are composed of lipids, like phospholipids, triglycerides and cholesterol.[68,69] Since these components are relatively safe and are derived from the natural base, they are widely being used as the carriers for anticancer drugs. The most common lipid-based nanocarriers are liposomes, solid lipid nanoparticles and lipid micelles. They offer a plethora of advantages such as high stability, ease of preparation, the capability of loading both hydrophilic and hydrophobic drugs with controlled-release mechanisms, and enhanced cellular uptake because of the natural tendency to interact with the cell membranes.[70,71] Liposomes consist of the phospholipid bilayer with the aqueous core, whereas lipid micelles are monolayered, which are formed by self-assembly in the aqueous media when the lipid concentration exceeds their critical micellar concentrations (CMCs).[72] The success of liposome-based formulation is already reflected by Doxil, the first formulation to be approved for clinical application. It consists of the pegylated lipids to escape the reticulo-endothelial system leading to efficient accumulation in tumors and cholesterol to enhance the liposome stability in the physiological environment. Solid lipid nanoparticles, on the other hand, have a lipophilic core and are unique since they remain solid at room and body temperatures.[73]

1.8.2. Inorganic nanocarriers

The most commonly used inorganic nanocarriers for cancer therapy include gold nanoparticles, magnetic and mesoporous silica nanoparticles. Usually, they are composed of the core and shell, which are usually different materials from each other.[74] These nanocarriers are in the limelight nowadays because of their various advantages. These include large surface-to-volume ratios, possibilities of surface modification with different moieties to enhance tumor targeting and unique intracellular properties that ease cellular imaging processes.[75,76] In addition to the delivery of anticancer drugs, inorganic nanocarriers are now being studied for gene delivery by either forming the complex between positively charged particles with negatively charged genetic material or by conjugating the genetic material to nanocarriers with a linker.[77]

1.8.2.1. Gold nanoparticles (AuNPs)

Gold nanoparticles (AuNPs) offer various advantages like biocompatibility, easy synthesis with a wide range of sizes, and the possibility of surface functionalization for cancer targeting.[78] Based on the shape, size and physicochemical properties, AuNPs can be further classified into gold nanorods, nanoshells and nanocages.[79] AuNPs are widely being studied for cancer diagnosis, in radiotherapy and for the delivery of small drug molecules, nucleic acids and proteins.[78,80,81]

1.8.2.2. Magnetic nanoparticles (MNPs)

The most common magnetic nanoparticles include superparamagnetic iron oxide nanoparticles composed of the iron oxide core coated with organic materials.[82] These nanostructures are being investigated for more than three decades for biomedical applications.[83] Particularly, in medicine, they are used for various purposes like magnetic cell separation and magnetic resonance imaging (MRI).[84] In oncology, they find the vital role for the targeted delivery of drugs which relies on the external magnetic field applied.[83] Moreover, MNPs can be used to generate heat to induce localized cell death, commonly known as magnetic hyperthermia (MH).[82,83]

1.8.2.3. Mesoporous silica nanoparticles (MSNPs)

MSNPs are widely being used in biomedical applications, including controlled drug delivery, gene delivery, treatment against infections and bone tissue regeneration.[85–88] They possess unique properties, including uniform mesopores, tunable pore size and structure, biocompatibility, and ease of surface modifications because of high silanol density.[89] The high surface area and pore

compartments provide the possibility of building the multifunctional theranostic agent. Usually, the pores in MSNPs are used to lodge drugs, genes or other contrast agents, whereas the surfaces are modified with targeting moieties.[87]

1.8.3. Carbon-based nanocarriers

Carbon-based nanocarriers are of great interest because of the various physical and chemical properties including mechanical strength, high electrical conductivity, and structural diversity.[90] The most widely studied carbon-based nanocarriers include carbon nanotubes, fullerenes and graphene quantum dots. They are particularly interesting as the delivery agents because of their ability to cross the biological barriers, irrespective of the cell type and functional groups on the surface. The other advantages include a higher surface area that allows multiple-molecule attachment, biocompatibility, and the possibility of surface modifications.[91] In cancer therapy, they are being explored to deliver various anticancer agents as well as in cancer diagnostics.[92,93]

1.8.4. Protein-mediated nanocarriers

Protein-based nanocarriers are an attractive platform for the delivery of therapeutics because of their biodegradability, safety, presence of hydrophilic and hydrophobic sites that facilitate the delivery of both hydrophilic and hydrophobic moieties.[94] Moreover, they can be prepared with ease and scaled up.[95,96] They are less opsonized by the reticuloendothelial system (RES) and possess various functional properties like foaming, gelation and emulsification.[96,97] The proteins generally used for the preparation of nanocarriers are either derived from animals (gelatin, albumin, casein) or plants (zein, soy, gliadin) or recombinant (silk, ferritin).[98]

1.9 Current status of nanocarriers in cancer

With the rapid advances in the field of nanomedicines, nanocarriers for the delivery of antitumor agents have gained tremendous attention both in cancer diagnosis and therapy. Some of the most prominent nanocarriers approved by FDA/EMA or in clinical trials are listed in Table 1. The clinically most advanced nanoparticles in cancer are mostly liposome-based (Doxil, DaunoXome, Myocet) or protein-based (Abraxane). The protein-based nanoparticles, especially those based on albumin are of particular interest because of the biocompatibility, biosafety and endogenous nature of albumin. Moreover, the clinical success of Abraxane, along with the preclinical and early

clinical trials with albumin-based nanocarriers have suggested that the delivery vehicle using albumin may result in superior efficacy in cancer, while minimizing the toxic side effects. Hence, in this doctoral thesis, the nanocarriers based on albumin will be discussed in detail to deliver chemotherapeutics and nucleic acids in cancer therapy.

Nanocarrier Type/drug	**Base composition**	**Clinical applications**	**Clinical Trials identifier/ References**
Doxil	Pegylated nano-liposomes with doxorubicin	FDA (1995) and EMA (1996) approved for ovarian cancers, HIV-associated Kaposi´s sarcoma and multiple myeloma	[99]
Magnablate I	Magnetic responsive iron nanoparticles	Phase 0 clinical trials for prostate cancer	NCT02033447
NANOM	Iron oxide shells in gold nanoparticles	Phase I clinical trial for stem cell therapy	NCT01436123
NU-0129	Gold nanoparticles with nucleic acids on the surface	Phase 0 clinical trials for recurrent glioblastoma	NCT03020017
Quantom dots	Veldoreotide coated CdS/ZnS core	Phase I clinical trial for suppression and bio imaging of breast cancers	NCT04138342
Abraxane	Paclitaxel loaded albumin nanoparticles	FDA (2005) and EMA (2008) approved for non-small cell lung cancer, metastatic breast cancer and pancreatic cancer	[100]

HSA-MTX	Methotrexate loaded HSA nanoparticles	Phase II clinical trial for advanced solid tumors or lymphomas	NCT01163071
Abi-008, Nab-docetaxel	Docetaxel loaded HSA nanoparticles	Phase I/II clinical trials for hormone-refractory prostate cancer	NCT00477529

Table 1. List of nanoparticles for cancer approved by FDA/EMA and those undergoing clinical trials.

1.10. Albumin

The term albumin is derived from a Latin word, ¨albumen¨, which means the egg white surrounding the yolk.[101] Albumin has an overall negatively charged surface, which makes it highly water-soluble.[26] Interestingly, albumin transcytosis is mediated by various receptors like GP60, also known as albondin, SPARC, also known as osteonectin, GP18 and GP30. GP18 and GP30 receptors are mostly responsible for the lysosomal degradation of deleterious albumin since these receptors have an affinity to the modified albumin like oxidized or glycated ones.[27,102] The unique properties of albumin, including long half-life, the ability of cellular receptor-mediated transcytosis and surface properties aiding in the conjugation of other moieties (oligonucleotides, antibodies, polymers, drugs) as shown in Figure 6 make it a suitable candidate for the preparation of nanocarriers. In this sense, the most commonly used albumins include ovalbumin, bovine serum albumin (BSA) and human serum albumin (HSA).[96]

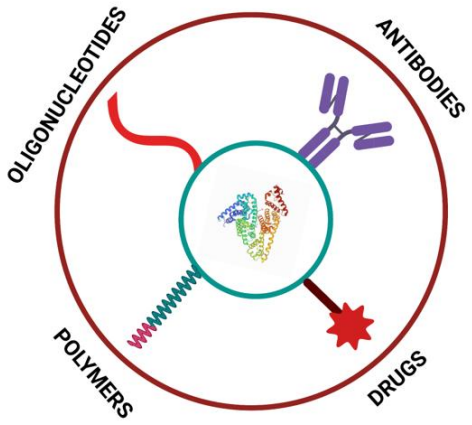

Figure 6. Various moieties for the surface modification of albumin that provides specificity and improved internalization to the cancer sites.

1.10.1. Ovalbumin

Ovalbumin is a major protein found in the egg white (60-65% content) with a molecular mass of 45000 Da and 385 amino acids.[96,103] It contains four free sulfhydryl groups and six cysteines with a disulphide bond between Cys74 and Cys121.[103] Compared to other proteins, it is easily available and has the lowest cost ($40-$60 per kg).[96,103] It possesses various properties like stabilization of emulsions, ability to form gel networks, pH- and temperature-sensitive properties.[104] Hence, it is used for the controlled delivery of drugs, which can be controlled by the regulation of the structure-forming conditions.[105]

1.10.2. Bovine serum albumin (BSA)

Bovine serum albumin (BSA) is a globular protein derived from the serum albumin of cow. It consists of 583 amino acid residues, has a molecular weight of around 69 kDa and an isoelectric point of 4.7 in water at 25 ℃. It is stabilized by 35 cysteine residues resulting in 17 disulfide bonds[106]. The secondary structure of BSA consists of α-helix and β-sheets, whereas the tertiary structure contains three homologous domains, namely, domains I, II and III. In addition, it consists of two tryptophan residues in domain I and domain II which are responsible for the intrinsic fluorescence[107]. BSA plays a vital role in the maintenance of blood pH and the lipid oxidation process. BSA is most widely accepted because of its low cost, abundance, ligand binding properties for specific targeting and ease of purification.[96]

1.10.3. Human serum albumin (HSA)

HSA, with a molecular weight of around 67 kDa, is the most abundant protein in human blood, which is synthesized in the liver and has a circulation half-life of approximately 19 days.[27] It consists of 585 amino acid residues and has various ligand binding sites, namely sudlow´s site I, which mainly binds the dicarboxylic acids and bulky heterocyclic molecules and, sudlow´s site II (indole-benzodiazepine site), which has an affinity towards the aromatic carboxylic acids.[108] The high stability of albumin is attributed to the disulfide bonds formed internally by 34 cysteine residues.[109] In addition, it has one free cysteine residue on the outer surface, responsible for the conjugation of ligands.[27,109] In comparison to BSA, HSA is more expensive, however, it is required to avoid any immunological response in humans.[96]

1.11. Albumin in cancer therapy

Albumin is being investigated extensively in cancer therapy due to its excellent properties as a selective carrier in this type of disease. This is due to many factors that lead to a preferable accumulation of the albumin structures in the tumor. For instance, the high albumin concentration in the blood (40 mg/mL) compared to the interstitial concentration of 14 mg/mL aids in diffusional transport of albumin to tumour sites.[110,111] In addition, albumin is preferentially internalized as the source of amino acids to cope with the enhanced cellular growth by the cancer cells expressing oncogenic Ras, whose activation is associated with cancer.[26] This property can be utilized to deliver the cargo encapsulated in albumin to cancer cells. Moreover, there are albumin-binding proteins, namely gp60 and SPARC, overexpressed in the cancer cells, which provide specificity to targeting the tumour sites.[112] The protein Cav-1 responsible for the formation of caveolae is upregulated in cancer cells, and since endocytosis of albumin is mainly mediated through caveolae, the accumulation of albumin in cancer sites is further enhanced.[26,113] For these reasons, albumin is being used in pharmaceutical applications as a biocompatible and biodegradable carrier for the delivery of anti-cancer agents, such as chemotherapeutics, biologics and immunomodulatory drugs.

1.12. Albumin nanocarriers for drug delivery in cancer

In this regard, the success of albumin nanocarriers in drug delivery is reflected by the FDA and EMA approved formulation, Abraxane, consisting of the chemotherapeutic paclitaxel, employed

for metastatic breast cancer. Inspired by the success of Abraxane, various studies are being conducted to enhance the efficacy of albumin-based nanocarriers either by incorporating different drugs or imaging agents in the same formulations. These nanocarriers have shown promising results in preclinical and clinical trials, improving the biodistribution, pharmacokinetic profiles, specific targeting and circulation half-life of the administered drug.[26]

1.13. Albumin nanocarrier for gene therapy in cancer

Considering the excellent properties of albumin as a nanocarrier, and its success in the delivery of chemotherapeutics, it has also been evaluated as a suitable carrier for gene delivery. In this sense, several studies are ongoing to assess the potential use of this approach to deliver different nucleic acids to the tumours for cancer gene therapy. Many reports have demonstrated the potential of albumin nanocarriers in the protection of encapsulated genome from degradation in the bloodstream and delivery to the target sites.[114,115] Moreover, various intrinsic properties of albumin, including good biocompatibility, low immunogenicity and entirely natural origin, make it a suitable choice.

1.14. Types of albumin nanocarriers

The most studied albumin-based delivery systems in cancer therapy are nanoparticles, nanoconjugates, and polyplexes, which are represented below (Figure 7).

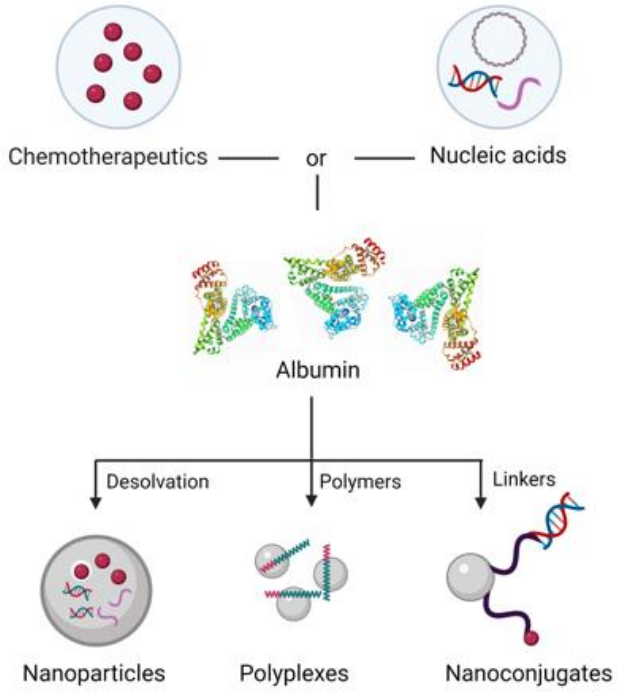

Figure 7. Schematic illustration of various albumin-based nanocarriers for the delivery of chemotherapeutics and nucleic acids.

1.14.1. Nanoparticles

One of the most widely used methods of utilizing albumins (BSA and HSA) as a carrier in cancer therapy is by encapsulation of the desired cargo into albumin-based nanoparticles.[116] These structures can be prepared by various techniques, including desolvation, thermal gelation, emulsification, nano spray drying, and self-assembly. Among all those methods, desolvation is the most commonly practiced method using ethanol as a desolvating agent and glutaraldehyde as a cross-linker.[117–119] The albumin nanoparticles protect the integrity of encapsulated cargo, enhances the bioavailability and prevent their enzymatic degradation. They enter the cells via an energy-dependent mechanism, primarily through caveolae- and clathrin-mediated endocytotic pathways.[117] Albumin nanoparticles have been employed to deliver chemotherapeutics and nucleic acids, such as plasmids, oligonucleotides and siRNAs.

1.14.2. Polyplexes

Another type of nanostructures based on albumin employed in the delivery of nucleic acids are polyplexes. These structures contain positively charged polymers that interact with the

negatively charged nucleic acids, inducing their condensation into smaller structures. The formation of this complex protects the nucleic acids against degradation by nucleases and also increases their internalization, since the positive charges present in the surface of the nanoparticle interact with the negatively charged cell membranes.[120,121] Despite the excellent properties reported for the transfection of nucleic acids, they present some toxicity, which has motivated the search for complementary transfection systems or additives to mitigate this drawback. In this regard, several studies have reported that albumin can enhance the transfection efficiency of polyplexes and improve cell viability.[114,115]

For instance, in a study conducted by Syga and co-workers, the use of albumin in a PEI-pDNA polyplex accelerated and enhanced the transfection in HeLa cells.[114] They prepared two types of polyplexes, Type 1, where BSA was placed between the plasmid pGFP and PEI, and Type 2, where albumin was added at the end, on the surface of previously formed polyplexes (PEI + pGFP). The experiments revealed that transfection efficiency was better with Type 1 polyplexes as the release of plasmid was easier from the loosely formed polyplexes than the Type 2 polyplexes with strong interaction between PEI and plasmid. Similarly, in a study conducted by Nicoli and co-workers, enhancement in cellular uptake was observed in metastatic breast cancer epithelial cells when HSA was incorporated in branched polyethylenimine (bPEI)-siRNA polyplexes.[122]

1.14.3. Nanoconjugates

Albumin nanoconjugates are obtained by the interaction of albumin with other moieties like polymers, nucleic acids, or metals. The interaction may be either non-covalent (hydrophobic and electrostatic) or covalent (thiol-maleimide coupling, Michael addition reaction and carbodiimide coupling reactions).[28] Nanoconjugates are smaller (~10 nm) than the typical nanoparticles (~100 nm) and can overcome the limitations associated with the nanoparticles, like limited biodistribution and toxicity.[123] However, these small conjugates are rapidly metabolized, excreted in vivo, and less effective in exploiting the EPR effect to reach the tumor sites than conventional nanoparticles.[124]

The nanoconjugates can be employed both for the delivery of chemotherapeutics and nucleic acids in cancer therapy. For instance, Chung and co-workers conjugated doxorubicin to albumin

by maleimide functionalization, which resulted in the improvement of circulation half-life of the drug from around 30 minutes to 19 hours.[125] Similar improvements were observed in-vivo when methotrexate was conjugated to human serum albumin.[126] In a study conducted by Carver and co-workers, HSA nanoconjugates with RGD-623 oligonucleotides having a size of about 13 nm were prepared.[127] Interestingly, the resulting HSA-RGD-623 conjugate could penetrate into a 3D tumor spheroid, whereas the conventional nanoparticles could deliver their payload only on the exterior cells of the spheroid, limiting the induction of splice correction of both GFP654 and Luc705 reporter genes. Similarly, in a study by Sarett and co-workers, serum albumin was used as a carrier in vivo for siRNAs modified with a diacyl lipid moiety (siRNA-L_2), which enhanced the pharmacokinetic properties of siRNA. This nanoconjugate showed 19-fold more tumor accumulation and 46-fold cellular uptake than the commercial siRNA nanocarrier jetPEI, in a mouse orthotopic model of human triple-negative breast cancer.[128] Hence, a nanocarrier system that can combine the advantages of nanoconjugates, with the properties of conventional nanoparticles could be of great interest for gene therapy in cancer.

1.15. Albumin as a coating agent

Besides its use as nanocarrier, albumin can be used as a coating agent for a variety of nanostructures, thus the advantages mentioned before on the use of albumin can be implemented in other nanostructures.[129–131] In a study conducted by Xu and co-workers, a chitosan complex with siRNAs to suppress tumor cell proliferation, was coated with pH-responsive detachable BSA to enhance recognition by human hepatocellular carcinoma cells.[130] In this case, the mRNA silencing obtained by the chitosan NPs was improved from 46.9% to 61.8% by introducing a BSA coating.

Albumin has been used as a coating agent in various lipid-based nanocarriers, to minimize their interaction with serum proteins and improve their delivery to the target sites.[131,132] For instance, HSA was used to coat lipid nanoparticles loaded with siRNA targeted against GFP(HSA-LNPs-siRNA) and their activity was evaluated in breast cancer cells and the corresponding xenograft mouse model.[131] In the cell experiments, the nanoparticles containing HSA significantly reduced the GFP fluorescence, compared to uncoated lipid nanoparticles. This result was also obtained in the animal model, where a 37% reduction in the GFP expression was

achieved after systemic administration of the HSA-coated nanoparticles. In another study, HSA was employed to coat lipid nanoparticles loaded with an antisense oligonucleotide against Bcl-2, which were evaluated in KB human oral carcinoma cells.[132] Interestingly, the authors reported that the efficiency of the Bcl-2 down-regulation depended on the molar ratio of HSA employed. The optimum down-regulation was observed with HSA to liposome ratio of 3:100 after which the increment in HSA decreased the efficiency.

1.16. Albumin nanocarriers for Immunotherapy

Cancer immunotherapy aims to exploit the patients' own immune system to treat cancer. For instance, some cancer immunotherapy approaches include immune checkpoint blockade, cancer vaccines, adoptive cell transfer therapy and oncolytic virotherapy.[29] In this regard, a variety of nucleic acids (e.g., siRNA, shRNA, ASOs, plasmids, aptamers, CRISPR gene-editing tools) are employed in cancer vaccination, gene regulation and adoptive T-cell therapy.[133] In this context, albumin-based nanocarriers are being investigated in a variety of cancers. For instance, Cheng and co-workers developed HSA NPs complexed with stearyl PEI (*st*PEI), which was non-covalently bound to plasmid (CRISPR/Cas9) and a siRNA that silenced the expression of programmed cell death ligand-1 (PD-L1) for cancer immunotherapy.[134] This combined approach produced a synergistic effect where the PD-L1 expression was inhibited by 21.2%.

In summary, immunotherapy against cancer mediated by nucleic acids has enormous potential, as highlighted by the recent developments, such as chimeric antigen receptors (CARs), to treat leukemia (e.g., Kymriah[135]), or CRISPR/Cas9 approaches employed to enhance T-cell mediated gene therapy[136]. However, such systems can be further improved by nanocarriers, such as those based on albumin.

1.17. Current challenges with albumin-based nanocarriers and possible solutions

Despite the plethora of advantages imparted by albumin-based nanocarriers, there are still some challenges that need attention. The most common method for the preparation of albumin-based nanoparticles include desolvation using glutaraldehyde as a cross-linker. However, using glutaraldehyde imparts some challenges including toxicity, interaction with the encapsulated drug, and presence of residual aldehyde, which limit the *in-vivo* applications. The alternative cross-linkers with better safety profile and release properties are hence of utter importance.

Moreover, most of the problems with albumin nanocarriers arise due to the negative charge at physiological conditions that prevent the binding of anionic nucleic acids.[137,138] Also, other parameters such as the circulation time, specific site targeting, internalization and release of encapsulated cargo, might require some improvement to ease their clinical translation.[139] In this regard, the modification of albumin-based nanostructures with selected moieties seems to be the most suitable approach.[140] The availability of functional groups such as carboxyl (e.g., asparaginic, glutaminic acid), amino (e.g., lysine) and hydroxyl groups (e.g., tyrosine) on albumin ease the surface modification of the nanostructures. The most widely used moieties for surface modification include polymers (e.g., PEG, PEI) and targeting agents (e.g., aptamers, antibodies).

Moreover, the production of albumin nanocarriers, or proteins in general, face problems related to the batch-to-batch reproducibility, which is critical issue during the scale-up processes in the industrial production.[141] A possible solution for it could be the implementation of approaches based on recombinant protein technologies. However, the interaction of these nanocarriers with the immune system should be first evaluated since it may affect the overall safety profile of the particles. In addition, the immunogenicity of exogenous albumin should be properly studied though albumin is predicted to be well tolerated in vivo.[142]

1.18. Aim and Objectives

This thesis aims to develop nanocarrier systems based on albumin for the delivery of anticancer drugs (hydrophilic and hydrophobic drugs, like doxorubicin, SN38 and volasertib) and nucleic acids to cancer cells. The nanocarriers described herein have been obtained either by desolvation method using ethanol as a desolvating agent, or by the formation of polyplexes with polymers (PEI, PEG). Various polymers were prepared and characterized, and further used in albumin nanocarriers. The prepared nanocarrier systems were characterized for size, surface charge, stability, and loading efficiency. The in-vitro cytotoxicity studies were conducted in various cells lines including, breast, cervical, and pancreatic cancer cell lines.

In this doctoral thesis, the following two objectives will be discussed in detail:

1. Development of albumin-based nanoparticles for the delivery of anticancer drugs for breast cancer and cervical cancer.

- Due to the aforementioned drawbacks of the most commonly used cross-linker, glutaraldehyde, the first objective was to select the optimum cross-linker with better release and safety profile for the preparation of albumin-based nanoparticles. The cross-linkers based on disulphide, amide bonds or on electrostatic interaction were prepared and the nanoparticles prepared with those cross-linkers were characterized for physicochemical properties and their activities in cells.
- Secondly, the feasibility of the most optimum system was tested by encapsulating various hydrophilic (Doxorubicin) as well as hydrophobic (SN38 and Volasertib) drugs. The prepared nanoparticles were characterized, and their efficiency in vitro were evaluated in various cell lines.
- The internalization of nanoparticles was then conducted in both 2D monolayer and 3D cancer spheroids. The 2D monolayer was selected because of the simplicity, good reproducibility, and possibility of growing wide range of cells. The internalization and activity of the nanoparticles was further tested in 3D cancer models because of their abilities to mimic the in vivo tumors and comparable growth kinetics to the solid tumors.

- Furthermore, the effects of using various albumin-based nanoparticles in the murine and human macrophages were evaluated since the use of new cross-linkers and exogenous albumin can trigger or suppress the immune system.

2. Development of albumin-based polyplexes for the delivery of plasmid.

- The polymers based on PEI and PEG were first designed and BSA was conjugated to the polymer to improve the cytotoxicity profile. The properties of this system were optimized using a GFP plasmid.
- The prepared nanostructures were characterized for physicochemical properties, including size, surface charge, and encapsulation efficiency.
- The system was then used to deliver a CRISPR/Cas plasmid designed to target the oncogenic mutated gene P53, leading to a decrease in cancer cell viability.

References

1. Roy, P.S.; Saikia, B.J. Cancer and cure: A critical analysis. *Indian J Cancer* **2016**, *53*, 441–442.

2. Hofmarcher, T.; Bradvik, G.; Svedman, C.; Lindgren, P.; Jonsson, B.; Wilking, N. Comparator Report on Cancer in Europe 2019 - Disease Burden, Costs and Access to Medicines, IHE, Lund, Sweden 2019.

3. Cavenee, Webster K., R.L.W. The Genetic Basis of Cancer. *Sci. Am.* **1995**, *272*, 72–79.

4. Trichopoulos, D.; Li, F.P.; Hunter, D.J. What causes cancer? *Sci. Am.* **1996**, *275*, 80–87, doi:10.1038/scientificamerican0996-80.

5. Anand, P.; Kunnumakara, A.B.; Sundaram, C.; Harikumar, K.B.; Tharakan, S.T.; Lai, O.S.; Sung, B.; Aggarwal, B.B. Cancer is a preventable disease that requires major lifestyle changes. *Pharm. Res.* **2008**, *25*, 2097–2116, doi:10.1007/s11095-008-9661-9.

6. Hanahan, D.; Weinberg, R.A. The Hallmarks of Cancer. *Cell* **2000**, *100*, 57–70.

7. Hanahan, D.; Weinberg, R.A. Hallmarks of cancer: The next generation. *Cell* **2011**, *144*, 646–674, doi:10.1016/j.cell.2011.02.013.

8. Price, P.; Sikora, K. Cancer Care: Today and Tomorrow. In *Treatment of Cancer*; CRC Press, 2021; pp. viii–xxiii.

9. OECD *Addressing Challenges in Access to Oncology Medicines*; 2020;

10. Statello, L.; Guo, C.J.; Chen, L.L.; Huarte, M. Gene regulation by long non-coding RNAs and its biological functions. *Nat. Rev. Mol. Cell Biol.* **2021**, *22*, 96–118, doi:10.1038/s41580-020-00315-9.

11. Ou, X.; Ma, Q.; Yin, W.; Ma, X.; He, Z. CRISPR/Cas9 Gene-Editing in Cancer Immunotherapy: Promoting the Present Revolution in Cancer Therapy and Exploring More. *Front. Cell Dev. Biol.* **2021**, *9*, 1–12, doi:10.3389/fcell.2021.674467.

12. Fitzmaurice, C.; Allen, C.; Barber, R.M.; Barregard, L.; Bhutta, Z.A.; Brenner, H.; Dicker, D.J.; Chimed-Orchir, O.; Dandona, R.; Dandona, L.; et al. Global, regional, and national cancer incidence, mortality, years of life lost, years lived with disability, and disability-adjusted life-years for 32 cancer groups, 1990 to 2015: A Systematic Analysis for the Global Burden of Disease Study Global Burden . *JAMA Oncol.* **2017**, *3*, 524–548, doi:10.1001/jamaoncol.2016.5688.

13. Siegel, R.L.; Miller, K.D.; Ahmedin Jemal, D. Cancer statistics , 2020. *CA Cancer J CLin* **2020**, *70*, 7–30, doi:10.3322/caac.21590.

14. Islami, F.; Miller, K.D.; Siegel, R.L.; Zheng, Z.; Zhao, J.; Han, X.; Ma, J.; Jemal, A.; Yabroff, K.R. National and State Estimates of Lost Earnings from Cancer Deaths in the United States. *JAMA Oncol.* **2019**, *5*, 3–10, doi:10.1001/jamaoncol.2019.1460.

15. Roy, P.; Saikia, B. Cancer and cure: A critical analysis. *Indian J Cancer* **2016**, *53*, 441–442.

16. National Cancer Institute *Cancer Statistics*; **2020**; NCI Press Release.

17. Milenic, D.E.; Brady, E.D.; Brechbiel, M.W. Antibody-targeted radiation cancer therapy. *Nat. Rev. Drug Discov.* **2004**, *3*, 488–498, doi:10.1038/nrd1413.

18. Cabanas, R.M. An approach for the treatment of penile carcinoma. *Cancer* **1977**, *39*, 456–466, doi:10.1002/1097-0142(197702)39:2<456::AID-CNCR2820390214>3.0.CO;2-I.

19. Cancer Quest *Cancer Treatments*; **2021**; Emory Winship Cancer Institute.

20. Tepper, J.N.J.A.J.D.M.K.J. Surgical interventions in cancer. In *Abeloff's Clinical Oncology*; Philadelphia, Pa.: Churchill Livingstone Elsevier, 2014.

21. Nair, C.K.K.; Parida, D.K.; Nomura, T. Radioprotectors in Radiotherapy. *J. Radiat. Res.* **2001**, *42*, 21–37, doi:10.1269/jrr.42.21.

22. Citrin, D.E. Recent developments in radiotherapy. *N. Engl. J. Med.* **2017**, *377*, 1065–1075, doi:10.1056/nejmra1608986.

23. Van Herk, M. Errors and Margins in Radiotherapy. *Semin. Radiat. Oncol.* **2004**, *14*, 52–64, doi:10.1053/j.semradonc.2003.10.003.

24. Kwatra, D.; Venugopal, A.; Anant, S. Nanoparticles in radiation therapy: A summary of various approaches to enhance radiosensitization in cancer. *Transl. Cancer Res.* **2013**, *2*, 330–342, doi:10.3978/j.issn.2218-676X.2013.08.06.

25. Desai, N. Challenges in development of nanoparticle-based therapeutics. *AAPS J.* **2012**, *14*, 282–295, doi:10.1208/s12248-012-9339-4.

26. Hoogenboezem, E.N.; Duvall, C.L. Harnessing albumin as a carrier for cancer therapies. *Adv. Drug Deliv. Rev.* **2018**, *130*, 73–89, doi:10.1016/j.addr.2018.07.011.

27. Larsen, M.T.; Kuhlmann, M.; Hvam, M.L.; Howard, K.A. Albumin-based drug delivery : harnessing nature to cure disease. *Mol. Cell. Ther.* **2016**, *4*, 1–12, doi:10.1186/s40591-016-0048-8.

28. Kudarha, R.R.; Sawant, K.K. Albumin based versatile multifunctional nanocarriers for cancer therapy: Fabrication, surface modification, multimodal therapeutics and imaging approaches. *Mater. Sci. Eng. C* **2017**, *81*, 607–626, doi:10.1016/j.msec.2017.08.004.

29. Kirkwood, J.M.; Butterfield, L.H.; Tarhini, A.A.; Zarour, H.; Kalinski, P.; Ferrone, S. Immunotherapy of cancer in 2012. *CA CANCER J CLIN* **2012**, *62*, 309–335, doi:10.3322/caac.20132.

30. Franiak-Pietryga, I. Nanoparticles could Improve the Efficiency of CAR-T Immunotherapy for Cancer OPEN ACCESS. *Am. J. Leuk. Res.* **2018**, *2*, 1–2.

31. Laheru, D.; Yeo, C.; Biedrzycki, B.; Solt, S.; Lutz, E.; Onners, B.; Tartakovsky, I.; Herman, J.; Hruban, R.; Piantadosi, S.; et al. A safety and efficacy trial of lethally irradiated allogeneic pancreatic tumor cells transfected with the GM-CSF gene in combination with adjuvant chemoradiotherapy for the treatment of adenocarcinoma of the pancreas. *J. Clin. Oncol.*

2007, *25*.

32. Hargadon, K.M.; Johnson, C.E.; Williams, C.J. Immune checkpoint blockade therapy for cancer: An overview of FDA-approved immune checkpoint inhibitors. *Int. Immunopharmacol.* **2018**, *62*, 29–39, doi:10.1016/j.intimp.2018.06.001.

33. Hager, S.; Fittler, F.J.; Wagner, E.; Bros, M. Nucleic Acid-Based Approaches for Tumor Therapy. *Cells* **2020**, *9*, 1–53, doi:10.3390/cells9092061.

34. Shen, T.; Zhang, Y.; Zhou, S.; Lin, S.; Zhang, X.; Zhu, G. Nucleic Acid Immunotherapeutics for Cancer. *ACS Appl Bio Mater.* **2021**, *3*, 2838–2849, doi:10.1021/acsabm.0c00101.Nucleic.

35. Bassal, M.; Mertens, A.C.; Taylor, L.; Neglia, J.P.; Greffe, B.S.; Hammond, S.; Ronckers, C.M.; Friedman, D.L.; Stovall, M.; Yasui, Y.Y.; et al. Risk of selected subsequent carcinomas in survivors of childhood cancer: A report from the childhood cancer survivor study. *J. Clin. Oncol.* **2006**, *24*, 476–483, doi:10.1200/JCO.2005.02.7235.

36. Sharifi, N.; Gulley, J.L.; Dahut, W.L. Androgen deprivation therapy for prostate cancer. *JAMA* **2005**, *294*, 238–244, doi:10.1007/978-3-319-99286-0_1.

37. Patil, P.M.; Chaudhari, P.D.; Sahu, M.; Duragkar, N.J. Review article on gene therapy. *Int. J. Genet.* **2012**, *4*, 74–79.

38. Hannon, G.J. RNA interference. *Nature* **2002**, *418*, 244–251.

39. Belete, T.M. The current status of gene therapy for the treatment of cancer. *Biol. Targets Ther.* **2021**, *15*, 67–77, doi:10.2147/BTT.S302095.

40. Sung, Y.K.; Kim, S.W. Recent advances in the development of gene delivery systems. *Biomater. Res.* **2019**, *23*, 1–7, doi:10.1186/s40824-019-0156-z.

41. Ramamoorth, M.; Narvekar, A. Non viral vectors in gene therapy - An overview. *J. Clin. Diagnostic Res.* **2015**, *9*, GE01–GE06, doi:10.7860/JCDR/2015/10443.5394.

42. Cagan, R.; Meyer, P. Rethinking cancer: Current challenges and opportunities in cancer research. *DMM Dis. Model. Mech.* **2017**, *10*, 349–352, doi:10.1242/dmm.030007.

43. Brannon-Peppas, L.; Blanchette, J.O. Nanoparticle and targeted systems for cancer therapy. *Adv. Drug Deliv. Rev.* **2004**, *56*, 1649–1659, doi:10.1016/j.addr.2004.02.014.

44. Bawa, R.; Bawa, S.R.; Maebius, S.B.; Flynn, T.; Wei, C. Protecting new ideas and inventions in nanomedicine with patents. *Nanomedicine Nanotechnology, Biol. Med.* **2005**, *1*, 150–158, doi:10.1016/j.nano.2005.03.009.

45. Hulla, J.E.; Sahu, S.C.; Hayes, A.W. Nanotechnology: History and future. *Hum. Exp. Toxicol.* **2015**, *34*, 1318–1321, doi:10.1177/0960327115603588.

46. Emerich, D.F.; Thanos, C.G. Nanotechnology and Medicine. *Expert Opin. Biol. Ther* **2003**, *3*, 655–663, doi:10.1148/radiol.2302031698.

47. Mobasser, S.; Firoozi, A.A. Review of Nanotechnology Applications in Science and Engineering. *J. Civ. Eng. Urban.* **2016**, *6*, 84–93.

48. Moghimi, S.M.; Hunter, A.C.; Murray, J.C. Nanomedicine: current status and future prospects. *FASEB J.* **2005**, *19*, 311–330, doi:10.1096/fj.04-2747rev.

49. Peer, D.; Karp, J.M.; Hong, S.; Farokhzad, O.C.; Margalit, R.; Langer, R. Nanocarriers as an emerging platform for cancer therapy. *Nat. Nanotechnol.* **2007**, *2*, 751–760, doi:10.1038/nnano.2007.387.

50. Poole, C.P.J.; Owens, F.J. *Introduction to Nanotechnology*; John Wiley & Sons, 2003; ISBN 0471079359, 9780471079354.

51. Sciau, P. Nanoparticles in Ancient Materials: The Metallic Lustre Decorations of Medieval Ceramics. In *The Delivery of Nanoparticles*; Hashim, A.A., Ed.; InTech, 2012; pp. 525–540.

52. Reibold, M.; Paufler, P.; Levin, A.A.; Kochmann, W.; Pätzke, N.; Meyer, D.C. Carbon nanotubes in an ancient Damascus sabre. *Nature* **2006**, *444*, 286.

53. Elsabahy, M.; Nazarali, A.; Foldvari, M. Non-viral nucleic acid delivery : key challenges and future directions non-viral nucleic acid delivery : key challenges and future directions. *Curr. Drug Deliv.* **2011**, *8*, 235–244, doi:10.2174/156720111795256174.

54. Din, F. ud; W; Aman, A.; Ullah, I.; Qureshi, O.S.; Mustapha, O.; Shafique, S.; Zeb, A. Effective use of nanocarriers as drug delivery systems for the treatment of selected tumors. *Int. J. Nanomedicine* **2017**, *12*, 7291–7309.

55. Prabhakar, U.; Blakey, D.C.; Maeda, H. Challenges and key considerations of the enhanced permeability and retention effect (EPR) for nanomedicine drug delivery in oncology. *Cancer Res.* **2013**, *73*, 2412–2417, doi:10.1158/0008-5472.CAN-12-4561.

56. Liu, Y.; Tan, J.; Thomas, A.; Ou-Yang, D.; Muzykantov, V.R. The shape of things to come: Importance of design in nanotechnology for drug delivery. *Ther. Deliv.* **2012**, *3*, 181–194, doi:10.4155/tde.11.156.

57. Haley, B.; Frenkel, E. Nanoparticles for drug delivery in cancer treatment. *Urol. Oncol. Semin. Orig. Investig.* **2008**, *26*, 57–64, doi:10.1016/j.urolonc.2007.03.015.

58. Torchilin, V. Tumor delivery of macromolecular drugs based on the EPR effect. *Adv. Drug Deliv. Rev.* **2011**, *63*, 131–135, doi:10.1016/j.addr.2010.03.011.

59. Packirisamy, G.; Kumar, U.; Matai, I.; Bhushan, B.; Malwal, D.; Sachdev, A.; Dubey, P. *Cancer nanotheranostics ch. 5*; Springer, Singapore: Singapore, 2015; ISBN 9789812874351.

60. Dai, L.; Liu, J.; Luo, Z.; Li, M.; Cai, K. Tumor therapy: Targeted drug delivery systems. *J. Mater. Chem. B* **2016**, *4*, 6758–6772, doi:10.1039/c6tb01743f.

61. Tannock, I.F.; Rotin, D. Acid pH in tumors and its potential for therpeutic exploitation. *Cancer Res.* **1989**, *49*, 4373–4384, doi:2545340.

62. Kato, Y.; Ozawa, S.; Miyamoto, C.; Maehata, Y.; Suzuki, A.; Maeda, T.; Baba, Y. Acidic extracellular microenvironment and cancer. *Cancer Cell Int.* **2013**, *13*, 1–8, doi:10.1186/1475-2867-13-89.

63. Jerzy, G.; Roman, R.; Jerzy, R. Glutathione. *Ann. Re. Biochem* **1983**, *52*, 711–760.

64. Chen, D.; Bobko, A.A.; Gross, A.C.; Evans, R.; Marsh, C.B.; Khramtsov, V. V.; Eubank, T.D.; Friedman, A. Involvement of tumor macrophage HIFs in chemotherapy effectiveness: Mathematical modeling of oxygen, pH, and glutathione. *PLoS One* **2014**, *9*, e107511, doi:10.1371/journal.pone.0107511.

65. Chen, W.; Meng, F.; Cheng, R.; Zhong, Z. pH-Sensitive degradable polymersomes for triggered release of anticancer drugs: A comparative study with micelles. *J. Control. Release* **2010**, *142*, 40–46, doi:10.1016/j.jconrel.2009.09.023.

66. Prajapati, R.; Gontsarik, M.; Yaghmur, A.; Salentinig, S. pH-responsive nano-self-assemblies of the anticancer drug 2-Hydroxyoleic acid. *Langmuir* **2019**, *35*, 7954–7961, doi:10.1021/acs.langmuir.9b00838.

67. Wang, X.; Cai, X.; Hu, J.; Shao, N.; Wang, F.; Zhang, Q.; Xiao, J.; Cheng, Y. Glutathione-triggered “off-On” release of anticancer drugs from dendrimer-encapsulated gold nanoparticles. *J. Am. Chem. Soc.* **2013**, *135*, 9805–9810, doi:10.1021/ja402903h.

68. Rawat, M.; Singh, D. Lipid Carriers : A Versatile Delivery Vehicle for Proteins and Peptides. *Pharm. Soc. Japan* **2008**, *128*, 269–280, doi:10.1248/yakushi.128.269.

69. Bee, S.; Banerjee, A.; Önyüksel, H. Improvement of drug safety by the use of lipid-based nanocarriers. *J. Control. Release* **2012**, *163*, 34–45, doi:10.1016/j.jconrel.2012.06.002.

70. Niu, Z.; Conejos-sánchez, I.; Grif, B.T.; Driscoll, C.M.O.; Alonso, M.J. Lipid-based nanocarriers for oral peptide delivery. *Adv. Drug Deliv. Rev.* **2016**, *106*, 337–354, doi:10.1016/j.addr.2016.04.001.

71. Bee, S.; Banerjee, A.; Önyüksel, H. Improvement of drug safety by the use of lipid-based nanocarriers. *J. Control. Release* **2012**, *163*, 34–45, doi:10.1016/j.jconrel.2012.06.002.

72. Mallick, S.; Choi, J.S. Liposomes : Versatile and Biocompatible Nanovesicles for Efficient Biomolecules Delivery. *J. Nanosci. Nanotechnol.* **2014**, *14*, 755–765, doi:10.1166/jnn.2014.9080.

73. Gohla, S.; Ma, K.; Mu, R.H. Solid lipid nanoparticles (SLN) for controlled drug delivery - a review of the state of the art. *Eur. J. Pharm. Biopharm.* **2000**, *50*, 161–177.

74. Chaudhuri, R.G.; Paria, S. Core / Shell Nanoparticles : Classes , Properties , Synthesis Mechanisms , Characterization , and Applications. *Chem. Rev.* **2012**, *112*, 2373–2433.

75. Ma, P.; Xiao, H.; Li, C.; Dai, Y.; Cheng, Z.; Hou, Z.; Lin, J. Inorganic nanocarriers for platinum drug delivery. *Biochem. Pharmacol.* **2015**, *18*, 554–564, doi:10.1016/j.mattod.2015.05.017.

76. Lin, G.; Mi, P.; Chu, C.; Zhang, J.; Liu, G. Inorganic Nanocarriers Overcoming Multidrug Resistance for Cancer Theranostics. **2016**, 1–14, doi:10.1002/advs.201600134.

77. Loh, X.J.; Lee, T.-C.; Doua, Q.; Deen, G.R. Utilising inorganic nanocarriers for gene delivery. *Biomater. Sci.* **2016**, *4*, 70–86, doi:10.1039/c5bm00277j.

78. Lim, Z.Z.J.; Li, J.E.J.; Ng, C.T.; Yung, L.Y.L.; Bay, B.H. Gold nanoparticles in cancer therapy. *Acta Pharmacol. Sin.* **2011**, *32*, 983–990, doi:10.1038/aps.2011.82.

79. Cai, W.; Gao, T.; Hong, H.; Sun, J. Applications of gold nanoparticles in cancer. *Nanotechnol. Sci. Appl.* **2008**, *1*, 17–32, doi:10.4018/978-1-5225-3158-6.ch035.

80. Hainfeld, J.F.; Dilmanian, F.A.; Slatkin, D.N.; Smilowitz, H.M. Radiotherapy enhancement with gold nanoparticles. *J. Pharm. Pharmacol.* **2008**, *60*, 977–985, doi:10.1211/jpp.60.8.0005.

81. Haume, K.; Rosa, S.; Grellet, S.; Śmiałek, M.A.; Butterworth, K.T.; Solov'yov, A. V.; Prise, K.M.; Golding, J.; Mason, N.J. Gold nanoparticles for cancer radiotherapy: a review. *Cancer Nanotechnol.* **2016**, *7*, doi:10.1186/s12645-016-0021-x.

82. Tietze, R.; Zaloga, J.; Unterweger, H.; Lyer, S.; Friedrich, R.P.; Janko, C.; Pöttler, M.; Dürr, S.; Alexiou, C. Magnetic nanoparticle-based drug delivery for cancer therapy. *Biochem. Biophys. Res. Commun.* **2015**, *468*, 463–470, doi:10.1016/j.bbrc.2015.08.022.

83. Goya, G.F.; Grazú, V.; Ibarra, M.R. Magnetic nanoparticles for cancer therapy. *Curr. Nanosci.* **2008**, *4*, 1–16, doi:10.1515/ntrev-2013-0011.

84. Jurgons, R.; Seliger, C.; Hilpert, A.; Trahms, L.; Odenbach, S.; Alexiou, C. Drug loaded magnetic nanoparticles for cancer therapy. *J. Phys. Condens. Matter* **2006**, *18*, S2893–S2902, doi:10.1088/0953-8984/18/38/S24.

85. Li, Z.; Barnes, J.C.; Bosoy, A.; Stoddart, J.F.; Zink, J.I. Mesoporous silica nanoparticles in biomedical applications. *Chem. Soc. Rev.* **2012**, *41*, 2590–2605, doi:10.1039/c1cs15246g.

86. Lozano, D.; Trejo, C.G.; Gómez-Barrena, E.; Manzano, M.; Doadrio, J.C.; Salinas, A.J.; Vallet-Regí, M.; García-Honduvilla, N.; Esbrit, P.; Buján, J. Osteostatin-loaded onto mesoporous ceramics improves the early phase of bone regeneration in a rabbit osteopenia model. *Acta Biomater.* **2012**, *8*, 2317–2323, doi:10.1016/j.actbio.2012.03.014.

87. Giret, S.; Wong Chi Man, M.; Carcel, C. Mesoporous-Silica-Functionalized Nanoparticles for Drug Delivery. *Chem. Eur. J.* **2015**, *21*, 13850–13865, doi:10.1002/chem.201500578.

88. Polo, L.; Gómez-Cerezo, N.; García-Fernández, A.; Aznar, E.; Vivancos, J.L.; Arcos, D.; Vallet-Regí, M.; Martínez-Máñez, R. Mesoporous Bioactive Glasses Equipped with Stimuli-Responsive Molecular Gates for Controlled Delivery of Levofloxacin against Bacteria. *Chem. - A Eur. J.* **2018**, *24*, 18944–18951, doi:10.1002/chem.201803301.

89. Wu, S.H.; Hung, Y.; Mou, C.Y. Mesoporous silica nanoparticles as nanocarriers. *Chem. Commun.* **2011**, *47*, 9972–9985, doi:10.1039/c1cc11760b.

90. Maiti, D.; Tong, X.; Mou, X.; Yang, K. Carbon-Based Nanomaterials for Biomedical Applications: A Recent Study. *Front. Pharmacol.* **2019**, *9*, 1–16, doi:10.3389/fphar.2018.01401.

91. Fabbro, C.; Ali-Boucetta, H.; Da Ros, T.; Bianco, A.; Kostarelos, K.; Prato, M. Targeting carbon nanotubes against cancer. *Chem. Commun.* **2012**, *48*, 3911–3926, doi:10.1039/c2cc17995d.

92. Ji, S. rong; Liu, C.; Zhang, B.; Yang, F.; Xu, J.; Long, J.; Jin, C.; Fu, D. liang; Ni, Q. xing; Yu, X. jun Carbon nanotubes in cancer diagnosis and therapy. *Biochim. Biophys. Acta - Rev. Cancer* **2010**, *1806*, 29–35, doi:10.1016/j.bbcan.2010.02.004.

93. Ebbesen, T.W. Carbon nanotubes. *Phys. Today* **1996**, *1*, 26–32.

94. Chattopadhyay, A. Protein-Based Multifunctional Nanocarriers for Imaging, Photothermal Therapy, and Anticancer Drug Delivery. *ACS Appl. Mater. Interfaces* **2017**, *9*, 19495–19501, doi:10.1021/acsami.6b06099.

95. Elzoghby, A.O.; El-fotoh, W.S.A.; Elgindy, N.A. Casein-based formulations as promising controlled release drug delivery systems. *J. Control. Release* **2011**, *153*, 206–216, doi:10.1016/j.jconrel.2011.02.010.

96. Elzoghby, A.O.; Samy, W.M.; Elgindy, N.A. Albumin-based nanoparticles as potential controlled release drug delivery systems. *J. Control. Release* **2012**, *157*, 168–182, doi:10.1016/j.jconrel.2011.07.031.

97. Chen, L.; Remondetto, E.; Subirade, M. Food protein-based materials as nutraceutical delivery systems. *Trends Food Sci. Technol. 17* **2006**, *17*, 272–283, doi:10.1016/j.tifs.2005.12.011.

98. Donsi, F.; Mcclements, D.J. Protein-Based Delivery Systems for the Nanoencapsulation of Food Ingredients. *ComprehensiveReviews inFoodScienceandFoodSafety* **2018**, *17*, 920–936, doi:10.1111/1541-4337.12360.

99. Barenholz, Y. Doxil® - The first FDA-approved nano-drug: Lessons learned. *J. Control. Release* **2012**, *160*, 117–134, doi:10.1016/j.jconrel.2012.03.020.

100. Stinchcombe, T.E.; Socinski, M.A.; Walko, C.M.; O'Neil, B.H.; Collichio, F.A.; Ivanova, A.; Mu, H.; Hawkins, M.J.; Goldberg, R.M.; Lindley, C.; et al. Phase I and pharmacokinetic trial of carboplatin and albumin-bound paclitaxel, ABI-007 (Abraxane®) on three treatment schedules in patients with solid tumors. *Cancer Chemother. Pharmacol.* **2007**, *60*, 759–766, doi:10.1007/s00280-007-0423-x.

101. Fanali, G.; Di Masi, A.; Trezza, V.; Marino, M.; Fasano, M.; Ascenzi, P. Human serum albumin: From bench to bedside. *Mol. Aspects Med.* **2012**, *33*, 209–290, doi:10.1016/j.mam.2011.12.002.

102. Merlot, A.M.; Kalinowski, D.S.; Richardson, D.R. Unraveling the mysteries of serum albumin — more than just a serum protein. *Front. Physiol.* **2014**, *5*, 1–7,

doi:10.3389/fphys.2014.00299.

103. Huntington, J.A.; Stein, P.E. Structure and properties of ovalbumin. *J. Chromatogr. B Biomed. Sci. Appl.* **2001**, *756*, 189–198, doi:10.1016/S0378-4347(01)00108-6.

104. Wongsasulak, S.; Patapeejumruswong, M.; Weiss, J.; Supaphol, P.; Yoovidhya, T. Electrospinning of food-grade nanofibers from cellulose acetate and egg albumen blends. *J. Food Eng.* **2010**, *98*, 370–376, doi:10.1016/j.jfoodeng.2010.01.014.

105. Wongsasulak, S.; Yoovidhya, T.; Bhumiratana, S.; Hongsprabhas, P. Physical properties of egg albumen and cassava starch composite network formed by a salt-induced gelation method. *Food Res. Int.* **2007**, *40*, 249–256, doi:10.1016/j.foodres.2006.03.011.

106. Wang, J.; Zhang, B. Bovine Serum Albumin as a Versatile Platform for Cancer Imaging and Therapy. *Curr. Med. Chem.* **2017**, *25*, 2938–2953, doi:10.2174/0929867324666170314143335.

107. Tayeh, N.; Rungassamy, T.; Albani, J.R. Fluorescence spectral resolution of tryptophan residues in bovine and human serum albumins. *J. Pharm. Biomed. Anal.* **2009**, *50*, 107–116, doi:10.1016/j.jpba.2009.03.015.

108. Krach-Hansen, U.; Chuang, V.T.G.; Otagiri, M. Practical aspects of the ligand-binding and enzymatic properties of human serum albumin. *Biol. Pharm. Bull.* **2002**, *25*, 695–704, doi:10.1248/bpb.25.695.

109. Quinlan, G.J.; Martin, G.S.; Evans, T.W. Albumin : biochemical properties and therapeutic potential. *Hepatology* **2005**, *41*, 1211–1219, doi:10.1002/hep.20720.

110. Evans, T.W. Review article : albumin as a drug — biological effects of albumin unrelated to oncotic pressure. *Aliment Pharmacol Ther* **2002**, *16*, 6–11, doi:10.1046/j.1365-2036.2002.00190.x.

111. Kratz, F. Albumin, a versatile carrier in oncology. *Int J Clin Pharmacol Ther* **2010**, *48*, 453–455.

112. An, F.; Zhang, X. Strategies for Preparing Albumin-based Nanoparticles for Multifunctional Bioimaging and Drug Delivery. *Theranostics* **2017**, *7*, 3667–3689, doi:10.7150/thno.19365.

113. Chatterjee, M.; Ben-josef, E.; Robb, R.; Vedaie, M.; Seum, S.; Thirumoorthy, K.; Palanichamy, K.; Harbrecht, M.; Chakravarti, A.; Williams, T.M. Caveolae-mediated endocytosis is critical for albumin cellular uptake and response to albumin-bound chemotherapy. *Cancer Res.* **2017**, *77*, 5925–5938, doi:10.1158/0008-5472.CAN-17-0604.

114. Syga, M.I.; Nicolì, E.; Kohler, E.; Shastri, V.P. Albumin incorporation in polyethylenimine-DNA polyplexes influences transfection efficiency. *Biomacromolecules* **2016**, *17*, 200–207, doi:10.1021/acs.biomac.5b01308.

115. Kumari, M.; Liu, C.H.; Wu, W.C. Efficient gene delivery by oligochitosan conjugated serum albumin: Facile synthesis, polyplex stability, and transfection. *Carbohydr. Polym.* **2018**, *183*, 37–49, doi:10.1016/j.carbpol.2017.11.013.

116. Yedomon, B.; Fessi, H.; Charcosset, C. Preparation of bovine serum albumin (BSA) nanoparticles by desolvation using a membrane contactor : a new tool for large scale production. *Eur. J. Pharm. Biopharm.* **2013**, *85*, 398–405, doi:10.1016/j.ejpb.2013.06.014.

117. Mo, Y.; Barnett, M.E.; Takemoto, D.; Davidson, H.; Kompella, U.B. Human serum albumin nanoparticles for efficient delivery of Cu , Zn superoxide dismutase gene. *Mol. Vis.* **2007**, *13*, 746–757.

118. Wagh, J.; Patel, K.J.; Soni, P.; Desai, K.; Upadhyay, P.; Soni, H.P. Transfecting pDNA to E. coli DH5α using bovine serum albumin nanoparticles as a delivery vehicle. *jounal Biol. Chem. Lumin.* **2015**, *30*, 583–591, doi:10.1002/bio.2789.

119. Steinhauser, I.; Langer, K.; Strebhardt, K.; Spänkuch, B. Uptake of plasmid-loaded nanoparticles in breast cancer cells and effect on Plk1 expression. *J. Drug Target.* **2009**, *17*, 627–637, doi:10.1080/10611860903118823.

120. Hall, A.; Lächelt, U.; Bartek, J.; Wagner, E.; Moghimi, S.M. Polyplex evolution : understanding biology , optimizing performance. *Mol. Ther.* **2017**, *25*, 1476–1490, doi:10.1016/j.ymthe.2017.01.024.

121. Boussif, O.; LezoualC'H, F.; Zanta, M.A.; Mergny, M.D.; Scherman, D.; Demeneix, B.; Behr, J.P. A versatile vector for gene and oligonucleotide transfer into cells in culture and in vivo: Polyethylenimine. *Proc. Natl. Acad. Sci. U. S. A.* **1995**, *92*, 7297–7301, doi:10.1073/pnas.92.16.7297.

122. Nicolì, E.; Syga, M.I.; Bosetti, M.; Shastri, V.P. Enhanced gene silencing through human serum albumin-mediated delivery of polyethylenimine-siRNA polyplexes. *PLoS One* **2015**, *10*, 1–16, doi:10.1371/journal.pone.0122581.

123. Kang, H.; Alam, R.; Dixit, V.; Fisher, M.; Juliano, R.L. Cellular delivery and biological activity of antisense oligonucleotides conjugated to a targeted protein carrier. *Bioconjug Chem* **2008**, *19*, 2182–2188, doi:10.1021/bc800270w.Cellular.

124. Matsumura, Y.; Maeda, H. A New concept for macromolecular therapeutics in cancer chemotherapy: mechanism of tumoritropic accumulation of proteins and the antitumor agent smancs. *Cancer Res.* **1986**, *46*, 6387–6392.

125. Chung, S.W.; Choi, J. uk; Lee, B.S.; Byun, J.; Jeon, O.C.; Kim, S.W.; Kim, I.S.; Kim, S.Y.; Byun, Y. Albumin-binding caspase-cleavable prodrug that is selectively activated in radiation exposed local tumor. *Biomaterials* **2016**, *94*, 1–8, doi:10.1016/j.biomaterials.2016.03.043.

126. Burger, A.M.; Hartung, G.; Stehle, G.; Sinn, H.; Fiebig, H.H. Pre-clinical evaluation of a methotrexate-albumin conjugate (MTX-HSA) in human tumor xenografts in vivo. *Int. J. Cancer* **2001**, *92*, 718–724, doi:10.1002/1097-0215(20010601)92:5<718::AID-IJC1257>3.0.CO;2-D.

127. Carver, K.; Ming, X.; Juliano, R.L. Multicellular tumor spheroids as a model for assessing delivery of oligonucleotides in three dimensions. *Mol. Ther.* **2014**, *3*, e153, doi:10.1038/mtna.2014.5.

128. Sarett, S.M.; Werfel, T.A.; Lee, L.; Jackson, M.A.; Kilchrist, K. V; Brantley-sieders, D.; Duvall, C.L. Lipophilic siRNA targets albumin in situ and promotes bioavailability , tumor penetration , and carrier-free gene silencing. *Proc. Natl. Acad. Sci.* **2017**, *114*, 1–8, doi:10.1073/pnas.1621240114.

129. Ghahremani, F.; Shahbazi-gahrouei, D.; Kefayat, A.; Motaghi, H.; Mehrgardi, M.A.; Javanmarde, S.H. AS1411 aptamer conjugated gold nanoclusters as a targeted radiosensitizer for megavoltage radiation therapy of 4T1 breast cancer cells. *RSC. Adv.* **2018**, *8*, 4249–4258, doi:10.1039/c7ra11116a.

130. Bohui, X.; Yan, X.; Gaoxing, S.; Hongyan, Z.; Li, Z. A multifunctional nanoparticle constructed with a detachable albumin outer shell and a redox- sensitive inner core for efficient siRNA delivery to hepatocellular carcinoma cells. *J. Drug Target.* **2018**, *26*, 941–954, doi:10.1080/1061186X.2018.1455840.

131. Piao, L.; Li, H.; Teng, L.; Yung, B.C.; Sugimoto, Y.; Brueggemeier, R.W.; Lee, R.J. Human serum albumin-coated lipid nanoparticles for delivery of siRNA to breast cancer. *Nanomedicine Nanotechnology, Biol. Med.* **2013**, *9*, 122–129, doi:10.1016/j.nano.2012.03.008.

132. Weecharangsan, W.; Yu, B.; Zheng, Y.; Liu, S.; Pang, J.X.; Lee, L.J.; Marcucci, G.; Lee, R.J. Efficient delivery of antisense oligodeoxyribonucleotide G3139 by human serum albumin-coated liposomes. *Mol. Pharm.* **2009**, *6*, 1848–1855.

133. Mukalel, A.J.; Riley, R.S.; Zhang, R.; Mitchell, M.J. Nanoparticles for nucleic acid delivery : Applications in cancer immunotherapy. *Cancer Lett.* **2019**, *458*, 102–112, doi:10.1016/j.canlet.2019.04.040.

134. Cheng, W.; Sheu, M.; Lin, H. Stearyl polyethylenimine complexed with plasmids as the core of human serum albumin nanoparticles noncovalently bound to CRISPR / Cas9 plasmids or siRNA for disrupting or silencing PD-L1 expression for immunotherapy. *Int. J. Nanomedicine* **2018**, *13*, 7079–7094.

135. FDA FDA approval brings first gene therapy to the United States. *FDA News Press Release* 2017.

136. Levi, J.R.; Kathrin, S.; Kole, T.R.; Ga, R.E.; Ye, C.J.; Lim, W.A.; Marson, A. CRISPR / Cas9-mediated PD-1 disruption enhances anti-tumor efficacy of human chimeric antigen receptor T cells. *Sci. Rep.* **2017**, *7*, 1–10, doi:10.1038/s41598-017-00462-8.

137. Look, J.; Wilhelm, N.; Briesen, H. Von; Noske, N.; Gu, C.; Langer, K.; Gorjup, E. Ligand-modified human serum albumin nanoparticles for enhanced gene delivery. *Mol. Pharm.* **2015**, *12*, 3202–3213, doi:10.1021/acs.molpharmaceut.5b00153.

138. Fischer, D.; Bieber, T.; Bru, S.; Elsa, H.; Kissel, T. Cationized human serum albumin as a non-viral vector system for gene delivery ? Characterization of complex formation with plasmid DNA and transfection efficiency. *Int. J. Pharm.* **2001**, *225*, 97–111.

139. Steinhauser, I.; Spa, B.; Strebhardt, K.; Langer, K. Trastuzumab-modified nanoparticles :

Optimisation of preparation and uptake in cancer cells. *Biomaterials* **2006**, *27*, 4975–4983, doi:10.1016/j.biomaterials.2006.05.016.

140. Choi, J.; Meghani, N. Impact of surface modification in BSA nanoparticles for uptake in cancer cells. *Colloids Surfaces B Biointerfaces* **2016**, *145*, 653–661, doi:10.1016/j.colsurfb.2016.05.050.

141. Langer, K.; Anhorn, M.G.; Steinhauser, I.; Dreis, S.; Celebi, D.; Schrickel, N.; Faust, S.; Vogel, V. Human serum albumin (HSA) nanoparticles: Reproducibility of preparation process and kinetics of enzymatic degradation. *Int. J. Pharm.* **2008**, *347*, 109–117, doi:10.1016/j.ijpharm.2007.06.028.

142. Segura, S.; Gamazo, C.; Irache, J.M.; Espuelas, S. Gamma interferon loaded onto albumin nanoparticles: In vitro and in vivo activities against Brucella abortus. *Antimicrob. Agents Chemother.* **2007**, *51*, 1310–1314, doi:10.1128/AAC.00890-06.

Chapter 2. Materials and methods

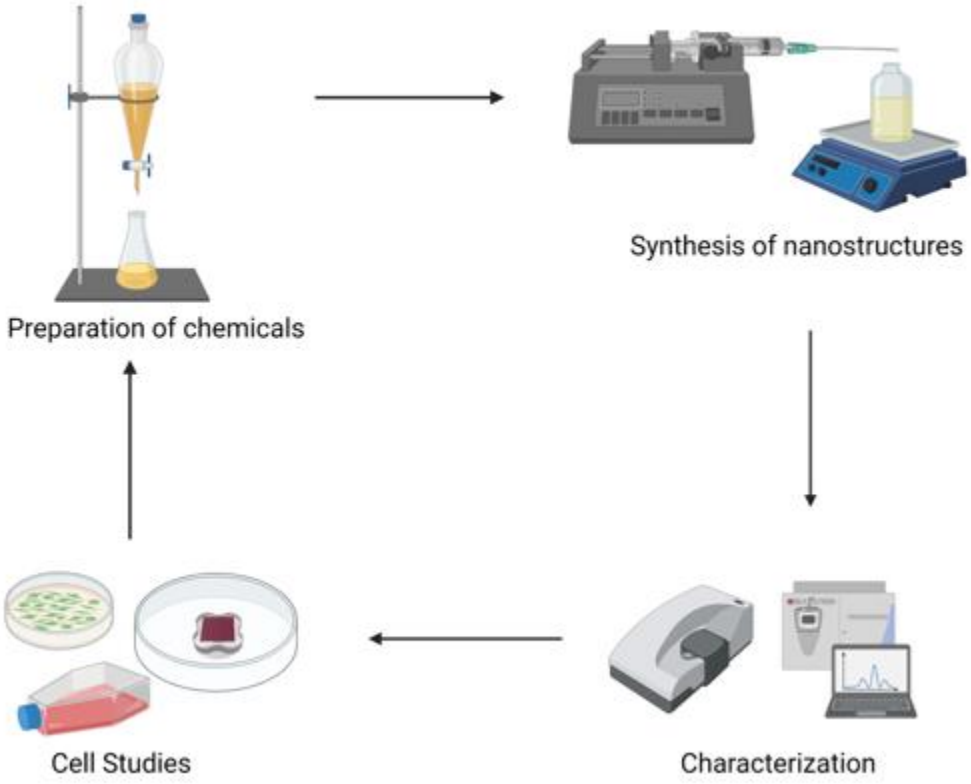

2.1. General Methods

2.1.1. Materials

All the solvents and chemical reagents were purchased from Sigma-Aldrich (San Luis, MO, USA), abcr GmbH (Karlsruhe, Germany), Thermo Fisher Scientific (Waltham, MA, USA), Scharlab (Sentmenat, Barcelona, Spain), FluoroChem (Hadfield, UK), and VWR (Radnor, PA, USA). Modified Eagle Medium (DMEM), streptomycin–penicillin (100X), fetal bovine serum (FBS), L-glutamine (100X), trypsin (10X), phosphate-buffered saline (PBS), and cell culture plasticware were purchased from VWR.

2.1.2. Surface Charge and Size Characterization of nanostructures

The Z-potential, size, and size distribution of all the prepared nanostructures were measured using a Zetasizer Nano ZS equipped with a 633 nm laser (Malvern Instruments, Worcestershire, UK). Prior to measurements at 25 °C and at 173° scattering angle, the samples were diluted 1/100 in water. ζ-potential was calculated by Zetasizer Software 7.11 (Malvern Instruments, Malvern, USA) using Smoluchowski equation:

$$\mu_e = \varepsilon_r \, \varepsilon_0 \, \zeta / \eta$$

Where, μ_e is the electrophoretic mobility, ε_r is the dielectric constant of water, ε_0 is the permittivity of vacuum, and η is the viscosity of the solvent (water). The measurements were done in triplicate and averaged.

For different polymers used for the preparation of polyplexes, the samples were diluted 1/100 in water and the surface charge was measured at different pH ranging from 3 to 11 (readjusted with 0.1 % acetic acid or 0.1% NaOH).

2.1.3. Scanning electron Microscopy (SEM)

The morphology of Dox-loaded albumin nanoparticles, BSA-PEI and BSA-PEI-PEG polymers in a dry state was observed using Scanning Electron Microscopy (SEM). Firstly, the samples were diluted 10 times in water. Then, 5µL of sample was loaded onto 100-mesh carbon-coated copper grid and was air-dried at room temperature with natural convection for 24 h. The samples were then observed using a Carl Zeiss AURIGA scanning electron microscope (Zeiss, Jana).

2.1.4 Cell culture

2.1.4.1 Maintenance and amplification of cell lines

The cell lines used were MCF-7, MDA-MB-231, PANC-1, HeLa and MCF-10A. Human breast adenocarcinoma (MCF-7 and MDA-MB-231), human breast epithelial cells (MCF-10A) and human pancreatic adenocarcinoma (PANC-1) cells were obtained from American Type Culture Collection (ATCC)®. Human cervical cancer cells (HeLa) were kindly donated by Dr. Angel Ayuso, IMDEA Nanociencia. MCF-7, MDA-MB-231, HeLa and PANC-1 cells were grown in DMEM containing 10% FBS, 1% streptomycin-penicillin, and 1% L-glutamine in a humidified incubator with 5% CO_2 and 95% air at 37 °C. MCF-10A cells were grown in HUMEC basal serum-free medium containing HUMEC supplement, bovine pituitary extract (BPE), and 1% streptomycin-penicillin. The cells were observed every 2-3 days using an inverted optical microscope. After the cells reached 80% confluency, sub-cultures were carried out.

The cell lines used for immunomodulatory studies were murine RAW 264.7 and human THP-1 cells. Both the cells lines were kindly donated by Dr. Fransisco Sanchez, CNIC. RAW 264.7 cells were grown in DMEM containing 10% FBS, 1% streptomycin-penicillin, and 1% L-glutamine. THP-1 cells were cultured in RPMI 1640 medium (Biowest) supplemented with 10% (v/v) fetal bovine serum (FBS), 2mM L-Glutamine and 1% Penicillin/Streptomycin. All the cells were incubated at standard conditions of 37 °C in an atmosphere of 5% CO2. Both RAW 264.7 and THP-1 cells were used within 5 passages. Before using the cells for the studies, THP-1 monocytes were differentiated into macrophages by incubation with 50 ng/mL phorbol 12-myrisate 13-acetate (PMA) for 48 hours followed by 24 hours incubation in RPMI medium.

2.1.4.2. Subcultures

For subcultures, the medium was removed, and the cells were washed twice with PBS 1X followed by the addition of trypsin-EDTA 1X. The culture plates were incubated at 37 °C for 2-5 minutes to allow the detachment of the cells. The cells were then suspended in the complete growth medium and new cultures were made with the dilution range of 1:4 to 1:10 depending on the cell line being used. The plates were then incubated at 37 °C in an atmosphere of 5% CO2. All the experiments were conducted before the cells reached 25 passages.

2.1.4.3 Freeze/Thaw of the cells

For long-term storage, cells were preserved in liquid nitrogen. During the subculture, after trypsinization step, the cells were counted in a hemocytometer. 2 x 10^6 cells were then resuspended in 1 mL of 10% dimethyl sulfoxide (DMSO) in fetal bovine serum (FBS). The suspensions were then frozen in cryovials (Thermo Fisher) and placed in an isopropanol chamber to gradually freeze them to -80 °C at a rate of 1 °C/min.

For thawing of the cells, the cryovials containing cells were first warmed in a water bath at 37°C. The whole content of the vial was then added to a falcon tube containing 5 mL of the complete medium. It was then centrifuged at 1000 rpm for 5 minutes and the supernatant was discarded. The pellets were resuspended in 10 mL of the complete medium and added to the flask. The flask was finally incubated at 37 °C in an atmosphere of 5% CO_2.

2.1.4.4. Preparation of the cells for experiments

For the use of cells for any experiment, the cells in the culture plate were first trypsinized and counted with a hemocytometer. The desired number of cells suspended in complete medium were then seeded to the plates (6, 12, 24 or 96 well cell culture plates). The number of cells used highly depended on the type of plate used, experiment, and cell line. The plates were used when the cells reached approximately 80% confluency.

2.1.4.5 Cytotoxicity Assay

The cell viability of the prepared drug loaded nanoparticles and polyplexes in various cell lines was determined by alamarBlue assay. The cells in 100 µL of DMEM medium with 10% FBS, 1% streptomycin-penicillin, and 1% L-glutamine were seeded in 96-well plate (5 × 10^3 cells per well) at 37 °C in a Binder CB210 incubator (5% CO_2). After the cells reached 60% confluency, nanostructures were added to each well. After 24, 48 and 72 h of incubation, the medium was removed, and 150 µL of DMEM with 1% resazurin was added. The supernatant was removed after 4 h of incubation at 37 °C, and the fluorescence was measured at excitation and emission wavelengths at 550 nm and 590 nm, respectively. The cell viability after 24, 48 and 72 h was calculated as follows:

$$Cell\ viability = \frac{Sample\ data - data\ of\ resazurin\ solution}{Data\ of\ untreated\ cells - data\ of\ resazurin\ solution} \times 100\% \qquad (3)$$

Where, the positive control corresponds with untreated cells, while a resazurin solution without cells serves as a negative control.

2.1.4.6. Internalization of nanoparticles in cells

Various cell studies were carried out to observe the internalization and release of Dox (in MCF-7 and MDA-MB 231), Vola (in MCF-7 and HeLa) and GFP from polyplexes (in MCF-7 and PANC-1). For this purpose, firstly, the cells were seeded on P-6 polystyrene tissue-culture plates. After the cells reached 60% confluency, they were treated with various nanostructures. After 24 h of incubation, the cells were washed twice with PBS and the cells were examined for fluorescence using Beckman Coulter Cytomics 500 Flow Cytometer (Beckman Coulter, Indianapolis, IN, USA). The acquired data were analyzed with FloJo™ v10.7 software (Ashland, USA). All these experiments were performed in the Flow Cytometry Service at the CNB-CSIC.

For the Vola loaded nanoparticles, a fluorescent dye was conjugated on the surface and the internalization was quantified using a flow cytometer as described above in HeLa and MCF-7 cells. In addition, for the polyplexes treated cells, after 24 hours of incubation, the cells were washed twice with PBS and the cells were also examined under a fluorescence microscope using 10X objective.

2.1.4.7. Study of Mechanism of Internalization

To analyze the mechanism of internalization of ABN-SPDP in cells, MCF-7 cells were seeded in a 96-well plate at a density of 5×10^3 cells/well. After the cells reached 60% confluency, they were washed with PBS followed by the addition of either 150 µM genistein or 5 µg/mL filipin (inhibitors for caveolae-mediated endocytosis), or chlorpromazine (10 µg/mL, an inhibitor for clathrin-mediated endocytosis). After 2 h of adding the endocytosis inhibitors, the cells were washed thrice with PBS and treated with Dox- or Vola- loaded ABN-SPDP. The cells were washed again with PBS after 4 h of treatment, and new DMEM was added. Alamarblue assay, as described in Section 2.1.4.5, was conducted to compare the effect of endocytosis inhibitors in the internalization of nanoparticles.

For the polyplexes, PANC-1 cells were seeded in 24-well plates at a density of $3 \text{ X } 10^5$ cells/well. After the cells reached 60% confluency, the cells were washed twice with PBS, followed by the addition of 400 µL of DMEM medium and equilibration at 4 °C or 37 °C for 30 minutes. The medium in the plate for 37 °C was replaced with 400 µL of either medium or different endocytosis

inhibitors as mentioned earlier. The cells were then incubated at 37 °C for 2 hours, followed by washing with PBS twice and the addition of 400 µL of either BSA-PEI or BSA-PEI-PEG polyplexes at the biopolymer: GFP weight ratio of 90:1. Uptake at 4 °C was also initiated by replacing the medium with polyplexes. Incubation of the cells was carried out for 4 hours either at 37 °C or 4 °C, followed by washing the cells with PBS twice. The cells were then examined under a fluorescence microscope using 10X objective.

2.1.4.8. Western Blot Analysis

To study the effect of nanoparticles on different protein levels, 2 × 10^5 MCF-7, MDA-MB231 or PANC-1 cells per p6 well were seeded and allowed to adhere to the plate. After 72 h of culture, cells were washed with PBS1x and incubated with the different treatments (as indicated in Results) in fresh medium. After 24 h of incubation of the drug loaded nanoparticles, cells were washed with PBS1x, collected, and lysed with lysis buffer plus protein inhibitors (10 mM Tris-HCl pH 7.5, 5 mM EDTA, 150 mM NaCl, 10% glycerol, 0.5% Triton X-100, 50 mM sodium fluoride, 30 mM sodium pyrophosphate, 1 mM sodium orthovanadate, and 1 mM phenylmethylsulfonyl) and cell extracts were incubated for 30 min at 4 °C in a tube rotator. After clearing the total cell lysate by centrifugation for 15 min at 16100× *g* and 4 °C, supernatants were stored at −80 °C. Total protein amount was quantified by Bradford assay (Bio-Rad). Twenty milligrams of protein samples were separated on 12% SDS-polyacrylamide gels under reducing conditions and transferred to 0.45 µm nitrocellulose membrane (GE Healthcare Life science). Detection of specific proteins was performed by Western blot, employing the corresponding antibodies as indicated in the Results section. After incubating the membranes with 5% BSA in TBS-T (0. 0.1% Tween-Tris buffered saline) for 1 h at room temperature, the blots were incubated overnight at 4 °C with the corresponding first antibody solution in 3% BSA in TBS-T. Conditions for each antibody are the following: anti-p53 (1:500; sc-263), anti-cyclin B1 (1:500; sc-245), anti-cyclin E (1:500; sc-377100), and anti-GAPDH (1:500; sc-47724). After three washes with TBS-T, blots were incubated with peroxidase-labelled anti-mouse (1:5000; sc-516102) with 3% BSA in TBS-T blocking solution for 1 h at room temperature. The blots were washed three times with TBS-T and membrane-bound antibody was detected with enhanced chemiluminescence detection

reagent (Bio-Rad). All antibodies were purchased from Santa Cruz Biotechnology. Densitometry analysis was performed using Fiji software (ImageJ).

In case of the polyplexes, similar process was followed. PANC-1 cells were washed with PBS 1X and fresh medium was added after 24 hours of treating with different polyplexes. The cells were incubated at 37°C in 5% CO_2 atmosphere for 48 hours more. After 48 hours, the cells were washed with PBS, collected, and lysed with lysis buffer plus protein inhibitors. The antibodies used were anti-p53 (1:500; sc-263) and anti-GAPDH (1:500; sc-47724).

2.1.5. Statistical Analysis

The results are presented as the mean ± standard deviation (SD). The statistical analysis was performed in R Project for Statistical Computing (R-3.2.5) software (R Development Core Team, Vienna, Austria) [22]. One-way analysis of variance (ANOVA) was used to compare the mean value of each condition versus the control. Significant differences between the means were accepted when the p-value was lower than 0.05 (*), 0.01 (**), and 0.001 (***). When the statistical difference was observed, Tukey's test was performed to compare the mean values by pairs.

2.2. Albumin-based nanoparticles for the delivery of chemotherapeutics

2.2.1. Preparation of BSA Nanoparticles (ABNs)

ABNs were prepared by the desolvation method, with ethanol as the desolvating agent. Depending upon the reagents used for the cross-linking of BSA, the ABNs were formed either by amide or disulfide bonds or by electrostatic stabilization. The preparation of nanoparticles was optimized using doxorubicin as a model drug and in vitro characterization was carried out. Later, the optimized system was used for the encapsulation of other hydrophobic drugs, including SN38 and volasertib.

2.2.1.1 Formation of Amide Bonds

Use of glutaraldehyde: For the preparation of nanoparticles using GLU (ABN-GLU), 20 mg/mL of BSA in an aqueous solution was incubated with 0.5 mg/mL doxorubicin HCl for 2 h at room temperature. To this solution, 2.7 mL of anhydrous ethanol was added dropwise with the syringe pump at the constant flow rate of 1 mL/min. After the solution became turbid, 7 µL of 8% glutaraldehyde was added for cross-linking. The solution was stirred at 550 rpm for 18 h. Then,

the free albumin, unbound Dox, ethanol, and excess glutaraldehyde, were removed by 3 cycles of centrifugations at 13,200 rpm for 15 min. After each centrifugation cycle, the pellets were redispersed in 1 mL of water. The mechanism by which the nanoparticles are formed is shown in Figure 8.

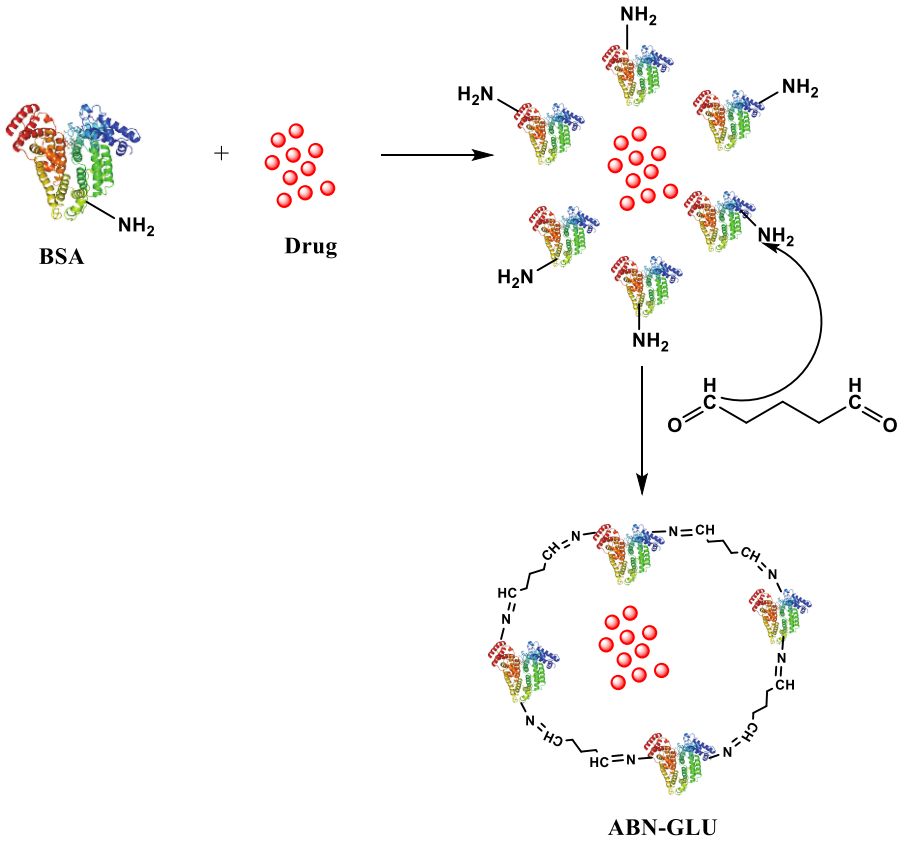

Figure 8. Formation of BSA nanoparticles using glutaraldehyde as a cross-linker (ABN-GLU)

Use of EDC: For the preparation of ABNs using EDC (ABN-EDC), a freshly prepared aqueous solution of EDC (2 mg/mL) was added to the turbid solution of BSA after the desolvation process. The mixture was left rotating at 550 rpm for 3 h and purified by three cycles of centrifugation to remove the unreacted EDC and ethanol.

2.2.1.2. Formation of Disulfide Bonds

Use of glutathione: Firstly, the intramolecular disulfide bonds in albumin were cleaved by using glutathione (GSH), which is one of the major endogenous antioxidants in vivo. After the pre-treatment, it was purified using NAP-10 column and incubated with 0.5 mg/mL doxorubicin HCl for 2 h, followed by desolvation with ethanol to precipitate albumin into Dox-loaded ABNs (ABN-GSH). Then, ethanol and unbound Dox were removed through centrifugation at 13,200 rpm for

15 min.

Use of N-succinimidyl 3-(2-pyridyldithio) propionate (SPDP): The schematic representation for the preparation of ABNs by using SPDP (ABN-SPDP) is depicted in Figure 9. Firstly, thiol groups were introduced in BSA with 2-iminothiolane, commonly known as Traut's reagent. In parallel, the same amount of BSA was modified with SPDP. The modified BSAs were purified with NAP-10 column and the resulting solutions combined. The mixture was incubated with DOX for 2 h, followed by preparation of NPs by desolvation method as described earlier in Section 2.2.1.

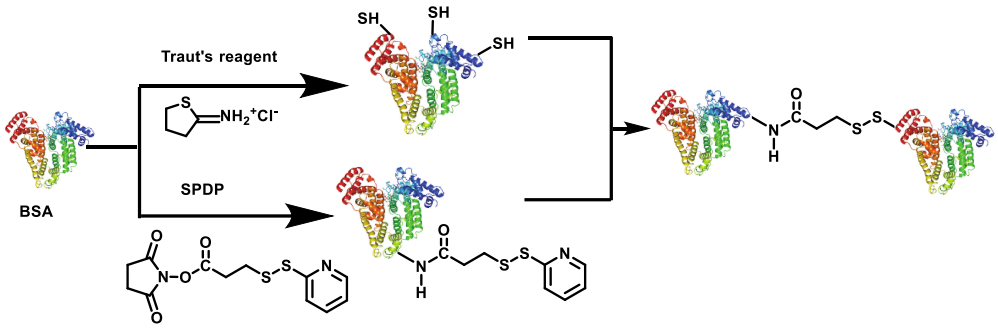

Figure 9. Surface modification of BSA with Traut's reagent and SPDP, followed by their conjugation through the formation of disulfide bonds to yield the corresponding BSA nanoparticles (ABN-SPDP)

Use of modified polyethylene glycol (PEG): The schematic representation of the synthesis of this derivative is provided in Figure 10. The preparation of this modified PEG is as follows: to a solution of $PEG(NH_2)_2$ (3000 M.W.) (**1**) (100 mg, 33 µmol) in THF (6 mL) at 0 °C, a solution of SPDP (41.5 mg, 0.13 mmol) in THF (3 mL) was added. The reaction was allowed to warm up to room temperature under vigorous stirring for 16 h. Then, the solvent was removed under vacuum and re-dissolved in methanol (3 mL). The product was purified by dialysis using a 3.5 KDa. dialysis membrane for 16 h at 4 °C against distilled water. After this time, the solution turned cloudy, and the solvent was removed under vacuum. The desired product (**2**) was isolated as a greyish oil (44% of yield, 48.3 mg) (linker/polymer ratio 2:1). The product was characterized by NMR and MS (Figure 11). ^{1}H NMR (D_2O, 400 MHz): δ 8.26 (d, 2H), 7.71 (m, 4H), 7.17 (td, 2H), 3.56 (m, 264H), 3.21 (t, 4H), 2.93 (t, 4H). ^{13}C NMR (D_2O, 101 MHz): δ 173.74, 158.67, 149.03, 138.61, 121.69, 120.08, 38.83, 34.37, 33.56. MS (MALDI): theoretical mass: 3296.97, calculated mass: 3295.8.

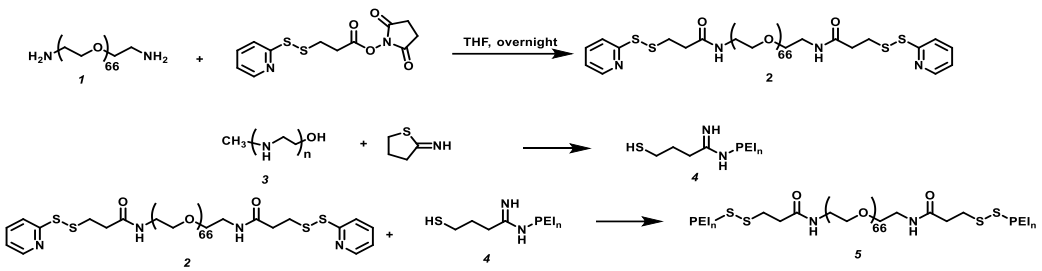

Figure 10. Schematic illustration of the preparation of PEI-PEG based polymer

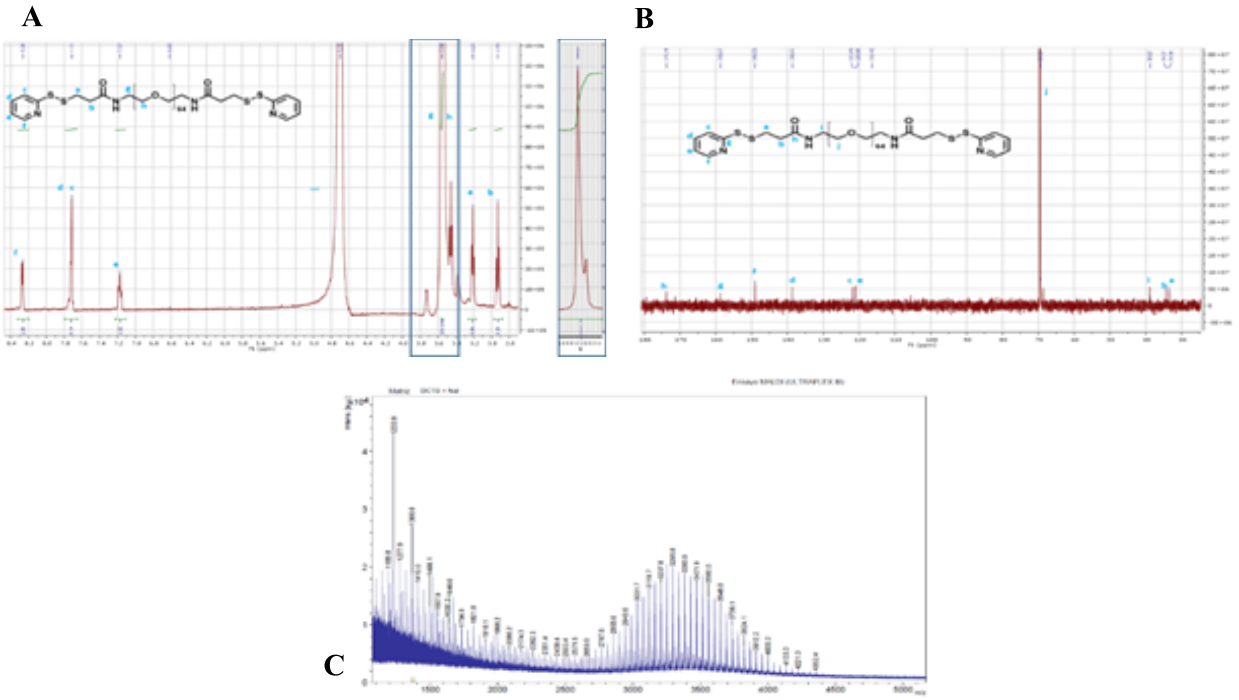

Figure 11. ^{1}H (A) ^{13}C NMR (B) and MS (C) of NH_2-PEG-NH_2 modified with SPDP.

Finally, the obtained product (**2**) was mixed with BSA modified with 2-iminothiolane at RT for 16 h, followed by incubation with Dox for 2 h and desolvation with ethanol to obtain the desired ABNs with modified PEG (ABN-PEG).

2.2.1.3. Electrostatic Stabilization

For this approach, a polymer based on PEI and PEG, (PEI-PEG) was prepared through a three steps reaction. The synthetic process is schematically represented in Figure 10. The amine groups in 2 kDa linear PEI (**3**) were activated with 2-iminothiolane, commonly known as Traut's reagent, to yield the derivative **4**, which contains the required thiols. Then, compound **4** was combined with the previously obtained compound **2**, and the mixture was stirred for 24 h at 400 rpm (at room

temperature). The product was finally dialyzed against water to remove unreacted PEI, PEG, and 2-iminothiolane, leading to the desired compound **4**. (Figure 12). ^{1}H NMR (400 MHz, D_2O) δ 3.71 (s, 291 H), 3.27 —2.21 (m, 305 H). ^{13}C NMR (101 MHz, D_2O) δ 174.07, 127.64, 121.90, 69.58, 68.81, 52.88, 51.03, 47.41, 45.52, 39.37, 39.02, 38.58, 37.55, 34.88, and 33.21. Finally, polymer **4** was incubated with 20 mg/mL BSA in water. The ABNs stabilized with PEI-PEG (ABN-PEI-PEG) and encapsulating DOX were then prepared, as discussed earlier in Section 2.2.1.

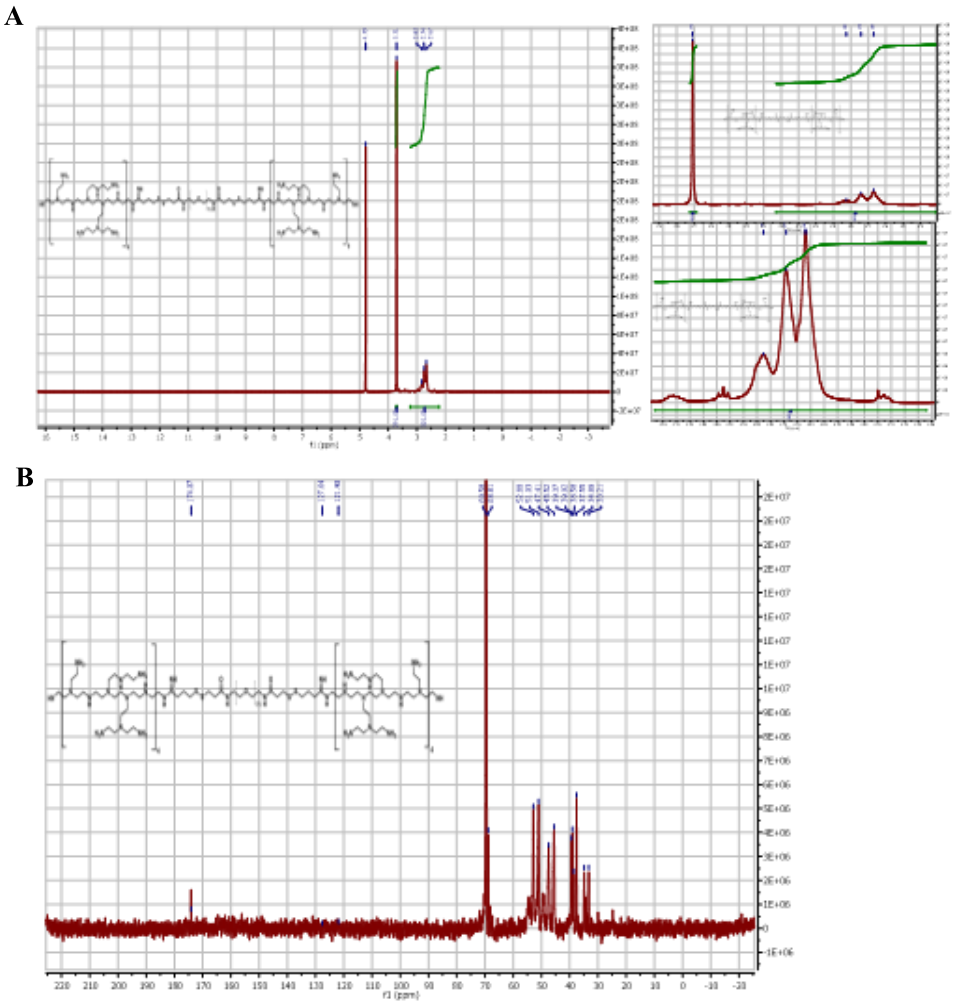

Figure 12. ^{1}H (A) and ^{13}C NMR (B) of PEI-PEG-PEI. In ^{1}H NMR, the PEG/PEI signal integrates in the ratio of 1:1.05, which corresponds approximately to the bi-functionalized PEG with PEI. In ^{13}C NMR, the characteristics peaks of the PEG at 70 ppm, and the peaks of PEI distributed between 50 and 35 ppm can be observed that correspond to the ethylene groups.

2.2.2. Preparation of nanoparticles encapsulating SN38 or Volasertib with the optimum cross-linking process.

After the preparation of albumin nanoparticles with various cross-linkers, the optimum system was selected based on the results obtained from size, encapsulation efficiency and activity in the cells. The selected system (ABN-SPDP) was then used to encapsulate hydrophobic drugs (SN38 and Volasertib) following the procedure described in Section 2.2.1.2

2.2.3. Quantification of Nanoparticle Formation

To quantify the amount of BSA converted to nanoparticles, the Bradford protein assay was performed [20]. The calibration curve was made with the known concentrations of BSA standards. The nanoparticles were first separated by centrifugation at 13,200 rpm for 15 min at room temperature and the supernatant was analyzed spectrophotometrically at 595 nm. The nanoparticle yield was then calculated by using Equation (1) [21].

$$NPs\ yield = \frac{Initial\ amount\ of\ BSA - amount\ of\ BSA\ in\ supernatant}{Initial\ amount\ of\ BSA} \times 100\% \qquad (1)$$

2.2.4. Drug Loading of NPs

The amount of Dox/Vola/SN38 incorporated in different ABNs was determined by an indirect method, i.e., by measuring the amount of the drug in the supernatant. The ABNs were separated by centrifugation, and the supernatant was analyzed spectrophotometrically at 495 nm for Dox, 318 nm for Vola and 370 nm for SN38. The drug loading capacity was then calculated following Equation (2).

$$Drug\ loading = \frac{Drug\ added - amount\ of\ drug\ in\ supernatant}{Drug\ added} \times 100\% \qquad (2)$$

2.2.5. In Vitro Release Studies

The release of Dox and Vola from ABNs prepared by various methods was evaluated under the physiological pH of 7.4, an acidic pH of 5 adjusted with 0.1% acetic acid, and/or presence of 1 mM glutathione (GSH) to mimic the intracellular environment of tumor sites. At various time points, the aliquots of the sample were centrifuged at 13,200 rpm for 15 min at room temperature, and the supernatant was analyzed spectrophotometrically at 495 or 318 nm. The drug release was then calculated from a standard calibration curve of the free Dox/Vola solution.

2.2.6. Stability Studies

The prepared ABN-SPDP suspension was stored either at 4 °C or at room temperature. Their stability was estimated by comparing the changes in their hydrodynamic size, zeta potential, and drug release every week for 2 months.

2.2.7. Determination of Cell Cycle Phase

Cells were harvested in 6-well plates. When the cells reached a 60% confluency, they were treated with ABN-SPDP encapsulating Dox or Vola at various concentrations. After 48 h, the samples were trypsinized, fixed with ethanol 70% (*v*/*v*), washed with PBS, and centrifuged at 100× *g* for 5 min in an Eppendorf centrifuge 5804 R (Eppendorf, Hamburg, Germany). For each sample, 10 µg RNase A and 20 µg propidium iodide (PI) were added. PI stains DNA that allows the differentiation of cells in G0/G1, S, and G2/M phases and aneuploid population. However, it also stains RNA in addition to DNA, and hence the cells need to be treated with RNase after fixing with ethanol to measure the cell cycle accurately. The cell cycle analysis was then performed using a flow cytometer.

2.2.8. Determination of Induction of Apoptosis/Necrosis

Cells were seeded in 6-well plates. When the cells reached a 60% confluency, they were treated with ABN-SPDP encapsulating Dox or Vola at various concentrations. After 24 h, the supernatant was collected, and the cells were trypsinized, washed with PBS, and centrifuged at 100× *g* for 5 min in an Eppendorf centrifuge 5804 R (Eppendorf, Hamburg, Germany). The cells were suspended in 100 µL of 1X binding buffer followed by the addition of 10 µL Annexin V 1X and incubated at 4 °C in darkness for 15 min. In each sample, 380 µL binding buffer 1X and 10 µL propidium iodide 1 mg/mL were added before analyzing them in a flow cytometer.

2.2.8. Measurement of intracellular ROS

To measure the intracellular ROS production, cells were seeded in 96-well plates. After 60% confluency was reached, the cells were treated with Vola, ABN-SPDP, or ABN-SPDP loaded with Vola. After 24 hours of incubation, the cells were washed twice with PBS 1X and incubated with 5 µM 2',7'- dichlorofluorescein (DFC-DA) for 15 minutes at 37 °C. The cells were then washed twice with PBS and the fluorescence was measured with multimode plate reader (λexc 485 nm and λem 535 nm) (Synergy H4 Hybrid reader (BioTEK)). After the measurement, the cells were washed with PBS and alamarblue assay was carried out. The values of the DFC-DA fluorescence

were then normalized on cell viability results. The process was repeated after 48 and 72 hours of treatment. For the imaging of the ROS production, the cells were seeded in 24 well plates treated with DFC-DA as described above. After incubation and washing with PBS 1X, the cells were immediately photographed under fluorescent microscope.

2.2.9. Detection of autophagosomes formation

To quantify the formation of autophagosomes, cells were incubated with monodansylcadaverine (MDC), a selective fluorescent probe for the detection of autophagosomes. The cells were seeded in 96-well plates and after they reached 60% confluency, they were treated with either Vola, ABN-SPDP or ABN-SPDP loaded with Vola. After 24 hours, cells were washed with PBS 1X and incubated with 50 μM monodansylcadaverine (MDC) for 15 minutes at 37 °C. The cells were then washed twice with PBS followed by fluorescence measurement using a multimode plate reader (λexc 340 nm and λem 535 nm) (Synergy H4 Hybrid reader (BioTEK)). Afterwards, the values were normalized with the cell viability from alamarBlue assay. The process was repeated 48 and 72 hours post treatment.

2.3. Overcoming biological barriers with albumin-based nanoparticles

2.3.1. Cellular uptake of the nanoparticles

To study the internalization of albumin nanoparticles (HSA-GLU and HSA-SPDP conjugated with AlexaFluor-488), HeLa and MCF-7 cells were incubated with different nanoparticles for 4 hours at 37 °C. The cells were then washed 3 times with HBSS to remove any residual extracellular particles. The plasma membrane was then stained with either DiR or DiO (1 μM) in 300 μL of HBSS for 12 minutes at room temperature, followed by washing with HBSS thrice. The dishes were then visualized under a confocal fluorescence microscope (FV1000, Olympus). The images were obtained using 100X oil objective (N.A. 1.40). For HSA-GLU, the particles were visualized with the excitation wavelength of 635 nm and the membrane staining DiO was imaged using a 488 nm laser. Meanwhile, for HSA-SPDP, the particles were imaged using the excitation wavelength of 488 nm and the membrane staining DiR was visualized using 635 nm. In both cases, a DM 405/488/559/635 was chosen as the primary dichroic mirror. In each case, Z-stack method was used to collect a set of images by changing the focal length from the bottom to the top of a single cell. This method offers an orthogonal view of the cell thickness cross-section on the x/y-

axis as a clear proof of the particles' internalization in the cells. The images were finally analyzed using FV-10-ASW Viewer software.

2.3.2. Mechanism of cellular uptake of the nanoparticles

MCF-7 and HeLa cells were seeded in the 15 mm culture dishes at a density of 10,000 cells/dish. After 24 hours, the cells were washed with PBS followed by the addition of either 5 µg/mL filipin (inhibitor for caveolae-mediated endocytosis), or chlorpromazine (10 µg/mL, an inhibitor for clathrin-mediated endocytosis). After 2 h of adding the endocytosis inhibitors, the cells were washed thrice with PBS and treated with either HSA-GLU or HSA-SPDP conjugated with AlexaFluor-488. The cells were incubated at 37 °C for 4 hours followed by washing thrice with HBSS. The membrane staining was performed with either DiO or DiR using the procedure previously described in section 2.3.1. The fluorescence intensities were quantified using ImageJ, and compared to the results obtained without the endocytosis inhibitors.

2.3.3. Endolysosomal escape of human serum albumin nanoparticles

To study the fate of nanoparticles in the cells, MCF-7 and HeLa cells were seeded on 15 mm culture dishes at the density of 10,000 cells/dish. After 24 hours, HSA-SPDP conjugated with AlexaFluor-488 or HSA-GLU was added to the cells. After incubating for 4 hours at 37℃, the cells were washed thrice with HBSS buffer to remove the residual extracellular particles. To track the acidic compartments, endo/lysosomes were stained either with Lysotracker Red (50 nM) or Lysotracker Green (250 nM) in HBSS for 15 minutes at room temperature. The cells were again washed with HBSS thrice and confocal images were obtained with FV 1000 Olympus microscope, with 100X oil objective (N.A. 1.40). For HSA-GLU, the nanoparticles and Lysostracker Green were imaged with the excitation wavelengths of 635 nm and 488 nm, respectively. On the other hand, for HSA-SPDP, the nanoparticles and Lysotracker Red were imaged with the excitation wavelengths of 488 nm and 561 nm, respectively. A DM 405/488/559/635 was chosen as the main dichroic mirror. The images were then processed using FV10-ASW Viewer Software.

2.3.4. Preparation of spheroids

For the preparation of the spheroids, agarose-mold was first produced by placing agarose 2% (w/v in 0.9% Nacl) in micro-molds (3D Petri Dish®, Microtissues Inc., Providence RI, US).[21] After the agarose was gelled, micro-mold was flexed to remove the 3D Petri Dish® into a cell culture

plate. Cell culture medium was then added to equilibrate the 3D Petri Dish and incubated for 15 minutes. The medium was replaced with fresh medium and the process was repeated twice. The medium surrounding the 3D Petri Dish and cell seeding chamber was removed carefully. The cell suspension (107,000 cells/190 µL) was then added dropwise into the cell seeding chamber and was allowed for 10 minutes to settle the cells in the dish. Additional medium was then added outside the 3D Petri Dish. The tissue culture plate was then incubated at 37°C and the medium was exchanged every two days. The Hela cells were grown for 10 days to allow the spheroids formation through cellular aggregation, whereas spheroids with MCF-7 cells were formed within 3 days. The schematic illustration for the preparation of spheroids is depicted in Figure 13.

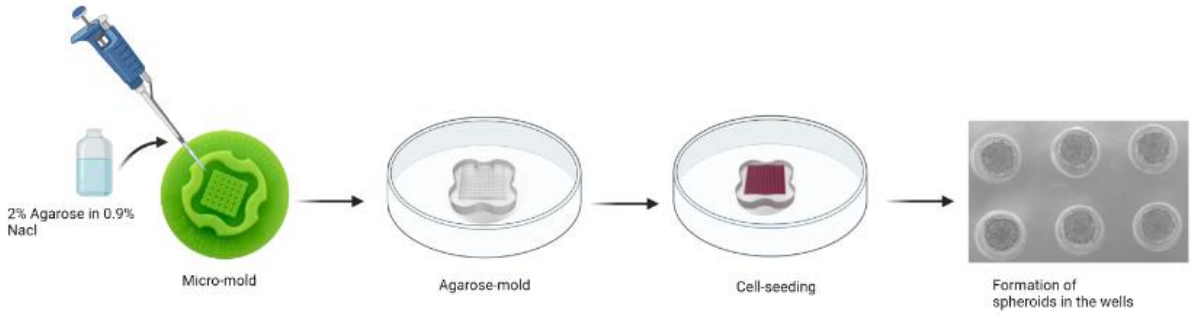

Figure 13. Schematic representation of the preparation of cancer spheroids using agarose micro-molds.

2.3.5. Internalization of albumin nanoparticles in cancer spheroids

To study the internalization of nanoparticles in the cancer spheroids, 20 µM HSA-GLU or HSA-SPDP conjugated with AlexaFluor-488 in 190 µL of medium was added dropwise to the spheroids in agarose-molds. After incubation at 37 °C for 24 hours, the medium was slowly removed from the dish. The spheroids were then recovered by splashing with 500 µL PBS 3 times in the micro-molds and collected in an Eppendorf tube. The spheroids were then washed twice with PBS, followed by fixation with PFA 4% (w/v in PBS) for 15 minutes. Subsequently, spheroids were washed 3 times with PBS and 200 µL Triton 0.1% was added, incubated for 20 minutes and then washed 3 times again with PBS. The fixed spheroids were then stained either with phalloidin 488 (for the spheroids treated with HSA-GLU) or phalloidin 647 (for the spheroids treated with HSA-SPDP) in 3% BSA. The spheroids were incubated at room temperature for 24 hours protected from light. The excess of dye was then removed by washing 3 times with PBS.

For imaging, the spheroids were loaded into the perfusion chamber fixed in the glass slide and visualized under a Las X microscope (Leica). The images were obtained using 25X water objective. For HSA-GLU, the particles were visualized in single photon with the excitation wavelength of 635 nm and cytoskeleton staining phalloidin 488 was imaged using a multiphoton 488 nm laser. On the contrary, for HSA-SPDP, the particles and phalloidin 647 were imaged using a multiphoton 488 nm laser and a single photon with an excitation wavelength of 635 nm, respectively. The Z-stack method was used to collect a set of images by changing the focal length from the bottom to the top of a single cell. The images were finally analyzed using Las X software.

2.3.6. Efficacy of drug-loaded nanoparticles in 3D cancer spheroids

The efficacy of the Vola-loaded HSA-SPDP and Dox-loaded HSA-SPDP was evaluated in 3D cancer spheroids by measuring the changes in the volume after various days of treatment. The spheroids were treated with various concentrations of the drug-loaded HSA nanoparticles and incubated for 24 hours. The medium was then replaced with the fresh medium, and the spheroids were further incubated at 37 ℃. On days 1, 3 and 5, after adding the particles, the spheroids were harvested, fixed with paraformaldehyde, and stained with phalloidin 488. The spheroids were then imaged using Leica sp8 2 photon Dive microscope. The diameter of the spheroids was then measured using Las X software and the volume of the spheroids was calculated using equation (1).[22,23]

$$V = 0.5 * (\text{short } \emptyset)^2 * \text{long } \emptyset$$

2.4. Immunomodulatory studies of the albumin-based nanoparticles

2.4.1. Preparation of albumin nanoparticles

The nanoparticles based on BSA, and HSA were prepared following the procedure provided in Section 2.2.1. HSA nanoparticles were prepared using SPDP as cross-linker to obtain the structures stabilized with disulfide bonds, whereas BSA nanoparticles were prepared either by using SPDP or glutaraldehyde (GLU) as a cross-linker.

2.4.2. Cell viability assay

Cell viability of the prepared NPs was assessed in murine RAW 264.7 and human THP-1 cells using cell titer-Glo luminescent assay. In this test, 7500 RAW 264.7 or THP-1 cells were seeded per well in 96-well plates. After 24 hours of incubation, varying concentrations of HSA NPs, BN-GLU or BN-

SPDP were added to the cells and incubated at 37 °C in an incubator at 5% CO2. After 24 hours, the cells were washed twice with PBS 1X, followed by the cell titer-Glo luminescent assay. To each well with 50 µL of PBS, 50 µL of cell titer-Glo reagent was added and the contents were mixed for 2 minutes in a shaker to induce cell lysis. The plate was then allowed to incubate at RT for 10 minutes to stabilize the luminescent signal. The luminescence reading was then taken at an integration time of 1 second per well. A blank with PBS mixed with cell titer-Glo reagent was used as a negative control. The cell viability was then calculated as below:

$$\text{Cell viability} = \frac{\text{Sample data} - \text{data of blank}}{\text{Data of untreated cells} - \text{data of resazurin solution}} \text{X}100\%$$

2.4.3. Nanoparticle uptake assay

RAW 264.7 and THP-1 cells were plated in 6-well tissue culture plates (2 x 106 cells/well) and incubated at 37 °C, 5% CO2 in a CO2 incubator for 24 h to form a confluent monolayer. The culture medium was replaced by DMEM containing 1 µM CY5-labeled NPs and incubated for 24 hours. To remove free nanoparticles, cells were washed twice with phosphate-buffered saline (PBS, pH 7.4). The cells were detached by trypsinization, collected, and centrifuged at 1000 rpm for 5 minutes. The cell pellets were washed twice with PBS and the fluorescence was measured using a flow cytometer.

2.4.4. Measurement of intracellular ROS

To measure the intracellular ROS production, RAW 264.7 or THP-1 cells were seeded in 96-well plates. After 60% confluency was reached, the cells were treated with various NPs (ABN-GLU, ABN-SPDP and HSA-SPDP). After 24-, 48- and 72- hours of incubation, the cells were washed twice with PBS 1X and incubated with 40 µM 2', 7'- dichlorofluorescein (DFC-DA) for 15 minutes at 37 °C. The cells were then washed twice with PBS and the fluorescence was measured with multimode plate reader (λ_{exc} 485 nm and λ_{em} 535 nm) (Synergy H4 Hybrid reader (BioTEK)). After the measurement, the cells were washed with PBS and cell viability was carried out using cell titer-Glo. The values of the DFC-DA fluorescence were then normalized on cell viability results.

2.4.5. Cell cycle analysis

RAW 264.7 and THP-1 cells were plated in 6-well tissue culture plates (2 x 10^6 cells/well) and incubated at 37 °C, 5% CO2 in a CO2 incubator for 24 h to form a confluent monolayer. When the

cells reached a 60% confluency, they were treated with ABN-GLU, ABN-SPDP or HSA-SPDP. After 24, 48 and 72 hours, the samples were trypsinized, fixed with ethanol 70% (*v*/*v*), washed with PBS, and centrifuged at 100× *g* for 5 min in an Eppendorf centrifuge 5804 R (Eppendorf, Hamburg, Germany). For each sample, 10 µg RNAse A and 20 µg propidium iodide (PI) were added. Then, the cell cycle analysis was performed using a flow cytometer.

2.4.6. Macrophage phenotype switch studies

RAW 264.7 and THP-1 cells were seeded in 12-well culture plates (100,000 cells/well) and incubated at 37 °C, 5% CO_2 in a CO_2 incubator for 24 h to form a confluent monolayer. The cells were treated with various albumin nanoparticles (ABN-GLU, ABN-SPDP and HSA-SPDP) at the concentration of 1 µM. Simultaneously, the cells were stimulated with 10 ng/mL LPS and 1 ng/mL IFN-γ, which were used as the M1 phenotype control; or by anti-inflammatory cytokines IL-4 and IL-13 (20 ng/mL each), which were used as M2 phenotype controls. After 24, 48 and 72 hours, the expression of CD80, CD86 and CD206 on the cell surfaces was detected by immunostaining with the respective antibodies.

Briefly, the cells were detached by adding 1 mM cold PBS-EDTA and collected in an Eppendorf tube. The collected cell pellets were centrifuged at 400 g for 5 minutes and the supernatant was removed. In each tube, 20 µL FC-block in cell staining buffer was added and incubated at room temperature for 10 minutes. After the incubation, 80 µL of antibodies markers was added to the cells (PE-CD80, APC-CD86 and FITC-CD206) and incubated for 20 minutes at 4 °C. The cell pellets were centrifuged and washed twice with cell staining buffer to remove any free markers, and subsequently analyzed by flow cytometry. In each group, cells without antibody staining were used as the negative control. All flow cytometry data were collected in triplicates and were processed by FlowJo software.

2.5. Albumin-based polyplexes for the delivery of nucleic acids

2.5.1 Synthesis of PEI-PEG-PEI polymer

The process is described in detail in Section 2.2.1.2.

2.5.2. Preparation of BSA-PEI and BSA-PEI-PEG polymers

BSA-PEI and BSA-PEI-PEG polymers were prepared using glutaraldehyde as reported with some modifications.[1] Briefly, 2 mg BSA in 500 µL distilled water was mixed with 60 µL 2 kDa PEI (1

mg/mL) or PEI-PEG-PEI obtained in Section 2.2.1.2.The conjugation between BSA and PEI/PEI-PEG-PEI was performed using 25% glutaraldehyde as a crosslinker. This conjugation process was carried out at room temperature for 2 h with constant vortexing. After the conjugation, 0.1 mg glycine was added, followed by an additional 1 h of vortexing. To remove the unreacted polymers, BSA and glutaraldehyde, ultracentrifugation with Amicon Ultra-0.5 centrifugal filter units with 50 kDa molecular weight cutoff was carried out. The product was washed 3 times with distilled water before further use.

2.5.3 Amplification of plasmid DNA

Plasmid encoding green fluorescence protein (GFP) was transformed firstly in E. coli to amplify the plasmid DNA. Secondly, it was purified by using MIDI prep purification kit. The concentration of the plasmid thus obtained was measured using Nanodrop Spectrophotometer.

2.5.4. Preparation and characterization of polyplexes

All the prepared BSA-PEI and BSA-PEI-PEG polymers were filtered through sterile 0.45 µm syringe filter before further use. Secondly, different weight ratios of polymers ranging from 10 to 90 µg was incubated with 1 µg of GFP plasmid in 50 µL of water at 37 °C for one hour. Finally, the prepared polyplexes were characterized for size and zeta potential using Dynamic Light Scattering (DLS).

2.5.5. DNA condensation assay of polyplexes

Agarose gel electrophoresis was carried out to evaluate the DNA retardation ability of polyplexes. Aliquots of 15 µL polyplexes, at varying weight ratios, were mixed with 3 µL of Ez-vision dye (a non-mutagenic fluorescent reagent that produces instant visualization of DNA bands upon UV illumination of agarose gels). Agarose gel (1%) was prepared in TAE buffer. The control plasmid and polyplexes with either BSA-PEI or BSA-PEI-PEG polymers at different weight ratios were loaded onto the gel. Electrophoresis was then performed at the constant voltage of 80 V for 1.5 hours in TAE buffer. The bands corresponding to the plasmid were detected under UV light and photographed.

Chapter 3. Albumin-based nanoparticles for the delivery of chemotherapeutics

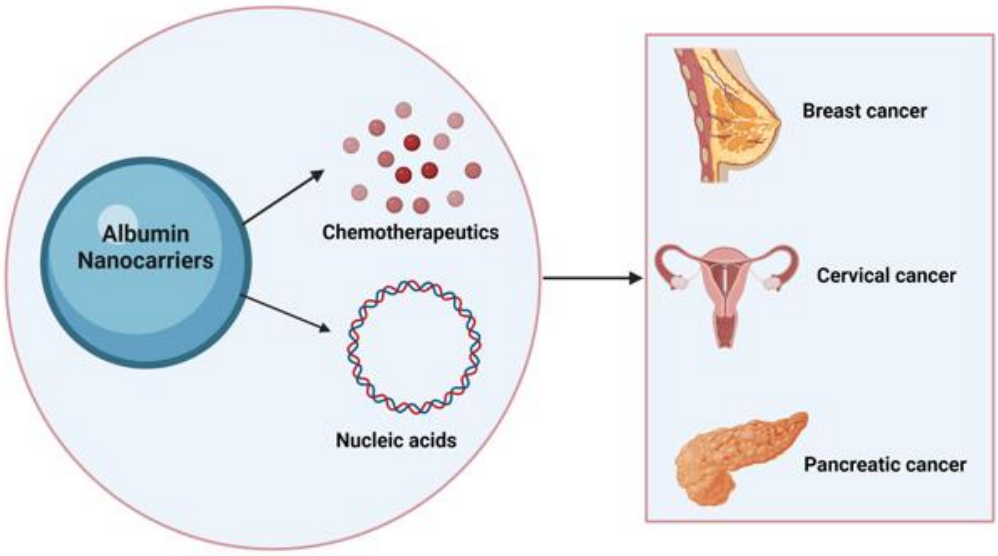

3.1. Albumin nanoparticles for the delivery of chemotherapeutics in breast cancer

3.1.1 Introduction

Breast cancer is a heterogeneous disease with different clinical behaviors, features, risk factors, and pathogenesis. It originates in the terminal duct–lobular unit of the mammary gland.[1] It is the most prevalent type of cancer in women and a common cause of death in women in the age range of 35 to 55.[2] It represents about 25% of all types of cancer in women and 1 in every 8-10 women are diagnosed with breast cancer in their lifetime. Generally, the occurrence of breast cancer increases with age during the reproductive period, however, the occurrence rate is much slower after menopause.[3] The incidence and mortality rate due to breast cancer vary widely around the world. Various factors contribute to breast cancer, including oral contraceptives, high-fat diets, alcohol consumption, smoking, family history for genetic predisposition to cancer, and exposure to ionizing radiation.[3–6]

In terms of the stages, breast cancer is divided into 4 stages from I-IV. Stage I breast cancers are smaller than 2 cm and do not involve the lymph nodes, whereas stage IV breast cancers are distant metastatic cancers.[7] In addition, based on the presence of the molecular markers for estrogen or progesterone receptors and human epidermal growth factor 2 (HER2), breast cancer is further divided into 3 different subtypes, namely, hormone receptor (HR) positive/HER2 negative, HER2 positive, and triple-negative breast cancers.[7]

1. HR +ve/ HER2 –ve breast cancer: It accounts for around 70% of the total breast cancer incidences. In this type of cancer, the estrogen receptor is responsible for the activation of oncogenic growth pathways. It is most prevalent in older women.
2. HER2 +ve breast cancer: The oncogene HER2, a tyrosine kinase receptor in the epidermal growth factor receptor family, is highly active in this type of cancer and accounts for around 15 to 20% of the total breast cancer incidences. The treatment of this cancer type is mostly through HER2 antibodies, including trastuzumab and pertuzumab.[8]
3. Triple-negative breast cancer (TNBC): In this type, the pathological criteria of estrogen, progesterone and HER2 are not met. It accounts for around 15% of total incidences, is highly aggressive, lacks homologous recombination linked to the loss of BRC1 function,

high immune cell infiltration, and has the worst prognosis.[9] Patients with triple-negative breast cancer have high chances of relapse in the first 5 years after diagnosis.

The treatment option varies widely depending on the type and stage of breast cancer. The main goal in non-metastatic breast cancer is to eradicate tumor and prevent the metastatic recurrence, whereas, for metastatic breast cancer, the goal is to prolong the survival of the patient and palliative cure.[7] Chemotherapy is one of the major treatment options for breast cancer, including triple-negative breast cancers. However, due to various shortcomings such as the high side effects, low aqueous solubility and rapid clearance of the drugs, their effective use in the clinical setting is still challenging. To overcome those issues, nanocarriers are being investigated widely, which enable the administration of both hydrophilic and lipophilic drugs without profound toxicities, enhance the targeted delivery of the drugs to tumor sites, increase the bioavailability and efficacy of the administered drugs.

In this chapter, we prepared albumin nanoparticles encapsulating two chemotherapeutics, doxorubicin and SN38 to treat breast cancer. The prepared nanoparticles were characterized, and in-vitro experiments were performed in three different cell lines, namely, MCF-7, MDA-MB-231 and MCF-10A.

3.1.2 Albumin Nanoparticles for the delivery of doxorubicin

Doxorubicin (Dox) is an antineoplastic agent widely used against various cancers, including breast cancer, Kaposi's sarcoma, osteosarcoma, oesophageal carcinoma, and Hodgkin's and non-Hodgkin's lymphomas.[10] It is an anthracycline antibiotic and has been practiced in oncology since the late 1960's. The primary pathway by which doxorubicin imparts anticancer effects is depicted in Figure 14. The mechanism involves the drug's ability to intercalate DNA which causes the breakage of DNA strands and inhibits DNA and RNA synthesis. Similarly, it disrupts topoisomerase-II-enzyme, generates free radicals, damages the cellular membranes, and inhibits the replication and transcription of DNA, leading to cell cycle arrest and apoptosis.[11,12]

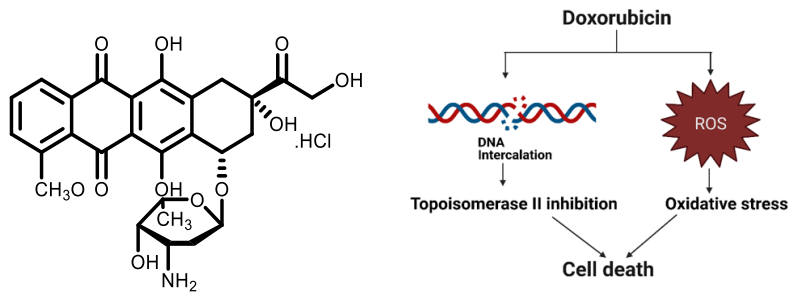

Figure 14. Structure of Doxorubicin (A) and mechanism of action of Doxorubicin (B)

Despite the great potential, the use of Dox is limited because of the increased toxicities, especially cardiotoxicity, mainly in those patients requiring dose escalations.[10,13] To enhance the therapeutic efficacy while decreasing the side effects, Dox was encapsulated in nanoparticles (NPs). In addition, the nanoparticles facilitate the passive tumor targeting through enhanced permeation and retention (EPR) effect and overcome the problems associated with multidrug resistance.[14,15]

In this regard, NPs based on albumin offer various advantages, including biocompatibility, safety, and convenient surface modification due to the presence of carboxylic and amino groups.[16,17] Albumin is the most abundant protein in human blood, with a molecular weight of around 67 kDa and a circulation half-life of approximately 19 days.[17] In the body, it acts as a carrier for various compounds, including bilirubin, metal ions like zinc and copper, and it helps in the solubilization and transportation of hydrophobic long-chain fatty acids.[18,19] The development of albumin-based nanocarriers for drug delivery is interesting because of the various binding sites that facilitate incorporating hydrophilic and hydrophobic drugs in the particle matrix.[20]

The tumoral uptake of albumin is enhanced by various factors, for instance, the higher concentration of albumin in blood than in the interstitial compartments allows the diffusion of albumin to tumor sites.[21,22] Moreover, various albumin receptors, namely, gp60 and SPARC, are overexpressed in cancer cells, which can further enhance the uptake of albumin-based cargos in the cancer sites.[23] For this reason, several approaches explore the use of albumin-based NPs for encapsulating Dox and increase the selective targeting to the tumor sites.[24,25]

Regarding the preparation of this type of nanostructures, various techniques are available, like desolvation, emulsification, nano spray drying, and NAB-technology. Among them, the most widely used method is desolvation using ethanol. In those cases, to increase the stability of the

final nanostructure, a cross-linking agent, such as glutaraldehyde, is usually employed.[26,27] However, the limitations associated with glutaraldehyde, including toxicity, interaction with the encapsulated drug, and presence of residual aldehyde, limit the *in-vivo* applications[28]. Therefore, stabilization strategies for albumin NPs are being searched for.[29,30] For instance, the use of glutathione to reduce the intramolecular disulfide bonds and stabilization of NPs by forming the intermolecular disulfide bonds was reported in previous studies.[28,31] Moreover, the surface of albumin can be modified with Traut's reagent to introduce sulfhydryl groups, which can be further used for the conjugation of other moieties, has also been evaluated.[32]

Breast cancer is one of the most common types of cancer with an increasing incidence. Hormone receptor-positive and human epidermal growth factor receptor 2-negative breast cancer represent the largest subtype of this neoplastic disease.[33] For the treatment of these cancers, in the present study, bovine serum albumin (BSA) nanoparticles (ABNs) were prepared by desolvation method using ethanol. Herein different stabilizing agents were evaluated, such as the cross-linking systems containing a disulfide bond to ease the release of the drugs inside the cells. Thus, the effect of various cross-linkers on drug loading, size, surface charge and nanoparticle yield was studied. Finally, *in-vitro* release studies and cell studies in MCF-7 and MDA-MB-231 breast cancer cells were performed.

3.1.3. Results and discussion

3.1.3.1. Preparation and Characterization of ABNs

For the preparation of ABNs, BSA was incubated with the drug (e.g., Dox) for 2 hours at RT, followed by the addition of ethanol at the rate of 1 mL/minute. The solution turns turbid due to the formation of ABNs, which are stabilized by the addition of cross-linkers. Depending on the cross-linker used, the mixture was incubated at RT for 3 hours to 18 hours. Then the samples were purified by centrifugation (Figure 15 A). In addition, we developed and evaluated different linkers to prepare this type of nanostructure and encapsulate the chemotherapeutic drug Dox (Figure 15 B). In the present study, three approaches have been explored, which can be classified based on the bond generated to stabilize the nanostructure. Particularly, the formation of amide and disulfide bonds was explored. Complementarily, the formation of nanostructures by electrostatic interactions was also studied.

The cross-linking agents employed (Figure 15 B) lead to the different nanostructures of this study. For the ABNs stabilized with amide bonds, EDC or GLU was used. In the case of glutaraldehyde (GLU), the procedure was based on previous studies where ganciclovir was loaded onto ABNs.[34] GLU reacts with the amino groups on the surface of BSA and hence cross-links the BSA molecules with each other. On the other hand, with the use of EDC as a cross-linker, a peptide bond is formed between the carboxyl and amide groups of BSA particles.[35] It is important to note that the preparation time of ABNs was reduced to 3 hours when EDC was used compared to overnight with GLU. Hence, it provides a rapid and straightforward technique for the preparation of ABNs. In the case of nanostructures stabilized by an amide bond (ABN-GLU and ABN-EDC), robust structures are expected, but the release of the chemotherapeutics might be limited.

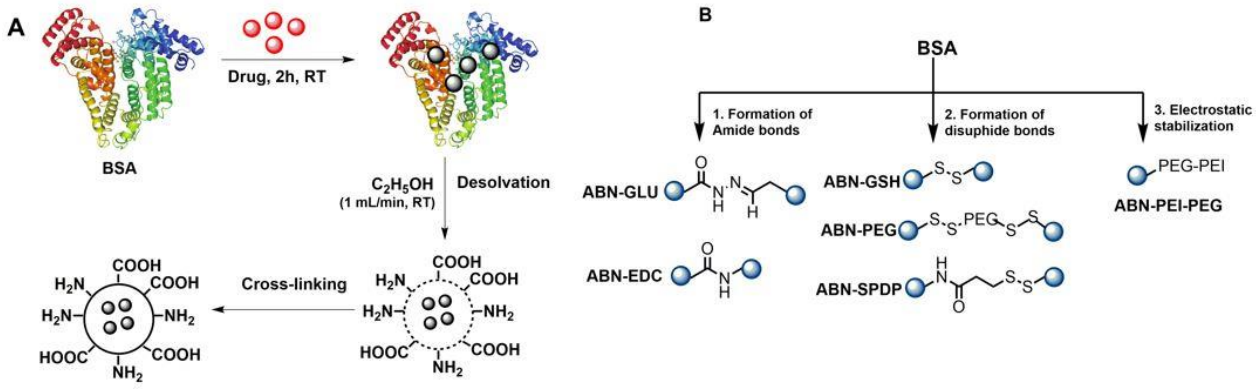

Figure 15. Schematic illustration of the preparation of ABNs. (A) Encapsulating a drug and (B) various approaches for the preparation of ABNs.

Regarding the formation of disulfide bonds, three approaches were assessed. In the first one, BSA was treated with GSH to cleave any possible intramolecular disulfide moiety, followed by a solvation process, where the available thiols could be oxidized to yield the corresponding intermolecular disulfide bonds. In another approach, PEG containing activated disulfide groups was mixed with thiolated BSA to produce the desired ABNs. In the last process involving disulfide bonds, an aqueous solution of BSA was modified with thiols, whereas another solution was treated with SPDP. Thus, the combination of both structures during the solvation process would yield a cross-linked structure due to the formation of disulfide bonds. When disulfide bonds are

used (ABN-GSH, ABN-PEG and ABN-SPDP), the release of the drugs can be promoted by glutathione present in the cells. Lastly, ABNs were also prepared where they were electrostatically stabilized with a tailor-made polymer based on PEI and PEG. These nanoparticles can be disassembled inside the cell due to the pH of lysosomes or ionic strength. In all the ABNs, the optimum concentration of Dox was chosen as 0.5 mg/mL.

The efficiency of the ABNs formulations was evaluated by the Bradford assay. In this case, the binding of the dye (Coomassie Brilliant Blue G-250) to protein causes the shift of maximum absorption of the dye from 465 to 595 nm, which could be used for the quantification of protein.[36] In all the cases, as shown in Figure 16 A, more than 90% of the added BSA was converted to ABNs, except when GSH was used (~75%). Next, the Dox encapsulated in each case was quantified using a UV-Vis spectrophotometer. In this regard, it is known that a variety of factors like the amount of drug added, type and amount of cross-linker used, and pH might affect the drug encapsulation.[25] In the present study, we focused on the effect of the different cross-linkers used to prepare ABNs on Dox loading. Particularly, the highest drug encapsulation (55%) was obtained using glutaraldehyde (GLU) as a cross-linker. On the other hand, when PEI-PEG was used to promote the formation of the nanostructure, the drug loading was the lowest (21%) (Figure 16 B).

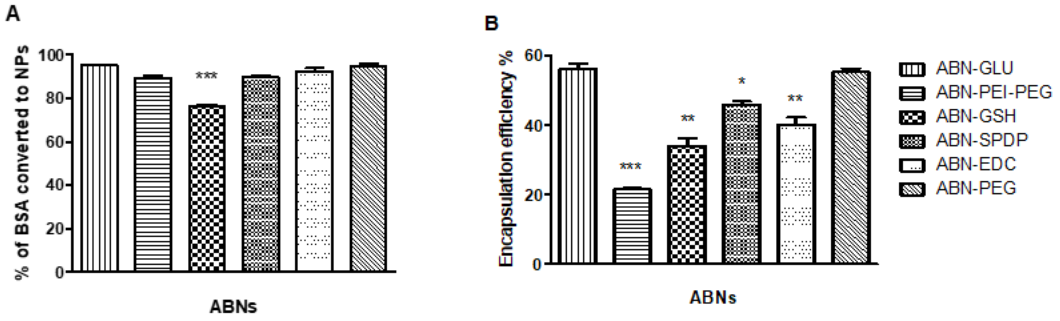

Figure 16. (A) Percentage of BSA converted to ABNs measured by Bradford assay and (B) Encapsulation efficiency of Dox in ABNs using various cross-linkers. Statistical analysis was performed using one-way ANOVA Tukey's test. * p-value < 0.01, ** p-value < 0.001, and *** p-value < 0.0001.

3.2.2.1. Size and Surface Charge Characterization of ABNs

It is important to gain insight into the size and surface charge characteristics of the prepared nanoparticles as they affect the colloidal stability, the nanoparticle cellular uptake, the pharmacokinetics, and the biodistribution after administration.[37–39] Moreover, the size of NPs plays a vital role in determining the fate inside biological systems. It has been observed that the NPs smaller than 6 nm are rapidly excreted by the kidney while those larger than 200 nm are accumulated in the spleen and liver[40]. In this sense, the ABN-SPDP with a size of around 156 nm measured by DLS (Figure 17 A), are optimal compared to other ABNs with sizes > 200 nm. The size analysis revealed that ABN-SPDP had the smallest size of 156 ± 1.5 nm, PDI of 0.09, whereas ABN-GSH had the largest size of 315 ± 4 nm, PDI of 0.7 (Figure 17 A).

It was also found that the surface charge of nanoparticles could play an essential role in modulating the biodistribution and their cellular uptake and translocation[41]. As expected, the ABNs with PEI-PEG polymer had a positive surface charge (+15.4 ± 0.4mV). All the other ABNs demonstrated the negative surface charge ranging from -24 ± 1.1 mV for ABN-EDC to -36.9 ± 0.3 mV for ABN-GLU. The nanoparticles prepared with SPDP as cross-linker were further analysed by SEM for morphology. These nanoparticles had a nanometric size and spherical morphology (Figure 17 C). Based on the results from the drug loading, percentage of albumin converted to the NPs and size characterization, the ABNs prepared with PEI-PEG and GSH were ruled out for further evaluation. Additionally, the ABNs prepared with PEG were also discarded since they were not stable for more than a week despite showing promising encapsulation efficiency of approximately 55%.

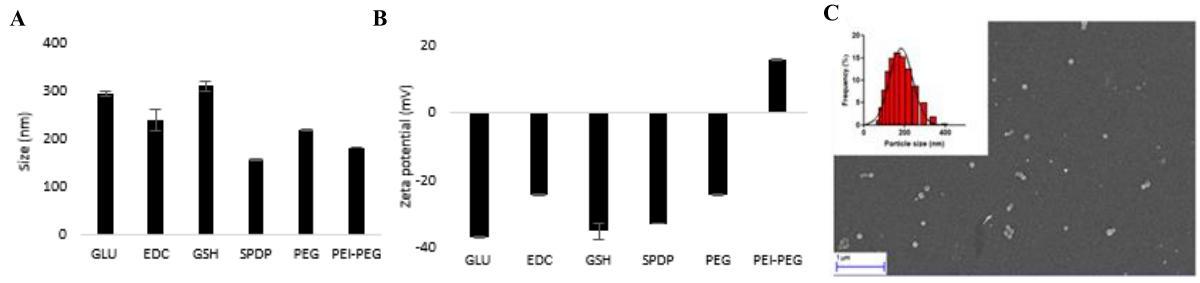

Figure 17. Size (A) and zeta potential (B) of Dox-loaded ABNs with various cross-linking methods; Size distribution of Dox-loaded ABN-SPDP observed with DLS and SEM (C).

3.2.2.2. In Vitro Release of Dox from ABNs

For enhanced drug efficacy and specificity, the nanoparticles that can respond to particular conditions in the tumor cells, like changes in pH, enzyme activity profile or redox state, are of great interest.[42] In this regard, pH-triggered drug release systems could be employed to increase the selectivity to cancer cells since the extracellular microenvironment of tumor cells has acidic pH of around 5.5-6.5 compared to healthy cells with a pH of 7.4.[43,44] This difference in pH of the target site may facilitate the specific drug targeting to the tumor sites. Moreover, solid tumors have elevated levels of glutathione (GSH), which can also be exploited to trigger the release of anticancer drugs.[45–48] In this regard, the disulfide bonds within the nanoparticles can be cleaved in the presence of GSH, enhancing the release of the drug.[49]

Hence, the effect of using different cross-linkers on the release of encapsulated Dox was thus studied at acidic pH of 5 and/or in the presence of glutathione at different time points. As shown in Figure 18, approximately 56% of encapsulated Dox was released from ABN-SPDP after 72 hours, whereas only around 26% was released from ABN-GLU. The release of Dox from ABN-EDC at the acidic pH was around 46% after 72 hours. Moreover, the release of the drug was enhanced by the use of 1 mM GSH in the case of ABN-SPDP. However, the release was not affected in ABNs with glutaraldehyde and EDC. The release of Dox from ABN-SPDP was highest in tumor mimicked environments, i.e., with acidic pH and in the presence of glutathione (Figure 18 C). This is because the ABNs are cross-linked with the disulfide bridges and hence the higher concentration of GSH in the tumor cells causes destabilization of ABNs, leading to a higher release of drug. However, the use of GLU results in the ABNs with a compact cross-linked matrix with smaller pores for drug diffusion that leads to lower drug release (Figure 18 A).[25]

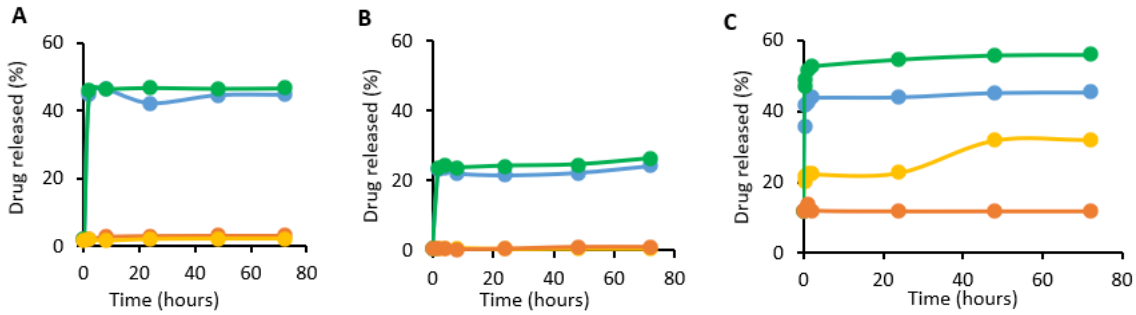

Figure 18. Release of Dox from ABNs with EDC (A), Glutaraldehyde (B), and SPDP (C) at different time points. The conditions tested were pH 5 (blue), GSH 1 mM (yellow), pH 5 and GSH 1 mM (green), and pH 7 with GSH 1 µM (orange).

3.1.3.4. Cell Viability Studies

The cell viability of MCF-7 cells 24- and 48-hours post-treatment with ABNs was carried out using the alamarBlue assay. All the ABNs without Dox showed more than 95% cell viability, which indicates the possible use of these systems to deliver Dox to the tumor sites. When Dox-loaded ABNs were used, the highest number of cells were killed when ABN-SPDP were used which was comparable to the free drug, followed by ABN-PEG, ABN-GLU, ABN-EDC, ABN-PEI-PEG and ABN-GSH, respectively (Figure 19).

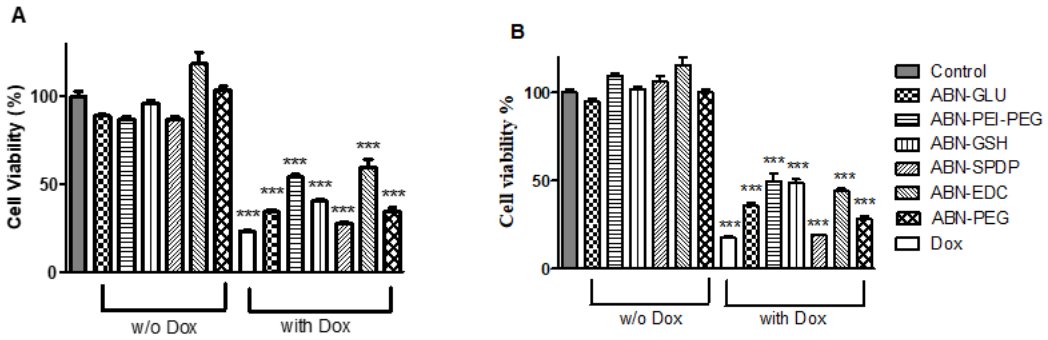

Figure 19. Cell viability assay of Dox-loaded ABNs with different cross-linkers in MCF-7 cells after 48 h (A) and 72 h (B) of treatment. In all the cases, the concentration of Dox used was 1 µM; 2–6: ABNs without Dox and 8–12: ABNs with Dox. Statistical analysis was performed using one-way ANOVA Tukey's test. * p-value < 0.01, ** p-value < 0.001, and *** p-value < 0.0001.

Based on these results, SPDP was selected as an optimum cross-linker to produce ABNs encapsulating doxorubicin. The findings support the idea that SPDP can be used as a cross-linking agent, which can serve as a possible alternative method to toxic glutaraldehyde. Furthermore, to assess the scope of the approach, a different type of drug was also evaluated. In this case, the hydrophobic drug SN38 (7-ethyl-10-hydroxycamptothecin) was used which is a camptothecin analog and inhibits topoisomerase I (TOP1), resulting in DNA breaks and apoptosis. Despite the fact that it shows enhanced anti-cancer activity, its use is limited because of its low aqueous solubility and stability at higher pH. Hence SN38 was encapsulated in ABN-SPDP, and the efficacy was analyzed in breast cancer cell lines.The drug concentration of up to 2 mg/mL could be loaded in these ABNs (encapsulation efficiency of 58.1 ± 4.2%), which resulted in the particles with the size of 215.1 ± 7.3 nm and zeta potential of -25.5 ± 1.6 mV. The ABNs resulted in the reduction of cell viability to approximately 25% and 23% in MCF-7 and MDA-MB-231 cells, respectively 48 hours post-treatment (Figure 20). Thus, these results confirm the potential of the approach for the encapsulation, delivery, and controlled release of hydrophobic and hydrophilic drugs such as SN38 and DOX, respectively.

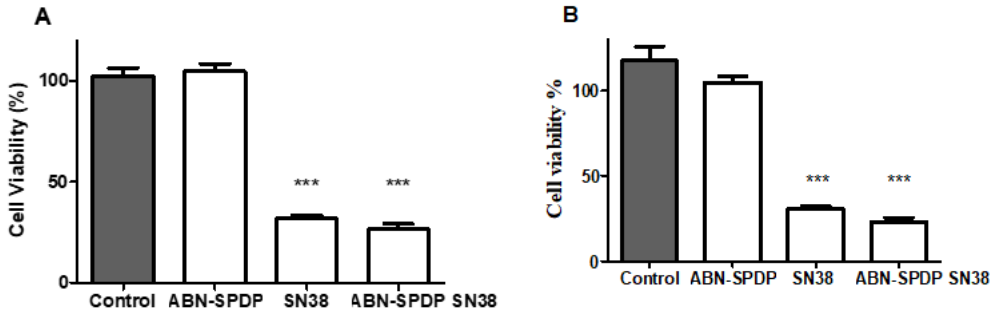

Figure 20. Cell viability assay with SN38 loaded ABN-SPDP in (A) MCF-7 and (B) MDA-MB-231 cells 48 hours post-treatment. Statistical analysis was performed using one-way ANOVA Tukey's test (*** p-value < 0.0001).

3.1.3.5. Stability Studies

The long-term colloidal stability of the nanoparticles was evaluated since it could be critical for future applications. Thus, ABN-SPDP were stored either at room temperature or at 4 ℃. The size distribution and surface potential of these nanoparticles were measured every week for 2 months. As seen in the Figure 21 A-C, the nanoparticles demonstrated constant size, surface

charge and drug release at both temperatures during the period of the study. These results suggest that the nanoaprticles are stable and maintained colloidal stability irrespective of the storage temperature. The great stability observed can be due to the repulsive forces between the particles, which might reduce the particle collisions and hence prevent particle aggregation.[50]

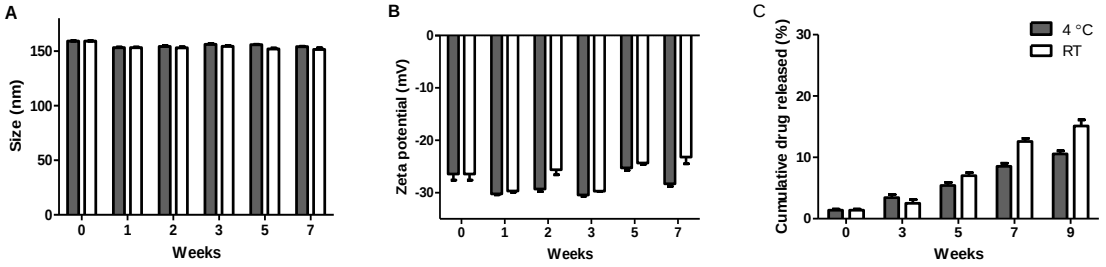

Figure 21. Change in size (A), zeta potential (B), and drug release (C) of Dox-loaded ABN-SPDP at different time points at two different temperature conditions, 4 °C (gray) and RT (white). Till the end of 2 months, the ABN-SPDP were stable. The data are presented as mean ± standard deviation (SD).

3.1.3.6. Cell Studies

The internalization of Dox-loaded ABN-SPDP was investigated in MCF-7 and MDA-MB-231 human breast cancer cells. The fluorescence of free Dox and encapsulated in ABN-SPDP was similar in both the cell lines (>98%) (Figure 22).

A

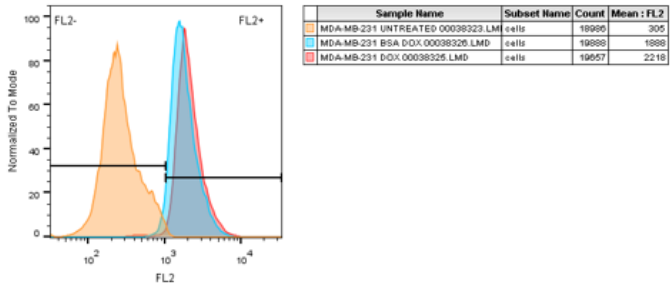

Sample Name	Subset Name	Count	Mean : FL2
MDA-MB-231 UNTREATED 00038323.LMD	cells	19986	305
MDA-MB-231 BSA DOX 00038326.LMD	cells	19888	1888
MDA-MB-231 DOX 00038325.LMD	cells	19657	2218

B

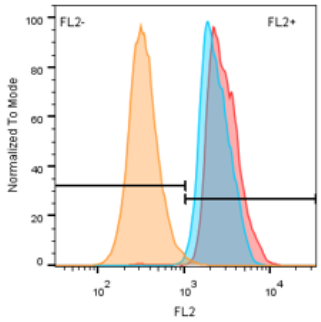

Sample Name	Subset Name	Count	Mean : FL2
MCF-7 UNTREATED 00038319.LMD	Ungated	27646	368
MCF-7 BSA DOX 00038322.LMD	cells	20601	2430
MCF-7 DOX 00038320.LMD	cells	22799	3038

Figure 22. Quantification of fluorescence of Dox using flow cytometry in MDA-MB-231 (A) and MCF-7 (B) cells 24 hours post-treatment.

Those ABNs were further tested in various cell lines (MCF-7, MDA-MB-231 and MCF-10 A). As shown in the Figure 23 A-C, the ABN-SPDP were not toxic in any cell line. The cell viability was significantly decreased when free Dox or Dox-loaded ABN-SPDP were used in MCF-7 and MDA-MB-231 cells. It is to be noted that when free Dox was administered in non-tumoral MCF-10 A cells, it was highly toxic, resulting in cell viability of around 20%. Remarkably, the cell viability when Dox-loaded in ABN-SPDP was administered was not significantly different from the untreated ones (Figure 23 C). This can be attributed to the fact that the release of drug from the ABNs employed is triggered by the acidic conditions and presence of glutathione which is favourable only in the tumor cells and not in the non-tumoral mammary epithelial cells (MCF-10A). Hence, these formulations could reduce the toxicity problems associated with the delivery of Dox and could revolutionize the treatment option in breast cancer therapy.

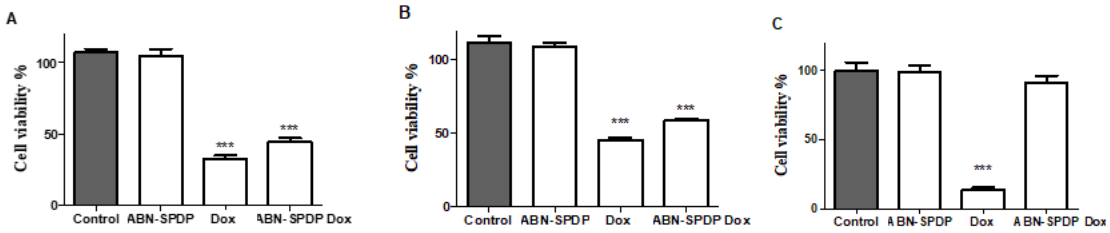

Figure 23. Cell viability assay with Dox-loaded ABN-SPDP 48 h post-treatment in (A) MCF-7 cells, (B) MDA-MB-231, and (C) MCF-10 A. In all the cases, the concentration of Dox used was 2 µM. Statistical analysis was performed using one-way ANOVA Tukey's test (*** p-value < 0.0001).

3.1.3.7. Effect on Apoptosis/Necrosis of the Cells

Furthermore, it was of interest to study the mechanism by which Dox affects the cells. Hence, a study was conducted to verify the effect of Dox-loaded ABN-SPDP in the apoptosis/necrosis of MCF-7 and MDA-MB-231 cells. As shown in Table 2, the percentage of healthy cells decreased in a dose-dependent manner in both the cell lines when treated with 1 µM, 2 µM, and 4 µM Dox-loaded ABN-SPDP. There was an increase in apoptotic cells by 1.43, 1.8, and 2.13 folds when MCF-7 cells were treated with 1 µM, 2 µM, and 4 µM Dox-loaded ABN-SPDP, respectively. Moreover, the percentage of necrotic cells also increased from 17.45% to 24.05% when the concentration of Dox-loaded ABN-SPDP was increased from 1 µM to 4 µM. A similar result was obtained with MDA-MB-231 cells. The percentage of apoptotic cells increased by 5.7, 6.9, and 7.5% when treated with 1 µM, 2 µM, and 4 µM Dox-loaded ABN-SPDP, respectively. Moreover, the necrotic cells increased to 33.9% when treated with 4 µM Dox-loaded ABN-SPDP. Hence, Dox is found to induce apoptosis and necrosis in both MCF-7 and MDA-MB-231 cell lines irrespective of the receptor present. We also observed that both free Dox and encapsulated in ABN-SPDP showed a similar trend in cell apoptosis and necrosis in both the cell lines (Table 2).

	MCF-7			MDA-MB-231		
	Healthy Cells	Apoptotic Cells	Necrotic Cells	Healthy Cells	Apoptotic Cells	Necrotic Cells
Control	99.45 ± 0.45	0.15 ± 0.05	0.10 ± 0.10	99.75 ± 0.15	0.2 ± 0.10	0.05 ± 0.10
ABNs	95.15 ± 0.85	1.40 ± 0.10	4.00 ± 0.20	95.75 ± 3.15	1.15 ± 0.15	3.65 ± 0.25
Dox alone 2 µM	55.45 ± 0.85	3.70 ± 0.20	18.40 ± 0.10	72.00 ± 0.50	6.20 ± 0.10	12.95 ± 0.35
ABN-SPDP Dox 1 µM	65.70 ± 0.40	2.15 ± 0.15	17.45 ± 1.05	69.20 ± 0.51	5.65 ± 0.05	14.80 ± 0.10
ABN-SPDP Dox 2 µM	60.90 ± 0.40	2.70 ± 0.10	20.90 ± 3.80	63.80 ± 0.48	7.15 ± 0.25	21.00 ± 0.30
ABN-SPDP Dox 4 µM	50.95 ± 6.35	3.20 ± 1.00	24.05 ± 4.65	44.50 ± 2.48	7.30 ± 0.20	33.90 ± 0.40

Table 2. Percentage of healthy, necrotic, and apoptotic cells with varying concentrations of Dox-loaded ABN-SPDP 24 h post-treatment in MCF-7 and MDA-MB-231 cells.

3.1.3.8. Determination of Dominant Cell Cycle Phase

The cell cycle assay was carried out to detect the dominant cell cycle phase in MCF-7 and MDA-MB-231 cells. As shown in Figure 24, when MCF-7 cells were treated with 1 µM Dox alone or with Dox-loaded ABN-SPDP, the cells in cell cycle arrest (G0/G1) increased by 1.37 and 1.17 folds, respectively compared to the empty ABNs, whereas G2/M phase cells elevated by 1.11 and 1.52 folds. On the other hand, when MDA-MB-231 cells were treated with 1 µM Dox or Dox-loaded ABN-SPDP, the number of cells in G2/M phase increased by 1.59 and 1.63 folds, respectively, compared to the empty ABN-SPDP. The cycle arrest was evident in both G0/G1 and G2/M phases in MCF-7 cells, while it was most prominent in G2/M phase in MDA-MB-231 cells. Oncul and co-workers obtained similar results when Dox was used in MCF-7 and MDA-MB-231 cells to study multidrug resistance and apoptosis.[51] This differential effects in two breast cancer cell lines can be attributed to the variation in the p53 activity in the two cell lines. MCF-7, an estrogen-dependent cell line with the wild-type p53 gene, whereas MDA-MB-231, an estrogen-independent cell line, has p53 mutated and inactive.[52,53] The active P53 in MCF-7 cells after

DNA damage mediated by Dox treatment can induce p21 upregulation responsible for cell cycle arrest in G0/G1 phase. In contrast, p53 levels in MDA-MB-231 cells are not affected by Dox treatment and hence p21 levels do not change significantly and therefore induces the cell cycle arrest in G2/M phase.[52]

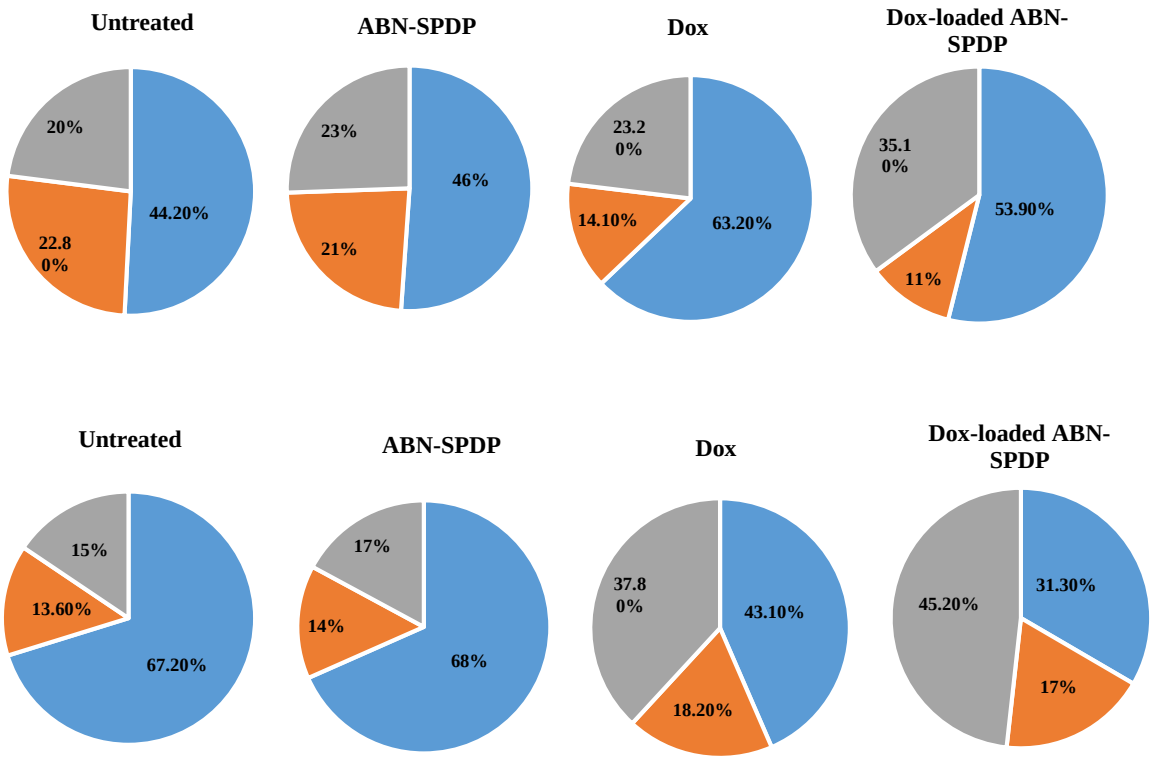

Figure 24. Percentage of cells in different phases of the cell cycle in MCF-7 cells (upper lane) and MDA-MB-231 cells (lower lane). The concentration of Dox used was 1 µM. The cells without any treatment and treated with ABN-SPDP were used as controls. Blue: cells in G0/G1 phase; orange: cells in S phase; grey: cells in G2/M phase.

3.1.3.9. Western Blot Analysis

Western blot assay was performed to assess the effect of free Dox and Dox-loaded ABN-SPDP on the expression of various proteins, namely, P53, cyclin B, and cyclin E. In the experiments, GAPDH with the molecular weight of 36 kDa was used as a control to assess the amount of protein loaded in each lane. As demonstrated in Figure 25, the levels of P53 were enhanced in MCF-7 cells when treated with free Dox or ABN-SPDP loaded with Dox. However, no change was observed in MDA-

MB-231 cells. This varying P53 activity in two breast cancer cell lines is attributed to the difference in cell cycle arrest phases by Dox, which was demonstrated by the levels of cyclins involved in cell cycles. The level of cyclin E, responsible for the cell cycle arrest in G0/G1 phase, was significantly enhanced in MCF-7 cells, while it was unchanged in MDA-MB-231 cells. However, the level of cyclin B, indicative of the cell cycle arrest in G2/M phase, was enhanced in both cell lines, most prominently in MDA-MB-231 cells, when treated with Dox-loaded ABN-SPDP. Hence, these results are in accordance with the observations from flow cytometry studies.

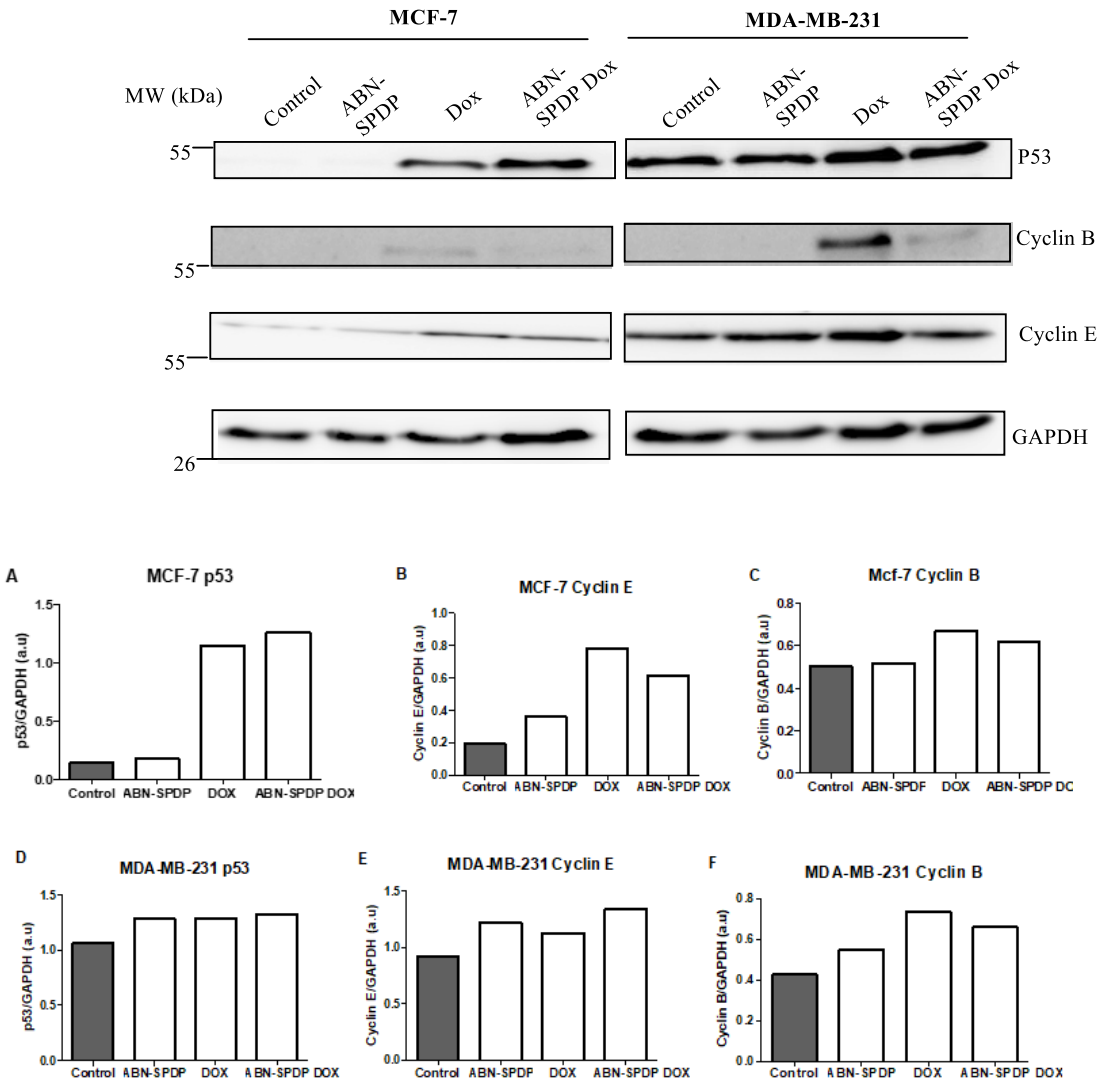

Figure 25. Western blot assay to assess the effect of Dox-loaded ABN-SPDP on the expression of P53 and cyclins in MCF-7 and MDA-MB-231 cells.

3.1.3.10. Determination of the Mechanism of Internalization of NPs

There are various pathways through which cells can uptake the nanoparticles, including clathrin-mediated endocytosis; caveolae-mediated endocytosis; and clathrin- and caveolae-independent pathways. In the present study, the intracellular trafficking of Dox-loaded ABN-SPDP was investigated using genistein or filipin (caveolae-mediated endocytosis inhibitors) or chlorpromazine (clathrin-mediated endocytosis inhibitor), and cell viability was measured after 24 h of treatment. As shown in Figure 26, the cell viability in MCF-7 cells was increased from 66% with Dox-loaded ABN-SPDP in the absence of any endocytosis inhibitors to 81% with genistein, 85% with filipin, and 72% with chlorpromazine. The obtained results indicate that the ABNs are internalized by both endocytotic pathways, with caveolae playing a more prominent role. These results are in agreement with a previous report where human serum albumin nanoparticles were used for gene delivery.[26]

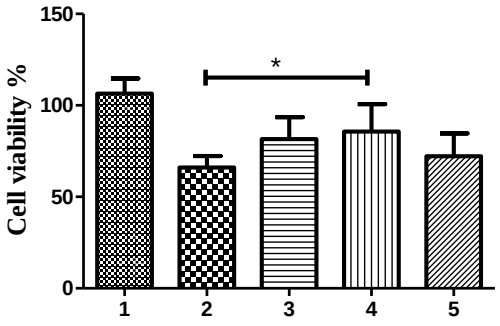

Figure 26. Cell viability assay with Dox-loaded ABN-SPDP in the presence of endocytosis inhibitors 24 h post-treatment in MCF-7 cells. 1: control, 2: ABN-SPDP Dox without endocytosis inhibitors, 3: in the presence of genistein, 4: filipin, and 5: chlorpromazine. Statistical analysis was performed using one-way ANOVA Tukey's test (*p-value < 0.05).

3.1.3.11. Use of HSA for the preparation of NPs

Finally, the feasibility of this approach for the preparation of nanostructures based on Human serum albumin (HSA) was studied, which might be required for the clinical translation. HSA is particularly useful to avoid any immunological response in studies involving humans.[54] Remarkably, HSA NPs prepared behaved similarly to ABN-SPDP with a similar size and zeta potential of 161.3 ± 4.6 nm and -31.2 ± 3.2 mV, respectively. Interestingly, the encapsulation

efficiency of Dox was increased to 62.9% when HSA was used instead of BSA. The in-vitro studies conducted in MCF-7 and MDA-MB-231 cells revealed improved activity in both the cell lines. The cell viability was reduced to 37% and 51%, respectively in MCF-7 and MDA-MB-231 cells when treated with Dox-loaded HSA NPs (Figure 27). Moreover, the cell cycle analysis in both the cell lines revealed elevated cell cycle arrest in G2/M phase (Figure 28). All these results obtained with HSA highlight the potential clinical translation of these nanocarrier systems.

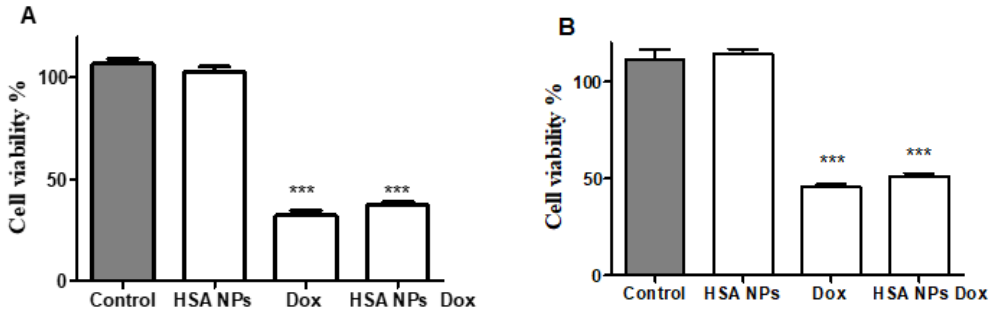

Figure 27. Cell viability assay with Dox-loaded HSA NPs in (A) MCF-7 and (B) MDA-MB-231 cells 48 hours post-treatment. Statistical analysis was performed using one-way ANOVA Tukey's test (*** p-value < 0.0001).

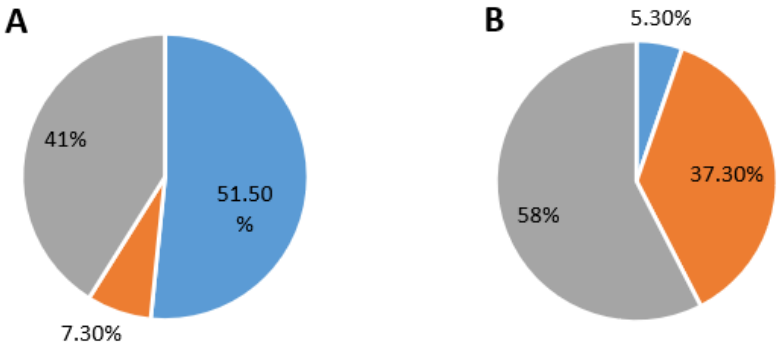

Figure 28. Percentage of cells in different phases of the cell cycle in (A) MCF-7 and (B) MDA-MB-231 cells treated with Dox-loaded HSA NPs. Blue: cells in G0/G1 phase; orange: cells in S phase; grey: cells in G2/M phase.

3.1.4. Conclusions

In the present study, different cross-linking processes were employed to prepare ABNs loaded with Dox to improve encapsulation efficiency, the in-vitro release of the drug, and enhancement of activity in the selected cell lines. When SPDP was used as a cross-linker, the release of drug

from ABNs was enhanced, demonstrated by in-vitro release in an acidic environment and in the presence of glutathione, and the activity in two cell lines, MCF-7 and MDA-MB-231. Interestingly, the NPs could target only the tumor cells and spared non-tumoral cells, demonstrated by the experiments in MCF-10A epithelial mammary cells.

The results presented here contribute to the fundamental understanding of the preparation of the optimum ABNs for encapsulation of the anticancer drug Dox. Moreover, this approach could be successfully used for the preparation of HSA NPs, which can ease the translation of this system to clinics. These experimental findings could guide the development of advanced cancer nanostructures for targeted delivery.

References

1. Weigelt, B.; Geyer, F.C.; Reis-Filho, J.S. Histological types of breast cancer: How special are they? *Mol. Oncol.* **2010**, *4*, 192–208, doi:10.1016/j.molonc.2010.04.004.

2. Harbeck, N.; Salem, M.; Nitz, U.; Gluz, O.; Liedtke, C. Personalized treatment of early-stage breast cancer: Present concepts and future directions. *Cancer Treat. Rev.* **2010**, *36*, 584–594, doi:10.1016/j.ctrv.2010.04.007.

3. Key, T.J.; Verkasalo, P.K.; Banks, E. Epidemiology of breast cancer. *Oncology* **2001**, *2*, 133–140, doi:10.1016/j.molcel.2019.06.002.

4. Smith-Warner, S.A.; Spiegelman, D.; Yaun, S.S.; Van Den Brandt, P.A.; Folsom, A.R.; Goldbohm, R.A.; Graham, S.; Holmberg, L.; Howe, G.R.; Marshall, J.R.; et al. Alcohol and breast cancer in women. *J. Am. Med. Assoc.* **1998**, *279*, 535–540, doi:10.1001/jama.279.7.535.

5. Calle, E.E.; Heath, C.W.; Miracle-McMahill, H.L.; Coates, R.J.; Liff, J.M.; Franceschi, S.; Talamini, R.; Chantarakul, N.; Koetsawang, S.; RachawatRachawat, D.; et al. Breast cancer and hormonal contraceptives: Collaborative reanalysis of individual data on 53 297 women with breast cancer and 100 239 women without breast cancer from 54 epidemiological studies. *Lancet* **1996**, *347*, 1713–1727, doi:10.1016/S0140-6736(96)90806-5.

6. Boice, J.; Land, C.; Preston, D. Ionizing radiation. *Cancer Epidemiol. Prev.* **1996**, 319–354.

7. Waks, A.G.; Winer, E.P. Breast Cancer Treatment. *JAMA - J. Am. Med. Assoc.* **2019**, *321*, 288–300, doi:10.1001/jama.2018.19323.

8. Piccart-Gebhart, M.J.; Procter, M.; Leyland-Jones, B.; Goldhirsch, A.; Untch, M.; Smith, I.; Gianni, L.; Baselga, J.; Bell, R.; Jackisch, C.; et al. Trastuzumab after Adjuvant Chemotherapy in HER2-Positive Breast Cancer. *N. Engl. J. Med.* **2005**, *353*, 1659–1672.

9. Denkert, C.; Liedtke, C.; Tutt, A.; von Minckwitz, G. Molecular alterations in triple-negative breast cancer—the road to new treatment strategies. *Lancet* **2017**, *389*, 2430–2442, doi:10.1016/S0140-6736(16)32454-0.

10. Singal, P.K.; Iliskovic, N. Doxorubicin-induced cardiomyopathy. *N. Engl. J. Med.* **1998**, *339*, 900–905.

11. Lv, L.; An, X.; Li, H.; Ma, L. Effect of miR-155 knockdown on the reversal of doxorubicin resistance in human lung cancer A549/dox cells. *Oncol. Lett.* **2016**, *11*, 1161–1166, doi:10.3892/ol.2015.3995.

12. Thorn, C.F.; Oshiro, C.; Marsh, S.; Hernandez-Boussard, T.; McLeod, H.; Klein, T.E.; Altman, R.B. Doxorubicin pathways. *Pharmacogenet. Genomics* **2011**, *21*, 440–446, doi:10.1097/fpc.0b013e32833ffb56.

13. Rivankar, S. An overview of doxorubicin formulations in cancer therapy. *J. Cancer Res. Ther.* **2014**, *10*, 853–858, doi:10.4103/0973-1482.139267.

14. Shi, Y.; van der Meel, R.; Chen, X.; Lammers, T. The EPR effect and beyond: Strategies to improve tumor targeting and cancer nanomedicine treatment efficacy. *Theranostics* **2020**, *10*, 7921–7924, doi:10.7150/thno.49577.

15. Kalyane, D.; Raval, N.; Maheshwari, R.; Tambe, V.; Kalia, K.; Tekade, R.K. Employment of enhanced permeability and retention effect (EPR): Nanoparticle-based precision tools for targeting of therapeutic and diagnostic agent in cancer. *Mater. Sci. Eng. C* **2019**, *98*, 1252–1276, doi:10.1016/j.msec.2019.01.066.

16. Hoogenboezem, E.N.; Duvall, C.L. Harnessing albumin as a carrier for cancer therapies. *Adv. Drug Deliv. Rev.* **2018**, *130*, 73–89, doi:10.1016/j.addr.2018.07.011.

17. Larsen, M.T.; Kuhlmann, M.; Hvam, M.L.; Howard, K.A. Albumin-based drug delivery : harnessing nature to cure disease. *Mol. Cell. Ther.* **2016**, *4*, 1–12, doi:10.1186/s40591-016-0048-8.

18. Curry, S.; Mandelkow, H.; Brick, P.; Franks, N. Crystal structure of human serum albumin complexed with fatty acid reveals an asymmetric distribution of binding sites. *Nat. Struct. Biol.* **1998**, *5*, 827–835.

19. Kragh-Hansen, U. Molecular Aspects of Ligand binding to serum albumin. *Pharmacol. Rev.* **1981**, *33*, 17–53.

20. Patil, G. V. Biopolymer albumin for diagnosis and in drug delivery. *Drug Dev. Res.* **2003**, *58*, 219–247, doi:10.1002/ddr.10157.

21. Evans, T.W. Review article : albumin as a drug — biological effects of albumin unrelated to oncotic pressure. *Aliment Pharmacol Ther* **2002**, *16*, 6–11, doi:10.1046/j.1365-2036.2002.00190.x.

22. Kratz, F. Albumin, a versatile carrier in oncology. *Int J Clin Pharmacol Ther* **2010**, *48*, 453–455.

23. An, F.; Zhang, X. Strategies for Preparing Albumin-based Nanoparticles for Multifunctional Bioimaging and Drug Delivery. *Theranostics* **2017**, *7*, 3667–3689, doi:10.7150/thno.19365.

24. Onafuye, H.; Pieper, S.; Mulac, D.; Cinatl, J.; Wass, M.N.; Langer, K.; Michaelis, M. Doxorubicin-loaded human serum albumin nanoparticles overcome transporter-mediated drug resistance. *Beilstein J Nanotechnol. 2* **2019**, *10*, 1707–1715.

25. Dreis, S.; Rothweiler, F.; Michaelis, M.; Cinatl, J.; Kreuter, J.; Langer, K. Preparation, characterisation and maintenance of drug efficacy of doxorubicin-loaded human serum albumin (HSA) nanoparticles. *Int. J. Pharm.* **2007**, *341*, 207–214, doi:10.1016/j.ijpharm.2007.03.036.

26. Mo, Y.; Barnett, M.E.; Takemoto, D.; Davidson, H.; Kompella, U.B. Human serum albumin nanoparticles for efficient delivery of Cu , Zn superoxide dismutase gene. *Mol. Vis.* **2007**, *13*, 746–757.

27. Wagh, J.; Patel, K.J.; Soni, P.; Desai, K.; Upadhyay, P.; Soni, H.P. Transfecting pDNA to E.

coli DH5α using bovine serum albumin nanoparticles as a delivery vehicle. *jounal Biol. Chem. Lumin.* **2015**, *30*, 583–591, doi:10.1002/bio.2789.

28. Wang, W.; Huang, Y.; Zhao, S.; Shao, T.; Cheng, Y. Human serum albumin (HSA) nanoparticles stabilized with intermolecular disulfide bonds. *Chem. Commun.* **2013**, *49*, 2234–2236, doi:10.1039/c3cc38397k.

29. Niknejad, H.; Mahmoudzadeh, R. Comparison of different crosslinking methods for preparation of docetaxel-loaded albumin nanoparticles. *Iran. J. Pharm. Res.* **2015**, *14*, 385–394, doi:10.22037/ijpr.2015.1639.

30. Amighi, F.; Emam-Djomeh, Z.; Labbafi-Mazraeh-Shahi, M. Effect of different cross-linking agents on the preparation of bovine serum albumin nanoparticles. *J. Iran. Chem. Soc.* 2020, *17*, 1223–1235.

31. Zhao, S.; Wang, W.; Huang, Y.; Fu, Y.; Cheng, Y. Paclitaxel loaded human serum albumin nanoparticles stabilized with intermolecular disulfide bonds. *Medchemcomm* **2014**, *5*, 1658–1663, doi:10.1039/c4md00200h.

32. Weber, C.; Reiss, S.; Langer, K. Preparation of surface modified protein nanoparticles by introduction of sulfhydryl groups. *Int. J. Pharm.* **2000**, *211*, 67–78, doi:10.1016/S0378-5173(00)00590-1.

33. Silvestri, M.; Cristaudo, A.; Morrone, A.; Messina, C.; Bennardo, L.; Nisticò, S.P.; Mariano, M.; Cameli, N. Emerging Skin Toxicities in Patients with Breast Cancer Treated with New Cyclin-Dependent Kinase 4/6 Inhibitors: A Systematic Review. *Drug Saf.* **2021**, doi:10.1007/s40264-021-01071-1.

34. Merodio, M.; Arnedo, A.; Renedo, M.J.; Irache, J.M. Ganciclovir-loaded albumin nanoparticles: Characterization and in vitro release properties. *Eur. J. Pharm. Sci.* **2001**, *12*, 251–259, doi:10.1016/S0928-0987(00)00169-X.

35. Jahanban-Esfahlan, A.; Dastmalchi, S.; Davaran, S. A simple improved desolvation method for the rapid preparation of albumin nanoparticles. *Int. J. Biol. Macromol.* **2016**, *91*, 703–709, doi:10.1016/j.ijbiomac.2016.05.032.

36. M.Bradford, M. A rapid and sensitive method for the quantitation of microgram quantities of protein utilizing the principle of protein-dye binding. *Anal. Biochem.* **1976**, *72*, 248–254.

37. Jiang, J.; Oberdörster, G.; Biswas, P. Characterization of size, surface charge, and agglomeration state of nanoparticle dispersions for toxicological studies. *J. Nanoparticle Res.* **2009**, *11*, 77–89, doi:10.1007/s11051-008-9446-4.

38. Borm, P.J.A.; Robbins, D.; Haubold, S.; Kuhlbusch, T.; Fissan, H.; Donaldson, K.; Schins, R.; Stone, V.; Kreyling, W.; Lademann, J.; et al. The potential risks of nanomaterials: A review carried out for ECETOC. *Part. Fibre Toxicol.* **2006**, *3*, 1–35, doi:10.1186/1743-8977-3-11.

39. Renwick, L.C.; Donaldson, K.; Clouter, A. Impairment of alveolar macrophage phagocytosis by ultrafine particles. *Toxicol. Appl. Pharmacol.* **2001**, *172*, 119–127,

doi:10.1006/taap.2001.9128.

40. Albanese, A.; Tang, P.S.; Chan, W.C.W. The effect of nanoparticle size, shape, and surface chemistry on biological systems. *Annu. Rev. Biomed. Eng.* **2012**, *14*, 1–16, doi:10.1146/annurev-bioeng-071811-150124.

41. Hoshino, A.; Fujioka, K.; Oku, T.; Suga, M.; Sasaki, Y.F.; Ohta, T.; Yasuhara, M.; Suzuki, K.; Yamamoto, K. Physicochemical properties and cellular toxicity of nanocrystal quantum dots depend on their surface modification. *Nano Lett.* **2004**, *4*, 2163–2169, doi:10.1021/nl048715d.

42. Qiu, Y.; Park, K. Environment-sensitive hydrogels for drug delivery. *Adv. Drug Deliv. Rev.* **2012**, *64*, 49–60, doi:10.1016/j.addr.2012.09.024.

43. Prajapati, R.; Gontsarik, M.; Yaghmur, A.; Salentinig, S. pH-responsive nano-self-assemblies of the anticancer drug 2-Hydroxyoleic acid. *Langmuir* **2019**, *35*, 7954–7961, doi:10.1021/acs.langmuir.9b00838.

44. Tannock, I.F.; Rotin, D. Acid pH in tumors and its potential for therapeutic exploitation. *Cancer Res.* **1989**, *49*, 4373–4384.

45. Catanzaro, G.; Curcio, M.; Cirillo, G.; Spizzirri, U.G.; Besharat, Z.M.; Abballe, L.; Vacca, A.; Iemma, F.; Picci, N.; Ferretti, E. Albumin nanoparticles for glutathione-responsive release of cisplatin: New opportunities for medulloblastoma. *Int. J. Pharm.* **2017**, *517*, 168–174, doi:10.1016/j.ijpharm.2016.12.017.

46. Kennedy, L.; Sandhu, J.K.; Harper, M.E.; Cuperlovic-culf, M. Role of glutathione in cancer: From mechanisms to therapies. *Biomolecules* **2020**, *10*, 1–27, doi:10.3390/biom10101429.

47. Estrela, J.M.; Ortega, A.; Obrador, E. Glutathione in cancer biology and therapy. *Crit. Rev. Clin. Lab. Sci.* **2006**, *43*, 143–181, doi:10.1080/10408360500523878.

48. Ballatori, N.; Krance, S.M.; Notenboom, S.; Shi, S.; Tieu, K.; Hammond, C.L. Glutathione dysregulation and the etiology and progression of human diseases. *Biol. Chem.* **2009**, *390*, 191–214, doi:10.1515/BC.2009.033.

49. Curcio, M.; Blanco-Fernández, B.; Costoya, A.; Concheiro, A.; Puoci, F.; Alvarez-Lorenzo, C. Glucose cryoprotectant affects glutathione-responsive antitumor drug release from polysaccharide nanoparticles. *Eur. J. Pharm. Biopharm.* **2015**, *93*, 281–292, doi:10.1016/j.ejpb.2015.04.010.

50. KIPP, J. The role of solid nanoparticle technology in the parenteral delivery of poorly water-soluble drugs. *Int. J. Pharm.* **2004**, *284*, 109–122, doi:10.1016/j.ijpharm.2004.07.019.

51. Oncul, S.; Ercan, A. Discrimination of the effects of doxorubicin on two different breast cancer cell lines on account of multidrug resistance and apoptosis. *Indian J. Pharm. Sci.* **2017**, *79*, 599–607, doi:10.4172/pharmaceutical-sciences.1000268.

52. Bar-On, O.; Shapira, M.; Hershko, D.D. Differential effects of doxorubicin treatment on cell cycle arrest and Skp2 expression in breast cancer cells. *Anticancer. Drugs* **2007**, *18*, 1113–

1121, doi:10.1097/CAD.0b013e3282ef4571.

53. Troester, M.A.; Hoadley, K.A.; Sørlie, T.; Herbert, B.S.; Børresen-Dale, A.L.; Lønning, P.E.; Shay, J.W.; Kaufmann, W.K.; Perou, C.M. Cell-type-specific responses to chemotherapeutics in breast cancer. *Cancer Res.* **2004**, *64*, 4218–4226, doi:10.1158/0008-5472.CAN-04-0107.

54. Elzoghby, A.O.; Samy, W.M.; Elgindy, N.A. Albumin-based nanoparticles as potential controlled release drug delivery systems. *J. Control. Release* **2012**, *157*, 168–182, doi:10.1016/j.jconrel.2011.07.031.

3.2 Albumin nanoparticles for the delivery of volasertib

3.2.1. Introduction

Polo-like kinases (PlKs) are serine or threonine kinases that regulate various cell cycle stages, such as centrosome maturation, mitotic entry or exit and maintenance of the bipolar spindle.[1] The overexpression of PlK1 was first observed in lung and breast cancer.[2] Later, it was also detected in other tumors, including uterine cancer, colorectal carcinoma, skin cancer, stomach cancer and acute myeloid leukemia (AML).[3–5] The Plk overexpression is associated with poor cancer prognosis, the potential of metastasis, low survival rates, development of drug resistance to several chemotherapeutics, including doxorubicin, gemcitabine and paclitaxel.[4,6,7] Thus, it has motivated research in the development of chemotherapeutics targeting these kinases. Among the 5 mammalian homologs of PlKs (PlK1 to Plk5), PlK1 is best characterized to date. In addition to being involved in the regulation of the cell cycle, PlK1 is reported to be responsible also for DNA replication and maintaining the dynamics between chromosomes and microtubules.[8] Hence, it is an attractive target for the treatment of various types of cancer.

In this sense, Volasertib (BI6727), developed by Boehringer Ingelheim is an ATP-competitive kinase inhibitor of PlK1, which has been studied in various cancers. It is a dihydropteridinone derivative (Figure 29 A) and selectively inhibits PlK1, PlK2 and PlK3 with IC50 of 0.87, 5 and 56 nM, respectively.[9] Volasertib (Vola) is the most clinically advanced Plk inhibitor and has been shown to inhibit the proliferation of various cell lines, including colon carcinoma, neuroblastoma, melanoma, breast cancer, cervical cancer, and lung cancer.[9,10] It exerts its anticancer effect via the inhibition of Plk-1, which reduces the phosphorylation of a wide range of target substrates, including ORC2 and P3F (Figure 29 B).[11] Vola is currently in phase II clinical trial both in monotherapy and in combination therapy with pemetrexed.[12]

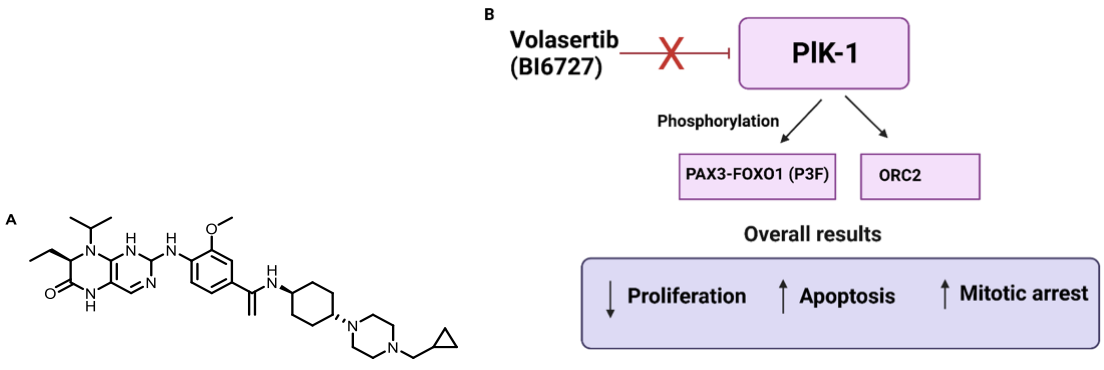

Figure 29. (A) Structure of volasertib and (B) Mechanism of action of Volasertib in cancers

Despite the broad potential of Vola in cancer therapy, its delivery is still a challenge. The major problems arise due to its highly hydrophobic nature, like poor aqueous solubility and burst release. Hence, a suitable carrier for specific targeting is desired. In this regard, albumin-based nanocarriers have shown remarkable results.[13–15] Unlike the conventional drug delivery systems, which have challenges regarding poor bioavailability, low therapeutic index, and off-target effects, albumin nanoparticles have great potential in terms of enhanced biocompatibility, stability, and controlled drug release.

Thus, in this chapter, we assessed the potential use of ABN for the delivery of volasertib. The method for the preparation of ABN-SPDP was optimized using doxorubicin in Chapter 3.1. The feasibility of the system was confirmed in both the hydrophilic (Dox) and hydrophobic (SN38) drugs. Hence, it was of great interest to encapsulate the novel drug, Vola, in the ABN-SPDP to use them in cancer therapy. The objective of the present work was to prepare ABN-SPDP encapsulating Vola, characterize for size, surface charge, encapsulation efficiency and activity in different cell lines (HeLa and MCF-7). These cell lines are associated with the overexpression of PlK-1 and hence, evaluation of Vola activity was carried out as its mechanism of action is based on the inhibition of PlK-1. SPDP was used as a cross-linking agent based on the results obtained in Chapter 3.1.

3.2.2. Results and discussion

3.2.2.1. Preparation and characterization of Vola loaded ABN-SPDP

ABN-SPDP were prepared using ethanol as a desolvating agent and SPDP as a cross-linking agent as discussed in detail in Chapter 3.1. The nanoparticles were prepared to encapsulate various

concentrations of Vola, ranging from 0.25 to 1 mg/mL. The prepared ABN-SPDP were characterized using dynamic light scattering for size and surface charge. As shown in the Figure 30, irrespective of the amount of the drug loaded, ABN-SPDP showed uniform size ranging from 120 to 140 nm. Similar results were obtained regarding the surface charge of the prepared NPs, from -21 to -25 mV. These results demonstrate that Vola loading does not affect the size and zeta potential of the resulting NPs. However, the NPs with the drug concentration of 1 mg/mL aggregated after 10 days of preparation and resulted in the formation of particles with sizes >500 nm.

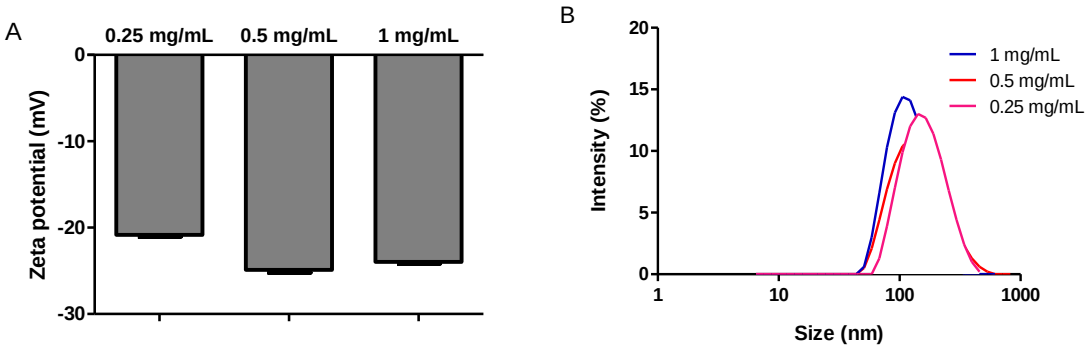

Figure 30. Surface charge (A) and size (B) characterization of volasertib-loaded ABN-SPDP using DLS.

The encapsulation efficiency of the NPs was also evaluated. As shown in the figure, the encapsulation of Vola was about 35% in all the cases, irrespective of the drug concentrations used (Figure 31). For all the further experiments, the concentration of the drug was chosen as 0.5 mg/mL.

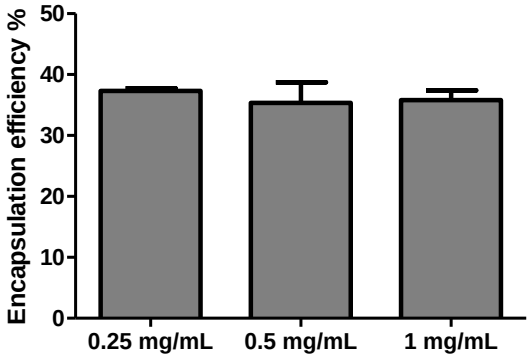

Figure 31. Encapsulation efficiency of Vola in ABN-SPDP with varying concentrations of the drug. The data were collected in triplicates and presented as Mean ± SD.

3.2.2.2 In vitro release of Volasertib from ABN-SPDP

Since the intracellular pH and the reducing environment in the tumor sites play an essential role in the release of drugs from the nanocarriers, it was interesting to analyze the release of the drug under various physiological conditions. The release of Vola from the prepared ABN-SPDP was hence studied under various conditions (at the acidic pH of 5 and/or in the presence of glutathione) at different time points. At 96 h, 36% of encapsulated Vola was released at pH of 5, whereas this value increased to 65% and 85%, respectively, when the conditions with glutathione 1 mM and pH 5 with glutathione 1 mM were used (Figure 32). Therefore, an additive effect was seen in the drug release when the tumor environment was mimicked using acidic pH and with glutathione, which is present in the higher concentration in the tumor cells. The glutathione breaks the disulphide bond and destabilizes the albumin nanoparticles causing the improved release of drug from the nanocarriers.

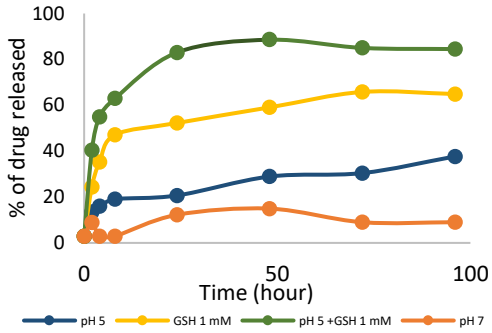

Figure 32. Release of Vola from ABN-SPDP at different time points. The conditions tested were pH 5 (blue), GSH 1 mM (yellow), pH 5 and GSH 1 mM (green) and pH 7 with GSH 1 µM (orange).

3.2.2.3 Cell studies

Since Vola cannot be tracked in the cells, Vola-loaded ABN-SPDP were conjugated with the fluorescent dye Cy5, to quantify the internalization of nanoparticles in the cells. The nanoparticles were incubated at RT overnight with 10 µM CY5-NHS-ester. The free CY5 was then removed by two cycles of centrifugation. The internalization was then studied in HeLa and MCF-7 cancer cells. As shown in Figure 33, the fluorescence of free Cy5 and conjugated in Vola-loaded ABN-SPDP was similar in both the cell lines (>98%).

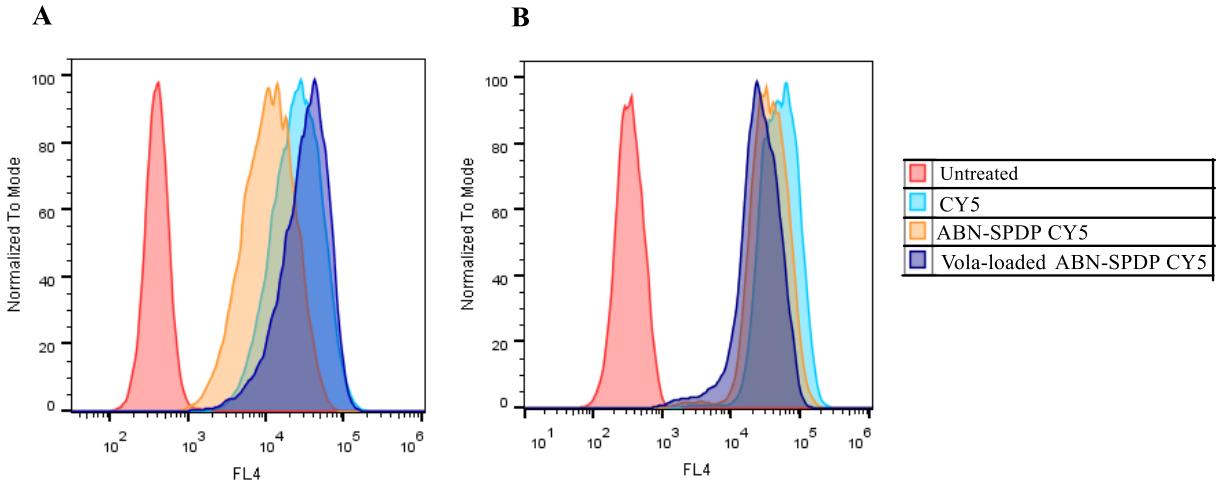

Figure 33. Quantification of fluorescence of Cy5 conjugated Vola-loaded ABN-SPDP using flow cytometry in HeLa and MCF-7 cells 24 hours post-treatment.

After confirming the internalization of Vola-loaded ABN-SPDP in cells using flow cytometry, the cell viability was studied in two cancer cell lines, HeLa and MCF-7, using the alamarBlue assay. As

shown in Figure 34, the free Vola and Vola encapsulated in ABN-SPDP both showed toxicity against both MCF-7 and HeLa cells. The decrease in cell viability was similar with free Vola and in the drug encapsulated in ABN-SPDP in both the cell lines. The cell viability decreased from around 59% after 24 h to 41% after 72 h with free Vola compared to 73% and 48% in HeLa cells. Similarly, the viability decreased to 55% and 23% in MCF-7 cells with free Vola. However, with Vola-loaded in ABN-SPDP, the cell viability after 24 and 72 h was almost similar (around 30%). Moreover, the empty ABN-SPDP did not affect the viability of cells, highlighting the negligible toxicity of ABN-SPDP. In this regard, previous studies have reported the excellent biocompatibility of the albumin nanocarriers.[16,17] The free Vola displayed a half-maximal inhibitory concentration (IC50) of 11.7 ± 1.17 nM in HeLa cells, which was 5.7-fold lower than Vola-loaded in ABN-SPDP (67.2 ± 1.13 nM) (Figure 35 A). However, in MCF-7 cells, the free drug or encapsulated in ABN-SPDP showed similar IC50 values of around 12.5 nM (Figure 35 B).

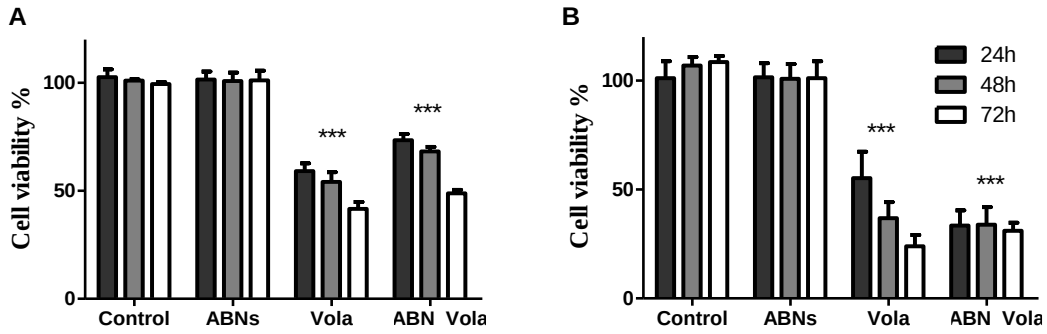

Figure 34. Cell viability assay with volasertib loaded ABN-SPDP 24, 48 and 72 h post-treatment in (A) HeLa cells and (B) MCF-7. In all the cases, the concentration of Vola used was 50 nM.

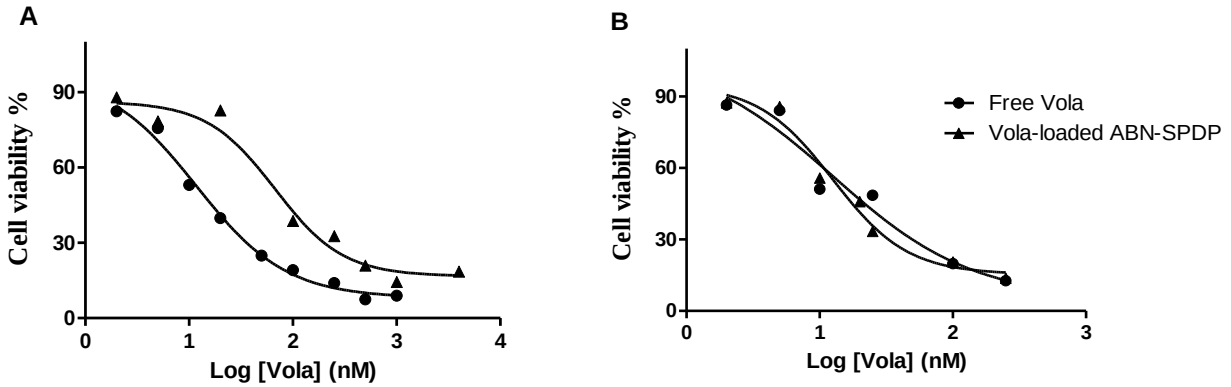

Figure 35. The half-maximal inhibitory concentration (IC50) of free Vola and Vola-loaded ABN-SPDP in (A) HeLa and (B) MCF-7 cells.

3.2.2.4 Study of apoptosis/necrosis of the cells

To analyze the mechanism of cell death mediated by Vola, the two most common mechanisms, namely apoptosis and necrosis, were investigated. In the HeLa cells, the percentage of necrotic cells increased drastically when treated with Vola alone (7.7 folds) or Vola -loaded ABN-SPDP (4.1 folds). Moreover, the apoptotic cells also increased by 3.2 folds and 3.7 folds when treated with Vola and Vola-loaded ABN-SPDP, respectively (Table 3). Similar results were observed in necrotic MCF-7 cells, increasing by 5.3 folds compared to ABN-SPDP. Moreover, there were 2.2- and 1.7-folds increase in the apoptotic cells after treatment with Vola and Vola-loaded ABN-SPDP, respectively. These results are in accordance with the previous studies, where Vola was shown to induce apoptosis in lung cancer and acute myeloid leukemia.[18,19]

	HeLa			MCF-7		
	Healthy Cells	**Apoptotic Cells**	**Necrotic Cells**	**Healthy Cells**	**Apoptotic Cells**	**Necrotic Cells**
Control	100.0 ± 0.2	0.1 ± 0.05	0.01 ± 0.02	100.0 ± 0.18	0.11 ± 0.10	0.03 ± 0.02
ABN-SPDP	81.50 ± 0.55	0.97 ± 0.10	7.31 ± 0.30	95.05 ± 1.05	1.19 ± 0.25	0.83 ± 0.28
Vola	6.31 ± 0.30	3.18 ± 0.21	56.6 ± 0.13	71.80 ± 0.30	2.62 ± 0.19	4.44 ± 0.23
Vola-loaded ABN-SPDP	22.2 ± 0.30	3.64± 0.31	30.5 ± 0.95	69.20 ± 1.50	2.1 ± 0.09	4.47 ± 0.20

Table 3. Percentage of healthy, necrotic, and apoptotic cells with varying concentrations of Vola-loaded ABN-SPDP 24 h post-treatment in HeLa and MCF-7 cells.

3.2.2.5 Study of dominant cell cycle phase

The overexpression of PlK1 is prevalent in a broad spectrum of cancers and is associated with a poor prognosis. PlK1 is a serine/threonine kinase and has a prominent role in the G2/M transition via cytokinesis[20]. Since PlK1 is primarily involved in regulating mitotic cell division via the effects on chromosome segregation, the cell cycle distribution in HeLa and MCF-7 cells was investigated after 24 hours of treatment with Vola-loaded ABN-SPDP. As shown in Figure 36, there was

prominent cell cycle arrest in G2/M phase in both the cell lines after PlK1 exposure, whereas a minimal effect was observed with empty ABN-SPDP. The cells in G2/M phase increased by 1.5 folds and 2.4 folds in HeLa and MCF-7 cells, respectively, compared to the control when treated with Vola-loaded ABN-SPDP.

Thus, the cytotoxic effect of Vola may be explained by the persistent G2/M phase arrest in prophase. A similar result was obtained in a study conducted by Bossche and co-workers in lung cancer cells when volasertib was used.[19] The treatment with volasertib hence accumulates the cells in G2/M phase, which is the most radiosensitive phase and hence can be used in combination therapy with radiotherapy.[21] It is to be emphasized that the enhanced cell cycle arrest in MCF-7 cells can be attributed to the wild-type p53 in MCF-7 cells compared to HeLa cells, which have absent or at least reduced wild-type p53 function because of the expression of HPV-encoded E6 and E7 oncoproteins leading to p53 degradation.[22]

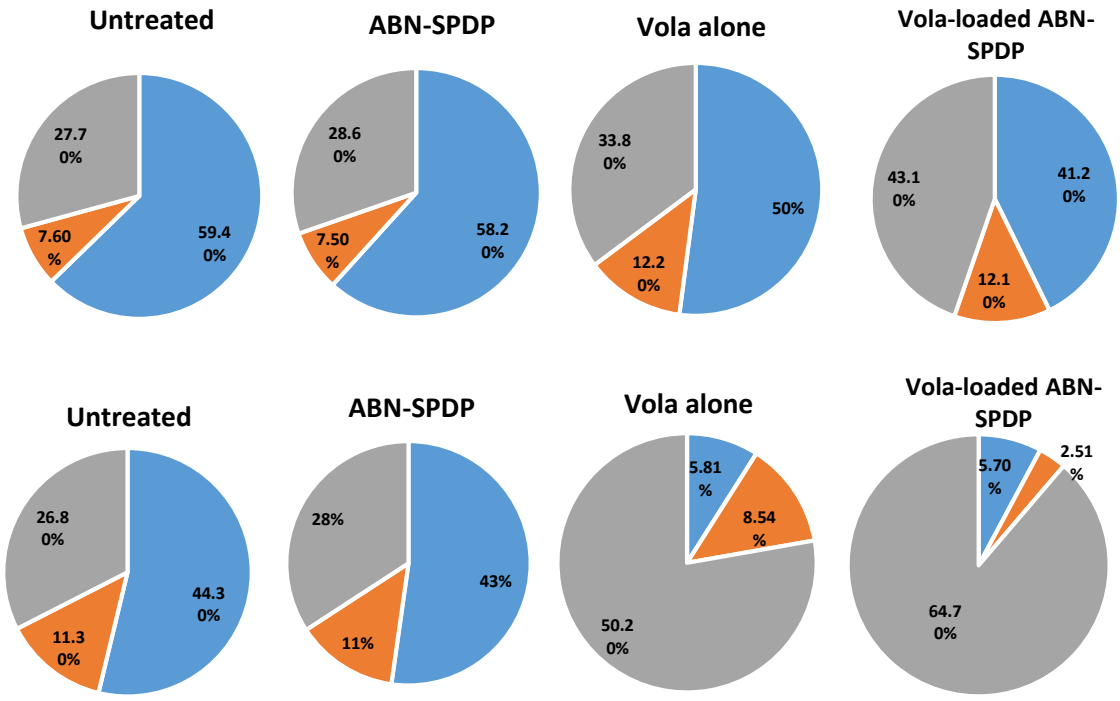

Figure 36. Flow cytometry analysis of the cell cycle 24 h post- treatment in HeLa (upper lane) and MCF-7 (lower lane) cells. The amount of Vola used in each case was 50 nM. Blue: cells in G0/G1 phase; orange: cells in S phase; grey: cells in G2/M phase.

3.2.2.6 Study of mechanism of internalization

The internalization of ABN-SPDP loaded with Vola was confirmed by flow cytometry studies with the nanoparticles conjugated with fluorescent CY5. Hence, it was interesting to study the mechanism by which those nanoparticles are being internalized in the cells. Various pathways, namely, clathrin-mediated endocytosis, caveolae-mediated endocytosis, and clathrin-, caveolae-independent pathways, may be involved in the internalization of the prepared nanoparticles. Thus, we studied the intracellular trafficking of Vola-loaded ABN-SPDP in the presence of various endocytosis inhibitors. Genistein or filipin, the caveolae-mediated endocytosis inhibitors or chlorpromazine, a clathrin-mediated endocytosis inhibitor, was used, and cell viability was investigated after 48 h of treatment with ABN-SPDP. As shown in Figure 37, the cell viability with Vola-loaded ABN-SPDP was around 29% in the absence of endocytosis inhibitors. However, this value was increased to 48%, 58% and 57% in the presence of genistein, filipin and chlorpromazine, respectively. Hence, it can be concluded that the nanoparticles are internalized by both caveolae and clathrin-dependent endocytosis pathways.

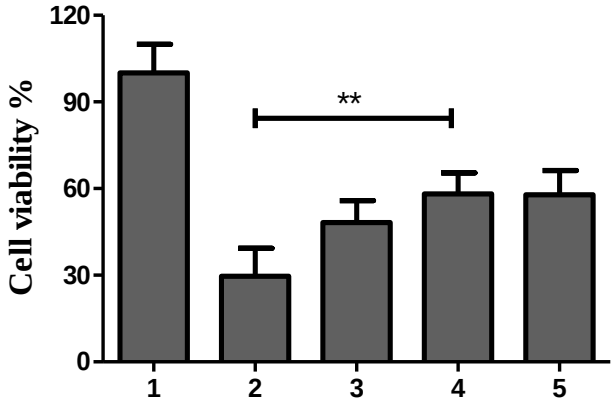

Figure 37. Cell viability assay with Vola-loaded ABN-SPDP in the presence of endocytosis inhibitors 24 h post-treatment in HeLa cells. 1: control, 2: Vola-loaded ABN-SPDP without endocytosis inhibitors, 3: in the presence of genistein, 4: filipin, and 5: chlorpromazine.

3.2.2.7 Study of intracellular ROS production

Many studies have demonstrated the elevated levels of ROS in most cancers and are unique biological stimuli for the efficient and targeted delivery of chemotherapeutics.[23,24] Most current cancer therapies and ionization radiation exploit ROS production to induce cancer cell

deaths.[25] To measure ROS produced by cells, 2',7'-dichlorofluorescin diacetate (DCF-DA) was used, which passively diffuses through the cell membrane. It is deacetylated to dichlorofluorescein (DCFH) by esterases which then reacts with ROS to form the green fluorophores, DFC which can be detected.[26,27]

It was observed that both free Vola and the Vola-loaded ABN-SPDP increased ROS levels predominantly after 48 hours of treatment in both the cell lines investigated (Figure 38). The level of ROS production was significantly higher with free Vola in HeLa cells compared to the encapsulated drug. However, there was no significant difference in the levels of ROS produced in MCF-7 cells. These results justify the low IC50 value observed with the free drug compared with the drug encapsulated in ABN-SPDP in HeLa, whereas similar IC50 in MCF-7 cells. Moreover, there was no change in the ROS levels with the ABN-SPDP without the drug. Hence, we can conclude that the ABN-SPDP does not play a role in ROS production at the concentrations used in both the cell lines of study. The cytotoxic effect observed with ABN-SPDP Vola may be related to ROS in both HeLa and MCF-7 cells.

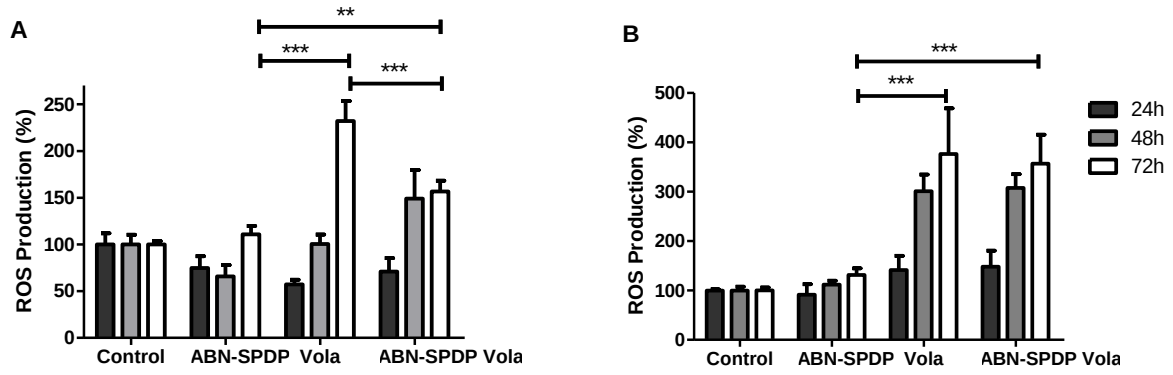

Figure 38. Quantification of ROS levels by detection of oxidized DCF-DA 24, 48 and 72 h post-treatment in (A) HeLa and (B) MCF-7 cells. Data represent means ± SD. The concentration of Vola used in each case was 50 nM.

The results were further confirmed by the fluorescence microscopy images. The free Vola and the Vola-loaded ABN-SPDP both enhanced the levels of ROS in a time-dependent manner in both HeLa and MCF-7 cells. As shown in the Figure 39, no fluorescence was observed when both the

cell lines were treated with empty ABN-SPDP. The ROS production was more prominent after 72 h post-treatment in MCF-7 cells, whereas it could be observed after 48 hours in Hela cells.

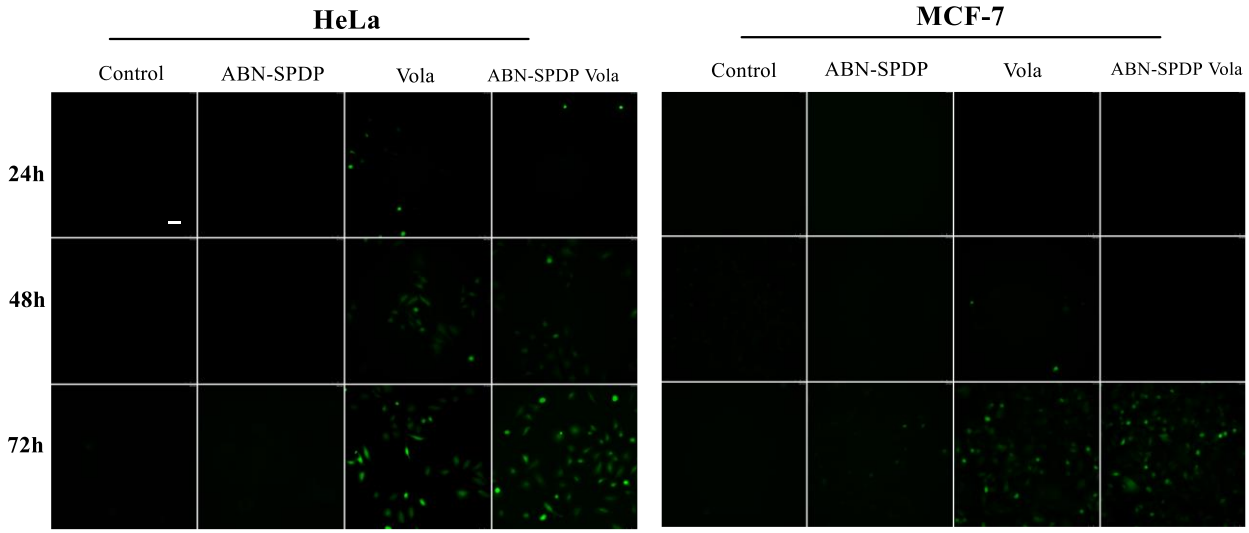

Figure 39. Fluorescence microscopic images for the detection of ROS production in HeLa and MCF-7 cells 24-, 48- and 72- hours post-treatment with ABN-SPDP, free Vola, and Vola-loaded ABN-SPDP. Scale bar: 75 µm.

3.2.2.8 Detection of autophagosomes formation

Autophagy is defined as an intracellular degradative process, which initiates the process of autophagosomes formation in various stressful conditions.[28,29] The autophagosomes are responsible for the delivery of degraded cytoplasmic components like misfolded proteins and damaged organelles to the lysosome to be recycled during various stressful conditions.[30] There are some studies that describe autophagy as the regulator of tumor suppressor genes, while other studies suggest the involvement of autophagy in both the promotion and inhibition of cancers.[31,32] The chemotherapeutics that regulate autophagy can be hence involved in cancer cell proliferation or death.[32]

In the present study, we investigated the role of the ABN-SPDP in the formation of autophagosomes. As shown in the Figure 40, both free Vola and Vola-loaded ABN-SPDP did not show any effect in autophagy till 48 h post-treatment in HeLa and MCF-7 cells. However, after 72 h of treatment, there was an increment in the formation of autophagosomes in both cell lines. The result suggests the autophagy-mediated cell death after 72 h of treatment by the free Vola

and Vola-loaded ABN-SPDP. However, there was no role of autophagy in cell death after 24 and 48 h of treatment. The increase in the autophagosomes was also reported in the previous studies with PlK1 inhibitors (RO3280 and BI2536) in myeloid leukemia[33].

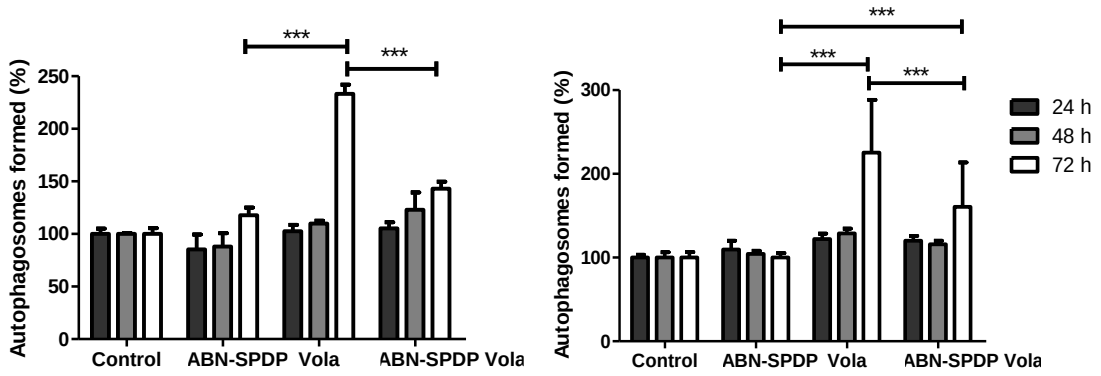

Figure 40. Quantification of autophagosome formation by measuring the fluorescence of MDC 24, 48 and 72 h post-treatment in (A) HeLa and (B) MCF-7 cells.

3.2.3 Conclusions

In the present study, the previously optimized system with ABN-SPDP was used to encapsulate the novel PlK-1 inhibitor, Volasertib. The prepared nanoparticles were characterized, and their efficacy was analysed in two different cancer cell lines, HeLa, and MCF-7. The Vola-loaded ABN-SPDP showed prominent efficacy in both the cell lines via induction of apoptosis and consequent cell cycle arrest in G2/M phase. Moreover, the treatment with the drug-loaded nanoparticles resulted in the production of ROS and autophagosomes, which might have played a role in the efficacy in both the cell lines. The results obtained in the study indicate the successful use of ABN-SPDP for the encapsulation and delivery of hydrophobic drugs like Volasertib, which otherwise face many challenges in delivery to the target sites.

References

1. Zitouni, S.; Nabais, C.; Jana, S.C.; Guerrero, A.; Bettencourt-Dias, M. Polo-like kinases: Structural variations lead to multiple functions. *Nat. Rev. Mol. Cell Biol.* **2014**, *15*, 433–452, doi:10.1038/nrm3819.

2. Yuan, J.; Hörlin, A.; Hock, B.; Stutte, H.J.; Rübsamen-Waigmann, H.; Strebhardt, K. Polo-like kinase, a novel marker for cellular proliferation. *Am. J. Pathol.* **1997**, *150*, 1165–1172.

3. Renner, A.G.; Dos Santos, C.; Recher, C.; Bailly, C.; Créancier, L.; Kruczynski, A.; Payrastre, B.; Manenti, S. Polo-like kinase 1 is overexpressed in acute myeloid leukemia and its inhibition preferentially targets the proliferation of leukemic cells. *Blood* **2009**, *114*, 659–662, doi:10.1182/blood-2008-12-195867.

4. Gjertsen, B.T.; Schöffski, P. Discovery and development of the Polo-like kinase inhibitor volasertib in cancer therapy. *Leukemia* **2015**, *29*, 11–19, doi:10.1038/leu.2014.222.

5. Tsykunova, G.; Reikvam, H.; Ahmed, A.B.; Nepstad, I.; Gjertsen, B.T.; Bruserud, Ø. Targeting of polo-like kinases and their cross talk with Aurora kinases possible therapeutic strategies in human acute myeloid leukemia? *Expert Opin. Investig. Drugs* **2012**, *21*, 587–603, doi:10.1517/13543784.2012.668525.

6. Strebhardt, K.; Ullrich, A. Targeting polo-like kinase 1 for cancer therapy. *Cancer* **2006**, *6*, 321–330.

7. Gutteridge, R.E.A.; Ndiaye, M.A.; Liu, X.; Ahmad, N. Plk1 inhibitors in cancer therapy: From laboratory to clinics. *Mol. Cancer Ther.* **2016**, *15*, 1427–1435, doi:10.1158/1535-7163.MCT-15-0897.

8. Bossche, J. Van den; Lardon, F.; Deschoolmeester, V.; Pauw, I. De; Vermorken, J.B.; Specenier, P.; Pauwels, P.; Peeters, M.; Wouters, A. Spotlight on Volasertib: Preclinical andClinical Evaluation ofa Promising Plk1 Inhibitor. *Med. Res. Rev.* **2016**, *36*, 749–786, doi:10.1002/med.

9. Rudolph, D.; Steegmaier, M.; Hoffmann, M.; Grauert, M.; Baum, A.; Quant, J.; Haslinger, C.; Garin-Chesa, P.; Adolf, G.R. BI 6727, a polo-like kinase inhibitor with improved pharmacokinetic profile and broad antitumor activity. *Clin. Cancer Res.* **2009**, *15*, 3094–3102, doi:10.1158/1078-0432.CCR-08-2445.

10. Grinshtein, N.; Datti, A.; Fujitani, M.; Uehling, D.; Prakesch, M.; Isaac, M.; Irwin, M.S.; Wrana, J.L.; Al-awar, R.; Kaplan, D.R. Small molecule kinase inhibitor screen identifies polo-like kinase 1 as a target for neuroblastoma tumor-initiating cells. *Cancer Res.* **2011**, *71*, 1385–1395, doi:10.1158/0008-5472.CAN-10-2484.

11. Gatz, S.A.; Aladowicz, E.; Casanova, M.; Chisholm, J.C.; Kearns, P.R.; Fulda, S.; Geoerger, B.; Schäfer, B.W.; Shipley, J.M. A Perspective on Polo-Like Kinase-1 Inhibition for the Treatment of Rhabdomyosarcomas. *Front. Oncol.* **2019**, *9*, 1–7, doi:10.3389/fonc.2019.01271.

12. Boehringer Ingelheim Trial of BI 6727 (Volasertib) Monotherapy and BI 6727 in Combination With Pemetrexed Compared to Pemetrexed Monotherapy in Advanced NSCLC.

13. Prajapati, R.; Larsen, S.W.; Yaghmur, A. Citrem-phosphatidylcholine nano-self-assemblies: Solubilization of bupivacaine and its role in triggering a colloidal transition from vesicles to cubosomes and hexosomes. *Phys. Chem. Chem. Phys.* **2019**, *21*, 15142–15150, doi:10.1039/c9cp01878f.

14. Wang, J.; Zhang, B. Bovine Serum Albumin as a Versatile Platform for Cancer Imaging and Therapy. *Curr. Med. Chem.* **2017**, *25*, 2938–2953, doi:10.2174/0929867324666170314143335.

15. Elzoghby, A.O.; Samy, W.M.; Elgindy, N.A. Albumin-based nanoparticles as potential controlled release drug delivery systems. *J. Control. Release* **2012**, *157*, 168–182, doi:10.1016/j.jconrel.2011.07.031.

16. Woods, A.; Patel, A.; Spina, D.; Riffo-Vasquez, Y.; Babin-Morgan, A.; De Rosales, R.T.M.; Sunassee, K.; Clark, S.; Collins, H.; Bruce, K.; et al. In vivo biocompatibility, clearance, and biodistribution of albumin vehicles for pulmonary drug delivery. *J. Control. Release* **2015**, *210*, 1–9, doi:10.1016/j.jconrel.2015.05.269.

17. Geng, T.; Zhao, X.; Ma, M.; Zhu, G.; Yin, L. Resveratrol-Loaded Albumin Nanoparticles with Prolonged Blood Circulation and Improved Biocompatibility for Highly Effective Targeted Pancreatic Tumor Therapy. *Nanoscale Res. Lett.* **2017**, *12*, 1–10, doi:10.1186/s11671-017-2206-6.

18. Rudolph, D.; Impagnatiello, M.A.; Blaukopf, C.; Sommer, C.; Gerlich, D.W.; Roth, M.; Tontsch-Grunt, U.; Wernitznig, A.; Savarese, F.; Hofmann, M.H.; et al. Efficacy and mechanism of action of volasertib, a potent and selective inhibitor of polo-like kinases, in preclinical models of acute myeloid Leukemia. *J. Pharmacol. Exp. Ther.* **2015**, *352*, 579–589, doi:10.1124/jpet.114.221150.

19. Van den Bossche, J.; Deben, C.; De Pauw, I.; Lambrechts, H.; Hermans, C.; Deschoolmeester, V.; Jacobs, J.; Specenier, P.; Pauwels, P.; Vermorken, J.B.; et al. In vitro study of the Polo-like kinase 1 inhibitor volasertib in non-small-cell lung cancer reveals a role for the tumor suppressor p53. *Mol. Oncol.* **2019**, *13*, 1196–1213, doi:10.1002/1878-0261.12477.

20. Schmit, T.L.; Ledesma, M.C.; Ahmad, N. Modulating Polo-Like Kinase 1 as a Means for Cancer Chemoprevention. *Pharm. Res.* **2010**, *27*, 989–998, doi:10.1007/s11095-010-0051-8.Modulating.

21. Lund-Andersen, C.; Patzke, S.; Nähse-Kumpf, V.; Syljuåsen, R.G. PLK1-inhibition can cause radiosensitization or radioresistance dependent on the treatment schedule. *Radiother. Oncol.* **2014**, *110*, 355–361, doi:10.1016/j.radonc.2013.12.014.

22. Wsierska-Gdek, J.; Schloffer, D.; Kotala, V.; Horky, M. Escape of p53 protein from E6-mediated degradation in HeLa cells after cisplatin therapy. *Int. J. Cancer* **2002**, *101*, 128–136, doi:10.1002/ijc.10580.

23. Liou, G.Y.; Storz, P. Reactive oxygen species in cancer. *Free Radic. Res.* **2010**, *44*, 479–496, doi:10.3109/10715761003667554.

24. Shim, M.S.; Xia, Y. A Reactive Oxygen Species (ROS)-Responsive Polymer for Safe, Efficient, and Targeted Gene Delivery in Cancer Cells. *Angew. Chemie* **2013**, *125*, 7064–7067, doi:10.1002/ange.201209633.

25. Srinivas, U.S.; Tan, B.W.Q.; Vellayappan, B.A.; Jeyasekharan, A.D. ROS and the DNA damage response in cancer. *Redox Biol.* **2019**, *25*, 101084, doi:10.1016/j.redox.2018.101084.

26. Lin, C.W.; Lu, K.Y.; Wang, S.Y.; Sung, H.W.; Mi, F.L. CD44-specific nanoparticles for redox-triggered reactive oxygen species production and doxorubicin release. *Acta Biomater.* **2016**, *35*, 280–292, doi:10.1016/j.actbio.2016.02.005.

27. Kalyanaraman, B.; Darley-Usmar, V.; Davies, K.J.A.; Dennery, P.A.; Forman, H.J.; Grisham, M.B.; Mann, G.E.; Moore, K.; Roberts, L.J.; Ischiropoulos, H. Measuring reactive oxygen and nitrogen

species with fluorescent probes: Challenges and limitations. *Free Radic. Biol. Med.* **2012**, *52*, 1–6, doi:10.1016/j.freeradbiomed.2011.09.030.

28. Mizushima, N. Autophagy: Process and function. *Genes Dev.* **2007**, *21*, 2861–2873, doi:10.1101/gad.1599207.

29. Mizushima, N. The pleiotropic role of autophagy: From protein metabolism to bactericide. *Cell Death Differ.* **2005**, *12*, 1535–1541, doi:10.1038/sj.cdd.4401728.

30. Yun, C.W.; Lee, S.H. The roles of autophagy in cancer. *Int. J. Mol. Sci.* **2018**, *19*, 1–18, doi:10.3390/ijms19113466.

31. Gewirtz, D.A. The four faces of autophagy: Implications for cancer therapy. *Cancer Res.* **2014**, *74*, 647–651, doi:10.1158/0008-5472.CAN-13-2966.

32. Rosenfeldt, M.T.; Ryan, K.M. The multiple roles of autophagy in cancer. *Carcinogenesis* **2011**, *32*, 955–963, doi:10.1093/carcin/bgr031.

33. Tao, Y.F.; Li, Z.H.; Du, W.W.; Xu, L.X.; Ren, J.L.; Li, X.L.; Fang, F.; Xie, Y.; Li, M.; Qian, G.H.; et al. Inhibiting PLK1 induces autophagy of acute myeloid leukemia cells via mammalian target of rapamycin pathway dephosphorylation. *Oncol. Rep.* **2017**, *37*, 1419–1429, doi:10.3892/or.2017.5417.

Chapter 4: Imaging and therapeutic activity of albumin-based nanoparticles in 2D and 3D cancer models

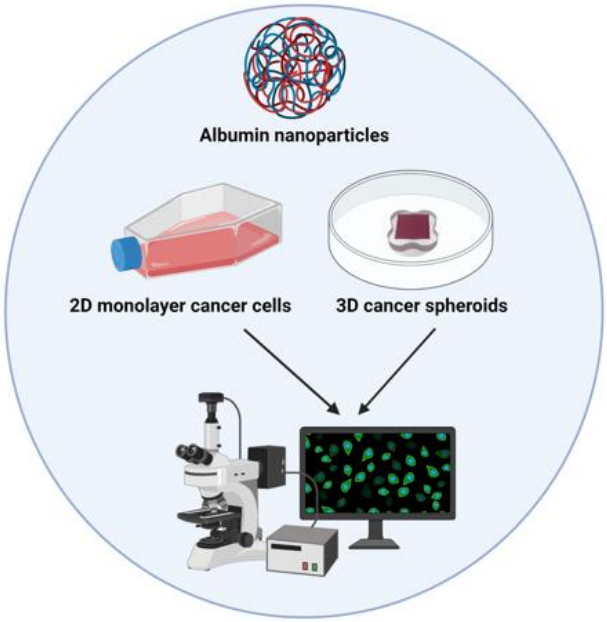

4.1. Introduction

In recent years, the use of nanocarriers has highlighted the potential for the diagnosis and treatment of various cancers. It has particularly attracted immense attention because of numerous advantages when applied to current therapies, including the ability to accumulate in tumors preferentially by the EPR effect, improvement in the solubility, and the pharmacokinetic properties of the drugs.[1,2] However, there are still some challenges that these novel approaches need to overcome to make a better impact in the clinic. For instance, various factors like degradation by lysosomes, elimination by the reticuloendothelial system (RES), opsonization and clearance of the particles by the macrophages and dense collagen tumoral matrix, inefficient tumor penetration and release of the cargo, must be properly solved for the success of these nanocarriers in cancer therapy.[3–5]

In this sense, we decided to study albumin-based nanocarriers' ability to overcome the biological barriers in cancer therapy. The studies were conducted in 2D and 3D cancer cell models. In the 2D cell cultures, cells grow in a monolayer and provide the preliminary study for the interaction of nanocarriers with the cells. 2D cell studies are widely prevalent in cancer research because of the cost-effectiveness, ease of experimental methods, good reproducibility, and possibility of growing a wide range of cells.[6,7] However, these 2D models cannot mimic the tumor environment conferred by the complexity present in the human body and can often lead to inaccurate biological performance results of the cancer therapeutics.[8] Therefore, 3D cell culture models are gaining tremendous attention for the screening of cancer therapeutics as they show various in vivo tumor characteristics like gene expression heterogeneity, cell-cell interaction, production of extracellular matrix, proliferation and hypoxia.[9,10]

The 3D cell cultures can either be scaffold-based (cells anchored to 3D platforms, in which growth resembles the extracellular matrix) or non-scaffold based (formed by self-aggregation of cells resulting in spheroids).[11,12] The non-scaffold method for the preparation of spheroids is particularly interesting in oncology because of its ability to mimic the in vivo tumors.[13–15] The growth kinetics of the spheroids is comparable to the solid tumors, with the necrotic cells accumulated in the core surrounded by non-proliferating or quiescent cells and finally an outer layer of rapidly proliferating and loosely attached cells (Figure 41).[16,17] The outermost cell

layer has easier access to oxygen and nutrients, which gradually decreases towards the core and leads to senescent and necrotic cells in the center.[18] Moreover, the cells convert pyruvate to lactate in the hypoxic environment and hence results in extracellular acidosis, which is characteristic of the in vivo solid tumors.[18,19]

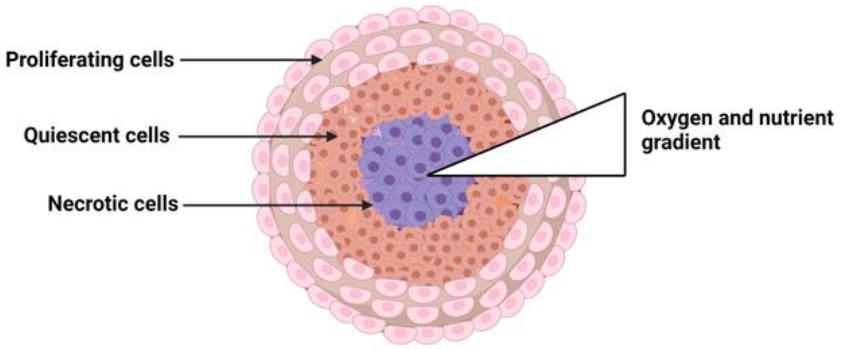

Figure 41. Schematic representation of the cancer spheroid with outermost proliferating cells (pink), non-proliferating quiescent cells in the middle (orange) and necrotic cells in the core (purple). The cellular density is lowest in the outside layer.

These studies have been done with nanoparticles based on HSA, because of their excellent activity in various cancer cell lines, as demonstrated in Chapter 3.1. In this chapter, HSA nanoparticles were obtained using two different cross-linkers, glutaraldehyde (HSA-GLU) and SPDP (HSA-SPDP). Then, their mechanism of internalization and intracellular localisation were first studied in the 2D cell cultures. These two cross-linkers were chosen since glutaraldehyde is the most widely used cross-linker for the preparation of albumin nanoparticles, while SPDP was found to enhance efficacy and cancer targeting in our recent study.[20] The internalization of the nanoparticles was further studied in MCF-7 and HeLa spheroids to evaluate the process in a more complex and realistic scenario, compared to the 2D system. For drug delivery applications, HSA-SPDP were loaded with different chemotherapeutics (Volasertib and Doxorubicin) and their cytotoxic effect was monitored by the decrease in the volumes of the spheroids. All these experiments were carried out in Rocha Lab, KU Leuven, Belgium, under the supervision of Assistant Professor Dr. Susana Rocha and Dr. Beatrice Fortuni.

4.2. Results and discussion

4.2.1. Conjugation of fluorescent dye to albumin nanoparticles

HSA nanoparticles were first prepared using either glutaraldehyde (GLU) or SPDP as a cross-linker as described in Chapter 3. When GLU was used, the nanoparticles exhibited intrinsic fluorescence, hence, they could be tracked in vitro without labeling agents. As observed in the emission spectra, when excited at a wavelength between 320 nm and 600 nm, the emission peaks shifted from 510 nm to 550 nm, which results in green and red fluorescence, respectively (Figure 42). Similar green and red fluorescent hydrogels were obtained when glutaraldehyde was used with HSA and bovine serum albumin (BSA).[21]

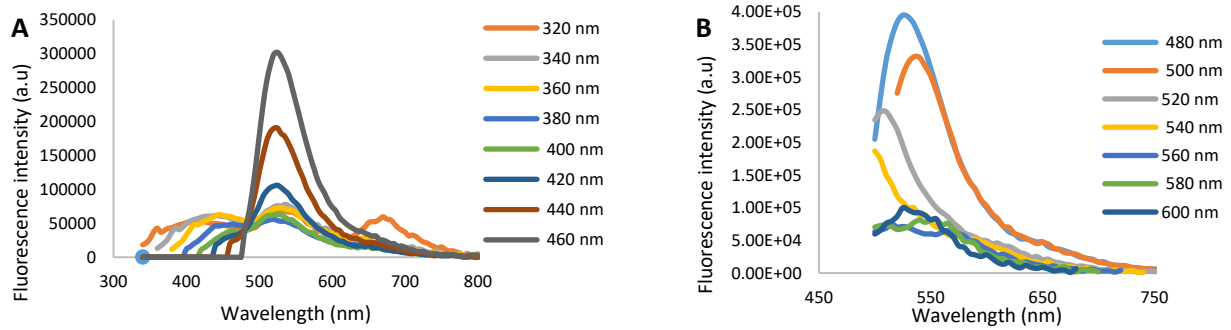

Figure 42. (A) and (B) Emission scans when excited between λ = 320nm and λ = 600nm, split into two figures for the sake of clear display.

For tracking HSA-SPDP in the cells, the nanoparticles were conjugated to the fluorescent dye, AlexaFluor-488 modified with NHS-ester. The schematic illustration is given in Figure 43. The conjugation of the dye to the nanoparticles was confirmed by fluorescence spectrum with an excitation peak at 488 nm and emission at 530 nm.

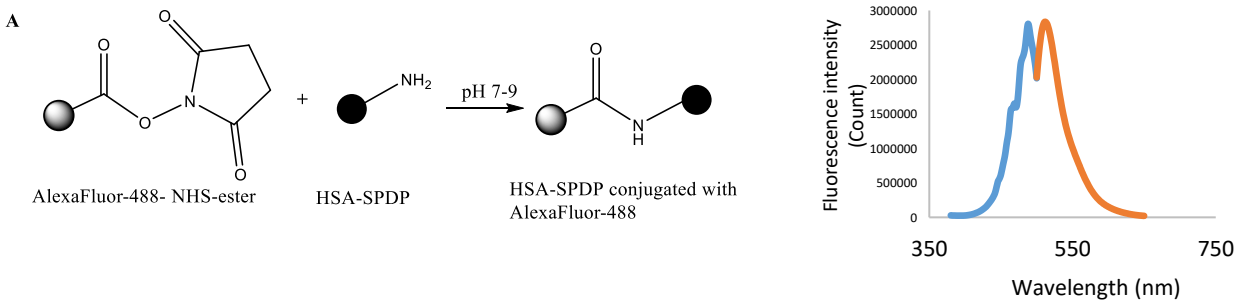

Figure 43. A) Conjugation of AlexafFluor-488 to the amino groups of HSA-SPDP to facilitate the

tracking inside the cells and B) Fluorescence excitation (blue) and emission spectra (orange) of the dye conjugated HSA-SPDP.

4.2.2. Internalization of nanoparticles in HeLa and MCF-7 cells

The internalization of HSA-GLU and HSA-SPDP was evaluated in two different cell lines, HeLa and MCF-7 cells. Figure 45 shows the fluorescence images in both cell lines after 4 h of incubation with different nanoparticles. The plasma membranes were stained with the fluorescent dyes DiO and DiR, when HSA-GLU and HSA-SPDP were used, respectively. Both types of nanoparticles were successfully internalized in both the cancer cell lines. However, there was better internalization of albumin nanoparticles in HeLa cells than in MCF-7, for both types of nanoparticles employed (Figure 44 A, B). Based on our results, we can hypothesize that the albumin binding receptors (for example, SPARC and gp60) are present more abundantly in HeLa cells, which facilitate the internalization of the nanoparticles. However, further studies need to be conducted to test this hypothesis.

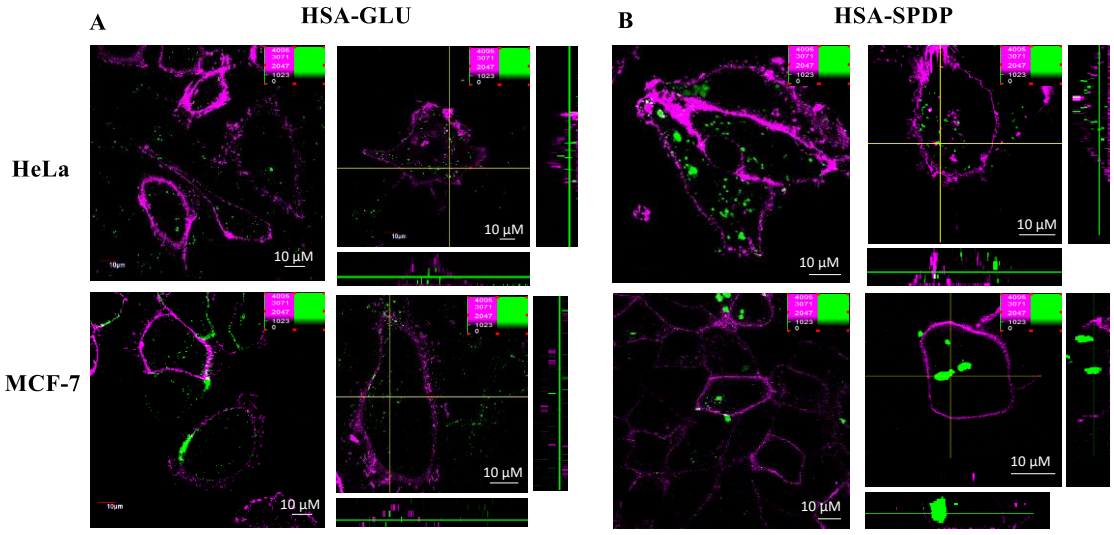

Figure 44. Internalization of HSA-GLU (A) and HSA-SPDP (B) in MCF-7 and HeLa cells 4 h post treatment. The right lane of each particle shows the central panel displaying a xy-plane within the cells, with right and bottom panels showing the yz and xz projections, respectively. The membrane is shown in magenta, while the nanoparticles are shown in green.

4.2.3. Lysosomal tracking of the nanoparticles in HeLa and MCF-7 cells

The lysosomes are subcellular organelles that are acidic and can cause the degradation of the nanocarriers leading to multidrug resistance. To explore the potential of the albumin-based nanoparticles to escape the lysosomal entrapment, the uptake of the NPs was conducted in the presence of lysosomal trackers. For HSA-GLU, Lysotracker green was used, whereas, for HSA-SPDP, Lysotracker Red was used, which are fluorescent markers and stain the late-endosomes or lysosomes. The co-localization was then studied by using confocal microscopy. As shown in the Figure 45, there was no co-localization of the nanoparticles with the lysosomal trackers with both kinds of nanoparticles in MCF-7 and HeLa cells. A similar result was obtained when the HSA nanoparticles loaded with plasmid were used in ARPE-19 cells.[22] This may indicate that the nanoparticles entered the cells through either caveolae-mediated pathways or clathrin-dependent endocytosis, from which they rapidly escaped the late endosomes and lysosomes.[22]

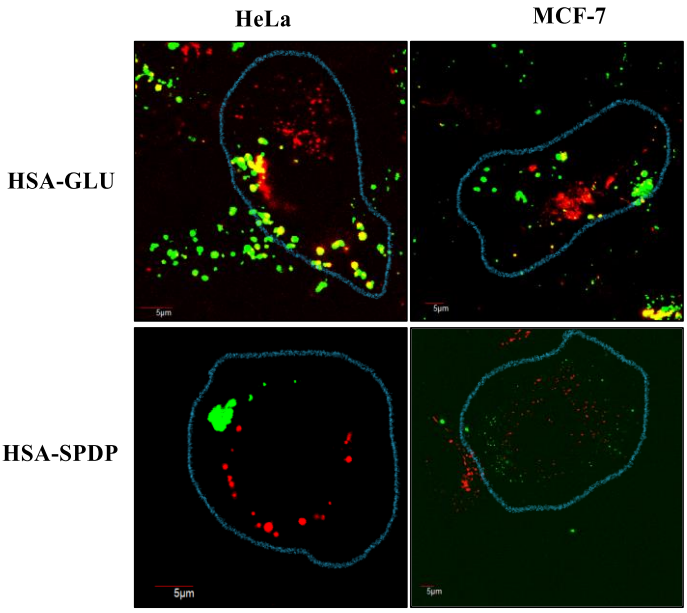

Figure 45. ABN-GLU (A, B) and ABN-SPDP (C, D) do not co-localize with lysosomes in both HeLa (A, C) and MCF-7 (B, D) cells after 4 h of incubation in the presence of lysotracker. With ABN-GLU, 250 nM Lysotracker green was used, whereas with ABN-SPDP conjugated with Alexa fluor, 50 nM Lysotracker red was used. Grey lines derived from DIC images were drawn to divide the intracellular and extracellular areas.

4.2.4. Effect of endocytosis inhibitors on the internalization of nanoparticles

The mechanism of internalization of albumin nanoparticles was studied using various endocytosis inhibitors (filipin and chlorpromazine). Both HeLa and MCF-7 cells with the particles (HSA-GLU and HSA-SPDP) in the presence/absence of endocytosis inhibitors were imaged with a confocal microscope after 4 h of incubation. The intensity of the particles inside the cells was then quantified using ImageJ. As shown in Figure 46, there was a significant reduction in the internalization of the particles when filipin or chlorpromazine was used, indicating the involvement of clathrin and caveolae-mediated endocytosis pathways. In particular, the reduction was more prominent when filipin was used, suggesting caveolae-mediated pathway to be more dominant in the internalization of albumin nanoparticles in both the cell lines studied. These findings are consistent with our previous results obtained using Dox-loaded HSA-SPDP in breast cancer cells, MCF-7.[20]

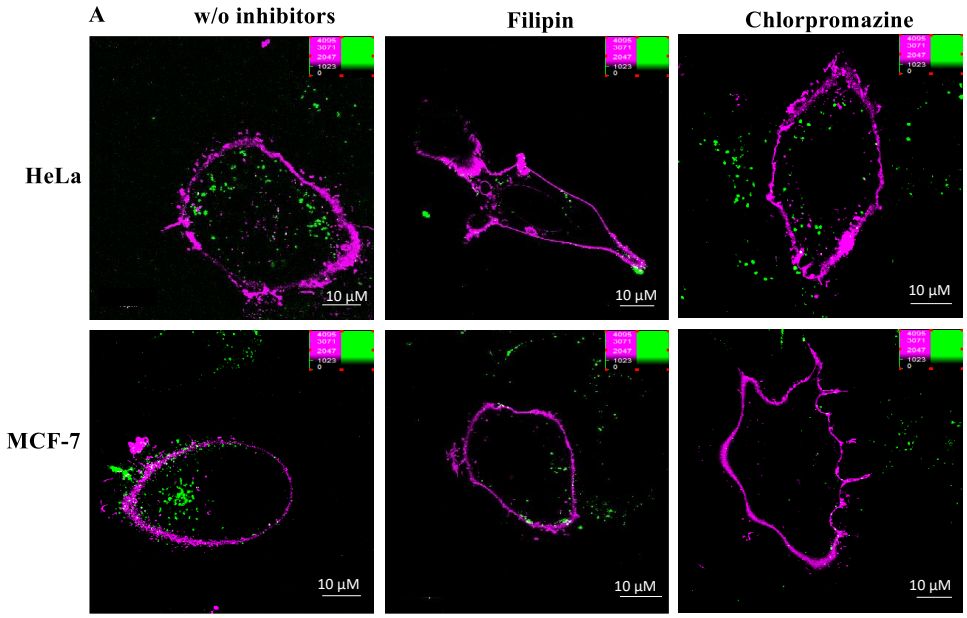

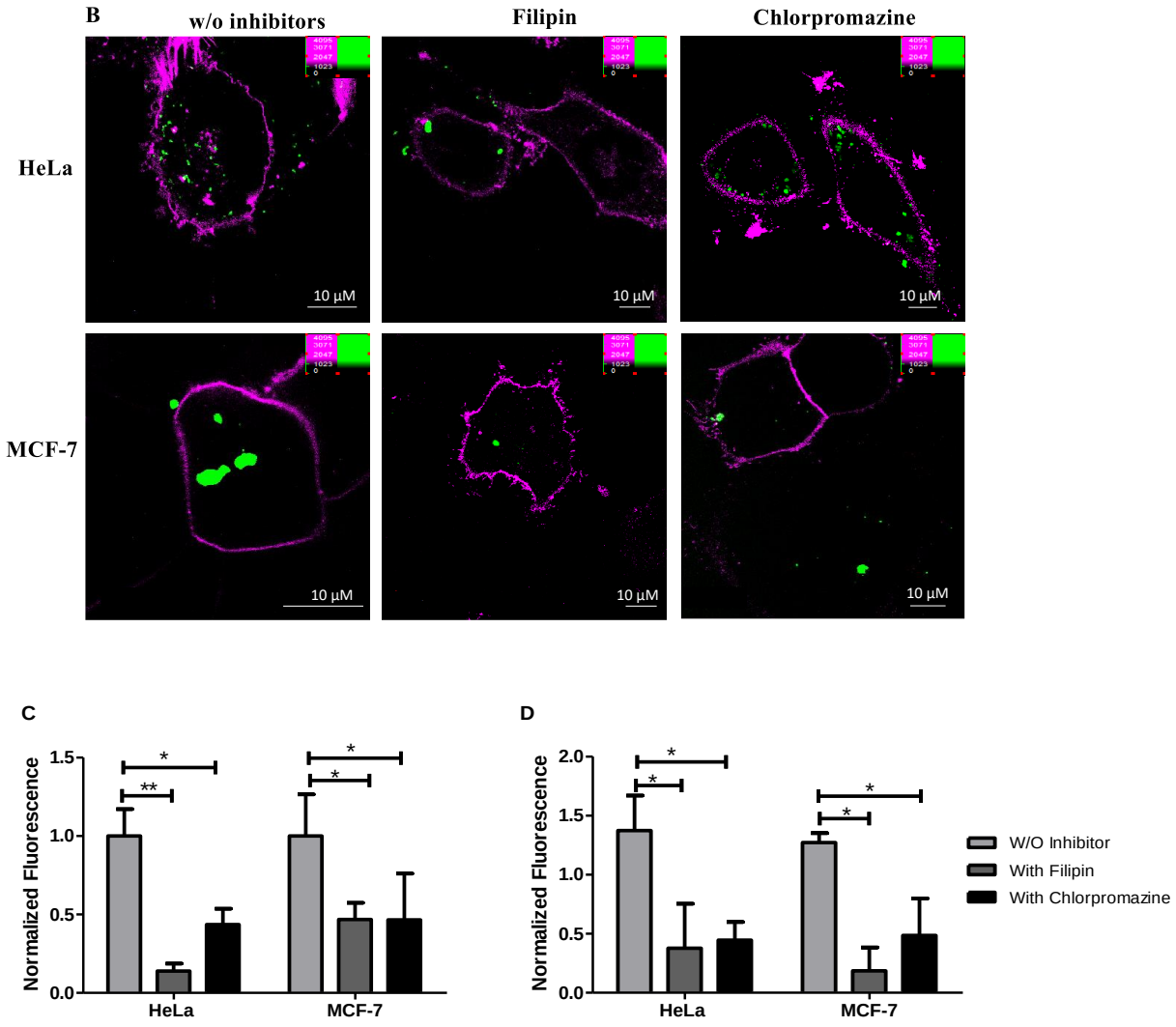

Figure 46. Effect of endocytosis inhibitors in the internalization of (A) HSA-GLU and (B) HSA-SPDP in HeLa and MCF-7 cells, 4 h post-treatment. The respective fluorescence intensities quantified employing ImageJ were plotted for (C) HSA-GLU and (D) HSA-SPDP. Statistical analysis was performed using one-way ANOVA Tukey's test. *p-value <0.01, ** p-value <0.001, and *** p-value <0.0001.

4.2.5. In cellulo release of Dox from albumin nanoparticles

After confirming the successful cellular internalization of albumin-based nanoparticles, it was interesting to study the in cellulo release of doxorubicin from HSA-SPDP. MCF-7 cells were treated with either Dox alone or with HSA-SPDP loaded with Dox for 3 h and the images were collected using confocal microscopy. The cells without any particles or drug were used as a

control. As shown in the Figure 47, Dox emission could be detected in the nucleus of the cells, meaning that it was released from the nanoparticles within 3 h of study.

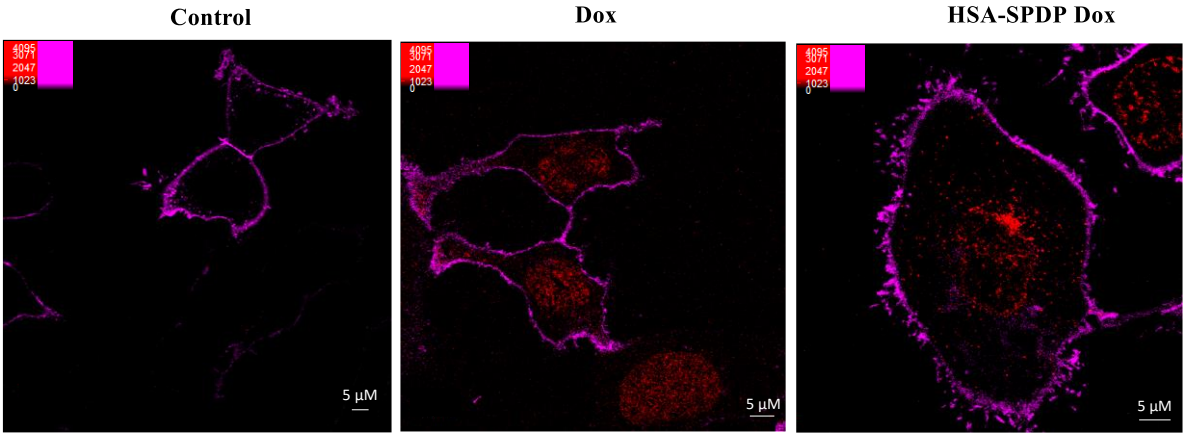

Figure 47. Fluorescence images of Dox and Dox-loaded HSA-SPDP in MCF-7 cells after 3 hours of treatment. Dox channel and DiR are shown in red and magenta, respectively. The contrast of red and magenta channels was kept constant in all the images.

4.2.6. Internalization of nanoparticles in 3D cancer spheroids

The internalization of HSA-GLU and HSA-SPDP was evaluated in 3D cell models, in particular in HeLa and MCF-7 spheroids (Figure 48). The spheroids were incubated for 24 h with the nanoparticles before evaluating the internalization using confocal microscopy. The internalization was observed in both HeLa and MCF-7 spheroids for both types of particles, however higher amount of nanoparticles could be detected in HeLa spheroids compared to MCF-7 spheroids, which was in accordance with the results obtained with the 2D monolayer cells.

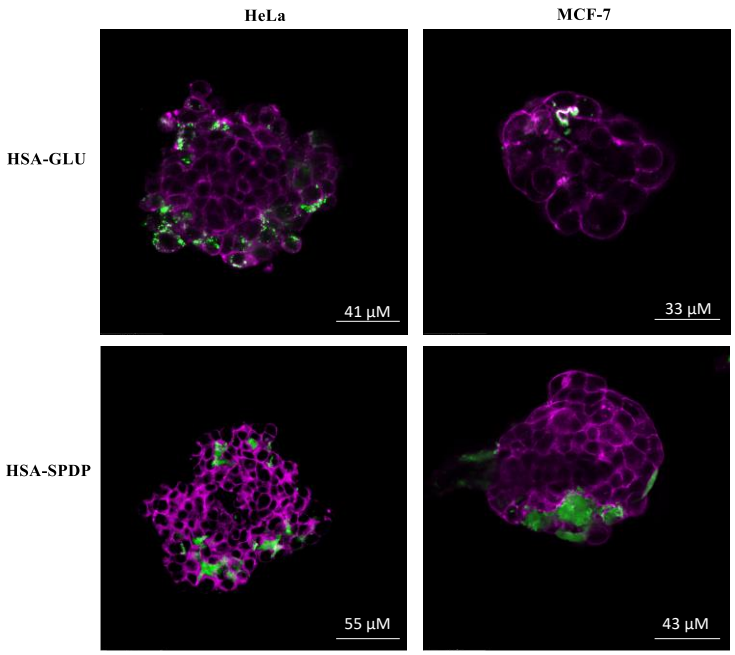

Figure 48. Confocal microscopy of HSA-GLU and HSA-SPDP incubated with HeLa and MCF-7 cellular spheroids. The cytoskeleton staining and the nanoparticles are shown in magenta and green, respectively.

4.2.7. Evaluation of cytotoxicity in 3D cancer spheroids

The cytotoxicity of the HSA-SPDP loaded with different chemotherapeutics was then studied in two different cancer spheroids (HeLa and MCF-7). HSA-SPDP loaded with Dox was tested in MCF-7 spheroids at the concentration of 40 µM, while HSA-SPDP loaded with Vola was tested in both MCF-7 and HeLa spheroids at the concentration of 20 µM. A control group without any particles was also included in the study. The cytotoxicity of the drug-loaded nanoparticles was then analyzed by monitoring the volumes variation of the spheroids over time. The volume of the spheroids was estimated assuming as approximate spherical symmetry of the multicellular aggregates.[23] Since the spheroids formed were not perfectly spherical in shape, the volumes were estimated using ellipsoid´s equation.[24] Figure 49 shows the changes in the volume of HeLa and MCF-7 spheroids when treated with different particles.

In all the cases, the volume of the spheroids increased gradually from day 1 to day 5 when no particles were added. When Dox alone was used in MCF-7 spheroids, the volume decreased significantly from day 1, with the decrease becoming more prominent on day 5. However, when

HSA-SPDP loaded with Dox was used, a decrease in the volume was observed only after day 3. The volume was not significantly different from the drug alone after day 5 (Figure 49 A). This can be attributed to the fact that the particles take some time to enter the densely packed spheroids and release the drug compared to the free drug.

HSA-SPDP loaded with Vola was studied in both MCF-7 and HeLa spheroids (Figure 49 B, C). In MCF-7 spheroids, unlike with HSA-SPDP loaded with Dox,, the particles loaded with the drug showed a significant reduction in volume on day 1. This can be due to the lower IC50 of Vola (approximately 11.5 nM) as mentioned in Chapter 3.2 compared to IC50 of Dox (approximately 1.2 µM).[25] There was no significant difference in the volume of spheroids treated with Vola alone or particles loaded with Vola after day 3 and day 5. The results obtained in HeLa were different than in MCF-7 spheroids (Figure 49 C). The volume of HeLa spheroids decreased drastically after day 1 when treated with Vola alone or particles loaded with Vola. At day 5, spheroids were completely erased in both cases. The enhanced cytotoxic activity in HeLa spheroids compared to MCF-7 can be due to the better internalization of particles in HeLa, as observed in Section 4.2.6.

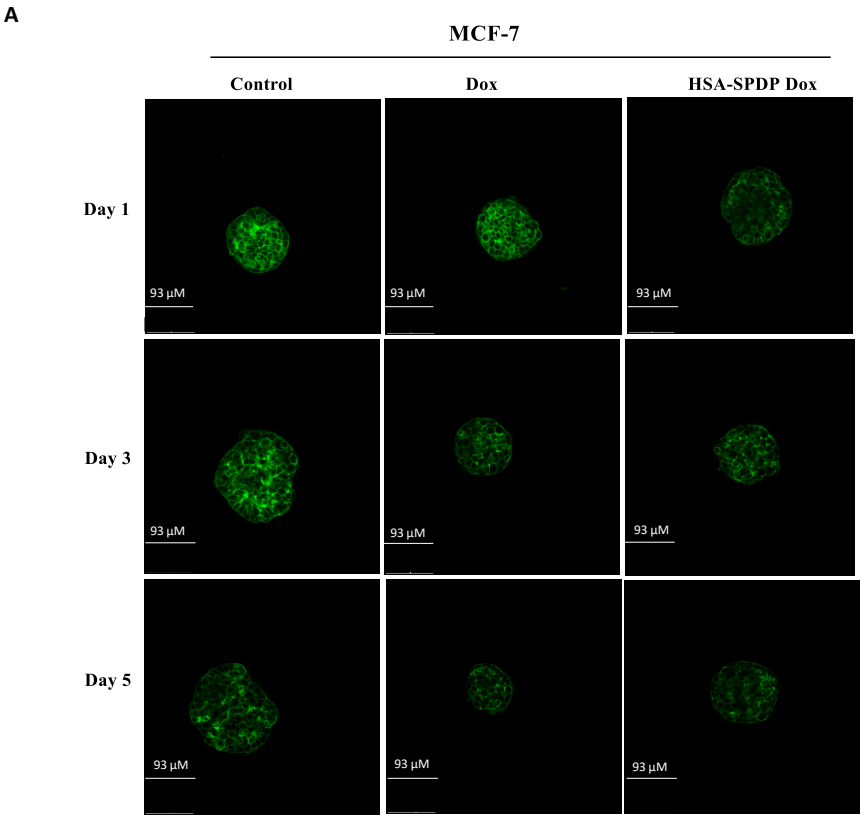

B

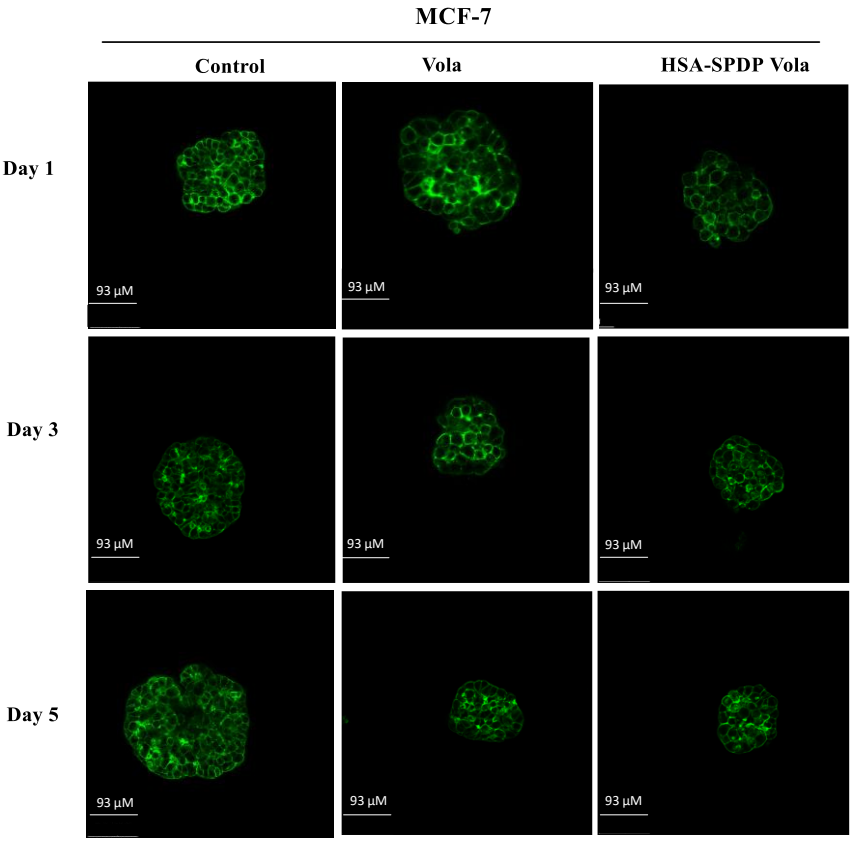
MCF-7
Control
Vola
HSA-SPDP Vola
Day 1
Day 3
Day 5
93 µM

C

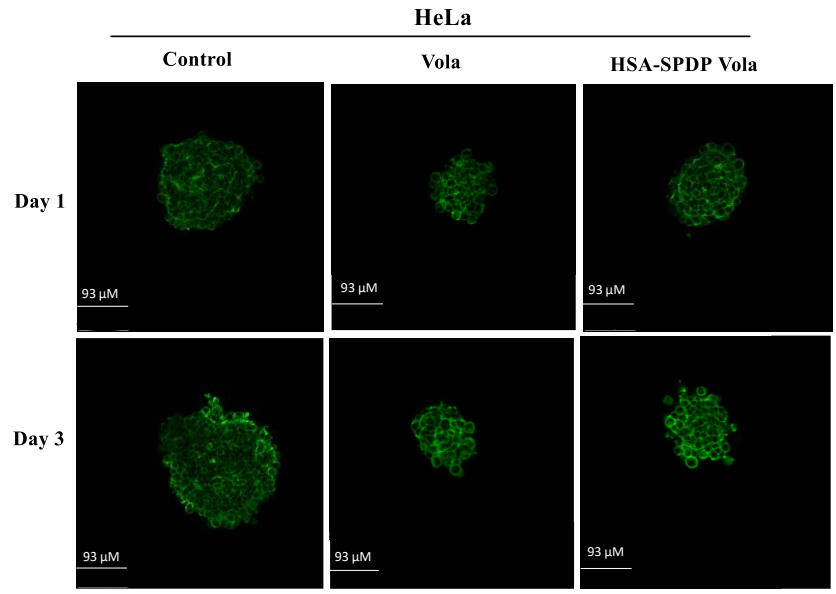
HeLa
Control
Vola
HSA-SPDP Vola
Day 1
Day 3
93 µM

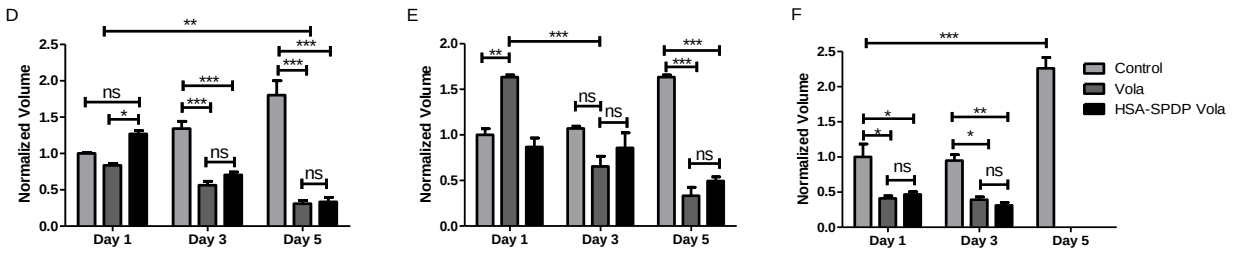

Figure 49. A-C represent the changes in volume when treated with HSA-SPDP loaded with Dox in MCF-7 spheroids, HSA-SPDP loaded with Vola in MCF-7 and HeLa spheroids, respectively. D-F represent the quantitative representation of the changes in volume. The concentration of drug used was 20 µM and 40 µM for Vola-loaded and Dox-loaded HSA-SPDP, respectively.Statistical analysis was performed using one-way ANOVA Tukey's test. ns p-value > 0.01, *p-value <0.01, ** p-value <0.001, and *** p-value <0.0001.

4.3. Conclusions

The main objective of the present study was to evaluate the ability of albumin-based nanoparticles to overcome the biological barriers and release the cargo in cancer cells. The accumulation of the particles in cancer sites, avoidance of endo-lysosomal entrapment and mechanism of internalization were studied. The studies were conducted in vitro, using 2D and 3D cancer cell models. Moreover, the versatility of the nanocarriers was evaluated by loading two different chemotherapeutic agents, doxorubicin and volasertib. The nanoparticles were internalized more in HeLa cells (both in 2D and 3D) than in MCF-7 cells. Moreover, both Dox and Vola-loaded HSA-SPDP showed reduction in the spheroid size over time. The change in the volume of spheroids treated with Dox-loaded HSA-SPDP was observed starting at day 3, whereas with Vola-loaded nanoparticles, the result was observed starting at day 1. This can be most probably due to different polarity and IC50 of the two drugs. These results pave the promising pathway for future in vivo experiments and potential use of these systems in cancer therapy.

References

1. Kumari, P.; Ghosh, B.; Biswas, S. Nanocarriers for cancer-targeted drug delivery. *J. Drug Target.* **2016**, *24*, 179–191, doi:10.3109/1061186X.2015.1051049.
2. Nehoff, H.; Parayath, N.N.; Domanovitch, L.; Taurin, S.; Greish, K. Nanomedicine for drug targeting: Strategies beyond the enhanced permeability and retention effect. *Int. J. Nanomedicine* **2014**, *9*, 2539–2555, doi:10.2147/IJN.S47129.
3. Bae, Y.H.; Park, K. Targeted drug delivery to tumors: Myths, reality and possibility. *J Control Release* **2011**, *153*, 198–205, doi:10.1016/j.jconrel.2011.06.001.Targeted.
4. Blanco, E.; Shen, H.; Ferrari, M. Principles of nanoparticle design for overcoming biological barriers to drug delivery. *Nat. Biotechnol.* **2015**, *33*, 941–951, doi:10.1038/nbt.3330.
5. Moghimi, S.M.; Patel, H.M. Serum-mediated recognition of liposomes by phagocytic cells of the reticuloendothelial system - The concept of tissue specificity. *Adv. Drug Deliv. Rev.* **1998**, *32*, 45–60, doi:10.1016/S0169-409X(97)00131-2.
6. Zimmermann, M.; Box, C.; Eccles, S.A. Two-dimensional vs. three-dimensional in vitro tumor migration and invasion assays. *Methods Mol. Biol.* **2013**, *986*, 227–252, doi:10.1007/978-1-62703-311-4.
7. Breslin, S.; O'Driscoll, L. Three-dimensional cell culture: The missing link in drug discovery. *Drug Discov. Today* **2013**, *18*, 240–249, doi:10.1016/j.drudis.2012.10.003.
8. Goodman, T.T.; Chee, P.N.; Suzie, H.P. 3-D tissue culture systems for the evaluation and optimization of nanoparticle-based drug carriers. *Bioconjug. Chem.* **2008**, *19*, 1951–1959, doi:10.1021/bc800233a.
9. Zanoni, M.; Piccinini, F.; Arienti, C.; Zamagni, A.; Santi, S.; Polico, R.; Bevilacqua, A.; Tesei, A. 3D tumor spheroid models for in vitro therapeutic screening: A systematic approach to enhance the biological relevance of data obtained. *Sci. Rep.* **2016**, *6*, 1–11, doi:10.1038/srep19103.
10. Fennema, E.; Rivron, N.; Rouwkema, J.; van Blitterswijk, C.; De Boer, J. Spheroid culture as a tool for creating 3D complex tissues. *Trends Biotechnol.* **2013**, *31*, 108–115, doi:10.1016/j.tibtech.2012.12.003.
11. Costa, E.C.; Moreira, A.F.; de Melo-Diogo, D.; Gaspar, V.M.; Carvalho, M.P.; Correia, I.J. 3D tumor spheroids: an overview on the tools and techniques used for their analysis. *Biotechnol. Adv.* **2016**, *34*, 1427–1441, doi:10.1016/j.biotechadv.2016.11.002.
12. Ricci, C.; Moroni, L.; Danti, S. Cancer tissue engineering-new perspectives in understanding the biology of solid tumours-a critical review. *OA Tissue Eng.* **2013**, *1*, 1–7, doi:10.13172/2052-9643-1-1-607.
13. Chan, H.F.; Zhang, Y.; Ho, Y.P.; Chiu, Y.L.; Jung, Y.; Leong, K.W. Rapid formation of multicellular spheroids in double-emulsion droplets with controllable microenvironment. *Sci. Rep.* **2013**, *3*, 3462, doi:10.1038/srep03462.
14. Yeon, S.E.; No, D.Y.; Lee, S.H.; Nam, S.W.; Oh, I.H.; Lee, J.; Kuh, H.J. Application of Concave Microwells to Pancreatic Tumor Spheroids Enabling Anticancer Drug Evaluation in a Clinically Relevant Drug Resistance Model. *PLoS One* **2013**, *8*, 1–12, doi:10.1371/journal.pone.0073345.

15. Lazzari, G.; Couvreur, P.; Mura, S. Multicellular tumor spheroids: A relevant 3D model for the: In vitro preclinical investigation of polymer nanomedicines. *Polym. Chem.* **2017**, *8*, 4947–4969, doi:10.1039/c7py00559h.
16. Van Zundert, I.; Fortuni, B.; Rocha, S. From 2d to 3d cancer cell models—the enigmas of drug delivery research. *Nanomaterials* **2020**, *10*, 1–30, doi:10.3390/nano10112236.
17. Ware, M.J.; Colbert, K.; Keshishian, V.; Ho, J.; Corr, S.J.; Curley, S.A.; Godin, B. Generation of homogenous three-dimensional pancreatic cancer cell spheroids using an improved hanging drop technique. *Tissue Eng. - Part C Methods* **2016**, *22*, 312–321, doi:10.1089/ten.tec.2015.0280.
18. Koppenol, W.H.; Bounds, P.L.; Dang, C. V. Otto Warburg's contributions to current concepts of cancer metabolism. *Nat. Rev. Cancer* **2011**, *11*, 325–337, doi:10.1038/nrc3038.
19. Görlach, A.; Acker, H. pO2- and pH-gradients in multicellular spheroids and their relationship to cellular metabolism and radiation sensitivity of malignant human tumor cells. *BBA - Mol. Basis Dis.* **1994**, *1227*, 105–112, doi:10.1016/0925-4439(94)90085-X.
20. Prajapati, R.; Garcia-Garrido, E.; Somoza, Á. Albumin-based nanoparticles for the delivery of doxorubicin in breast cancer. *Cancers (Basel).* **2021**, *13*, 1–17, doi:10.3390/cancers13123011.
21. Ma, X.; Sun, X.; Hargrove, D.; Chen, J.; Song, D.; Dong, Q.; Lu, X.; Fan, T.H.; Fu, Y.; Lei, Y. A Biocompatible and Biodegradable Protein Hydrogel with Green and Red Autofluorescence: Preparation, Characterization and in Vivo Biodegradation Tracking and Modeling. *Sci. Rep.* **2016**, *6*, 1–12, doi:10.1038/srep19370.
22. Mo, Y.; Barnett, M.E.; Takemoto, D.; Davidson, H.; Kompella, U.B. Human serum albumin nanoparticles for efficient delivery of Cu , Zn superoxide dismutase gene. *Mol. Vis.* **2007**, *13*, 746–757.
23. De Santis, I.; Tasnadi, E.; Horvath, P.; Bevilacqua, A.; Piccinini, F. Open-source tools for volume estimation of 3D multicellular aggregates. *Appl. Sci.* **2019**, *9*, 1616, doi:10.3390/app9081616.
24. Barbier, M.; Jaensch, S.; Cornelissen, F.; Vidic, S.; Gjerde, K.; De Hoogt, R.; Graeser, R.; Gustin, E.; Chong, Y.T.; Hickman, J.; et al. Ellipsoid segmentation model for analyzing light-attenuated 3D confocal image stacks of fluorescent multi-cellular spheroids. *PLoS One* **2016**, *11*, 1–19, doi:10.1371/journal.pone.0156942.
25. Fang, X.J.; Jiang, H.; Zhu, Y.Q.; Zhang, L.Y.; Fan, Q.H.; Tian, Y. Doxorubicin induces drug resistance and expression of the novel CD44st via NF-κB in human breast cancer MCF-7 cells. *Oncol. Rep.* **2014**, *31*, 2735–2742, doi:10.3892/or.2014.3131.

Chapter 5. Immunomodulatory studies of the albumin-based nanoparticles

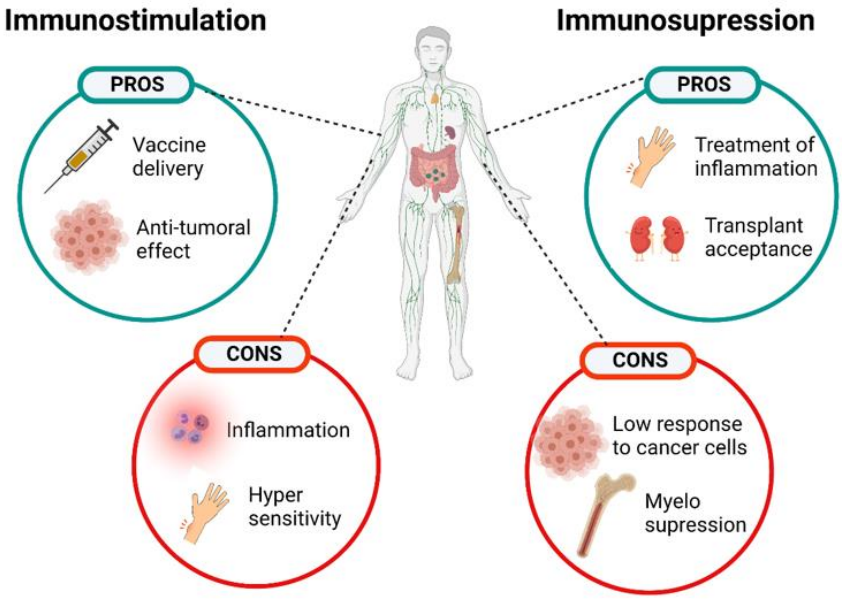

5.1. Introduction

The scope of nanoparticles is growing rapidly in the field of diagnostics, imaging and treatment of various diseases. They demonstrate enhanced performance compared to their corresponding bulk materials due to the improved surface properties and enhanced surface-to-volume ratios.[1] Despite their wide potential, nanoparticles have attracted increasing concerns regarding the potential adverse effects on the environment and human health.[2,3] Hence, the careful evaluation of the biosafety and toxicological profiles of nanoparticles is of utter importance, particularly in biological applications.

One of the major concerns of nanoparticles is their effect on the immune system, which is responsible for the protection from foreign substances, infections, and malignancies.[4,5] The immune system uses phagocytic cells like neutrophils, monocytes and macrophages, which can release the inflammatory mediators (basophils, mast cells and eosinophils) and natural killer cells.[6,7] However, it can be disturbed by the internal and external environment resulting in either immune stimulation or suppression. Therefore, a thorough evaluation should be done when foreign materials (chemical or biological entities) for therapeutic or diagnostic applications are used in live systems, to prevent undesired responses from the immune system. In this sense, nanoparticles have tremendous potential in cancer therapy, however, they may show unwanted interactions with the immune system. For instance, when carbon nanotubes were introduced into the abdominal cavity of mice, it led to asbestos-like pathogenic behavior, including inflammation and formation of granulomas.[8]

There are numerous studies reporting on the properties of nanoparticles, including their size, surface charge, particle coating, hydrophobicity/hydrophilicity, and the chemicals used in their preparation, which may affect the interaction of the nanoparticles with the immune system.[9–11] For instance, when Abraxane (paclitaxel-loaded albumin nano formulation) was used in patients with breast cancer, there was a lower incidence of grade 4 neutropenia compared to when the first generation of the paclitaxel formulation, containing Cremophor EL, was used.[12] Hence, the immunocompatibility of the nanocarriers is critical and must be evaluated before they are used in clinical settings.

Macrophages are the vital modulators and effector cells in the immune system and hence their activation is associated with other parts of the immune system.[13,14] Generally, macrophages are classified into three categories, namely pro-inflammatory (M1), non-activated or resting (M0) and anti-inflammatory (M2). M1 macrophages are responsible for the release of cytokines and chemokines, along with the use of lymphocytes in the inflamed areas, while M2 macrophages help in the control of inflammation through the release of various anti-inflammatory cytokines.[15] Hence, excessive activity of the M1 phenotype may lead to inflammatory diseases, whereas M2 activity may lead to tissue fibrosis and cancers.

In recent years, albumin-based nanoparticles have gained tremendous attention as delivery vehicles for chemotherapeutics, nucleic acids, and diagnostic tools.[16] Our previous study has also identified BSA and HSA nanoparticles as potential candidates for the delivery of chemotherapeutics such as Doxorubicin and SN38.[17] Many reports have claimed the safety and biocompatibility of the albumin-based nanocarriers. However, there are not any studies, to our knowledge, which assess the interactions of the albumin-based nanocarriers with the immune system. Hence, in the present study, the effect of various albumin nanoparticles will be discussed, by using murine RAW 264.7 and human THP-1 cells. The RAW 264.7 cells are monocyte/macrophage-like cells, originating from Abelson leukemia virus transformed cell line derived from BALB/c mice. On the other hand, THP-1 cells are the immortalized monocyte-like cell line derived from the peripheral blood of a childhood case of the acute monocytic leukemia.[18] These cells are being described as an appropriate model of macrophages.[19] We chose murine macrophages and human macrophages to facilitate the use of nanoparticles in animal studies and in clinical translation, respectively. The effect of using various albumin-based nanoparticles in the macrophage phenotype switching will also be discussed in detail.

5.2. Results and discussion

5.2.1. Cell viability assessment in RAW 264.7 and THP-1 cells

Firstly, the cytotoxicity of the prepared nanoparticles was tested in RAW 264.7 murine macrophage cells and THP-1 human monocytes. The cells were cultured with ABN-GLU, ABN-SPDP or HSA-SPDP for 24h, 48h or 72h, and the cell viability was evaluated by CellTiter-Glo luminescence assay. Interestingly, we observed different results in murine and human

macrophages. As shown in Figure 50 (A-C), all the nanoparticles, till the concentration of 1 µM had negligible cytotoxicity in RAW 264.7 cells, with the percentage of viable cells maintained above 90% after 72h of treatment. However, ABN-SPDP and ABN-GLU showed cytotoxicity when the concentration was increased to 3 µM after 72 hours. On the contrary, ABN-GLU and HSA-SPDP showed minimal cytotoxicity in THP-1 cells in all the concentration range tested, even after 72h Figure 50 (D-F). However, slight cytotoxicity was observed with ABN-SPDP after 72h, even at the concentration of 1 µM. These results indicate that HSA-SPDP is most tolerable in both murine and human cell lines among all the albumin nanoparticles studied. In the additional experiments, the nanoparticles were used at 1 µM, which is the highest tolerable concentration in RAW 264.7 and THP-1 cells. The non-toxic activity of the albumin-based nanoparticles was also demonstrated in previous studies where they were used as imaging and nanosensor systems.[20] The biocompatibility of the albumin nanoparticles strengthens the use of these systems as the delivery vehicle for various biomedical applications.

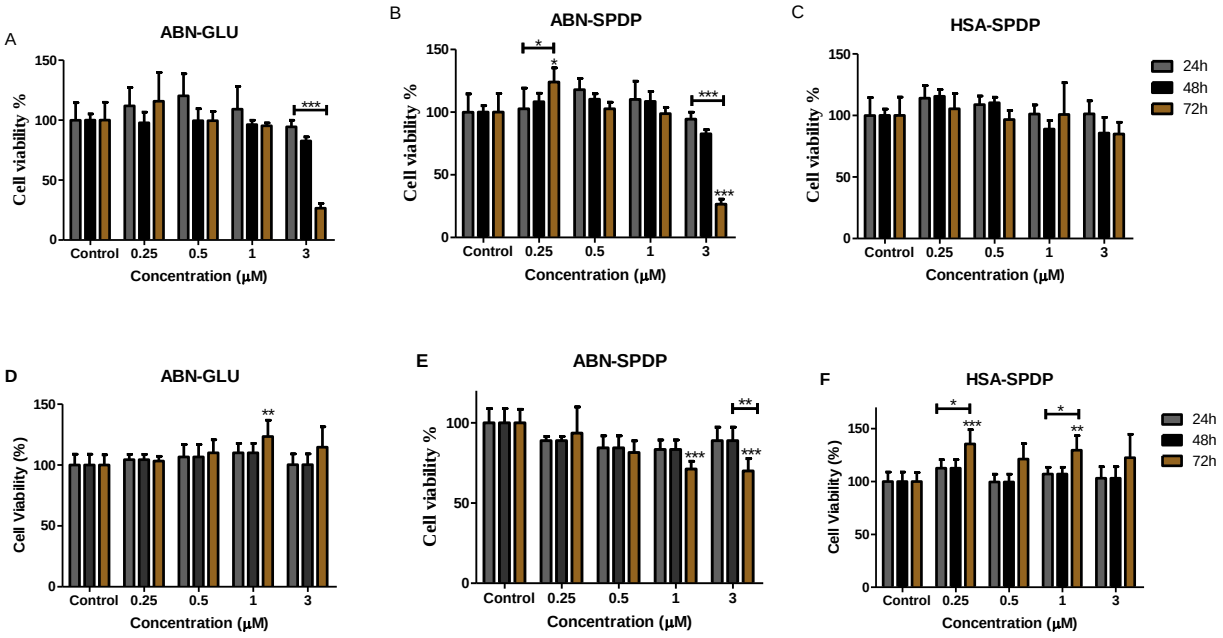

Figure 50. Cell viability of various nanoparticles at varying concentration in RAW 264.7 (A-C) and THP-1 (D-F) cells 24-, 48- and 72h post-treatment. The measurements were performed in triplicates and statistical analysis was performed using one-way ANOVA Tukey's test. * p-value < 0.01, ** p-value < 0.001, and *** p-value < 0.0001.

5.2.2. Cellular uptake of nanoparticles

The cellular uptake of the nanoparticles was then studied in RAW 264.7 and THP-1 cells. The HSA-SPDP and ABN-SPDP were first conjugated with CY5 to facilitate the tracking in the cells. The modified nanoparticles were then added to the cells and incubated for 24h. The fluorescence was then quantified using a flow cytometer. As shown in the Figure 51, both HSA-SPDP and ABN-SPDP were successfully internalized in both RAW 264.7 and THP-1 cells. The percentage of fluorescent positive cells was more than 90% in both the cell lines. These values were comparable to the free CY5, and hence, the nanoparticles can be internalized in both the murine macrophages and the human monocytes.

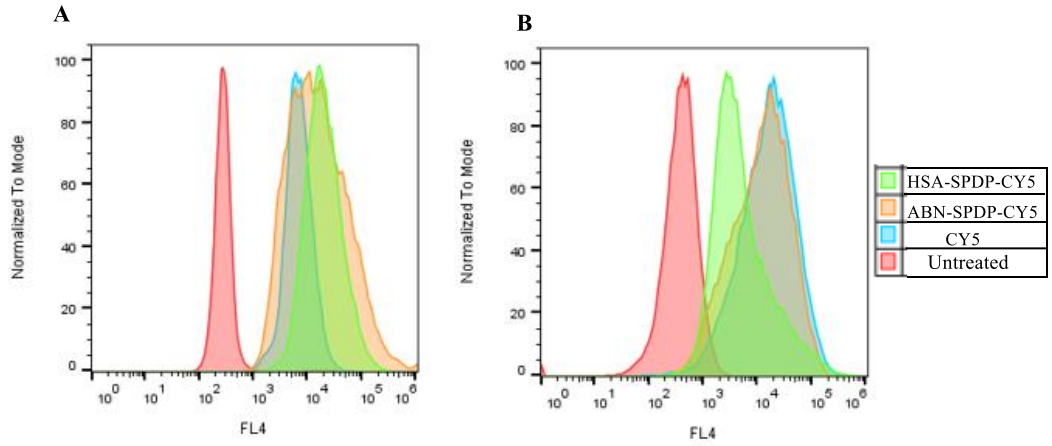

Figure 51. Quantification of fluorescence in RAW 264.7 (A) and THP-1 (B) cells 24 hours post-treatment with CY5 conjugated BSA-SPDP and HSA-SPDP.

5.2.3. Production of intracellular ROS

The ROS scavenging ability of the prepared nanoparticles was analyzed in RAW 264.7 and THP-1 cells. For this assay, the non-fluorescent DFC-DA, which can diffuse into the cytoplasm and be transformed into a fluorescent compound in the presence of ROS was used. In THP-1 cells, ABN-GLU and ABN-SPDP did not show significant changes in the levels of ROS compared to the untreated conditions (Figure 52). However, there was a decrease in the levels of ROS produced with HSA-SPDP after 72 h of treatment, even at the lower concentration of 0.25 µM. On the contrary, in RAW 264.7 cells, there were no significant changes in the levels of ROS produced when treated with HSA-SPDP. However, there was a substantial increase in the ROS levels after 48h when treated with ABN-GLU starting from the concentration of 0.25 µM. In the case of ABN-

SPDP, the increase was significant after 72h at 1 µM and from 48h when 3 µM was employed. The levels of ROS produced in both cell lines could be correlated with the cell viability assay performed except with ABN-GLU in RAW 264.7 since the ROS produced is not reflected in the reduction of cell viability at lower concentrations.

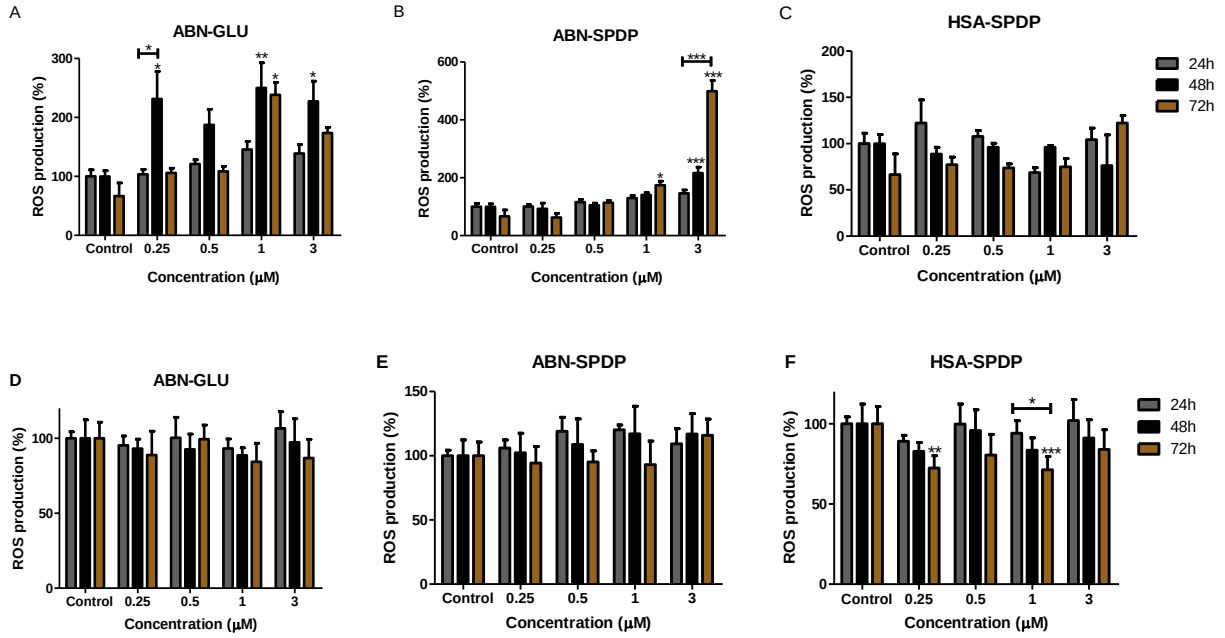

Figure 52. Production of intracellular ROS by various albumin-based nanoparticles at varying concentration in RAW 264.7 (A-C) and THP-1 (D-F) cells 24-, 48- and 72h post-treatment. The measurements were performed in triplicates and statistical analysis was performed using one-way ANOVA Tukey's test. * p-value < 0.01, ** p-value < 0.001, and *** p-value < 0.0001.

5.2.4. Cell cycle analysis

The effect of various albumin-based nanoparticles on the cell cycle was also studied in both cell lines. In these assays, the concentration of the nanoparticles used was 1 µM. As shown in Figure 53, there were no significant changes in the population of cells in G0/G1, S and G2/M phases of both murine and human macrophages. In RAW 264.7 cells, the percentage of cells in G0/G1, S and G2/M phases remained constant at around 55%, 8% and 36%, respectively, after 24 h of treatment. The population of cells in G0/G1 slightly increased to around 70%, while that in S and G2/M phase decreased to around 4% and 17%, respectively, both after 48 and 72h of treatment. However, in THP-1 cells, the percentage of cells in G0/G1, S and G2/M phases remained constant

at around 48%, 24% and 16%, respectively, irrespective of the treatment time and the types of nanoparticles used. These results suggest that the nanoparticles are non-cytotoxic.

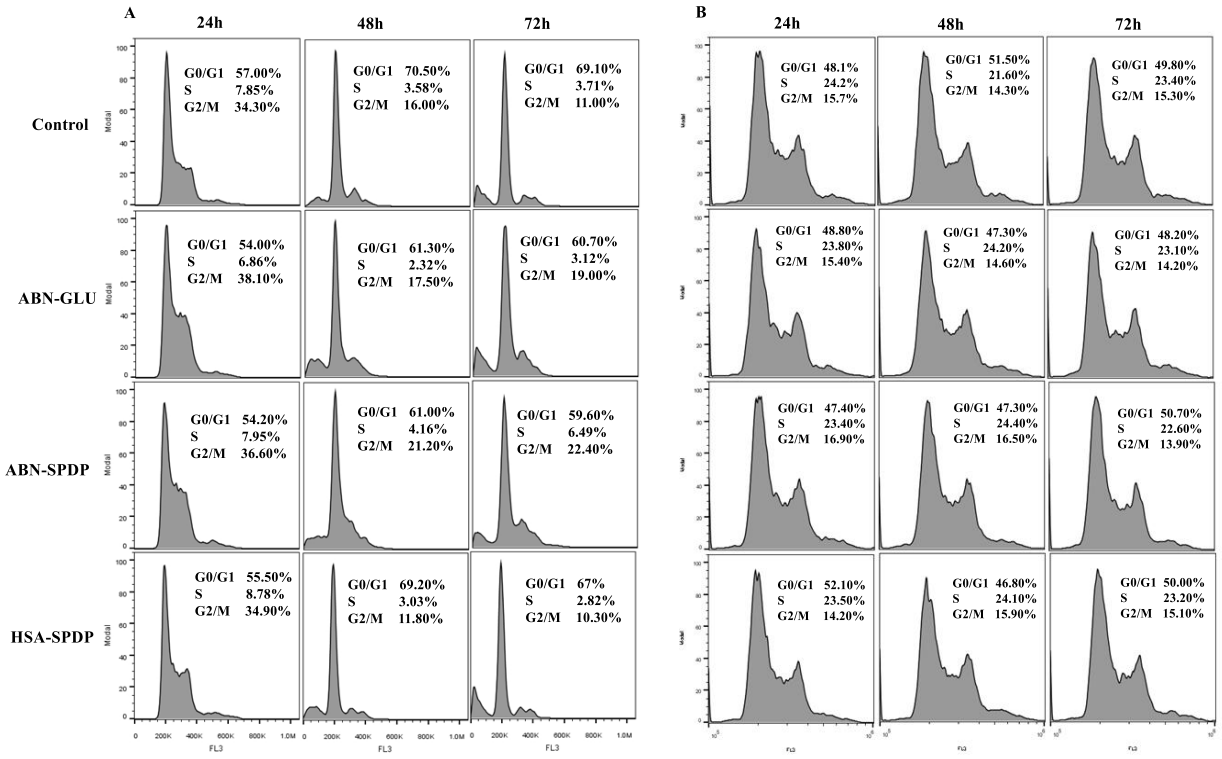

Figure 53. Cell cycle analysis of different albumin-based nanoparticles in (A) RAW 264.7 and (B) THP-1 cells after 24-, 48-, and 72h of treatment.

5.2.5. Macrophage phenotype switch study

The effect of the albumin nanoparticles in the switching of the phenotypes in the macrophages was next studied in RAW 264.7 and THP-1 cells. The cells stimulated with LPS and IFN-γ developed into M1 phenotype (M1 control), whereas the cells treated with cytokines evolved into M2 phenotype (M2 control). M1 and M2 phenotypes have unique markers on the surface of the cells (Figure 54), which can be exploited to monitor these processes and characterize them. In this case, the phenotype switch between M1 and M2 was carried out by the evaluation of the expression of CD80 and CD86 (M1 markers) and CD206 (M2 marker) by immunostaining and subsequent analysis through flow cytometry. Cells without any stimulations were used as the M0 controls.

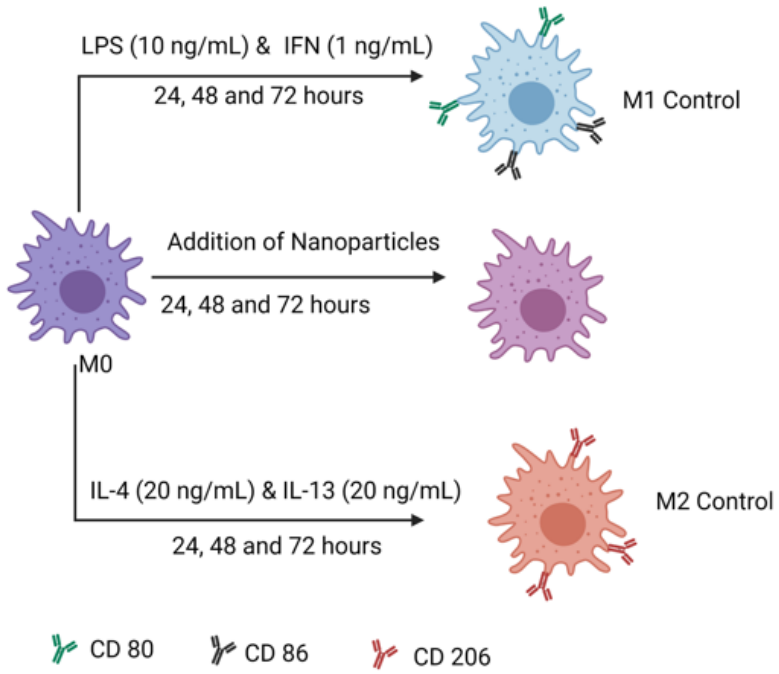

Figure 54. Schematic representation of the stimulation of macrophages to M1 and M2 stages and the treatment of the cells with the nanoparticles. The measurements were performed in triplicates and statistical analysis was performed using one-way ANOVA Tukey's test. * p-value < 0.01, ** p-value < 0.001, and *** p-value < 0.0001.

As shown in Figure 55 (A, B, E, F), there was 4.3 and 2.3 folds increment in the expression of CD80 and CD86, respectively, in M1 control compared to the resting stage M0 in RAW 264.7 cells. Both ABN-GLU and ABN-SPDP also showed the enhancement of both CD80 and CD86 expression. Similar pro-inflammatory effect was observed with BSA nanoparticles when histophathological analysis of the mice skin was conducted, which probably was due to the morphology of the nanoparticles.[21] However, there was no significant change in the levels of both CD80 and CD86 when treated with HSA-SPDP.

The results obtained were different in the human THP-1 cells as shown in Figure 55 (C, D, G, H). There was an approximately 3.7 fold increase in the expression of CD80 in M1 pro-inflammatory macrophages compared to M0 control. However, there were no significant changes in the levels of CD86. Similar to RAW 264.7 cells, ABN-GLU showed enhanced expression of CD80 (3.1 folds). However, both ABN-SPDP and HSA-SPDP showed no significant changes in the level of CD80.

These results in murine and human macrophages indicate that HSA-SPDP interacts least with the immune system, whereas ABN-GLU and ABN-SPDP may induce an inflammatory response, most prominently with ABN-GLU. The nanocarriers based on BSA may be problematic in terms of translation to animal models which has been reported also in the previous studies.[22] However, the results with HSA-SPDP opens the possibility of using these nanoparticles in mice studies instead of the more expensive murine albumin. In the similar trend, in the study conducted by Banerjee and co-workers,[23] HSA NPs were successfully used in atherosclerotic mice which further strengthens the use of HSA-SPDP in animal models without the prominent immunoreactivity.

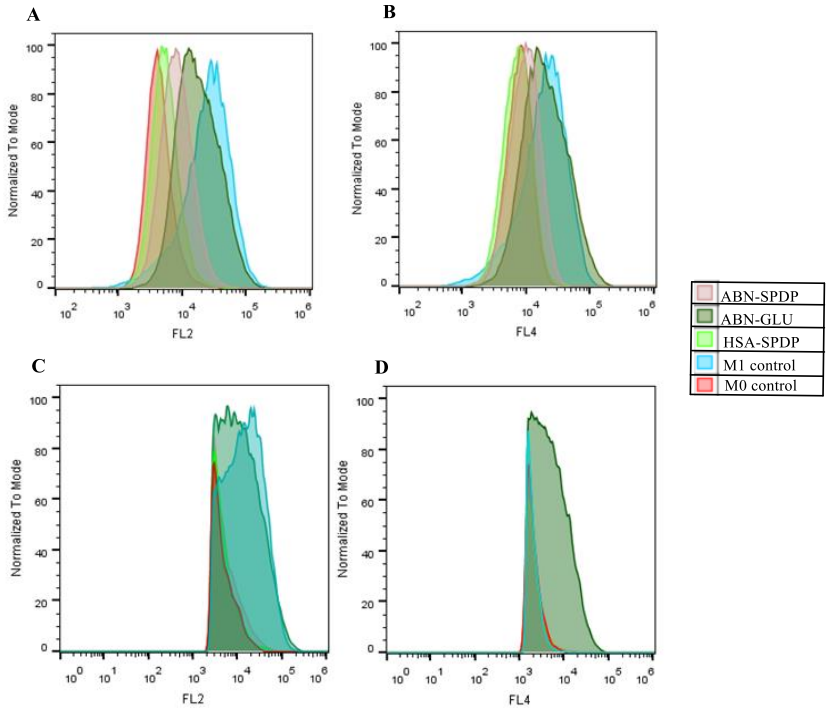

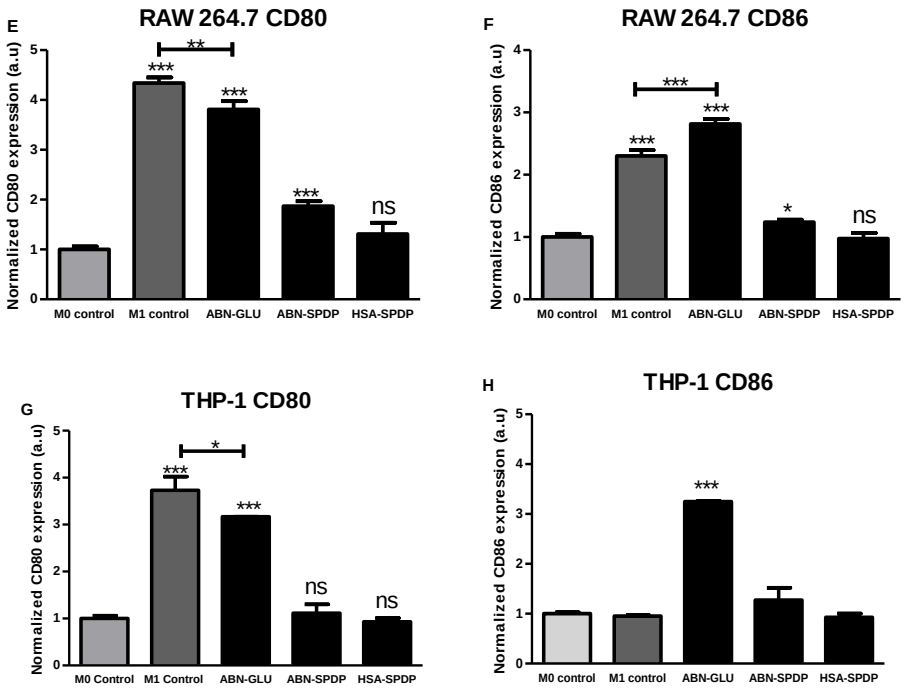

Figure 55. Expression of different markers (A, C) CD80 and (B, D) CD86 in RAW 264.7 (A, B) and THP-1 cells (C, D). The respective normalized expression of the markers is shown in the graph (E-H). The measurements were performed in triplicates, and statistical analysis was performed using one-way ANOVA Tukey's test. * p-value < 0.01, ** p-value < 0.001, and *** p-value < 0.0001.

5.3. Conclusions

The research involving nanoparticles for commercial application is growing exponentially and hence, the safety and toxicity of these nanoparticles have dramatically attracted the public attention. In this sense, albumin-based nanoparticles are not the exception, and therefore, it is essential to analyze their safety. In the present study, we focused on the effect of various albumin-based nanoparticles in the immune system, by analyzing their effect in murine RAW 264.7 and human THP-1 cells. The use of ABN-GLU, ABN-SPDP and HSA-SPDP in macrophages was evaluated in terms of cell viability, internalization, production of ROS, changes in cell cycle and macrophages phenotype switching. The results obtained in the study suggest that the nanoparticles are not cytotoxic in both the cell lines in a concentration till 1 µM. Moreover, the immunomodulatory studies reveal that ABN-GLU and ABN-SPDP could trigger the inflammatory responses in the murine and human macrophages, while HSA-SPDP showed no interaction. The

obtained results indicate the possibility of translating HSA-SPDP in animal models. However, further studies are required for a better understanding of the effects of albumin-based nanoparticles in immunomodulation, since immune system is quite complex and cannot be relied only on the effects on macrophages. The preliminary results from the present study however pave the path for the facil clinical translation of HSA nanoparticles with minimum undesirable immunogenic effects.

References

1. Jeevanandam, J.; Barhoum, A.; Chan, Y.S.; Dufresne, A.; Danquah, M.K. Review on nanoparticles and nanostructured materials: History, sources, toxicity and regulations. *Beilstein J. Nanotechnol.* **2018**, *9*, 1050–1074, doi:10.3762/bjnano.9.98.

2. Zhao, J.; Castranova, V. Toxicology of nanomaterials used in nanomedicine. *J. Toxicol. Environ. Heal. - Part B Crit. Rev.* **2011**, *14*, 593–632, doi:10.1080/10937404.2011.615113.

3. Scuri, M.; Chen, B.T.; Castranova, V.; Reynolds, J.S.; Johnson, V.J.; Samsell, L.; Walton, C.; Piedimonte, G. Effects of titanium dioxide nanoparticle exposure on neuroimmune responses in rat airways. *J. Toxicol. Environ. Heal. - Part A Curr. Issues* **2010**, *73*, 1353–1369, doi:10.1080/15287394.2010.497436.

4. Zolnik, B.S.; González-Fernández, Á.; Sadrieh, N.; Dobrovolskaia, M.A. Minireview: Nanoparticles and the immune system. *Endocrinology* **2010**, *151*, 458–465, doi:10.1210/en.2009-1082.

5. Parkin, J.; Cohen, B. An Overview of the Immune System. *Lancet* **2001**, *357*, 1777–1789, doi:10.1201/b15224-2.

6. Peter J. Delves; Roitt, I.M. The immune system. *Adv. Immunol.* **2000**, *343*, 37–49.

7. Iwasaki, A.; Medzhitov, R. Regulation of adaptive immunity by the innate immune system. *Science (80-.).* **2010**, *327*, 291–295, doi:10.1126/science.1183021.

8. Poland, C.A.; Duffin, R.; Kinloch, I.; Maynard, A.; Wallace, W.A.H.; Seaton, A.; Stone, V.; Brown, S.; MacNee, W.; Donaldson, K. Carbon nanotubes introduced into the abdominal cavity of mice show asbestos-like pathogenicity in a pilot study. *Nat. Nanotechnol.* **2008**, *3*, 423–428, doi:10.1038/nnano.2008.111.

9. Dobrovolskaia, M.A.; Aggarwal, P.; Hall, J.B.; McNeil, S.E. Preclinical studies to understand nanoparticle interaction with the immune system and its potential effects on nanoparticle biodistribution. *Mol. Pharm.* **2008**, *5*, 487–495, doi:10.1021/mp800032f.

10. Dobrovolskaia, M.A.; McNeil, S.E. Immunological properties of engineered nanomaterials.

Nat. Nanotechnol. **2007**, *2*, 469–478, doi:10.1142/9789814287005_0029.

11. Aggarwal, P.; Hall, J.B.; McLeland, C.B.; Dobrovolskaia, M.A.; McNeil, S.E. Nanoparticle interaction with plasma proteins as it relates to particle biodistribution, biocompatibility and therapeutic efficacy. *Adv. Drug Deliv. Rev.* **2009**, *61*, 428–437, doi:10.1016/j.addr.2009.03.009.

12. Stinchcombe, T.E.; Socinski, M.A.; Walko, C.M.; O'Neil, B.H.; Collichio, F.A.; Ivanova, A.; Mu, H.; Hawkins, M.J.; Goldberg, R.M.; Lindley, C.; et al. Phase I and pharmacokinetic trial of carboplatin and albumin-bound paclitaxel, ABI-007 (Abraxane®) on three treatment schedules in patients with solid tumors. *Cancer Chemother. Pharmacol.* **2007**, *60*, 759–766, doi:10.1007/s00280-007-0423-x.

13. Martinez, F.O.; Gordon, S. The M1 and M2 paradigm of macrophage activation: Time for reassessment. *F1000Prime Rep.* **2014**, *6*, 1–13, doi:10.12703/P6-13.

14. Jiao, Q.; Li, L.; Mu, Q.; Zhang, Q. Immunomodulation of nanoparticles in nanomedicine applications. *Biomed Res. Int.* **2014**, *2014*, 1–19, doi:10.1155/2014/426028.

15. Orekhov, A.N.; Orekhova, V.A.; Nikiforov, N.G.; Myasoedova, V.A.; Grechko, A. V.; Romanenko, E.B.; Zhang, D.; Chistiakov, D.A. Monocyte differentiation and macrophage polarization. *Vessel Plus* **2019**, *3*, 1–20, doi:10.20517/2574-1209.2019.04.

16. Elzoghby, A.O.; Samy, W.M.; Elgindy, N.A. Albumin-based nanoparticles as potential controlled release drug delivery systems. *J. Control. Release* **2012**, *157*, 168–182, doi:10.1016/j.jconrel.2011.07.031.

17. Prajapati, R.; Garcia-Garrido, E.; Somoza, Á. Albumin-based nanoparticles for the delivery of doxorubicin in breast cancer. *Cancers (Basel).* **2021**, *13*, 1–17, doi:10.3390/cancers13123011.

18. Tsuchiya, S.; Yamabe, M.; Yamaguchi, Y.; Kobayashi, Y.; Konno, T.; Tada, K. Establishment and characterization of a human acute monocytic leukemia cell line (THP-1). *Int. J. Cancer* **1980**, *26*, 171–176.

19. Taciak, B.; Białasek, M.; Braniewska, A.; Sas, Z.; Sawicka, P.; Kiraga, Ł.; Rygiel, T.; Król, M. Evaluation of phenotypic and functional stability of RAW 264.7 cell line through serial passages. *PLoS One* **2018**, *13*, 1–13, doi:10.1371/journal.pone.0198943.

20. Yang, Q.; Ye, Z.; Zhong, M.; Chen, B.; Chen, J.; Zeng, R.; Wei, L.; Li, H.W.; Xiao, L. Self-Assembled Fluorescent Bovine Serum Albumin Nanoprobes for Ratiometric pH Measurement inside Living Cells. *ACS Appl. Mater. Interfaces* **2016**, *8*, 9629–9634, doi:10.1021/acsami.6b00857.

21. Ingrid Oliveira da Silva, N.; Salvador, E.A.; Rodrigues Franco, I.; de Souza, G.A.P.; de Souza Morais, S.M.; Prado Rocha, R.; Dias Novaes, R.; Paiva Corsetti, P.; Malaquias, L.C.C.; Leomil Coelho, L.F. Bovine serum albumin nanoparticles induce histopathological changes and inflammatory cell recruitment in the skin of treated mice. *Biomed. Pharmacother.* **2018**, *107*, 1311–1317, doi:10.1016/j.biopha.2018.08.106.

22. Hassanin, I.; Elzoghby, A. Albumin-based nanoparticles: a promising strategy to overcome cancer drug resistance. *Cancer Drug Resist.* **2020**, *3*, 930–946, doi:10.20517/cdr.2020.68.

23. Banerjee, S.; Sengupta, J.; Aljarilla, A.I.; Setaro, F.; Makinen, P.; Wu, L.; Holappa, L.; de la Escosura, A.; Martinelli, C.; Trohopoulos, P.; et al. Human serum albumin nanoparticles loaded with phthalocyanine dyes for potential use in photodynamic therapy for atherosclerotic plaques. *Precis. Nanomedicine* **2019**, *2*, 278–302, doi:10.33218/prnano2(2).190411.1.

Chapter 6: Albumin-based nanostructures for the delivery of nucleic acids

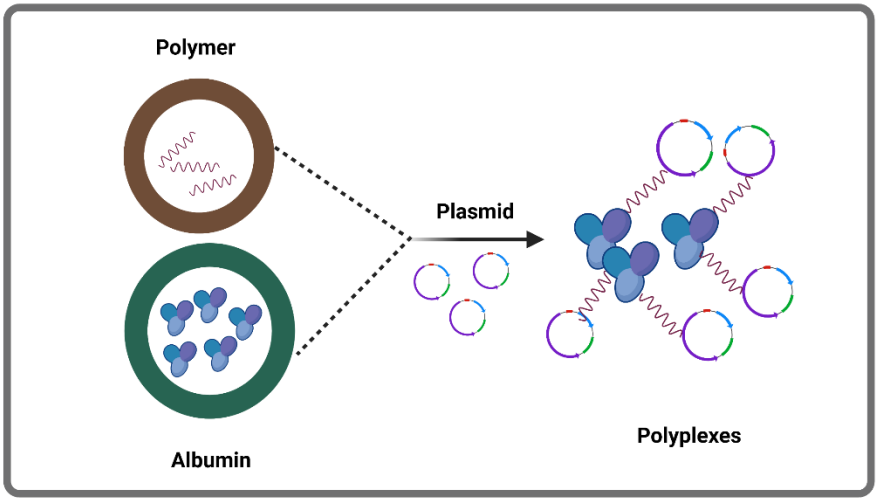

6.1. Albumin-based polyplexes for the delivery of nucleic acids in cancer

6.1.1. Introduction

With the advancement in the knowledge regarding molecular biology and pathophysiology of cancer, novel strategies against cancer have emerged in recent times.[1,2] In particular, nucleic acids are receiving growing attention because of their potential use in wide range of tumors. The most widely used nucleic acids for cancer therapy include small interfering RNA (siRNA), antisense oligonucleotides (ASOs), aptamers, micro RNAs (miRNA), and plasmid DNA (pDNA).[3,4] Their mechanisms of action vary widely, ranging from mRNA regulation to protein binding, which can be designed to promote the reduction in cancer cell proliferation, induction of apoptosis, enhancement of immune-stimulatory responses and inhibition of neoangiogenesis.[5–7] The small RNAs form an RNA-induced silencing complex (RISC), which silences the mRNA translation. In contrast, ASOs can act either by suppression of the ribonucleoprotein activity or by activation of the enzymatic cascade that enhances mRNA degradation.[8] The tremendous therapeutic potential of nucleic acids has been assessed in multiple experiments in cell culture or animal models.[9,10] However, some challenges need to be addressed to ease their path to the clinic.

6.1.1.1. Limitations associated with nucleic acids delivery

Despite the promising therapeutic applications of nucleic acids in cancer therapy, their effective delivery to the target sites is still challenging.[11,12] Particularly, the major drawbacks associated with nucleic acid delivery include difficulty in accessing deeply seated tumor sites, biological barriers, enzymatic degradation by nucleases, rapid clearance by kidney filtration, triggering of the immune system and effects in non-targeted genes. The naked nucleic acids cannot enter the cells because of their inherent properties like hydrophilicity, large size and negative charges.[13] Nucleic acids are rapidly degraded by intra- and extracellular enzymes even before reaching the target cells. This was demonstrated in a study conducted in mice where a pDNA was fully degraded within 5 minutes after the injection.[14] Hence, the sufficient amount of genes required to elicit the therapeutic effect cannot be reached at the target sites. The nucleic acids can also trigger the immune system resulting in the release of cytokines that may further lead to serious inflammatory responses.[15] In addition, inhibition or overexpression of a non-targeted gene, commonly called the “off-target” effect, is one major setback in nucleic acid therapy.[16]

The major limitations associated with the delivery of nucleic acids are demonstrated in Figure 56 along with the possible solutions.

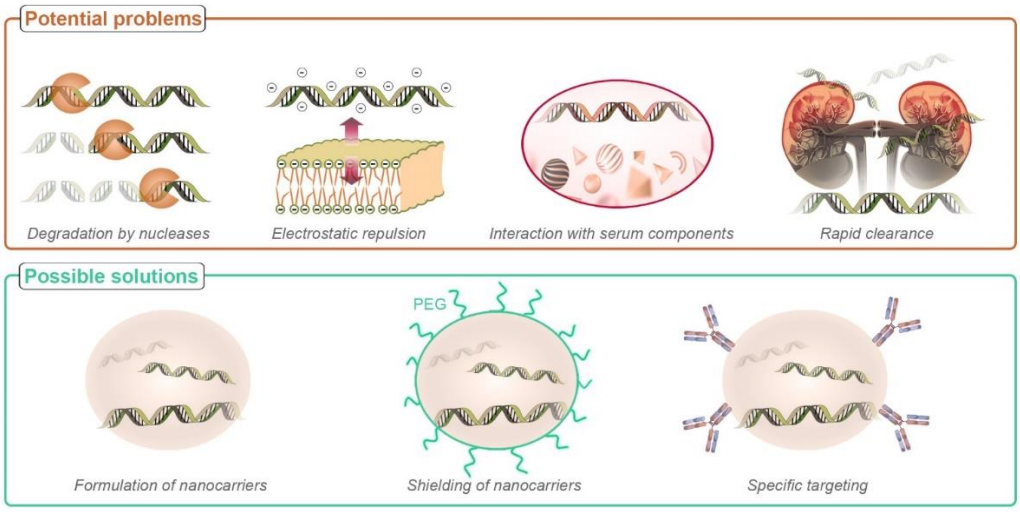

Figure 56. Various barriers to nucleic acid delivery and their possible solutions

6.1.1.2. Nanocarriers for nucleic acid delivery

To overcome the challenges associated with the delivery of nucleic acids to cancer sites, viral and non-viral vectors are being used extensively. The viral vectors show high transfection efficiency and possess strong promoters for the long-term expression of genes. However, carcinogenicity, inflammation, immunogenicity, and high production costs are still the primary concerns.[17] On the other hand, non-viral vectors based on lipids, proteins, polymers are considered relatively safe but show low and transient gene transfection. Hence, the development of biocompatible and biodegradable delivery vehicles possessing specificity to the target sites, and avoiding immune system activation is of utter importance.[18] In this regard, nanocarriers based on cationic polymers are gaining much popularity because of the ease of synthesis, safety, and low immune response.[19,20]

6.1.1.3. Use of cationic polymers

The cationic polymers, particularly polyethylenimine (PEI), a well-characterized, effective gene transfer vehicle,[21–23] is gaining increased attention because of its various properties like high buffering capacity and low immunogenicity.[23,24] The positively charged PEI can interact with the negatively charged nucleic acids condensing it to smaller sizes, forming the complexes called polyplexes. The polyplexes effectively protect the nucleic acids against degradation by nucleases

and enhance the cellular uptake because of the overall positive surface charge.[23,25] Moreover, PEI has the unique property of pumping protons into endosomes, increasing ionic strength and osmotic swelling, commonly known as the proton sponge effect.[26] This property helps in overcoming lysosomal degradation, one of the major barriers to efficient gene transfer.[23,27]

Despite the various advantages associated with PEI, the cytotoxicity of these cationic polymers, which limits their clinical application, cannot be neglected.[28] Numerous strategies to reduce the off-target cytotoxicity of polymers by PEGylation, thiolation, disulfide linkage, or fluorination are hence being employed.[29–31] The low molecular weight PEIs crosslinked with biodegradable disulfide bonds enhance rapid degradation after cellular internalization along with the release of cargo in the nucleus or cytosol due to the higher glutathione concentration inside the cells compared to the extracellular environment.[31,32] In addition, the introduction of hydrophilic non-cationic moieties like polyethylene glycol (PEG) drastically reduces cytotoxicity, primarily due to steric shielding of the surface charge.[33] In addition, PEGylation reduces the non-specific electrostatic interaction of polyplexes, inhibits the reticuloendothelial system activation and increases the half-life of polyplexes in the blood.[34,35]

Furthermore, various studies suggest the conjugation of cationic polymer with natural proteins to enhance transfection efficiency and reduce cytotoxicity. Hence, the use of biocompatible protein, preferably albumin, was considered in the present study. Albumin is the most abundant plasma protein in the human blood, reduces *in vivo* drug toxicity and aids in delivering hydrophobic drugs because of the hydrophobic core.[36–39] Based on these findings, bovine serum albumin (BSA) was conjugated either with PEI or PEI-PEG-PEI polymer, and further complexed with the plasmid. In the present study, a Green Fluorescent Protein (GFP) plasmid, was used as the model plasmid as its translocation into the cell can be easily monitored once the GFP is expressed.[40]

In the resulting polyplexes, the cationic charge density for the interaction with negatively charged plasmids is provided by the polymer while BSA provides stability to the nanostructures. In addition, BSA aids in protecting plasmid from nuclease degradation, PEI enhances endosomal escape and transfection efficiency, while PEG decreases the positive charge density of the polymer leading to improved cell viability. The prepared polyplexes were characterized for size,

surface charge, plasmid condensation properties, and the mechanism of internalization in the cells was also evaluated. Furthermore, the transfection efficiency of the prepared polyplexes was studied in two different cell lines, MCF-7, and PANC-1.

6.1.2. Results and discussion

Albumin-based delivery systems, such as nanoparticles, nanoconjugates and polyplexes, have been successfully employed for nucleic acids (Figure 57). In the present study, we aimed to either encapsulate the plasmid in albumin nanoparticles or electrostatically bind it to the polyplexes using our polymers.

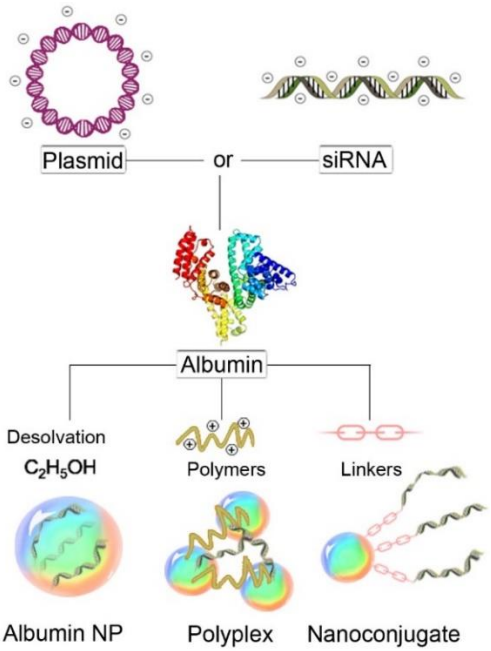

Figure 57. Schematic representation of different albumin nanocarriers for nucleic acid delivery.

6.1.2.1 Preparation of plasmid loaded BSA nanoparticles

For the preparation of nanoparticles, BSA was first modified using 2-iminothiolane. Then, the resulting derivative was treated with aldrithiol, modified PEG or PEI (Figure 58). The modified BSA was then mixed with the equal volume of thiol modified BSA. To the mixture, 100 µg of GFP plasmid was added and incubated for 15 minutes at room temperature. The nanoparticles were then prepared by the dropwise addition of 2.7 mL ethanol at the constant flow rate of 1 mL/min. For the nanoparticles without any modification, after the solution turned turbid, it was stabilized with 8% glutaraldehyde. The solution was stirred at 550 rpm for 18 hours. Free albumin and excess cross-linking agent were removed by iterative centrifugation.

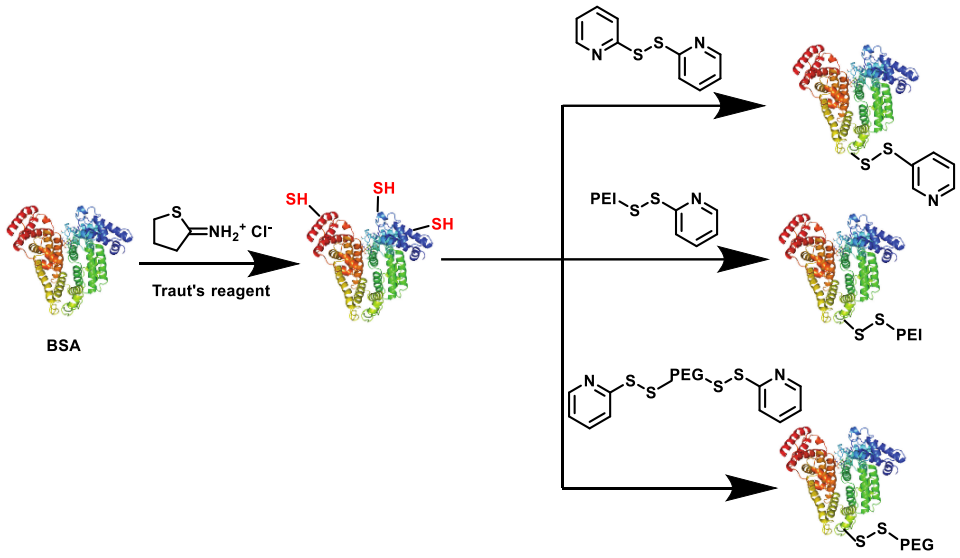

Figure 58. Schematic representation of BSA modification processes which were later used to prepare plasmid-loaded BSA nanoparticles.

Then, the size of prepared nanoparticles was determined. The nanoparticles with PEG (BSA-PEG) showed the lowest size of 184±2 nm followed by PEI (BSA-PEI), aldrithiol (BSA-Aldri) and glutaraldehyde (BSA-GLU) (Figure 59 A). The efficiency of the nanoparticle formation was assessed by the Bradford assay, revealing that more than 80% conversion of BSA to nanoparticles was achieved with all formulations (Figure 59 B). This result highlights the feasibility of our systems as delivery agents. Also, studies on the encapsulation efficiency revealed that BSA-Aldri could encapsulate the highest percentage of GFP (88%) followed by BSA-PEG (69%), BSA-PEI (64%) and BSA-GLU (58%) as shown in Figure 59 C. Moreover, all the prepared nanoparticles were not toxic in the PANC-1 cells 48 hours post treatment, which further strengthens the use of these nanocarriers to deliver nucleic acids (Figure 59 D).

Despite all the nanocarriers showing good physicochemical properties and favorable for the encapsulation of plasmids, efficient release of the plasmid could not be achieved from these nanoparticles in cancer cells (PANC-1 and MCF-7). This may be because of the large size of the plasmids, which impose problems during the release from the matrix of the nanoparticles. Hence, further optimization in the albumin-based nanoparticles is required for the efficient delivery of the plasmids.

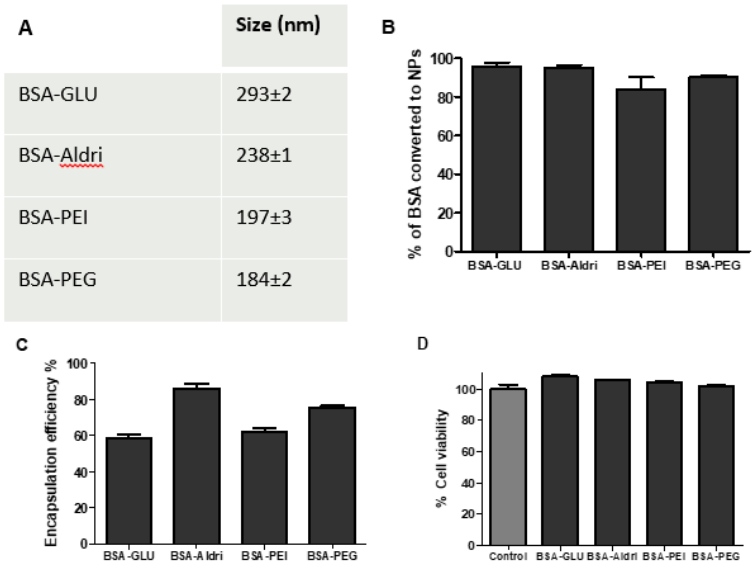

Figure 59. A) Size of the GFP loaded nanoparticles measured by DLS; B) Percentage of BSA converted to NPs analysed by Bradford assay; C) GFP encapsulation efficiency of various BSA Nanoparticles; D) Cell viability of the nanoparticles in PANC-1 cells 48 hours post-treatment.

6.1.2.2 Preparation of plasmid loaded polyplexes

The second approach employed herein to deliver nucleic acids involves the preparation of polyplexes, which is represented in Figure 60. Briefly, an aqueous solution of BSA was mixed with the polymer (PEI or PEI-PEG-PEI) and vortexed vigorously for 2 hours at room temperature in the presence of 25% glutaraldehyde. Then, an aqueous solution of glycine (0.1 mg/mL) was added to mask the free aldehyde groups, and prevent their reaction with biomolecules. The obtained polymers were further used for the preparation of polyplexes. For the polyplexes with GFP plasmid, BSA-PEI or BSA-PEI-PEG polymer was incubated with 1 µg of plasmid for one hour at 37 ℃. In all the polyplexes, the amount of GFP used was constant (1µg), whereas polymer was varied from 10 to 90 µg. The polyplexes were formed by the electrostatic interaction between the negative charged plasmid and the positively charged polymers.

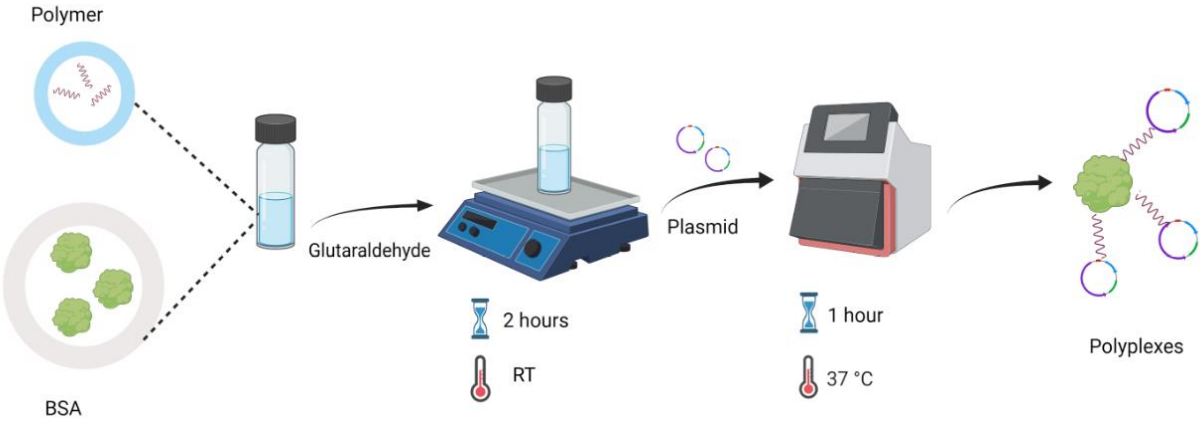

Figure 60. Schematic illustration for the preparation of polyplexes

6.1.2.3. Surface charge measurement of the polyplexes

It is essential to investigate the surface characteristics of the prepared polymers since it affects the stability, cellular uptake, transfection efficiency and cytotoxicity.[41,42] Particularly, the surface charge plays an important role in modulating the biodistribution, as well as cellular uptake and translocation of polyplexes.[43] Thus, the zeta potential of the polymers at varying pH was studied (Figure 61 A). Both BSA-PEI and BSA-PEI-PEG polymers presented a positive surface charge at physiological pH of 7.4. This charge can be exploited to form polyplexes with negatively charged DNA plasmids, due to electrostatic interactions.[44] When the pH was decreased from 7 to 5, the zeta potential increased from +6 mV to +10 mV for BSA-PEI and from +3 mV to +5 mV for BSA-PEI-PEG polymers. This can be attributed to the degree of protonation of amines in PEI which increased from 20% to 45% when pH was reduced from 7 to 5, hence increasing the surface charge.[27] In addition, it is important to note that BSA-PEI-PEG polymer demonstrated lower surface charge density than BSA-PEI at all the pH range measured (Figure 61 A). A similar result was obtained in the study conducted by Merdan and co-workers on PEGylated PEI for gene delivery to human ovarian carcinoma cells.[45] This reduced surface potential due to hindrance imposed by PEG, minimizes the interactions with plasma proteins, cellular blood components and endothelium.[45,46] This can aid in obtaining the stable nanostructures in vivo, prolonged circulation in blood, and reduction in overall cytotoxicity.[46]

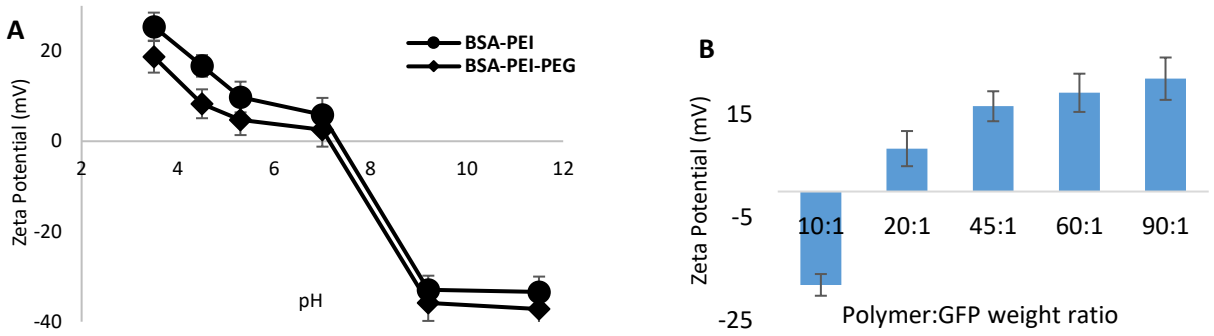

Figure 61. Zeta potentials of BSA-PEI and BSA-PEI-PEG polymers at pH range of 3-11 (A) and BSA-PEI-GFP polyplexes at different weight ratios (B). The error bar represents the mean ± SD (n=3).

Next, the surface charge of the polyplexes was determined with varying amounts of polymer while keeping the weight of GFP plasmid constant at 1 µg. As shown in Figure 61 B, the zeta potential of the polyplexes increased from -18.1 mV to +21.8 mV with increasing the weight ratio of polymer: GFP from 10:1 to 90:1. The polyplexes with low polymer: GFP ratio of 20:1 also showed the positive surface charge of +8.3 mV, suggesting its ability to condense pDNA even at lower polymer weight ratios. These cationic BSA-PEI polyplexes can be exploited to interact with the negatively charged plasma membrane and enhance cellular uptake leading to enhanced transfection efficacy.

6.1.2.4. Size characterization

The size of the nanostructures BSA-PEI and BSA-PEI-PEG was obtained by Dynamic Light Scattering (DLS), (Figure 62). The polyplexes obtained with BSA-PEI-PEG had an average size of 115 ± 92 nm with a PDI of 0.3. This size was slightly larger than polyplexes obtained with BSA-PEI, having an average size of 85 ± 39 nm with a PDI of 0.2. The increase in the size of the complexes with PEG can be attributed to the fact that the longer polymer was used for the complex formation. The population of the particles <60 nm present in both graphs corresponds to free BSA.

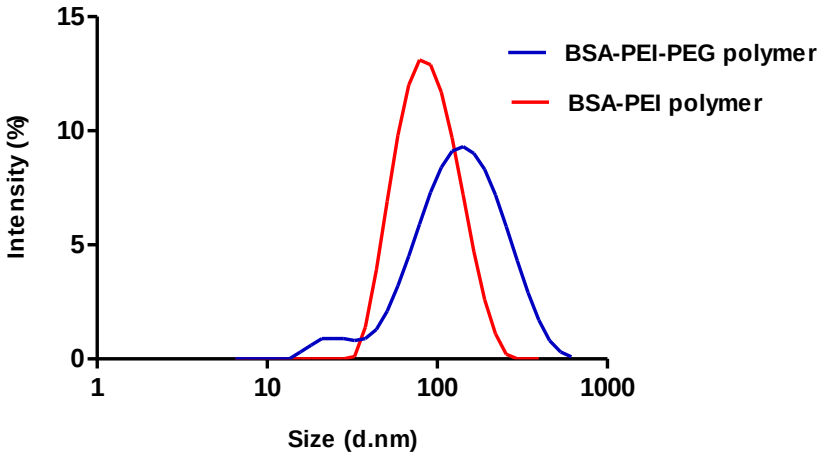

Figure 62. Size distribution of BSA-PEI (Red) and BSA-PEI-PEG (Blue) polymers observed by DLS.

Figure 63 represents SEM images of BSA-PEI and BSA-PEI-PEG polymers, which showed that both the complexes were pseudo-spherical. BSA-PEI polymers showed an average size of 100 nm compared to 120 nm with BSA-PEI-PEG. Hence, the results obtained from DLS and SEM show a good correlation.

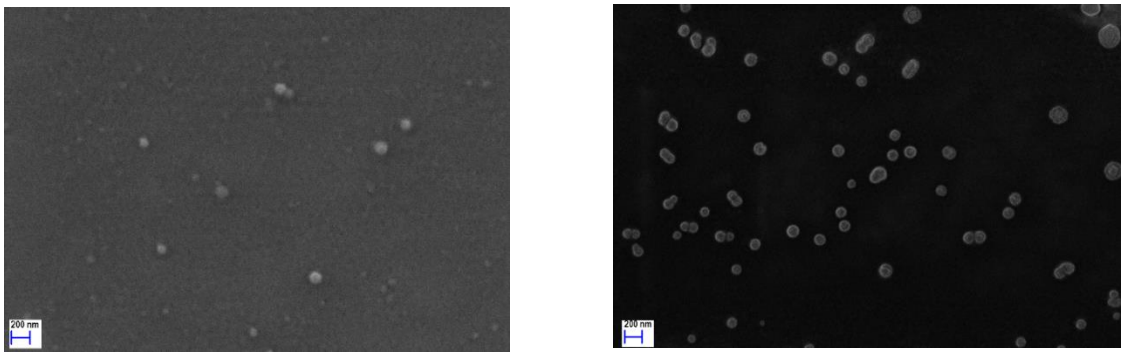

Figure 63. Size distribution of BSA-PEI (A) and BSA-PEI-PEG (B) polymers observed by SEM.

6.1.2.5. Agarose gel retardation assay

The plasmid delivery through polycation-based nanocarriers primarily relies on the formation of complexes through electrostatic interactions between nitrogen atoms of polymers and phosphate groups of the nucleotides.[47,48] The extent of such interaction can be evaluated using electrophoretic mobility shift assays (EMSAs), including polyacrylamide gels and agarose gels.[49] In the present study, agarose gel retardation assay was conducted to study the DNA complexation capacity of pDNA by BSA-PEI and BSA-PEI-PEG polymers at various polymer: GFP

weight ratios from 10:1 to 90:1 (Figure 64). In both kinds of polyplexes, the complexation increased with increasing polymer weight ratio. The polymers fully retarded the migration of GFP starting from the polymer: GFP ratio of 45:1. Similar results were obtained in previous reports.[44,48] A study conducted by *Neu et. al*. on polyplexes with PEI modified with high molecular weight PEG showed that PEG-modified PEI had a better ability to condense plasmid DNA.[48] However, in the current study, there was no significant difference in DNA condensation ability of BSA-PEI and BSA-PEI-PEG polymers, which may be due to the use of low molecular weight PEG for the modification of PEI.

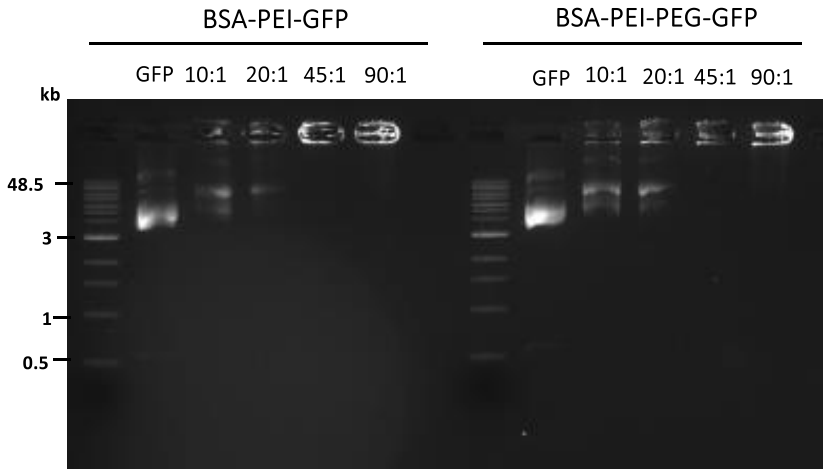

Figure 64. Agarose gel electrophoresis of polyplexes; Lane 2 was loaded with naked plasmid and used as a control. BSA-PEI-GFP and BSA-PEI-PEG-GFP polyplexes were loaded at the polymer: GFP weight ratios of 10:1, 20:1, 45:1 and 90:1.

6.1.2.6. Cytotoxicity assessment of the polyplexes

Once the structure of the polyplexes was evaluated, we studied the biological activity of these structures, particularly their cytotoxic effect in MCF-7 and PANC-1 cells, which is a critical parameter in the development of nanocarriers. It should be negligible, however, it is difficult to predict because various parameters, like size and surface charge, affect the cytotoxicity of the materials.[44,50] Thus, biological studies in this regard are required to assess the suitability of the nanostructures. In the present study, alamarBlue assay was performed to measure the cell viability of the prepared polyplexes in MCF-7 and PANC-1 cells. These experiments revealed that BSA-PEI-PEG has optimum cell tolerability (around 100%) at all concentrations after 72 hours of

incubation in both cell lines (Figure 65). In the case of BSA-PEI, the cell viability decreased from approximately 111% to 90% when the polymer concentration was increased from 20 µM to 120 µM after 72 hours of incubation in PANC-1 cells.

Despite the better transfection efficiency offered by PEI, dose-related toxicity remains a challenge with PEI-based delivery systems.[19] However, PEGylation and the use of glycine to mask free aldehydes of unreacted glutaraldehyde can contribute to the improved cell viability of the prepared polyplexes. This is because the free aldehyde groups of the unreacted glutaraldehyde cross-linker may react with the cell membrane of the cultured cells, leading to high cytotoxicity.[51] However, the reactivity of the aldehyde groups can be quenched by glycine and, hence, reduce the toxicity of the cross-linker.[44,51,52] In the present study, the cytotoxicity profile of the PEI-based polymers was drastically improved after quenching the free aldehydes with glycine and conjugation of the PEG group to PEI.

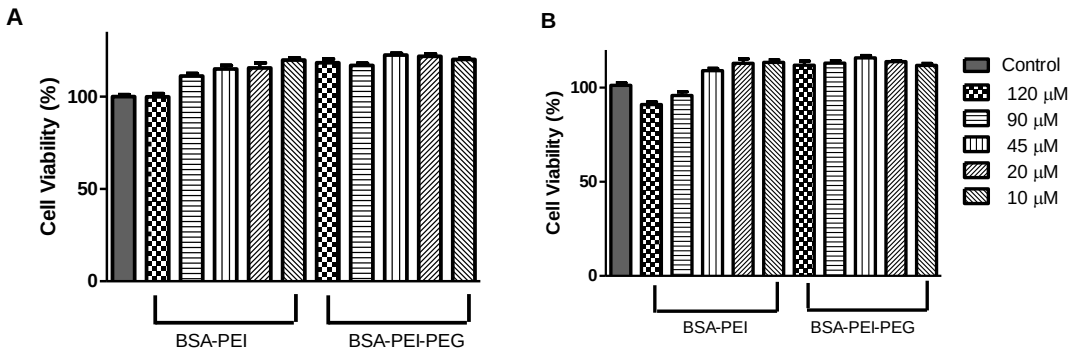

Figure 65. Cell viability assay of BSA-PEI and BSA-PEI-PEG polyplexes at different weight ratios in (A) MCF-7 and (B) PANC-1 cells after 72 hours of treatment

In PEI-PEG-PEI polymers, low molecular weight PEIs are linked by disulfide bonds which enhances the rapid degradation after cellular internalization and hence leads to a better cell viability profile. Moreover, PEG provides further reduction in cytotoxicity as it shields the surface charge by steric hindrance and decreases the non-specific polyplex interaction, in addition to increasing the circulation time of the polyplexes in blood. These factors enable BSA-PEI-PEG-GFP polyplexes to show optimum tolerability in the cell viability studies conducted in PANC-1 cells.

6.1.2.7. Mechanism of internalization of the polyplexes

Many studies have been carried out to investigate the mechanism of cellular uptake and intracellular trafficking of the polyplexes.[53–55] Various factors, including size, surface charge and shape of the particles, affect uptake and transfection efficiency.[56] Endocytosis routes like caveolae, clathrin, micropinocytosis or a combination of all those pathways are found to affect the cellular internalization of polyplexes.[53] A study conducted by Rejman and co-workers concluded that the particles <200 nm are uptaken into the cells via clathrin-dependent mechanism in contrast to the particles with sizes of 200-500 nm, which predominantly enter the cells via caveolae-mediated endocytosis.[57]

In the present study, the cellular uptake of polyplexes was studied at low temperature to investigate the influence of cellular energy deprivation in the process. Moreover, chlorpromazine, an inhibitor of clathrin-mediated[58] and filipin, an inhibitor of caveolae-mediated[56] endocytosis, were used to better assess the internalization mechanism of polyplexes into PANC-1 cells. As shown in Figure 66, there was a significant reduction in the expression of GFP with both BSA-PEI and BSA-PEI-PEG polyplexes when incubation temperature was decreased from 37 to 4 ℃, which indicates that the cellular uptake is an energy-dependent mechanism. Furthermore, the addition of endocytosis inhibitors, namely filipin and chlorpromazine, also inhibited the cellular uptake of both polyplexes, indicating that both, caveolae and clathrin dependent endocytosis, are responsible for the cellular uptake. As evident from Figure 67, filipin had a more inhibitory effect compared to chlorpromazine, which suggests that the cellular uptake of polyplexes is mediated primarily through caveolae-mediated endocytosis. This result is in accordance with a related study where PEI-DNA complexes were employed on COS-7 cells.[59] It is worth mentioning that those polyplexes that enter the cells via caveolae-mediated endocytosis can escape the lysosomal compartments and, hence provide better results.[60]

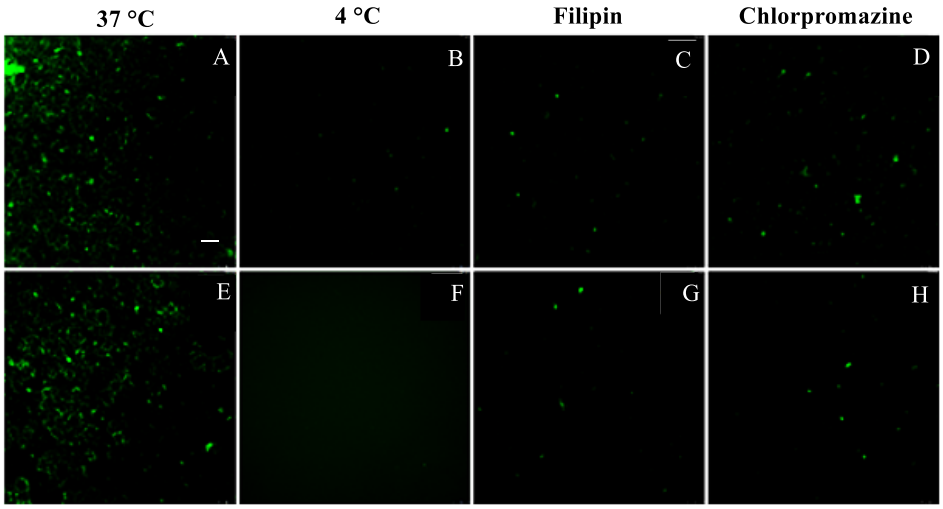

Figure 66. Fluorescence microscopy images of cellular uptake of BSA-PEI-GFP polyplexes (A-D) and BSA-PEI-PEG-GFP polyplexes (E-H).

The GFP fluorescence was further quantified using a flow cytometer in the presence of the endocytosis inhibitors. As shown in Figure 67, the fluorescence was decreased from 53% (without the endocytosis inhibitors) to around 12% and 9% when BSA-PEI-GFP polyplexes were used in the presence of filipin and chlorpromazine, respectively. Similarly, when BSA-PEI-PEG-GFP polyplexes were used, this value decreased from approximately 37% to 28% and 23%. These results correlate with the fluorescence images obtained previously and hence can be concluded that the internalization of the polyplexes is mediated through the endocytosis-mediated pathways.

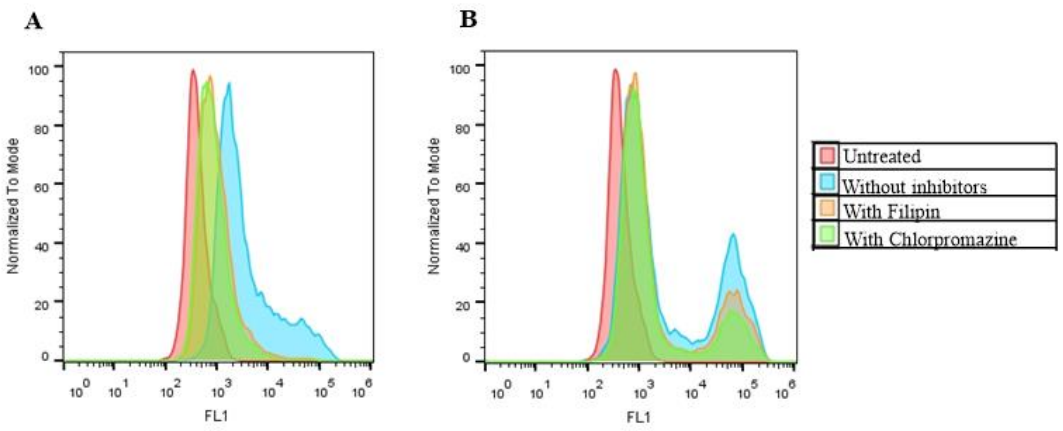

C	BSA-PEI-GFP	BSA-PEI-PEG-GFP
	% GFP positive cells	
Untreated	0.29	0.16
Without inhibitor	53	37.6
With Filipin	12.6	28.1
With Chlorpromazine	9.37	23.4

Figure 67. Percentage of fluorescent PANC-1 cells treated with BSA-PEI-GFP (A) or BSA-PEI-PEG-GFP (B) polyplexes 24-hour post treatment and in the presence of various endocytosis inhibitors. The percentage is shown in tabulated form for clarity (C).

6.1.2.8. Polyplexes induce efficient gene transfection

Finally, the transfection efficiency of different polyplexes was investigated in PANC-1 and MCF-7 cells. PANC-1 is a human pancreatic cancer cell line obtained from a pancreatic carcinoma of ductal cell origin, whereas MCF-7 is a human breast cancer cell line. Both these cell lines show efficient expression of GFP plasmid regulation and hence are used in our studies. In the polyplexes, the amount of GFP plasmid was kept constant (1 µg/well) and the polymer: GFP ratio was 90:1. The expression of GFP plasmid inside the cells was qualitatively studied by using fluorescence microscopy after 24 hours of incubation with the polyplexes. The cells transfected with GFP in the presence of lipofectamine 2000 were used as a positive control. It is evident from Figure 68 that both the polyplexes could successfully transfect both cell lines after 24 hours of treatment. This can be attributed to the fact that the positive surface charge of the polyplexes

facilitates the interaction with negatively charged cell membranes elevating the cellular uptake and hence the transfection efficiency.[27]

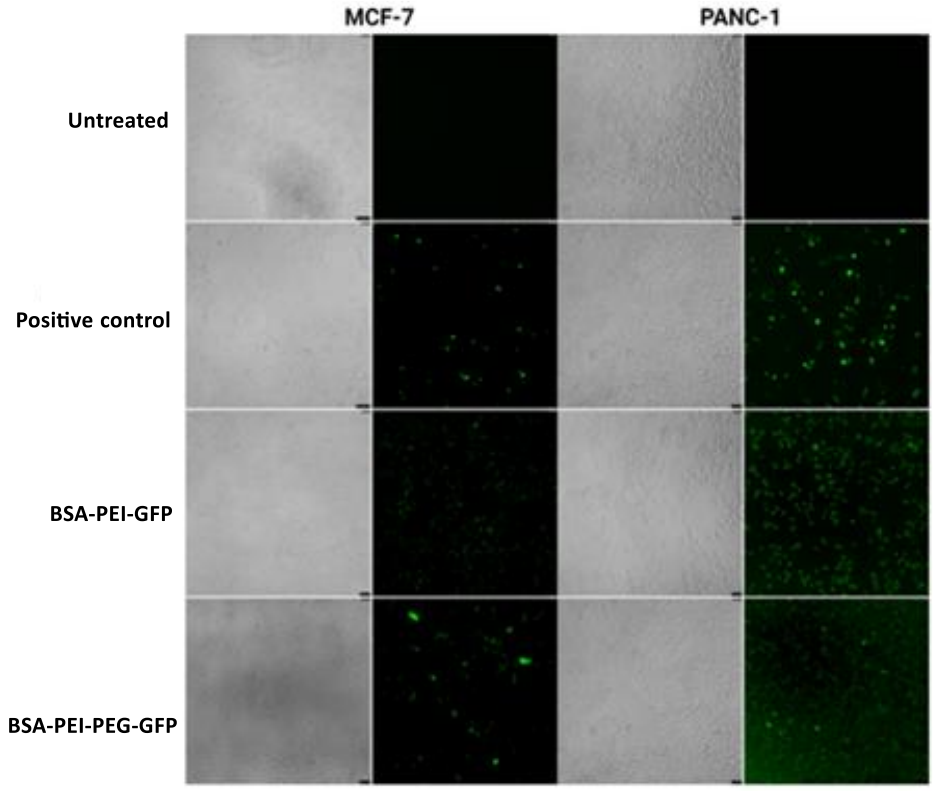

Figure 68. Expression of GFP plasmid in MCF-7 and PANC-1 cells at polymer: GFP weight ratios of 90:1, 24 hours post-treatment.

The result was further confirmed by the flow cytometry studies conducted in PANC-1 cells (Figure 69). After 24 hours of treatment, the transfection efficiency obtained with BSA-PEI-GFP polyplexes (52.6%) was slightly better than that obtained with BSA-PEI-PEG-GFP polyplexes (43.4%). In both cases, the transfection efficiency was lower than the positive control carried out with lipofectamine 2000 (84.8%). These results are in agreement with the fluorescence images obtained.

A

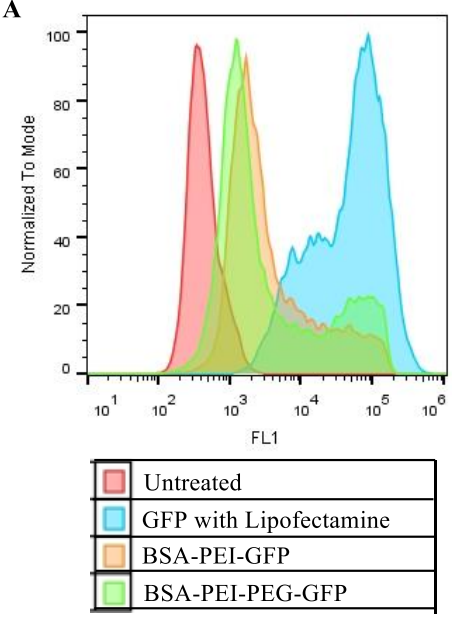

B

	Positive cells (%)
Untreated	0.31
GFP with Lipofectamine	84.8
BSA-PEI-GFP	52.6
BSA-PEI-PEG-GFP	43.4

Figure 69. Expression of GFP plasmid in PANC-1 cells transfected with BSA-PEI-GFP and BSA-PEI-PEG-GFP polyplexes at the polymer:GFP ratio of 90:1, 24 hours post treatment.

6.1.3. Conclusions

Nanostructures were obtained through the combination of BSA with polymers like PEI and PEI-PEG-PEI derivatives using glutaraldehyde as a crosslinker. The systems obtained with the PEI-PEG-PEI derivative presented a bigger size and less surface charge than the structures obtained with PEI. Despite this difference, all polyplexes could condense plasmid DNA efficiently. The polyplexes formed with BSA-PEI-PEG polymers showed low cytotoxicity compared to the ones prepared with BSA-PEI polymers. This can be attributed to the reduction of the positive charge density of the polymer, primarily due to the incorporation of PEG, which could shield the surface charge. This small reduction in charge could explain the reduction in transfection efficiency, which was 43.4% in the case of the PEG derivative vs 52.6% obtained with the structure containing only PEI. The results obtained herein contribute to the fundamental understanding of the polyplexes formation and in-vitro characterization. The presented experimental findings on the polyplexes could guide the development of advanced nanocarriers for the targeted gene delivery to the tumor sites.

6.2. Albumin based polyplexes for delivery of CRISPR plasmid for mutant p53 genome editing

6.2.1. Introduction

Gene editing or genome editing is the process of insertion, deletion, modification, or replacement of DNA in the genome. Due to the increasing clinical interest in gene editing, it has been developed extensively in the past few years and is one of the standard experimental strategies for gene manipulation nowadays. In this sense, the clustered, regularly interspaced, short palindromic repeat (CRISPR)/Cas (CRISPR-associated proteins) system is gaining tremendous attention from the scientific community and also from the general public, due to its ease of use for gene editing.[61]

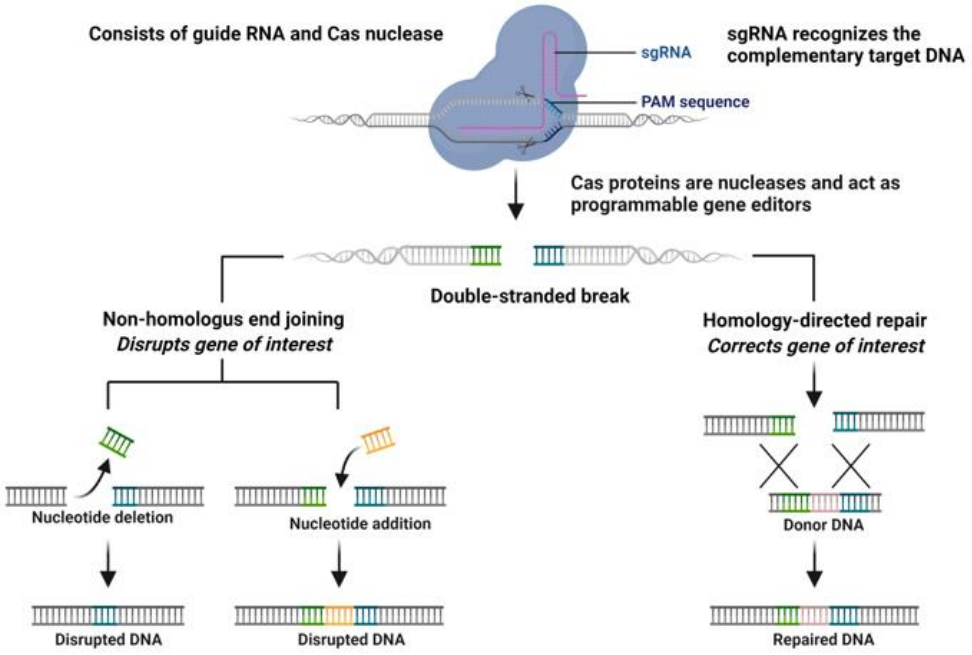

Figure 70. Schematic representation of genome editing by CRISPR/Cas system

The process requires a Cas protein that can act as a nuclease to cut the target DNA and a single guide RNA (sgRNA), which recognizes the specific sequence in the target genome called the protospacer.[62,63] This process is possible only if the specific sequence is followed by a Protospacer Adjacent Motif (PAM), which depends on the Cas protein employed.[63] The PAM recognition facilitates the annealing between the sgRNA and the target DNA.[64,65] Then, the Cas protein generates a double-stranded break (DSB) (Figure 70).[62] These breaks can be

repaired either via non-homologous end joining (NHEJ) or homology-directed repair (HDR).[66] NHEJ results in the generation of knock-outs by random insertion or deletion of the base pairs, while HDR results in knock-in generation by precise gene editing.[67] Thus, the potential of the CRISPR/Cas9 are immense for therapeutic use against bacteria, viruses, and cancers.[68–70] Particularly in cancer, this system is emerging as a promising gene-editing tool for targeted precision therapy.[66,71] In addition, it can be used to study various genes involved in cancer proliferation, migration, and cell signalling pathways.[71]

Despite the ever-growing potential of CRISPR/Cas9 system, safe, efficient, and targeted delivery of such system to tumor sites is still a challenge that needs to be addressed. It can be delivered as ribonucleoproteins (RNPs), mRNA or DNA. [72,73] The introduction of the CRISPR/Cas system using mRNA enhances the onset of gene editing, however, it is highly unstable and susceptible to degradation by nucleases. On the other hand, the delivery by RNPs enables rapid gene editing in the nucleus with high efficiency. However, it incurs a high cost and may trigger an immunological response, especially when the protein is of bacterial origin. The delivery system with plasmid DNA results in the slowest onset of gene editing, however, it yields a longer expression time in cells, which can facilitate the sustained expression for gene editing.[72] The longer half-life may, however, increase the risk of off-target effects and the possibility of DNA residual integration.

To date, various studies have been carried out for the successful delivery of Cas9 system. The major delivery problem arises from combining two large macromolecules (Cas9 with around 160 kDa and sgRNA, which is around 150 nucleotides long).[74] Various methods like electroporation, nucleofection, and different transfection reagents have been used to deliver the CRISPR system in vitro, however, they cannot be employed for in vivo applications.[67] Hence, suitable vehicles including, viral and non-viral vehicles, are being studied. The non-viral vectors, including nanocarriers are particularly of interest since they can overcome the issues related to the viral vectors like safety issues and low loading capacities.[75] In this regard, nanocarriers based on albumin are gaining tremendous attention because of the various advantages, including biosafety, biocompatibility, and possibilities of surface modification for specific targeting.

In the present study, we focused on the delivery of CRISPR/Cas9 plasmid targeting the mutant p53 using albumin-based polyplexes. The polyplexes were characterized for size, surface charge, DNA condensation abilities and their activities were analyzed in pancreatic cancer cells, PANC-1.

6.2.1.1. Mutant P53

p53 is a transcription factor that controls the expression of many coding and non-coding RNA. It plays an essential role in the tumor suppression and reduction in neoplastic transformation by acting as a sensitive collector of stress inputs, protection of cellular homeostasis and genome stability.[76,77] During the cancer progression, it plays a protective role by triggering cell senescence and apoptosis.[77] Due to its beneficial properties in the prevention of malignant tumors, p53 is commonly referred to as the "guardian of genome".[78]

The mutations in the gene p53 are the most frequently occurring gene mutation in human tumors and are prevalent in more than half of the cancers.[79] Most of these mutations are in the central DNA-binding domain (DBD) of the p53 gene.[80] It results in the mutant p53 proteins with the loss of beneficial activities of p53 and frequently acquire the oncogenic gain of function (GOF) that leads to tumorigenesis.[81] The mutant p53 proteins hence support the tumor proliferation and progression by protecting the tumor cells from oxidative and proteotoxic stress, immune system, metabolic imbalances, and DNA lesions (Figure 71). In addition, it also regulates the expression of various genes involved in chemo- and radio-resistance.[82]

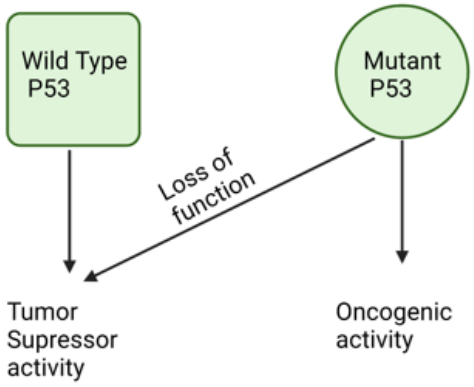

Figure 71. The effect of p53 mutations in cancer progression

Due to the role of the mutant p53 in the progression of various cancers, it is one of the most prominent targets for cancer therapy. The therapeutic strategies can be either the restoration of the wild-type conformation of p53 or degradation of mutant p53 or induction of the synthetic lethality.[83] Recently, approaches based on chemotherapeutics, CRISPR/Cas9, and immunotherapies are being developed, which efficiently target the mutant p53.[80] Particularly, CRISPR/Cas9 systems have immense scope because of their wide potential in the restoration of wild-type p53 by genome editing or eliminate the p53-deficient cancer cells.[80,84] It induces double-strand DNA breaks, which further results in cell cycle arrest and apoptosis.

6.2.2. Results and discussion

6.2.2.1. Design of the CRISPR/Cas9 plasmid targeting p53

DNA plasmid with CRISPR/Cas9 targeting the mutant p53 was designed and prepared by Dr. Marco Cordani, a former member of our group. Firstly, three DNA sequences capable of being transcribed into the functional sgRNA, two sequences complementary to the p53 gene (p53.1 and p53.2) shown in Table 4, and one non-targeting (NT) for the control were designed. For the insertion of the sequences (p53.1, p53.2 and NT) in the plasmid, the duplexes were annealed and ligated into the plasmid after the U6 promoter. The plasmids with the sequence complementary to p53 and non-targeting sequence were then denoted as Cas9_p53.1, Cas9_p53.2 and Cas9_NT, respectively.

Guide 1 (p53.1)	Guide 1 sense	5'-CACCGCCTGAGTAGTGGTAATCTAC-3'
	Guide 1 antisense	5'-AAACGTAGATTACCACTACTCAGGC-3'
Guide 2 (p53.2)	Guide 2 sense	5'-CACCGACTGGGACGGAACAGCTTTG-3'
	Guide 2 antisense	5'-AAACCAAAGCTGTTCCGTCCCAGTC-3'

Table 4. Design of DNA duplexes for guides 1 and 2.

6.2.2.2. Delivery of plasmid using lipofectamine

The efficiency of the prepared CRISPR/Cas9 plasmids was first evaluated in PANC-1 cells using lipofectamine 2000 as a transfecting agent. The detailed procedure for transfection is presented in Section 2.1.4.6. The cells were incubated at 37 ℃ for 24 hours in the atmosphere with 5% CO_2 and washed twice with PBS 1X. The fresh medium was added, and the cells were further incubated for 48 hours. The internalization of the plasmid in PANC-1 cells was evaluated using

fluorescence microscopy (Figure 72). The images demonstrate that the plasmids are efficiently internalized in the cells following the transfection with lipofectamine 2000.

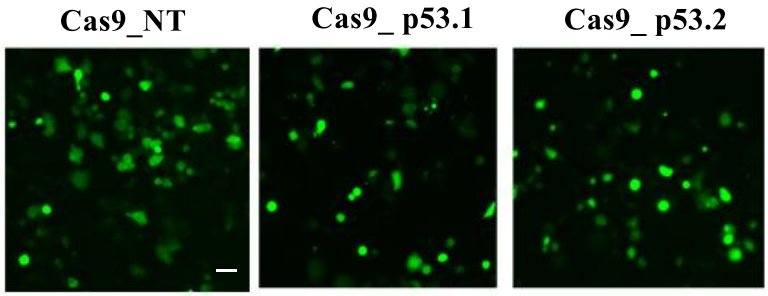

Figure 72. Fluorescence imaging in Panc-1 cells using lipofectamine; scale bar : 75 µm.

All the plasmids of interest showed fluorescence in the PANC-1 cells, and hence, the next step was to evaluate the efficacy of these plasmids in downregulating the mutant p53 in PANC-1 cells. Western blot analysis was performed to analyze the downregulation of mutant p53 72-hours post-treatment in PANC-1 cells. The plasmid Cas9_NT was used as a control in the study. In the experiment, GAPDH with the molecular weight of 36 kDa was used as a control to assess the amount of protein loaded in each lane. As shown in Figure 73, the levels of p53 were decreased in PANC-1 cells when treated with the plasmids Cas9_p53.1 and Cas9_p53.2. The decrease was most prominent with the plasmid Cas_p53.2. These results confirm the efficacy of the designed plasmids.

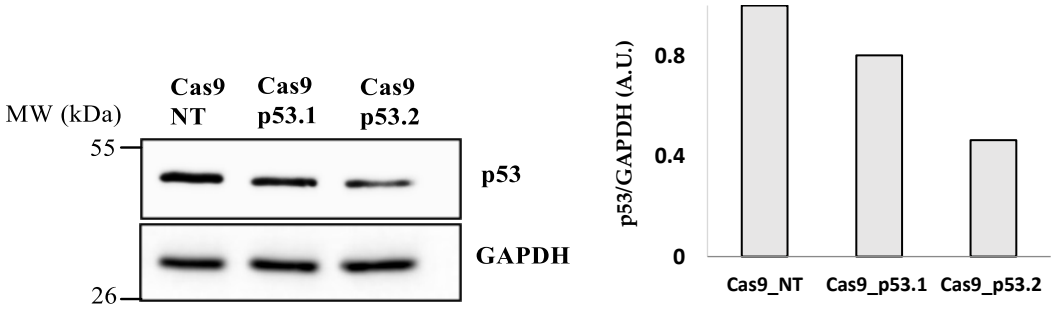

Figure 73. Western blot to confirm the activity of the designed plasmids in Panc-1 cells 72-hours post-treatment.

6.2.2.3. Delivery of CRISPR/Cas9 plasmid using albumin-based polyplexes

The polyplexes with CRISPR/Cas9 plasmid were prepared using albumin-PEI based polyplexes as described in Chapter 6.1. In each of the cases, the ratio of polymer to plasmid was fixed at 90:1 based on the results obtained with GFP, the model plasmid.

6.2.2.4. Size and surface charge characterization

The major limitation in the delivery of the plasmids arises due to their large size, negative surface charge that inhibits the interaction with the negatively charged biological membranes, and the possibility of degradation by nucleases. Hence, it was interesting to prepare the polyplexes by using the positively charged polymers that can condense the negatively charged plasmids by electrostatic interaction and can prevent enzymatic degradation.

The size and surface charge of the prepared polyplexes were measured using dynamic light scattering. The polyplexes could successfully condense the plasmids, resulting in structures with positive zeta potential (3.8 to 5.5 mV), as shown in Table 5. Moreover, the polyplexes demonstrated a similar size of about 130 nm with a low PDI of around 0.3.

	Size (nm)	PDI	Zeta potential (mV)
BSA-PEI Cas9_NT	135.4 ± 5.7	0.22	5.53 ± 0.18
BSA-PEI Cas9_p53.1	130.4 ± 3.8	0.31	4.01 ± 0.15
BSA-PEI Cas9_p53.2	129.3 ± 5.1	0.34	3.87 ± 0.12

Table 5. Size and surface charge characterization of the polyplexes prepared with BSA-PEI.

6.2.2.5. Agarose gel retardation assay

Based on the results obtained in Chapter 6.1, the polymer: plasmid ratio of 90:1 was used with Cas9_p53.1 and Cas9_p53.2 plasmids. As shown in Figure 74, the polyplexes completely retarded the migration of plamids at this weight ratio. The respective naked plasmids were used as the controls. The results were in agreement with the gel retardation capabilities of polyplexes with GFP.

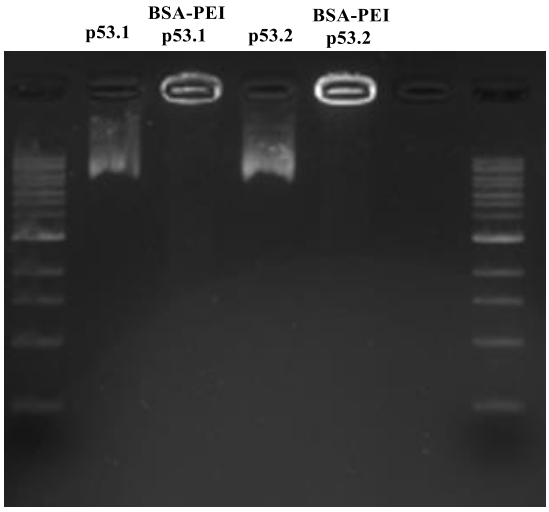

Figure 74. Retardation assay on an agarose gel of BSA-PEI polyplexes with Cas9_p53.1 and Cas9_p53.2 with a concentration of 1 µg. Naked plasmid (1 µg) was used as a control.

6.2.2.6. Fluorescence microscopy imaging of the polyplexes

To study the potential of BSA-PEI polyplexes to transfect the cells, in vitro transfection assay was performed in PANC-1 cells. The cells were incubated with the polyplexes at the polymer: plasmid ratio of 90:1 for 24 hours. After that, the medium was replaced with the fresh medium. After 24 hours, fluorescence imaging was carried out. The cells without polyplexes were used as control. As shown in Figure 75, the polyplexes could be internalized successfully in the cells with Cas9_p53.1 and Cas9_p53.2 plasmids. The result suggests that the plasmid electrostatically interacted with the positively charged polymers and could be successfully released in vitro.

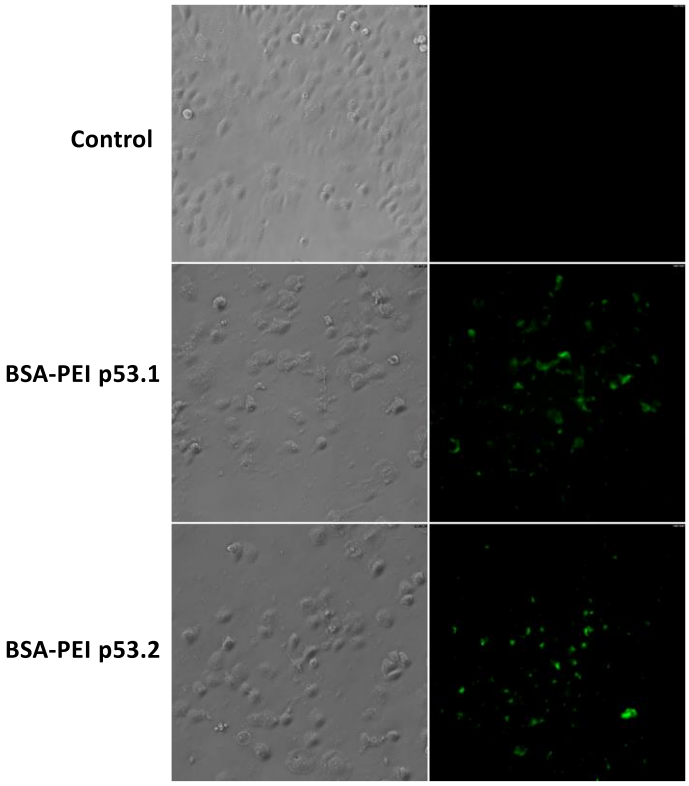

Figure 75. Fluorescence microscopy images to study the internalization of the BSA-PEI polyplexes in PANC-1 cells 48-hours post-treatment.

6.2.2.6. Western blot analysis

To analyse if the albumin-based polyplexes condensing the plasmids could show the desired effect in the pancreatic cell line, western blot analysis was carried out. The untreated cells, cells treated with the BSA-PEI polymer and the polyplexes with Cas9_NT were all used as the controls in the study. As shown in the Figure 76, the expression of p53 was reduced when treated with the polyplexes with Cas9_p53.1 and Cas9_p53.2, with the result more evident with polyplexes with Cas9_p53.2. This was similar to the result obtained when plasmid was delivered using lipofectamine as a transfection agent.

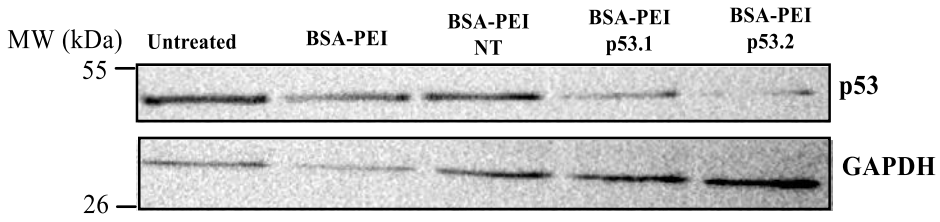

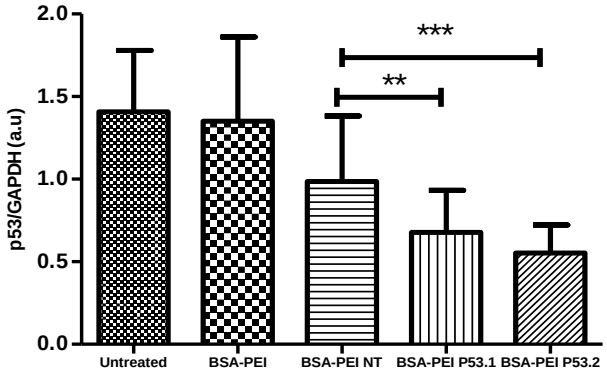

Figure 76. Western blot analysis to measure the expression of p53 levels in PANC-1 cells 72 h post-treatment with polyplexes with Cas9_p53.1 and Cas9_p53.2. (A) Gray values of the expressed protein bands and (B) Densitometric graphs of the expressed p53 levels. The graphs were constructed according to the gray values of the protein bands. Statistical analysis was performed using one-way ANOVA Tukey's test (**p-value < 0.01 and *** p-value < 0.001).

6.2.3. Conclusions

The present study highlights the potential of albumin-based polyplexes for delivering CRISPR/Cas9 plasmid for p53 mutant pancreatic cancers. The efficacy of plasmid was first demonstrated by using the transfecting agent, lipofectamine. However, despite the fact that lipofectamine enhances the internalization and transfection, its use is limited because of its cytotoxic nature and its inability to be used in the animal models. Thus, a nanocarrier system was designed and used to deliver CRISPR/Cas9 plasmid for pancreatic cancer. The described modular strategy will guide the delivery of other therapeutic nucleic acids in cancer therapy. However, these are only the preliminary results, and the system's efficacy needs to be studied thoroughly. Further studies regarding the effectiveness of the system in other cancer types with mutant p53 could be helpful to expand the use of the prepared polyplexes. Moreover, the potential off-site gene editing should be assessed, as well as the system's capabilities in animal models.

References

1. Hager, S.; Fittler, F.J.; Wagner, E.; Bros, M. Nucleic Acid-Based Approaches for Tumor Therapy. *Cells* **2020**, *9*, 1–53, doi:10.3390/cells9092061.

2. Alvarez-salas, L.M. Nucleic Acids as Therapeutic Agents. *Curr. Top. Med. Chem.* **2008**, *8*, 1379–1404, doi:10.2174/156802608786141133.

3. Li, J.; Wang, Y.; Zhu, Y.; Oupický, D. Recent Advances in Delivery of Drug-Nucleic Acid Combinations for Cancer Treatment. *J Control Release* **2014**, *172*, 1–30, doi:10.1016/j.jconrel.2013.04.010.Recent.

4. Izquierdo, M. Short interfering RNAs as a tool for cancer gene therapy. *Cancer Gene Ther.* **2005**, *12*, 217–227, doi:10.1038/sj.cgt.7700791.

5. Shir, A.; Ogris, M.; Wagner, E.; Levitzki, A. EGF receptor-targeted synthetic double-stranded RNA eliminates glioblastoma , breast cancer , and adenocarcinoma tumors in mice. *PLoS Med.* **2006**, *3*, 125–135, doi:10.1371/journal.pmed.0030006.

6. Zhou, G.; Wilson, G.; Hebbard, L.; Duan, W.; Liddle, C.; George, J.; Qiao, L. Aptamers : a promising chemical antibody for cancer therapy. *Oncotarget* **2016**, *7*, 13446–13463.

7. Parsel, S.M.; Grandis, J.R.; Thomas, S.M. Nucleic acid targeting : towards personalized therapy for head and neck cancer. *Oncogene* **2015**, *35*, 3217–3226, doi:10.1038/onc.2015.424.

8. Ramasamy, T.; Munusamy, S.; Ruttala, H.B.; Kim, J.O. Smart Nanocarriers for the Delivery of Nucleic Acid-Based Therapeutics: A Comprehensive Review. *Biotechnol. J.* **2021**, *16*, 1–14, doi:10.1002/biot.201900408.

9. Lu, W.; Sun, Q.; Wan, J.; She, Z.; Jiang, X. Cationic albumin – conjugated pegylated nanoparticles allow gene delivery into brain tumors via intravenous administration. *Cancer Res.* **2006**, *66*, 11878–11888, doi:10.1158/0008-5472.CAN-06-2354.

10. Zhu, Q.; Pan, X.; Sun, Y.; Wang, Z.; Liu, F.; Li, A.; Zhao, Z.; Wang, Y.; Li, K.; Mi, L. Biological nanoparticles carrying the Hmda-7 gene are effective in inhibiting pancreatic cancer in vitro and in vivo. *PLoS One* **2017**, *7*, 1–12.

11. Dachs, Gabi U.; Dougherty, Graeme J.; Stratford, Ian J.; Chaplin, D.J. Targeting Gene Therapy to Cancer: A Review. *Oncol. Res.* **1997**, *9*, 313–325.

12. Harrison, E.B.; Azam, S.H.; Pecot, C. V Targeting Accessories to the Crime : Nanoparticle Nucleic Acid Delivery to the Tumor Microenvironment. *Front. Pharmacol.* **2018**, *9*, 1–15, doi:10.3389/fphar.2018.00307.

13. Silva, A.C.; Lopes, C.M.; Lobo, J.M.S.; Amaral, M.H. Nucleic acids delivery systems : a challenge for pharmaceutical technologists. *Curr. Drug Metab.* **2015**, *16*, 3–16.

14. Harada-SHiba, M.; Yamauchi, K.; Harada, A.; Takamisawa, I.; Shimmokado, K.; Kataoka, K. Polyion complex micelles as vectors in gene therapy – pharmacokinetics and in vivo gene

transfer. *Gene Ther.* **2002**, *9*, 407–414, doi:10.1038/sj/gt/3301665.

15. Kariko, K.; Bhuyan, P.; Capodici, J.; Weissman, D. Small interfering RNAs mediate sequence-independent gene suppression and induce immune activation by signaling through toll-like receptor 3. *J. Immunol.* **2004**, *172*, 6544–6549, doi:10.4049/jimmunol.172.11.6545.

16. Oh, Y.; Park, T.G. siRNA delivery systems for cancer treatment. *Adv. Drug Deliv. Rev.* **2009**, *61*, 850–862, doi:10.1016/j.addr.2009.04.018.

17. Lundstrom, K.; Boulikas, T. Viral and non-viral vectors in gene therapy: technology development and clinical trials. *Technol. Cancer Res. Treat.* **2003**, *2*, 471–485, doi:10.1177/153303460300200513.

18. Elsabahy, M.; Nazarali, A.; Foldvari, M. Non-viral nucleic acid delivery : key challenges and future directions non-viral nucleic acid delivery : key challenges and future directions. *Curr. Drug Deliv.* **2011**, *8*, 235–244, doi:10.2174/156720111795256174.

19. Gao, J.Q.; Zhao, Q.Q.; Lv, T.F.; Shuai, W.P.; Zhou, J.; Tang, G.P.; Liang, W.Q.; Tabata, Y.; Hu, Y.L. Gene-carried chitosan-linked-PEI induced high gene transfection efficiency with low toxicity and significant tumor-suppressive activity. *Int. J. Pharm.* **2010**, *387*, 286–294, doi:10.1016/j.ijpharm.2009.12.033.

20. Leong, K.W.; Mao, H.Q.; Truong-Le, V.L.; Roy, K.; Walsh, S.M.; August, J.T. DNA-polycation nanospheres as non-viral gene delivery vehicles. *J. Control. Release* **1998**, *53*, 183–193, doi:10.1016/S0168-3659(97)00252-6.

21. Kleemann, E.; Jekel, N.; Dailey, L.A.; Roesler, S.; Fink, L.; Weissmann, N.; Schermuly, R.; Gessler, T.; Schmehl, T.; Roberts, C.J.; et al. Enhanced gene expression and reduced toxicity in mice using polyplexes of low-molecular-weight poly(ethylene imine) for pulmonary gene delivery. *J. Drug Target.* **2009**, *17*, 638–651, doi:10.1080/10611860903106414.

22. Tros de Ilarduya, C.; Sun, Y.; Düzgüneş, N. Gene delivery by lipoplexes and polyplexes. *Eur. J. Pharm. Sci.* **2010**, *40*, 159–170, doi:10.1016/j.ejps.2010.03.019.

23. Boussif, O.; LezoualC'H, F.; Zanta, M.A.; Mergny, M.D.; Scherman, D.; Demeneix, B.; Behr, J.P. A versatile vector for gene and oligonucleotide transfer into cells in culture and in vivo: Polyethylenimine. *Proc. Natl. Acad. Sci. U. S. A.* **1995**, *92*, 7297–7301, doi:10.1073/pnas.92.16.7297.

24. Syga, M.I.; Nicolì, E.; Kohler, E.; Shastri, V.P. Albumin incorporation in polyethylenimine-DNA polyplexes influences transfection efficiency. *Biomacromolecules* **2016**, *17*, 200–207, doi:10.1021/acs.biomac.5b01308.

25. Hall, A.; Lächelt, U.; Bartek, J.; Wagner, E.; Moghimi, S.M. Polyplex evolution : understanding biology , optimizing performance. *Mol. Ther.* **2017**, *25*, 1476–1490, doi:10.1016/j.ymthe.2017.01.024.

26. Akinc, A.; Thomas, M.; Klibanov, A.M.; Langer, R. Exploring polyethylenimine-mediated DNA transfection and the proton sponge hypothesis. *J. Gene Med.* **2005**, *7*, 657–663,

doi:10.1002/jgm.696.

27. Behr, J. The Proton Sponge: a Trick to Enter Cells the Viruses Did Not Exploit. *Chimia (Aarau).* **1997**, *2*, 34–36.

28. Fischer, D.; Li, Y.; Ahlemeyer, B.; Krieglstein, J.; Kissel, T. In vitro cytotoxicity testing of polycations : influence of polymer structure on cell viability and hemolysis. *Biomaterials* **2003**, *24*, 1121–1131.

29. Muthiah, M.; Che, H.; Kalash, S.; Jo, J.; Choi, S.; Jong, W.; Su, C.; Young, J.; Park, I. Formulation of glutathione responsive anti-proliferative nanoparticles from thiolated Akt1 siRNA and disulfide-crosslinked PEI for efficient anti-cancer gene therapy. *Colloids Surfaces B Biointerfaces* **2015**, *126*, 322–327, doi:10.1016/j.colsurfb.2014.12.022.

30. Huang, F.-W.; Wang, H.-Y.; Li, C.; Wang, H.-F.; Sun, Y.-X.; Feng, J.; Zhang, X.-Z.; Zhuo, R.-X. PEGylated PEI-based biodegradable polymers as non-viral gene vectors. *Acta Biomater.* **2010**, *6*, 4285–4295.

31. Gosselin, M.A.; Guo, W.; Lee, R.J. Efficient gene transfer using reversibly cross-linked low molecular weight polyethylenimine. *Bioconjug. Chem.* **2001**, *12*, 989–994.

32. Bauhuber, B.S.; Hozsa, C.; Breunig, M.; Achim Go¨pferich Delivery of nucleic acids via disulfide-based carrier systems. *Adv. Mater.* **2009**, *21*, 3286–3306, doi:10.1002/adma.200802453.

33. Ahn, C.; Chae, S.Y.; Bae, Y.H.; Kim, S.W. Biodegradable poly (ethylenimine) for plasmid DNA delivery. *J. Control. Release* **2002**, *80*, 273–282.

34. Schiffelers, R.M.; Ansari, A.; Xu, J.; Zhou, Q.; Tang, Q.; Storm, G.; Molema, G.; Lu, P.Y.; Scaria, P. V; Woodle, M.C. Cancer siRNA therapy by tumor selective delivery with ligand-targeted sterically stabilized nanoparticle. *Nucleic Acids Res.* **2004**, *32*, 1–10, doi:10.1093/nar/gnh140.

35. Ogris, M.; Walker, G.; Blessing, T.; Kircheis, R.; Wolschek, M.; Wagner, E. Tumor-targeted gene therapy : strategies for the preparation of ligand – polyethylene glycol – polyethylenimine / DNA complexes. *J. Control. Release* **2003**, *91*, 173–181.

36. Yogasundaram, H.; Bahniuk, M.S.; Singh, H.; Aliabadi, H.M.; Uludaˇ, H.; Unsworth, L.D. BSA Nanoparticles for siRNA Delivery : Coating Effects on Nanoparticle Properties , Plasma Protein Adsorption , and In Vitro siRNA Delivery. *Int. Jounal Biomater.* **2012**, *2012*, 1–10, doi:10.1155/2012/584060.

37. Larsen, M.T.; Kuhlmann, M.; Hvam, M.L.; Howard, K.A. Albumin-based drug delivery : harnessing nature to cure disease. *Mol. Cell. Ther.* **2016**, *4*, 1–12, doi:10.1186/s40591-016-0048-8.

38. Weber, C.; Kreuter, J.; Langer, K. Desolvation process and surface characteristics of HSA-nanoparticles. *Int. J. Pharm.* **2000**, *196*, 197–200.

39. Wang, G.; Press, S.; Uludag, H. Recent developments in nanoparticle-based drug delivery

and targeting systems with emphasis on protein-based nanoparticles. *Expert Opin. Drug Deliv.* **2008**, *5*, 499–515, doi:10.1517/17425247.5.5.499.

40. Morikawa, T.J.; Fujita, H.; Kitamura, A.; Ho, T. Dependence of fluorescent protein brightness on protein concentration in solution and enhancement of it. *Sci. Rep.* **2016**, *6*, 1–13, doi:10.1038/srep22342.

41. Kim, K.; Ryu, K.; Kim, T. Cationic methylcellulose derivative with serum-compatibility and endosome buffering ability for gene delivery systems. *Carbohydr. Polym.* **2014**, *110*, 268–277, doi:10.1016/j.carbpol.2014.03.073.

42. Jiang, J.; Oberdörster, G.; Biswas, P. Characterization of size, surface charge, and agglomeration state of nanoparticle dispersions for toxicological studies. *J. Nanoparticle Res.* **2009**, *11*, 77–89, doi:10.1007/s11051-008-9446-4.

43. Hoshino, A.; Fujioka, K.; Oku, T.; Suga, M.; Sasaki, Y.F.; Ohta, T.; Yasuhara, M.; Suzuki, K.; Yamamoto, K. Physicochemical properties and cellular toxicity of nanocrystal quantum dots depend on their surface modification. *Nano Lett.* **2004**, *4*, 2163–2169, doi:10.1021/nl048715d.

44. Kumari, M.; Liu, C.H.; Wu, W.C. Efficient gene delivery by oligochitosan conjugated serum albumin: Facile synthesis, polyplex stability, and transfection. *Carbohydr. Polym.* **2018**, *183*, 37–49, doi:10.1016/j.carbpol.2017.11.013.

45. Merdan, T.; Callahan, J.; Petersen, H.; Kunath, K.; Bakowsky, U.; Kopecˇkova´, P.; Kissel, T.; Kopecˇek, J. Pegylated Polyethylenimine - Fab' Antibody Fragment Conjugates for Targeted Gene Delivery to Human Ovarian Carcinoma Cells. *Bioconjug. Chem.* **2003**, *14*, 989–996.

46. Ogris, M.; Brunner, S.; Schu, S.; Kircheis, R.; Wagner, E. PEGylated DNA / transferrin – PEI complexes : reduced interaction with blood components , extended circulation in blood and potential for systemic gene delivery. *Gene Ther.* **1999**, *6*, 595–605.

47. Dunlap, D.D.; Maggi, A.; Soria, M.R.; Monaco, L. Nanoscopic structure of DNA condensed for gene delivery. *Nucleic Acids Res.* **1997**, *25*, 3095–3101.

48. Neu, M.; Germershaus, O.; Behe, M.; Kissel, T. Bioreversibly crosslinked polyplexes of PEI and high molecular weight PEG show extended circulation times in vivo. *J. Control. Release* **2007**, *124*, 69–80, doi:10.1016/j.jconrel.2007.08.009.

49. Ream, J.A.; Lewis, L.K.; Lewis, K.A. Rapid agarose gel electrophoretic mobility shift assay for quantitating protein:RNA interactions. *Anal Biochem.* **2016**, *511*, 36–41, doi:10.1016/j.ab.2016.07.027.Rapid.

50. Fischer, D.; Bieber, T.; Li, Y.; Elsässer, H.P.; Kissel, T. A novel non-viral vector for DNA delivery based on low molecular weight, branched polyethylenimine: Effect of molecular weight on transfection efficiency and cytotoxicity. *Pharm. Res.* **1999**, *16*, 1273–1279, doi:10.1023/A:1014861900478.

51. Lai, J. Biocompatibility of chemically cross-linked gelatin hydrogels for ophthalmic use. *J. Mater. Sci.* **2010**, *21*, 1899–1911, doi:10.1007/s10856-010-4035-3.

52. Matsuda, S.; Iwata, H.; Se, N.; Ikada, Y. Bioadhesion of gelatin films crosslinked with glutaraldehyde. *Bioadhesion gelatin Film.* **1999**, *45*, 20–27.

53. Ingle, N.P.; Hexum, J.K.; Reineke, T.M. Polyplexes Are Endocytosed by and Tra ffi cked within Filopodia. *Biomacromolecules* **2020**, doi:10.1021/acs.biomac.9b01610.

54. Qi, R.; Mullen, D.G.; Jr., J.R.B.; Holl, M.M.B. The Mechanism of Polyplexes Internalization into Cells: Testing the GM1/Caveolin-1-Mediated Lipid Raft Mediated Endocytosis Pathway. *Mol. Pharm.* **2010**, *7*, 267–279, doi:10.1021/mp900241t.The.

55. Gersdorff, K. Von; Sanders, N.N.; Vandenbroucke, R.; Smedt, S.C. De; Wagner, E.; Ogris, M. The Internalization Route Resulting in Successful Gene Expression Depends on both Cell Line and Polyethylenimine Polyplex Type. *Mol. Ther.* **2006**, *14*, 745–753, doi:10.1016/j.ymthe.2006.07.006.

56. Orlandi, P.A.; Fishman, P.H. Filipin-dependent inhibition of cholera toxin: evidence for toxin internalization and activation through caveolae-like domains. *J. Cell Biol.* **1998**, *141*, 905–915.

57. Rejman, J.; Oberle, V.; Zuhorn, I.S.; Hoekstra, D. Size-dependent internalization of particles via the pathways of clathrin- and caveolae-mediated endocytosis. *Biochem. J.* **2004**, *377*, 159–169.

58. Wang, L.; Rothberg, K.G.; Anderson, R.G.W. Mis-assembly of clathrin lattices on endosomes reveals a regulatory switch for coated pit formation. *J. Cell Biol.* **1993**, *123*, 1107–1117.

59. Aa, M.A.E.M. van der; Huth, U.S.; Ha¨fele, S.Y.; Schubert, R.; Oosting, R.S.; Mastrobattista, E.; Hennink, W.E.; Peschka-Su¨ss, R.; Koning, G.A.; Crommelin, D.J.A. Cellular Uptake of Cationic Polymer-DNA Complexes Via Caveolae Plays a Pivotal Role in Gene Transfection in COS-7 Cells. *Pharm. Res.* **2007**, *24*, 1590–1598, doi:10.1007/s11095-007-9287-3.

60. Rejman, J.; Bragonzi, A.; Conese, M. Role of Clathrin- and Caveolae-Mediated Endocytosis in Gene Transfer Mediated by Lipo- and Polyplexes. *Mol. Ther.* **2005**, *12*, 468–474, doi:10.1016/j.ymthe.2005.03.038.

61. Xue, W.; Chen, S.; Yin, H.; Tammela, T.; Papagiannakopoulos, T.; Joshi, N.S.; Cai, W.; Yang, G.; Bronson, R.; Crowley, D.G.; et al. CRISPR-mediated direct mutation of cancer genes in the mouse liver. *Nature* **2014**, *514*, 380–384, doi:10.1038/nature13589.

62. Jinek, M.; Chylinski, K.; Fonfara, I.; Hauer, M.; Doudna, J.A.; Charpentier, E. A programmable dual-RNA-guided DNA endonuclease in adaptive bacterial immunity. *Science (80-.).* **2012**, *337*, 816–821, doi:10.1126/science.1225829.

63. Jiang, F.; Doudna, J.A. CRISPR – Cas9 Structures and Mechanisms. *Annu. Rev. Biophys.* **2017**, *46*, 505–529.

64. Jiang, F.; Taylor, D.W.; Chen, J.S.; Kornfeld, J.E.; Zhou, K.; Thompson, A.J.; Nogales, E.; Doudna, J.A. Structures of a CRISPR-Cas9 R-loop complex primed for DNA cleavage. *Science (80-.).* **2016**, *351*, 867–871, doi:10.1126/science.aad8282.

65. Palermo, G.; Miao, Y.; Walker, R.C.; Jinek, M.; McCammon, J.A. Striking plasticity of CRISPR-Cas9 and key role of non-target DNA, as revealed by molecular simulations. *ACS Cent. Sci.* **2016**, *2*, 756–763, doi:10.1021/acscentsci.6b00218.

66. Sánchez-Rivera, F.J.; Jacks, T. Applications of the CRISPR-Cas9 system in cancer biology. *Nat. Rev. Cancer* **2015**, *15*, 387–395, doi:10.1038/nrc3950.

67. Escalona-Noguero, C.; López-Valls, M.; Sot, B. CRISPR/Cas technology as a promising weapon to combat viral infections. *BioEssays* **2021**, *43*, 1–16, doi:10.1002/bies.202000315.

68. Choudhary, E.; Thakur, P.; Pareek, M.; Agarwal, N. Gene silencing by CRISPR interference in mycobacteria. *Nat. Commun.* **2015**, *6*, 1–11, doi:10.1038/ncomms7267.

69. Liao, H.K.; Gu, Y.; Diaz, A.; Marlett, J.; Takahashi, Y.; Li, M.; Suzuki, K.; Xu, R.; Hishida, T.; Chang, C.J.; et al. Use of the CRISPR/Cas9 system as an intracellular defense against HIV-1 infection in human cells. *Nat. Commun.* **2015**, *6*, 1–10, doi:10.1038/ncomms7413.

70. Hemphill, J.; Borchardt, E.K.; Brown, K.; Asokan, A.; Deiters, A. Optical control of CRISPR/Cas9 gene editing. *J. Am. Chem. Soc.* **2015**, *137*, 5642–5645, doi:10.1021/ja512664v.

71. Yang, H.; Bailey, P.; Pilarsky, C. CRISPR Cas9 in Pancreatic Cancer Research. *Front. Cell Dev. Biol.* **2019**, *7*, 1–6, doi:10.3389/fcell.2019.00239.

72. Yip, B.H. Recent advances in CRISPR/Cas9 delivery strategies. *Biomolecules* **2020**, *10*, 1–16, doi:10.3390/biom10060839.

73. Kim, S.; Kim, D.; Cho, S.W.; Kim, J.; Kim, J.S. Highly efficient RNA-guided genome editing in human cells via delivery of purified Cas9 ribonucleoproteins. *Genome Res.* **2014**, *24*, 1012–1019, doi:10.1101/gr.171322.113.

74. Alsaiari, S.K.; Patil, S.; Alyami, M.; Alamoudi, K.O.; Aleisa, F.A.; Merzaban, J.S.; Li, M.; Khashab, N.M. Endosomal Escape and Delivery of CRISPR/Cas9 Genome Editing Machinery Enabled by Nanoscale Zeolitic Imidazolate Framework. *J. Am. Chem. Soc.* **2018**, *140*, 143–146, doi:10.1021/jacs.7b11754.

75. Luther, D.C.; Lee, Y.W.; Nagaraj, H.; Scaletti, F.; Rotello, V.M. Delivery approaches for CRISPR/Cas9 therapeutics in vivo: advances and challenges. *Expert Opin. Drug Deliv.* **2018**, *15*, 905–913, doi:10.1080/17425247.2018.1517746.

76. Pilley, S.; Rodriguez, T.A.; Vousden, K.H. Mutant p53 in cell-cell interactions. *Genes Dev.* **2021**, *35*, 433–448, doi:10.1101/gad.347542.120.

77. Mantovani, F.; Collavin, L.; Del Sal, G. Mutant p53 as a guardian of the cancer cell. *Cell Death Differ.* **2019**, *26*, 199–212, doi:10.1038/s41418-018-0246-9.

78. Toufektchan, E.; Toledo, F. The guardian of the genome revisited: P53 downregulates genes required for telomere maintenance, DNA repair, and centromere structure. *Cancers (Basel).* **2018**, *10*, doi:10.3390/cancers10050135.

79. Kandoth, C.; McLellan, M.D.; Vandin, F.; Ye, K.; Niu, B.; Lu, C.; Xie, M.; Zhang, Q.; McMichael, J.F.; Wyczalkowski, M.A.; et al. Mutational landscape and significance across 12 major cancer types. *Nature* **2013**, *502*, 333–339, doi:10.1038/nature12634.

80. Zhu, G.; Pan, C.; Bei, J.X.; Li, B.; Liang, C.; Xu, Y.; Fu, X. Mutant p53 in Cancer Progression and Targeted Therapies. *Front. Oncol.* **2020**, *10*, 1–9, doi:10.3389/fonc.2020.595187.

81. Alvarado-Ortiz, E.; de la Cruz-López, K.G.; Becerril-Rico, J.; Sarabia-Sánchez, M.A.; Ortiz-Sánchez, E.; García-Carrancá, A. Mutant p53 Gain-of-Function: Role in Cancer Development, Progression, and Therapeutic Approaches. *Front. Cell Dev. Biol.* **2021**, *8*, 1–24, doi:10.3389/fcell.2020.607670.

82. Lu, C.; El-Deiry, W.S. Targeting p53 for enhanced radio- and chemo-sensitivity. *Apoptosis* **2009**, *14*, 597–606, doi:10.1007/s10495-009-0330-1.

83. Parrales, A.; Iwakuma, T. Targeting oncogenic mutant p53 for cancer therapy. *Front. Oncol.* **2015**, *5*, 1–13, doi:10.3389/fonc.2015.00288.

84. Jiang, L.; Ingelshed, K.; Shen, Y.; Boddul, S. V CRISPR enriches for cells with mutations in a p53-related interactome , and this can be inhibited. *BioR* **2021**, 1–10.

Chapter 7. Conclusions and future perspectives

As discussed throughout the present thesis, cancer is one of the leading causes of death worldwide, and an overwhelming research is going on in this field recently. However, significant improvement still needs to be done in terms of the targeted delivery of the therapeutic agents with minimal off-target effects. In this regard, the present thesis is focused on the targeted delivery of various anti-cancer agents in different types of cancers, including breast, cervical and pancreatic cancers. The major conclusions that can be drawn from the present thesis are as follows:

- Albumin nanoparticles were prepared with various cross-linkers like glutaraldehyde, EDC, SPDP, polymers based on PEI and PEG. Optimization of the preparation of albumin-based nanoparticles was then done where SPDP was chosen as an optimum cross-linker.
- ABN-SPDP could be used for the delivery of hydrophilic (Doxorubicin) as well as hydrophobic (SN38, Volasertib) drugs. Moreover, this system could also be used with HSA, which can facilitate the clinical translation of these nanoparticles.
- The drug-loaded nanoparticles showed the targeted effect only in the tumor cells and had negligible effect in the healthy cells. This can be probably due to the difference in pH and reducing environment in the tumor and healthy cells which facilitates the release of cargo from albumin nanoparticles in cancer.
- Albumin nanoparticles could be successfully internalized in both 2D monolayer and 3D cancer spheroids. They further showed a promising reduction in the 3D cancer spheroids viability when HSA-SPDP loaded with various chemotherapeutics (Dox and Vola) were used.
- The immunological studies of the albumin nanoparticles conducted in murine RAW 264.7 and human THP-1 cells revealed that HSA-SPDP does not interact with the macrophages and hence are safe to be used as nanocarriers. ABN-GLU and ABN-SPDP however showed pro-inflammatory effect in murine and human macrophages.
- The polyplexes based on albumin and various polymers (PEI and PEI-PEG-PEI) could be successfully prepared with GFP and CRISPR/Cas9 plasmid targeting the mutant p53. The polyplexes could successfully deliver plasmid to the pancreatic cancer cells, where it downregulated the expression of the mutant p53.

Throughout this thesis, albumin was used as the key component for the delivery of both the chemotherapeutics and nucleic acids because of the biosafety, biocompatibility, and ease of production of these carriers. The feasibility of chosen system was reflected by its ability to encapsulate both hydrophobic and hydrophilic drugs, plasmids and their efficacy in wide range of cancer cell lines (MCF-7, MDA-MB-231, HeLa and PANC-1). The successful internalization of HSA-SPDP in 2D monolayer as well as 3D cancer spheroids further strengthens the possibility of using this system in cancer therapy. Moreover, the HSA nanoparticles prepared with novel cross-linker SPDP showed minimum interaction with both the murine and human macrophages. This further widens the possibility of using HSA-SPDP in cancer (delivery of both diagnostics and anti-cancer agents).

In addition, the successful conjugation and delivery of plasmid using albumin-based polyplexes further addresses the problem faced by the delivery of nucleic acids in cancer. The polyplexes could be used to deliver advanced system like CRISPR/Cas9 and hence opens the possibility of using other systems like CAR-T. Overall, the prepared nanocarriers show tremendous potential for the management of various types of cancers. However, use of various polymers like PEI and PEG during the preparation of polyplexes may affect the biosafety of these systems and hence extensive studies, including the interaction with immune system should be carried out.

Nevertheless, the results presented in the thesis only form the base for further development in nanocarriers for cancer therapy. The conclusions are solely derived from the studies conducted in 2D and 3D cancer spheroids. Hence, further animal studies with both pharmacodynamics and pharmacokinetics evaluation are required to confirm the potential therapeutic use of these modified nanocarriers. Moreover, safety studies, in addition to the interaction with macrophages should also be conducted for the successful clinical translation of those nanocarriers. Various experiments can also be conducted to further enhance the selective targeting of the nanocarriers in the tumor sites, for instance by using targeting moieties like aptamers and antibodies.

Scientific Contributions

1. **Prajapati, R.**; Garcia-Garrido, E.; Somoza, Á. Albumin-based nanoparticles for the delivery of doxorubicin in breast cancer. *Cancers (Basel).* **2021**, *13*, 1–17, doi:10.3390/cancers13123011.

2. **Prajapati, R.**; Somoza, Á. Albumin nanostructures for nucleic acid delivery in cancer: Current trend, emerging issues, and possible solutions. *Cancers (Basel).* **2021**, *13*, 1–16, doi:10.3390/cancers13143454.

3. **Prajapati, R.**; Cordani, M.; Somoza, Á. Albumin-based polyplexes for the delivery of CRISPR/Cas9 plasmid targeting the mutant p53. (*Under preparation*)

4. **Prajapati, R.**; Fortuni, B.; Rocha, S.; Somoza, Á. Albumin-based nanoparticles for the delivery of Volasertib in cancer therapy. (*Under preparation*)